

NOTTINGHAM TRENT UNIVERSITY



*Synthesis and Properties of Advanced Chiral and Racemic
Multifunctional Molecular Materials*

Elizabeth Kate Rusbridge

*A thesis submitted in partial fulfilment of the requirements of
Nottingham Trent University for the degree of Doctor of Philosophy*

February 2024

Declaration

I confirm that this is my own work and the use of all materials from other sources has been properly and fully acknowledged. No part of this thesis has already been, or is being currently submitted for any such degree, diploma or other qualification.

The copyright in this work is held by the author. You may copy up to 5% of this work for private study, or personal, non-commercial research. Any re-use of the information contained within this document should be fully referenced, quoting the author, title, university, degree level and pagination. Queries or requests for any other use, or if a more substantial copy is required, should be directed to the author.

Signed: *Elizabeth R*

Date: 28/02/2024

Elizabeth Rusbridge

1. Abstract

Superconductivity is one of the most interesting phenomena of our time. First observed in 1911, materials possessing this property have the ability to conduct large electrical currents with zero resistance indefinitely.¹ As a result of their powerful magnetic fields, *superconducting* materials are ideal for use in power transmission cables, superfast transport, as well as medical applications like that of MRI (magnetic resonance imaging). *Superconductors* have the ability to revolutionise vehicular and energy transport across the world. The main drawback for materials of this type is that they require expensive cryogenic cooling with liquid nitrogen or liquid helium to activate this *superconducting* state. Since the origin of *high-temperature superconductivity* and the ideal conditions required for a material to enter this state are not yet fully understood, this project aims to aid in providing theoretical information to allow explanation of this strange phenomenon. In this, a range of materials will be synthesised which possess both (*super*)*conducting* properties, as well as chirality; a combination that is not observed in nature, and in some cases, magnetism to yield a property trifecta. In doing so, it may be possible to understand the mechanisms of both *superconductivity* and eMChA (electrical magnetochiral anisotropy).

Three novel types of materials have been studied during this body of work, with particular focus on the first and second, whereby the third is included as a result of resistivity measurements performed by the author on materials synthesised by others within the research group. The first syntheses were based upon functionalisation of BEDT-TTF (bis(ethylenedithio)tetrathiafulvalene) to yield novel donors with varying chiral sidechains, following the published work by the Martin research group very recently.^{2,3} A series of eight novel unsymmetrically substituted enantiopure donors have been realised based upon this previously published research, which may now be employed in the synthesis of novel θ -type charge-transfer salts. In doing so, one may study the effect of chirality and *super(conductivity)* within enantiomeric and diastereomeric salts.

The second type of material studied includes salts of metal trisoxalate anions with BEDT-TTF. A number of novel charge-transfer salts have been synthesised successfully, with some interesting and surprising serendipitous discoveries. The synthetic method employed offers the potential for introducing a wide range of guest molecules, whereas previously these have been limited to solvent molecules. Such introductions may allow one to fine-tune the conducting properties *via* extension of the hexagonal cavity *b* axis, which in turn may

increase the superconducting T_c in this family of salts, whilst adding further functionality to the material alongside depending on the guest identity. Despite extensive syntheses reported here, these represent only a small number of the vast pool of guest molecules available for one to utilise in discovering novel chiral-magnetic-conducting salts. The full potential of those reported have yet to be realised and one is honoured to have already been able to add to the wealth of literature surrounding these salts.⁴

Finally, two novel charge-transfer salts of BEDT-TTF with spiroborate have been characterised *via* electrical resistivity measurements. The discovery of this family of salts was established by the Martin research group very recently, such that the potential of these novel materials remains relatively untapped.⁵⁻⁷ The extensive potential for an array of further bidentate ligands forms the basis of further work in this area, and the novel salts reported provide new additions of both *semiconducting* and *metallic-insulating* members to said family.

A new family of chiral donors has been synthesised which can be employed not only with TCNQ (tetracyanoquinodimethane), but with a multitude of different sized/shaped anions to potentially lead to further chiral (*super*)conductors and/or switching materials. Much study upon the materials synthesised in this body of work is still available for future researchers, and one postulates that all three types of material studied may even be employed to formulate novel families with one another, such that the newly-realised chiral BEDT-TTF motifs may be employed with both the metal trisoxalate anions, as well as the spiroborate anions to realise even further novel multifunctional molecular conducting materials. Moreover, inclusion of chiral guest molecules may be employed in these new families using the methods described here, which have shown that using chiral guests can lead to chiral induction, thereby yielding single enantiomers of the anions employed.

Acknowledgements

I would like to dedicate this body of work to my late grandmother, who has always been one of my biggest supporters and sources of joy, love and laughter. I am grateful to my family, who have provided much love and support throughout my degrees studied at NTU.

Thank you to Professor John Wallis for his endless NMR and XRD support, as well as general chatter and light-hearted fun. Thank you for keeping an eye on me and sharing your extensive knowledge of BEDT-TTF donors, as well as taking the time to assist in gathering all the necessary data for synthesised materials. Thank you for always being willing to lend a hand as well as an anecdote or two! One also extends thanks to Dr Songjie Yang, who taught me how to make my first novel donor molecules so that I may have all the necessary tools to synthesise further donors.

Thank you to both Dr Toby Blundell and Dr Joseph Ogar for their time spent analysing synthesised crystals *via* XRD and imparting shared knowledge of the characterisation technique.

Thank you to JSPS, for the opportunity to perform my PhD work in Osaka for two months in 2022 and spend time with collaborators of our research group. A special thank you to Professor Hiroki Akutsu of Osaka University for his wonderful role of host, temporary supervisor and supplier of lots of Japanese treats. Thank you for the wonderful experience and shared laughter whilst teaching me the ways of attaching tiny gold wires to tiny crystals for conductivity measurements. Gratitude is also offered for performing XRD, conductivity and SQUID measurements on synthesised materials during my PhD.

Thank you to Nottingham Trent University for the use of their facilities throughout my project and to the technical staff who not only kept the laboratories in order, but also provided comic relief on days when syntheses did not go to plan. The same thanks go to lab colleagues who were present in the initial years of my PhD studies.

Finally, my biggest acknowledgement goes to Dr Lee Martin for his role of supervisor and friend throughout my PhD. Without him, I would not have had the opportunity to study these interesting families of (*super*)conductors and this body of work would not exist. Thank you for sharing your extensive knowledge of the research area, as well as that of Japan and all it has to offer! I am grateful for all the support he has given me in all aspects of my PhD, especially during the writing phase.

List of Publications

T. J. Blundell, A. L. Morritt, E. K. Rusbridge, L. Quibell, J. Oakes, H. Akutsu, Y. Nakazawa, S. Imajo, T. Kadoya, J. I. Yamada, S. J. Coles, J. Christensen and L. Martin, Molecular conductors from bis(ethylenedithio)tetrathiafulvalene with tris(oxalato)gallate and tris(oxalato)iridate, *Mater Adv*, 2022, **3**, 4724–4735.

T. J. Blundell, E. K. Rusbridge, R. Pemberton, M. Brannan, A. L. Morritt, J. Ogar, J. D. Wallis, H. Akutsu, Y. Nakazawa, S. Imajo and L. Martin, Introduction of new guest molecules into BEDT-TTF radical-cation salts with tris(oxalato)ferrate, *CrystEngComm*, 2024, **26** (14), 1962-1975.

T.J. Blundell, E. K. Rusbridge, M. Brannan, J. Ogar, J. D. Wallis, H. Akutsu, Y. Nakazawa, S. Imajo and L. Martin, BEDT-TTF radical-cation salts with tris(oxalato)chromate and guest additives, *RSC advances*, 2024, **14** (26), 18444-18452.

E. K. Rusbridge, J. Ogar, T. J. Blundell, J.D. Wallis, A. Mantle, H. Akutsu, Y. Nakazawa and Lee Martin, Chiral conductors *via* spontaneous resolution of $\text{Fe}(\text{C}_2\text{O}_4)_3$ in BEDT-TTF radical-cation salts, *pending submission to Inorg.Chem.*

Abbreviations, Units and Symbols

Å	Angstrom Unit of Length
B ⁰	Applied magnetic field
BCS	Bardeen, Cooper and Schrieffer Theory
BEDT-TTF	Bis(ethylenedithio)tetrathiafulvalene
CT Salt	Charge-transfer Salt
eMChA	Electrical magnetochiral anisotropy
eV	Electron Volts
ξ	Coherence Length
H _c	Superconducting Critical Field
HRMS	High Resolution Mass Spectrometry
J _c	Superconducting Critical Current
K	Kelvin
κ	Ginzburg-Landau Parameter
ℓ	Electron Mean Free Path
λ / λ _L	(London) Penetration Depth
Pa	Pascal Unit of Pressure
P(OMe) ₃	Trimethyl Phosphite
MO	Molecular Orbital
NMR	Nuclear Magnetic Resonance
T ₃ P	Propyl phosphonic Anhydride Solution (≥50 wt. % in ethyl acetate)
T _c	Superconducting Critical Temperature
TCNQ	Tetracyanoquinodimethane
TMTSF	Tetramethyltetraselenafulvalene
TTF	Tetrathiafulvalene
XRD	X-Ray Diffraction
vdW	Van der Waals

Table of Contents

1. ABSTRACT	III
ACKNOWLEDGEMENTS	V
LIST OF PUBLICATIONS	VI
ABBREVIATIONS, UNITS AND SYMBOLS.....	VII
LIST OF FIGURES	XI
LIST OF SCHEMES	XIV
LIST OF TABLES	XV
2. INTRODUCTION AND LITERATURE REVIEW	1
2.1 ELECTRICAL CONDUCTIVITY	1
2.1.1 Bonding in Solids	1
2.1.2 Band Theory of Solids.....	2
2.1.3 Insulators.....	4
2.1.4 Semiconductors.....	4
2.1.5 Metallic conductors.....	5
2.2 CONDUCTIVITY IN ORGANIC MATERIALS	6
2.2.1 Conducting Polymers: Conjugated Systems.....	6
2.2.2 Charge-Transfer Complexes	7
2.3 A BRIEF HISTORY OF SUPERCONDUCTORS	8
2.3.1 The Meissner Effect	9
2.3.2 BCS Theory: Cooper Pairs	12
2.3.3 Type I and Type II Superconductors	14
2.3.4 The Josephson Effect	17
2.4 HIGH TEMPERATURE SUPERCONDUCTIVITY	18
2.5 ORGANIC SUPERCONDUCTIVITY	20
2.5.1 BEDT-TTF-based Materials	22
2.5.2 Chiral Molecular Conductors	27
2.6 COMBINING MAGNETISM, CHIRALITY AND SUPERCONDUCTIVITY.....	29
2.7 AIMS OF THIS BODY OF WORK.....	30
2.7.1 BEDT-TTF-Based Donors with TCNQ.....	30
2.7.2 BEDT-TTF salts with Metal Trisoxalate Anions.....	32
2.7.3 BEDT-TTF salts with Spiroborate Anions	33
3. BEDT-TTF-BASED DONORS WITH TCNQ.....	34
3.1 INTRODUCTION	34
3.2 EXPERIMENTAL	36
3.2.1 Synthesis of Bis(tetraethylammonium)bis(1,3-dithiol-2-thione-4,5-dithiol)zincate....	36
3.2.2 Synthesis of 4,5-Ethylenedithio-1,3-dithiole-2-thione	37
3.2.3 Synthesis of 4,5-Ethylenedithio-1,3-dithiole-2-one	38
3.2.4 Synthesis of 1,3-Dithiolane-2,4,5-trithione	39
3.2.5 Synthesis of 2-(2-Thioxo-5,6-dihydro-[1,3]dithiolo[4,5-b][1,4]dithiin-5-yl)acetic acid	40
3.2.6 Synthesis of the S,S & S,R-Diastereoisomers of N-(1'-phenyl-ethyl)-2-thioxo-5,6-	
dihydro-[1,3]dithiolo[4,5-b][1,4]dithiin-5-yl-acetamide	41
3.2.7 Synthesis of the S,S-Diastereoisomer of N-(1'-phenylethyl)-(BEDT-TTF)-acetamide...43	
3.2.8 Synthesis of the S,R-Diastereoisomer of N-(1'-phenylethyl)-(BEDT-TTF)-acetamide...44	
3.2.9 Synthesis of the R,R & R,S-Diastereoisomers of N-(1'-phenyl-ethyl)-2-thioxo-5,6-	
dihydro-[1,3]dithiolo[4,5-b][1,4]dithiin-5-yl-acetamide	45
3.2.10 Synthesis of the R,R-Diastereoisomer of N-(1'-phenylethyl)-(BEDT-TTF)-acetamide	47
3.2.11 Synthesis of the R,S-Diastereoisomer of N-(1'-phenylethyl)-(BEDT-TTF)-acetamide.48	

3.2.12	Synthesis of the S,S & S,R-Diastereoisomers of N-(1'-(2'-Pyridyl)-ethyl)-2-thioxo-5,6-dihydro-[1,3]dithiolo[4,5- b][1,4]dithiin-5-yl-acetamide.....	49
3.2.13	Synthesis of the S,S-Diastereoisomer of N-(1'-(2'-Pyridyl)-ethyl)-(BEDT-TTF)-acetamide	51
3.2.14	Synthesis of the S,R-Diastereoisomer of N-(1'-(2'-Pyridyl)-ethyl)-(BEDT-TTF)-acetamide	52
3.2.15	Synthesis of the R,R & R,S-Diastereoisomers of N-(1'-(2'-Pyridyl)-ethyl)-2-thioxo-5,6-dihydro-[1,3]dithiolo[4,5- b][1,4]dithiin-5-yl-acetamide.....	53
3.2.16	Synthesis of the R,R-Diastereoisomer of N-(1'-(2'-Pyridyl)-ethyl)-(BEDT-TTF)-acetamide	55
3.2.17	Synthesis of the R,S-Diastereoisomer of N-(1'-(2'-Pyridyl)-ethyl)-(BEDT-TTF)-acetamide	56
3.2.18	Synthesis of the S,S & S,R-Diastereoisomers of N-(1'-(4''-Methylphenyl)-ethyl)-2-thioxo-5,6-dihydro-[1,3]dithiolo[4,5- b][1,4]dithiin-5-yl-acetamide	57
3.2.19	Synthesis of the S,S-Diastereoisomer of N-(4''-Methylphenyl)-ethyl)-(BEDT-TTF)-acetamide	59
3.2.20	Synthesis of the S,R-Diastereoisomer of N-(4''-Methylphenyl)-ethyl)-(BEDT-TTF)-acetamide	61
3.2.21	Synthesis of Charge-Transfer Salts from Novel Donor Molecules with TCNQ	63
3.2.21.1	S,S-N-(1'-phenylethyl)-(BEDT-TTF)-acetamide.....	63
3.2.21.2	S,R-N-(1'-phenylethyl)-(BEDT-TTF)-acetamide.....	63
3.2.21.3	R,R-N-(1'-phenylethyl)-(BEDT-TTF)-acetamide	63
3.2.21.4	R,S-N-(1'-phenylethyl)-(BEDT-TTF)-acetamide.....	64
3.2.21.5	S,S-N-(4''-methylphenyl)-ethyl)-(BEDT-TTF)-acetamide	64
3.2.21.6	S,R-N-(4''-methylphenyl)-ethyl)-(BEDT-TTF)-acetamide	64
3.2.22	Characterisation Techniques	65
3.3	RESULTS AND DISCUSSION	68
3.3.1	Analysis of Synthesised Novel Organic Donor Molecules and their Precursors	68
3.3.1.1	Synthesis of Bis(tetraethylammonium)bis(1,3-dithiol-2-thione-4,5-dithiol)zincate	68
3.3.1.2	Synthesis of 4,5-ethylenedithio-1,3-dithiole-2-thione.....	68
3.3.1.3	Synthesis of 4,5-ethylenedithio-1,3-dithiole-2-one	69
3.3.1.4	Synthesis of 1,3-dithiolane-2,4,5-trithione.....	69
3.3.1.5	Synthesis of 2-(2-thioxo-5,6-dihydro-[1,3]dithiolo[4,5-b][1,4]dithiin-5-yl)acetic acid	70
3.3.1.6	Synthesis of the S,S & S,R-Diastereoisomers of N-(1'-phenyl-ethyl)-2-thioxo-5,6-dihydro-[1,3]dithiolo[4,5-b][1,4]dithiin-5-yl-acetamide	70
3.3.1.7	Synthesis of Enantiopure S,S- and S,R-Diastereoisomers of N-(1'-phenylethyl)-(BEDT-TTF)-acetamide.....	71
3.3.1.8	Synthesis of the R,R & R,S-Diastereoisomers of N-(1'-phenyl-ethyl)-2-thioxo-5,6-dihydro-[1,3]dithiolo[4,5-b][1,4]dithiin-5-yl-acetamide	73
3.3.1.9	Synthesis of Enantiopure R,R & R,S-Diastereoisomers of N-(1'-phenylethyl)-(BEDT-TTF)-acetamide.....	74
3.3.1.10	Synthesis of the S,S & S,R-Diastereoisomers of N-(1'-(2'-Pyridyl)-ethyl)-2-thioxo-5,6-dihydro-[1,3]dithiolo[4,5- b][1,4]dithiin-5-yl-acetamide	75
3.3.1.11	Synthesis of Enantiopure S,S & S,R-Diastereoisomers of N-(1'-(2'-Pyridyl)-ethyl)-(BEDT-TTF)-acetamide.....	76
3.3.1.12	Synthesis of the R,R & R,S-Diastereoisomers of N-(1'-(2'-Pyridyl)-ethyl)-2-thioxo-5,6-dihydro-[1,3]dithiolo[4,5- b][1,4]dithiin-5-yl-acetamide	76
3.3.1.13	Synthesis of Enantiopure R,R & R,S-Diastereoisomers of N-(1'-(2'-Pyridyl)-ethyl)-(BEDT-TTF)-acetamide.....	77

3.3.1.14	Synthesis of the S,S & S,R-Diastereoisomers of N-(1'-(4''-Methylphenyl)-ethyl)-2-thioxo-5,6-dihydro-[1,3]dithiolo[4,5-b][1,4]dithiin-5-yl-acetamide	78
3.3.1.15	Synthesis of Enantiopure S,S- and S,R-Diastereoisomers of N-((4''-Methylphenyl)-ethyl)-(BEDT-TTF)-acetamide	80
3.3.2	Cyclic Voltammetry	81
3.3.3	Analysis of the Synthesis of Charge-Transfer Salts Under Reflux Conditions	82
3.4	CONCLUSION	85
4.	BEDT-TTF SALTS WITH METAL TRISOXALATE ANIONS	87
4.1	INTRODUCTION	87
4.2	EXPERIMENTAL	90
4.2.1	BEDT-TTF salts with Metal Trisoxalates and Benzonitrile	90
4.2.2	BEDT-TTF salts with Metal Trisoxalates and New Guest Molecules	91
4.2.3	Electrocrystallisation using H-cells	92
4.2.4	X-ray Crystallography	93
4.2.5	Resistivity Measurements	93
4.3	RESULTS AND DISCUSSION	95
4.3.1	BEDT-TTF salts with Metal Trisoxalates and Benzonitrile.....	95
4.3.1.1	pseudo- κ -(BEDT-TTF) ₄ [(H ₃ O)Ir(C ₂ O ₄) ₃].PhCN ⁴	95
4.3.2	BEDT-TTF salts with Metal Trisoxalate and New Guest Molecules.....	99
4.3.2.1	β'' -(BEDT-TTF) ₅ [Ir(C ₂ O ₄) ₃].ethanol	100
4.3.2.2	β'' -(BEDT-TTF) ₄ [(H ₃ O)M(C ₂ O ₄) ₃].toluene (M = Cr or Fe)	105
4.3.2.3	β'' - β'' -(BEDT-TTF) ₄ [(H ₂ O/H ₃ O)Fe(C ₂ O ₄) ₃].1-phenylethane-1,2-diol	109
4.3.2.4	α''' -(BEDT-TTF) ₄ [Fe(C ₂ O ₄) ₂ (kojate)]	113
4.3.2.5	α -(BEDT-TTF) ₅ [Fe(C ₂ O ₄) ₃].(tartaric acid) ₂	118
4.4	CONCLUSIONS.....	121
4.4.1	BEDT-TTF salts with Metal Trisoxalate and Benzonitrile.....	121
4.4.2	BEDT-TTF salts with Metal Trisoxalate and New Guest Molecules	121
5.	BEDT-TTF SALTS WITH SPIROBORATE ANIONS	122
5.2.1	X-ray Crystallography	124
5.2.2	Resistivity Measurements.....	124
6.	FINAL CONCLUSIONS AND FUTURE WORK.....	130
	REFERENCES	134

List of Figures

FIGURE 2.1: A MOLECULAR ORBITAL DIAGRAM OF HYDROGEN.....	2
FIGURE 2.2 - A SIMPLIFIED MOLECULAR ORBITAL DIAGRAM TO ILLUSTRATE THE FORMATION OF ENERGY BANDS IN RESPONSE TO INCREASING ATOMS. FOR CLARITY, THE BLUE COLOUR DEPICTS A 'FILLED' BAND.....	3
FIGURE 2.3 - A SIMPLIFIED BAND-STRUCTURE DIAGRAM OF A) A METALLIC CONDUCTOR, B) A SEMICONDUCTOR AND C) AN INSULATOR. FOR CLARITY, THE BLUE COLOUR DEPICTS A 'FILLED' BAND.	4
FIGURE 2.4 - VARIATION OF ELECTRICAL CONDUCTIVITY AS A FUNCTION OF VARYING TEMPERATURE FOR SOLIDS CLASSIFIED AS A METALLIC CONDUCTOR, A SEMICONDUCTOR AND A SUPERCONDUCTOR. ¹¹	6
FIGURE 2.5 – ELECTRON DONATING MOLECULES; A) P-PHENYLENEDIAMINE (TMPD), B) TETRATHIAFULVALENE (TTF) AND C) BIS(ETHYLENEDITHIO)TETRATHIAFULVALENE (BEDT-TTF).....	7
FIGURE 2.6 - ELECTRON ACCEPTING MOLECULES; A) TETRACYANOQUINODIMETHANE (TCNQ) AND B) CHLORANIL.....	8
FIGURE 2.7 - KAMERLINGH-ONNES' ORIGINAL PLOT OF RESISTANCE (OHMS, Ω) AGAINST ABSOLUTE TEMPERATURE (K) MARKING THE DISCOVERY OF SUPERCONDUCTIVITY IN MERCURY AT 4.2K. ³⁰	9
FIGURE 2.8 - VISUAL REPRESENTATION OF THE MEISSNER EFFECT WHEN A SUPERCONDUCTING SAMPLE IS COOLED BELOW T_c , WHERE B IS THE APPLIED MAGNETIC FIELD.....	10
FIGURE 2.9 - COMPARISON OF THE MAGNETIC BEHAVIOUR OF A PERFECT CONDUCTOR AND A SUPERCONDUCTOR COOLED UNDER AN APPLIED MAGNETIC FIELD (B^0), BEFORE THE FIELD IS TURNED OFF (A AND C) AND AFTER THE FIELD IS REMOVED (B AND D). ³⁶	10
FIGURE 2.10 - THE FORMATION OF A COOPER PAIR; ONE ELECTRON DISTORTS THE LATTICE ATTRACTING A SECOND ELECTRON, FORMING A LOWER ENERGY PAIR AS A RESULT OF THIS ELECTRON-LATTICE INTERACTION. ¹¹	13
FIGURE 2.11 - A MAGNETIC FIELD (H) VS TEMPERATURE (T) DIAGRAM FOR A TYPE I SUPERCONDUCTOR (LEFT) AND A TYPE II SUPERCONDUCTOR (RIGHT), ALLOWING VISUAL REPRESENTATION BETWEEN THE TWO DIFFERENT PHASE TRANSITIONS. ¹²	15
FIGURE 2.12 – SIMULTANEOUS LINES OF FIELDS AND CURRENTS IN A VORTEX LATTICE IN THE VICINITY OF H_{c2} , GIVING RISE TO QUADRATIC ARRAYS OF VORTICES (LEFT) AND TRIANGULAR ARRAYS OF VORTICES (RIGHT). ⁵⁰	16
FIGURE 2.13 - VORTEX PINNING GIVING RISE TO LEVITATION OF A SUPERCONDUCTOR ABOVE A MAGNET (LEFT) AND SUSPENSION OF A SUPERCONDUCTOR BELOW A MAGNETIC (RIGHT) AS A RESULT OF THESE FLUX LINES. ¹²	16
FIGURE 2.14 - DISCOVERY OF LOW TEMPERATURE ELEMENTAL AND INTERMETALLIC SUPERCONDUCTORS FROM 1911 UNTIL 1980. ⁶⁶	18
FIGURE 2.15 - EVOLUTION OF SUPERCONDUCTING CRITICAL TEMPERATURES, WITH THE HIGH TEMPERATURE ERA STATING FROM THE 1980's. ⁷³	19
FIGURE 2.16 - CRYSTALLINE LATTICE STRUCTURE OF (TMTSF) ₂ PF ₆ , WHERE P ATOMS ARE PINK, C ATOMS ARE BLACK, F ATOMS ARE WHITE AND SE ATOMS ARE ORANGE. REGIONS OF NEGATIVE CHARGE LIE ALONG THE VERTICAL STACKS OF PF ₆ ⁻ (GREY SHADING), AND REGIONS OF POSITIVE CHARGE LIE ALONG THE VERTICAL STACKS OF TMTSF (PINK SHADING). ⁷⁹	21
FIGURE 2.17 - STRUCTURE OF BEDT-TTF (BIS(ETHYLENEDITHIO)TETRATHIAFULVALENE).....	23
FIGURE 2.18 - RING-OVER-BOND (RB) STACKING MOTIF, TOP, AND RING-OVER-ATOM (RA) STACKING MOTIF, BOTTOM. OVERLAP MODES VIEWED FROM TWO PLANES; LEFT IS PERPENDICULAR TO THE MOLECULAR PLANE AND RIGHT IS ALONG THE LONG AXIS. ⁹⁴	24
FIGURE 2.19 - B-TYPE PHASES ARISING FROM RA AND RB STACKING MOTIFS. ⁹⁴	25
FIGURE 2.20 – A VISUAL REPRESENTATION OF THE A-, B- AND Θ -TYPE STACKING MOTIFS BASED UPON RA AND RB OVERLAP AND THEIR RELEVANT INCLINATIONS; + INDICATES AN UPWARD INCLINATION AND – INDICATES A DOWNWARD INCLINATION OF THE BEDT-TTF MOLECULES. ⁹⁴	25
FIGURE 2.21 - A VISUAL REPRESENTATION OF THE Δ -, Δ' - AND A' -PHASES AND THEIR RELEVANT TWISTING AND RA/RB OVERLAPPING MOTIFS. ⁹⁶	26
FIGURE 2.22 - A VISUAL REPRESENTATION OF THE K-PHASE. ⁹⁵	26
FIGURE 2.23 - A) VISUAL ILLUSTRATION OF CHIRALITY WITH ITS LEFT AND RIGHT-HANDED NATURE, AND B) R-(+)- & S-(-)- THALIDOMIDE. THE SINGLE ENANTIOMERS AND THE RACEMIC FORM MAY DIFFER IN THEIR DOSAGES, EFFICACIES, SIDE EFFECT PROFILES, OR INDICATED USE.	27

FIGURE 2.24 - A SIMPLE DIAGRAM TO DEMONSTRATE EMCHA AND HOW CHIRALITY CAN AFFECT THE DIRECTION OF ELECTRICAL TRANSPORT. IN SIMPLE TERMS, THE 'LEFT-HANDED' MATERIAL MAY DIRECT THE ELECTRICAL CURRENT IN A CLOCKWISE FASHION, WHEREAS THE 'RIGHT-HANDED' MATERIAL DIRECTS IT IN AN ANTI-CLOCKWISE FASHION....	28
FIGURE 2.25 - NOVEL DONOR MOLECULE BASED ON BEDT-TTF, SYNTHESISED BY WALLIS ET AL. ³	31
FIGURE 2.26 - A) 4:1 B''-(BEDT-TTF) ₄ [(H ₃ O)Fe(C ₂ O ₄) ₃].PHBr WITH ALTERNATING LAYERS OF BEDT-TTF DONORS AND METAL TRISOXALATE, AND B) THE HEXAGONAL CAVITY ARISING IN THESE 4:1 SALTS, WITH BROMOBENZENE AS A CAVITY GUEST. ¹²⁹	32
FIGURE 3.1 - A GENERAL CYCLIC VOLTAMMETRY PLOT TO VISUALISE THOSE YIELDED BY ALL DONORS (WITH THE EXCEPTION OF THE PYRIDYL-TYPE DONORS DUE TO PURITY ISSUES). DATA USED FOR THIS GRAPH WAS THAT OF S,R-N-(1'-PHENYLETHYL)-(BEDT-TTF)-ACETAMIDE.	67
FIGURE 3.2 - MOLECULAR STRUCTURE OF FIRST (S,S)-FULL DONOR, SHOWING THE (S)-STEREOCHEMISTRY AT 5-C ON THE DITHIIN RING. ACETONE SOLVENT MOLECULE OMITTED FOR CLARITY.....	72
FIGURE 3.3 - PACKING OF THE DONOR MOLECULES WITHIN THE CRYSTAL STRUCTURE OF THE S,S-FULL DONOR; ONE OBSERVES INTERESTING HYDROGEN BONDING INTERACTIONS BETWEEN THE ACETONE SOLVENT AND DONORS, AS OPPOSED TO THE USUAL DONOR-DONOR H-BONDING MOTIFS OBSERVED IN PREVIOUSLY PUBLISHED MATERIALS. .	72
FIGURE 3.4 - MOLECULAR STRUCTURE OF THE FIRST (S,S)-HALF DONOR, SHOWING THE (S)-STEREOCHEMISTRY AT 5-C ON THE DITHIIN RING. NO SOLVENT APPEARS IN THIS STRUCTURE.....	79
FIGURE 3.5 - PACKING OF THE DONOR MOLECULES WITHIN THE CRYSTAL STRUCTURE OF THE S,S-HALF DONOR. FOR CLARITY, THE ACETONE SOLVENT MOLECULES ARE NOT DISPLAYED.	79
FIGURE 4.1 - PACKING ARRANGEMENTS OF THE ANION LAYER WITHIN THE 4:1 SALTS; THE PSEUDO-K PHASE ON THE LEFT SHOWS ALTERNATING ENANTIOMERS WITHIN THE SAME LAYER, WHEREAS THE B'' PHASE ON RIGHT SHOWS THE SINGLY-ENANTIOMERIC LAYER.	88
FIGURE 4.2 - PSEUDO-K-(BEDT-TTF) ₄ [(H ₃ O)Ir(C ₂ O ₄) ₃].BENZONITRILE VIEWED DOWN THE A AXIS. HYDROGEN ATOMS AND DISORDER OF TERMINAL ETHYLENE GROUPS OF BEDT-TTF OMITTED FOR CLARITY. ⁴	97
FIGURE 4.3 - PSEUDO-K-(BEDT-TTF) ₄ [(H ₃ O)Ir(C ₂ O ₄) ₃].BENZONITRILE DONOR LAYER. HYDROGEN ATOMS AND DISORDER OF TERMINAL ETHYLENES OF BEDT-TTF OMITTED FOR CLARITY. DISTINCT DONORS ARE CLARIFIED IN TERMS OF CHARGE IN FIGURE 4.7. ⁴	98
FIGURE 4.4 - PSEUDO-K-(BEDT-TTF) ₄ [(H ₃ O)Ir(C ₂ O ₄) ₃].BENZONITRILE ANION LAYER VIEWED DOWN THE C AXIS. HYDROGEN ATOMS OMITTED FOR CLARITY. ⁴	98
FIGURE 4.5 - PSEUDO-K-(BEDT-TTF) ₄ [(H ₃ O)Ir(C ₂ O ₄) ₃].BENZONITRILE ELECTRICAL RESISTIVITY. ⁴	98
FIGURE 4.6 - B''-(BEDT-TTF) ₅ [Ir(C ₂ O ₄) ₃].ETHANOL VIEWED DOWN THE B AXIS. HYDROGEN ATOMS AND DISORDER OF TERMINAL ETHYLENES OF BEDT-TTF OMITTED FOR CLARITY. ⁴	102
FIGURE 4.7 - B''-(BEDT-TTF) ₅ [Ir(C ₂ O ₄) ₃].ETHANOL DONOR LAYER. DONOR A = YELLOW, B = BLUE, C = RED. DONOR A FORMS A DIMER (CIRCLED), WHEREAS DONORS B AND C FORM A B-C-B TRIMER (DASHED CIRCLED). ⁴	103
FIGURE 4.8 - B''-(BEDT-TTF) ₅ [Ir(C ₂ O ₄) ₃].ETHANOL ANION LAYER VIEWED DOWN THE C AXIS. ⁴	103
FIGURE 4.9 - PACKING ARRANGEMENT OF DONOR LAYER FOR B''-(BEDT-TTF) ₅ [Ir(C ₂ O ₄) ₃].ETHANOL. A = YELLOW, B = BLUE, C = RED. ⁴	104
FIGURE 4.10 - B''-(BEDT-TTF) ₅ [Ir(C ₂ O ₄) ₃].ETHANOL ELECTRICAL RESISTIVITY. ⁴	104
FIGURE 4.11 - B''-(BEDT-TTF) ₄ [(H ₃ O)M(C ₂ O ₄) ₃].TOLUENE VIEWED DOWN THE A AXIS. HYDROGEN ATOMS AND DISORDER OF TERMINAL ETHYLENES OF BEDT-TTF OMITTED FOR CLARITY.	107
FIGURE 4.12 - B''-(BEDT-TTF) ₄ [(H ₃ O)M(C ₂ O ₄) ₃].TOLUENE DONOR LAYER. HYDROGEN ATOMS AND DISORDER OF TERMINAL ETHYLENE GROUPS OF BEDT-TTF GROUPS OMITTED FOR CLARITY.....	107
FIGURE 4.13 - B''-(BEDT-TTF) ₄ [(H ₃ O)M(C ₂ O ₄) ₃].TOLUENE ANION LAYER VIEWED DOWN THE C AXIS. HYDROGEN ATOMS OMITTED FOR CLARITY.	108
FIGURE 4.14 - B''-(BEDT-TTF) ₄ [(H ₃ O)M(C ₂ O ₄) ₃].TOLUENE ELECTRICAL RESISTIVITY. M = CR (TOP) AND FE (BOTTOM).	108
FIGURE 4.15 - B''-B''-(BEDT-TTF) ₄ [(H ₂ O/H ₃ O)Fe(C ₂ O ₄) ₃].1-PHENYLETHANE-1,2-DIOL VIEWED DOWN THE A AXIS.	111
FIGURE 4.16 - B''-B''-(BEDT-TTF) ₄ [(H ₂ O/H ₃ O)Fe(C ₂ O ₄) ₃].1-PHENYLETHANE-1,2-DIOL DONOR LAYERS. DONOR LAYER 1 (LEFT) IS ON THE EDGE OF THE UNIT CELL (C AXIS) DOCKING INTO ANION LAYERS FACING THE R GROUP OF THE GUEST MOLECULE. DONOR LAYER 2 (RIGHT) IS IN THE CENTRE OF THE UNIT CELL (C AXIS) DOCKING INTO ANION LAYERS FACING THE PHENYL GROUPS OF THE GUEST MOLECULE.....	112

FIGURE 4.17 - B''-B''-(BEDT-TTF) ₄ [(H ₂ O/H ₃ O)Fe(C ₂ O ₄) ₃]. 1-PHENYLETHANE-1,2-DIOL ANION LAYER VIEWED DOWN THE C AXIS.	112
FIGURE 4.18 - B''-B''-(BEDT-TTF) ₄ [(H ₂ O/H ₃ O)Fe(C ₂ O ₄) ₃]. 1-PHENYLETHANE-1,2-DIOL ELECTRICAL RESISTIVITY....	113
FIGURE 4.19 - A''''-(BEDT-TTF) ₄ [Fe(C ₂ O ₄) ₂ (KOJATE)] VIEWED DOWN THE A AXIS.....	116
FIGURE 4.20 - A''''-(BEDT-TTF) ₄ [Fe(C ₂ O ₄) ₂ (KOJATE)] DONOR LAYER; THE TOP FIGURE DISPLAYS THE DONOR LAYER IN A SIMPLE VIEW, WHEREAS THE BOTTOM FIGURE HIGHLIGHTS THE DIFFERENTLY CHARGED DONORS, DISTINGUISHED BY COLOURS. RESPECTIVE CHARGES ARE AS FOLLOWS; WHITE = 0.81+, GREEN = 0.74+, MAGENTA = 0.85+, RED = 0.91+, YELLOW = 0.70+, DARK BLUE = 0.67+, CLARET = 0.32+ AND LIGHT BLUE = 0.49+.	116
FIGURE 4.21 - A''''-(BEDT-TTF) ₄ [Fe(C ₂ O ₄) ₂ (KOJATE)] ANION LAYER VIEWED DOWN THE C AXIS.....	117
FIGURE 4.22 - A''''-(BEDT-TTF) ₄ [Fe(C ₂ O ₄) ₂ (KOJATE)] ELECTRICAL RESISTIVITY.....	117
FIGURE 4.23 - A-(BEDT-TTF) ₅ [Fe(C ₂ O ₄) ₃].(TARTARIC ACID) ₂ VIEWED DOWN THE A AXIS.	119
FIGURE 4.24 - A-(BEDT-TTF) ₅ [Fe(C ₂ O ₄) ₃].(TARTARIC ACID) ₂ DONOR LAYER.	119
FIGURE 4.25 - A-(BEDT-TTF) ₅ [Fe(C ₂ O ₄) ₃].(TARTARIC ACID) ₂ ANION LAYER VIEWED DOWN THE C AXIS.	120
FIGURE 4.26 - A-(BEDT-TTF) ₅ [Fe(C ₂ O ₄) ₃].(TARTARIC ACID) ₂ ELECTRICAL RESISTIVITY.	120
FIGURE 5.1 - SPIROBORATE ANION B(4-CHLOROSALICYLATE) ₂ ⁻	126
FIGURE 5.2 - B''-(BEDT-TTF) ₂ B(4-CHLOROSALICYLATE) ₂ VIEWED DOWN THE A AXIS.....	126
FIGURE 5.3 - B''-(BEDT-TTF) ₂ B(4-CHLOROSALICYLATE) ₂ ELECTRICAL RESISTIVITY.....	127
FIGURE 5.4 - SPIROBORATE ANION B(GLYCOLATE) ₂ ⁻	128
FIGURE 5.5 - B''-(BEDT-TTF) ₂ [B(GLYCOLATE) ₂] VIEWED DOWN THE B AXIS.....	128
FIGURE 5.6 - B''-(BEDT-TTF) ₂ [B(GLYCOLATE) ₂] ELECTRICAL RESISTIVITY.	128

List of Schemes

SCHEME 3.1 - SELF-ASSEMBLY REACTION FOR THE SYNTHESIS OF THE ZINC SALT, USING METHODS REPORTED BY WANG ET AL. ¹⁴⁷	68
SCHEME 3.2 - SYNTHESIS OF THE THIONE, USING METHODS REPORTED BY VARMA ET AL. ¹⁴⁹	68
SCHEME 3.3 - SYNTHESIS OF THE OXO-COMPOUND.....	69
SCHEME 3.4 - SYNTHESIS OF THE TRITHIONE.....	69
SCHEME 3.5 - SYNTHESIS OF CARBOXY-THIONE.	70
SCHEME 3.6 - SYNTHESIS OF THE HALF S,S- AND S,R- DIASTEREOMERIC ACETAMIDES USING S-A-METHYLBENZYLAMINE.....	70
SCHEME 3.7 - SYNTHESIS OF THE FULL S,S- AND S,R-DIASTEREOMERIC ACETAMIDES USING S-A-METHYLBENZYLAMINE.	71
SCHEME 3.8 - SYNTHESIS OF THE HALF R,R- AND R,S-DIASTEREOMERIC ACETAMIDES USING R-A-METHYLBENZYLAMINE.....	73
SCHEME 3.9 - SYNTHESIS OF THE FULL R,R- AND R,S-DIASTEREOMERIC ACETAMIDES USING R-A-METHYLBENZYLAMINE.....	74
SCHEME 3.10 - SYNTHESIS OF THE HALF S,S- AND S,R- DIASTEREOMERIC ACETAMIDES USING (S)-1-PYRIDIN-2-YL-ETHYLAMINE.	75
SCHEME 3.11 - SYNTHESIS OF THE FULL S,S- AND S,R-DIASTEREOMERIC ACETAMIDES USING (S)-1-PYRIDIN-2-YL-ETHYLAMINE.	76
SCHEME 3.12 - SYNTHESIS OF THE HALF R,R- AND R,S- DIASTEREOMERIC ACETAMIDES USING (R)-1-PYRIDIN-2-YL-ETHYLAMINE.	77
SCHEME 3.13 - SYNTHESIS OF THE FULL R,R- AND R,S-DIASTEREOMERIC ACETAMIDES USING (R)-1-PYRIDIN-2-YL-ETHYLAMINE.	78
SCHEME 3.14 - SYNTHESIS OF THE HALF S,S- AND S,R- DIASTEREOMERIC ACETAMIDES USING S-1-(P-TOLYL)ETHANAMINE.	78
SCHEME 3.15 - SYNTHESIS OF THE FULL S,S- AND S,R-DIASTEREOMERIC ACETAMIDES USING S-1-(P-TOLYL)ETHANAMINE.	80
SCHEME 3.16 - GENERAL REACTION SCHEME FOR THE SYNTHESIS OF CHARGE-TRANSFER SALTS WITH NEW DONORS AND TCNQ.....	82

List of Tables

TABLE 3.1 - CYCLIC VOLTAMMETRY DATA FOR SYNTHESISED DONORS, GIVING OXIDATION POTENTIALS FOR EACH DONOR MOLECULE, MEASURED RELATIVE TO Ag/AgCl, WITH N-BU ₄ NPF ₆ IN CH ₂ Cl ₂ AS THE CHARGE-CARRIER USING A SCAN RATE OF 100 mV s ⁻¹	81
TABLE 3.2 – RESULTS OF THE REFLUX REACTIONS BETWEEN NOVEL DONOR MOLECULES AND TCNQ.	83
TABLE 4.1 - SHORT S...S CONTACTS (>SUM VDW RADII) IN PSEUDO-K-(BEDT-TTF) ₄ [(H ₃ O)Ir(C ₂ O ₄) ₃].BENZONITRILE. ⁴	96
TABLE 4.2 - APPROXIMATION OF THE CHARGE OF BEDT-TTF MOLECULES IN PSEUDO-K-(BEDT-TTF) ₄ [(H ₃ O)Ir(C ₂ O ₄) ₃].BENZONITRILE FROM BOND LENGTHS (Å): Δ = (B + C)-(A + D), Q = 6.347-7.463Δ. ⁴ ..	97
TABLE 4.3 - DETAILS OF OTHER GUESTS THAT WERE TRIED BUT GAVE NO CRYSTALS OR CRYSTALS OF PHASES THAT ARE ALREADY PUBLISHED OR UNDESIRE PHASES.	99
TABLE 4.4 - SHORT S...S CONTACTS (>SUM VDW RADII) IN B''-(BEDT-TTF) ₅ [Ir(C ₂ O ₄) ₃].ETHANOL IN Å. ⁴	101
TABLE 4.5 - APPROXIMATION OF THE CHARGE OF BEDT-TTF MOLECULES IN B''-(BEDT-TTF) ₅ [Ir(C ₂ O ₄) ₃].ETHANOL FROM BOND LENGTHS (Å): Δ = (B + C)-(A + D), Q = 6.347-7.463Δ. ¹⁶⁴ *1 NORMALISED BY THE TOTAL CHARGE. *2 NORMALISED CHARGES OF DIMERS AND TRIMERS.	102
TABLE 4.6 - SHORT S...S CONTACTS (>SUM VDW RADII) IN B''-(BEDT-TTF) ₄ [(H ₃ O)M(C ₂ O ₄) ₃].TOLUENE; HERE, M= Fe.	106
TABLE 4.7 - APPROXIMATION OF THE CHARGE OF BEDT-TTF MOLECULES IN B''-(BEDT-TTF) ₄ [(H ₃ O)M(C ₂ O ₄) ₃].TOLUENE FROM BOND LENGTHS (Å): Δ = (B + C)-(A + D), Q = 6.347-7.463Δ; HERE M=Fe. ¹⁶⁴	107
TABLE 4.8 - SHORT S...S CONTACTS (>SUM VDW RADII) IN B''-B''-(BEDT-TTF) ₄ [(H ₂ O/H ₃ O)Fe(C ₂ O ₄) ₃].1-PHENYLETHANE-1,2-DIOL.....	110
TABLE 4.9 - APPROXIMATION OF THE CHARGE OF BEDT-TTF MOLECULES IN B''-B''-(BEDT-TTF) ₄ [(H ₂ O/H ₃ O)Fe(C ₂ O ₄) ₃].1-PHENYLETHANE-1,2-DIOL FROM BOND LENGTHS (Å): Δ = (B + C)-(A + D), Q = 6.347-7.463Δ. ¹⁶⁴	111
TABLE 4.10 - SHORT S...S CONTACTS (>SUM VDW RADII) IN A''''-(BEDT-TTF) ₄ [Fe(C ₂ O ₄) ₂ (KOJATE)]	114
TABLE 4.11 - APPROXIMATION OF THE CHARGE OF BEDT-TTF MOLECULES IN A''''-(BEDT-TTF) ₄ [Fe(C ₂ O ₄) ₂ (KOJATE)] FROM BOND LENGTHS (Å): Δ = (B + C)-(A + D), Q = 6.347-7.463Δ. ¹⁶⁴	115

2. Introduction and Literature Review

This section provides an extensive introduction into the area of electrical conductivity and *superconductivity* before specific focus turns to a review of charge-transfer salts based upon BEDT-TTF (BEDT-TTF = bis(ethylenedithio)tetrathiafulvalene). The focus of this research lies in the synthesis of functionalised BEDT-TTF-based charge-transfer salts with the view to design and characterise new materials with synergetic coexistence of multiple physical properties, namely chirality, conductivity and molecular switching. To end, a brief overview of the aims is provided.

2.1 Electrical Conductivity

Simply put, electrical conductivity pertains to the intrinsic ability of a material to carry an electric current, often related to temperature. Ohm's law is used to relate voltage (V), current (I) and resistance (R) according to the formula $V = RI$; whereby application of voltage to a material induces a proportional current with inversely proportional resistance. In general terms, application of voltage enables movement of (negatively charged) electrons through the material in question towards positive termini. Ease of electron mobility through a material in response to applied voltage (and temperature) allows us to separate materials into distinct categories; *insulators*, *semiconductors*, *metallic conductors* and *superconductors*. First, it is important to understand the types of bonding within solids of these types, leading onto the widely-accepted band theory of solids, which is largely based upon molecular orbital theory.

2.1.1 Bonding in Solids

The bonding within a solid may be one of three types; metallic, ionic or covalent. In metallic solids, electrons are delocalised across the whole structure of identical arrays of cations and therefore crystal structure is dependant more so on geometrical packing of atoms in an orderly array. Ionic solids are held together by ions dependent upon their Coulombic interactions to give an electronically neutral structure. The atoms of covalently-bonded solids are linked in specific, well-defined orientations throughout the crystal structure, and therefore depend upon stereochemical ordering as opposed to geometric packing. This gives rise to elaborate and extensive structures such as diamond and graphite. Metallic solids have a tendency to conduct electricity very well as a result of the delocalised electrons within their structures. Contrastingly, the valence electrons within ionic and covalently bonded structures are localised on individual atoms, ions or molecular orbitals and are not delocalised across

the structure as a whole. Those which conduct effectively are then classified based upon the variation of their electrical conductivity with temperature; the key to distinguishing a *semiconductor* from a *metallic conductor*. The bonding theory which accounts for delocalised electrons, and therefore separates solids into types of conduction, is the band theory of solids.

2.1.2 Band Theory of Solids

Molecular orbital theory is most commonly applied to small, finite molecules. In this, when atoms bond, there is an overlap and mixing of atomic orbitals which creates two types of distinct molecular orbitals; one bonding orbital and one antibonding orbital. Using diatomic H_2 as an example, an atomic orbital from one hydrogen atom overlaps that of the other hydrogen atom, forming two molecular orbitals that are delocalised across both atoms, *Figure 2.1*. The bonding orbital, sitting at the lowest energy, contains both electrons, and the higher energy antibonding orbital lies empty.

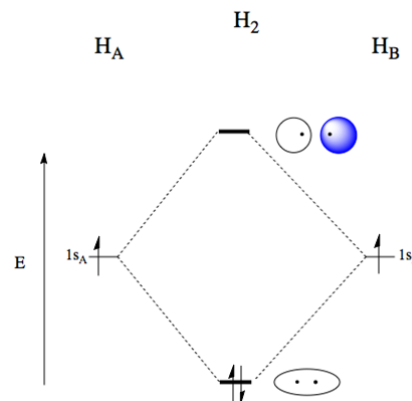


Figure 2.1: A molecular orbital diagram of hydrogen.

This molecular orbital theory can be extended to account for the electrical transport properties of many solids, whereby these near-infinite aggregations of atoms are simply regarded as single large molecules with very large numbers of molecular orbitals (MO's). The overlap of large quantities of atomic orbitals gives rise to equally large quantities of MO's; for every atomic orbital added to the system, a molecular orbital also forms. As this number increases, the average energy gap between individual molecular orbitals decreases, forming an almost continuous *band* of energy levels. The resultant *bands* are separated by *band gaps* with energy ranges associated to where orbitals are absent. The lowest energy band is referred to as the *valence* band, and the highest energy band is referred to as the *conduction* band, *Figure 2.2*.

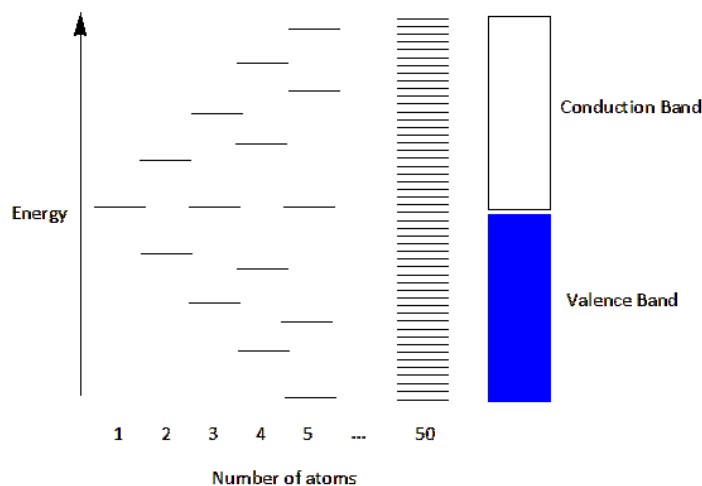


Figure 2.2 - A simplified molecular orbital diagram to illustrate the formation of energy bands in response to increasing atoms. For clarity, the blue colour depicts a 'filled' band.

The formation of bands is not governed by the type of atomic orbital, in the sense that bands may be formed from combinations of s and p orbitals, or p and d orbitals *via* orbital overlapping. The energies of each band, as well as whether they overlap or not, is dependent upon the energies of the contributing atomic orbitals, and bands can be empty, partially filled or full with regard to the number of electrons within the molecule.⁸

At zero Kelvin, the individual molecular orbitals of the bands are occupied by electrons in accordance with the Pauli Exclusion and Aufbau principles, with the lowest energy orbitals being occupied first. The highest occupied orbital within the structure of a *metallic conductor* is coined the *Fermi level*, and its position relative to the valence band is dependent upon the fullness of said band.⁹ For a band that is partially filled, the *Fermi level* lies near the middle of the band and electrons close to said level can be promoted to nearby empty levels. As such, the electrons are mobile and free to move through the solid thereby becoming a *metallic conductor*. For *insulators* and *semiconductors*, the *Fermi level* lies within the band gap, and conductivity is therefore dependent upon the required energy for electrons to move between the *valence* and *conduction* bands. Moreover, the differences between *metals*, *semiconductors* and *insulators* depend upon three main characteristics; the band structure of each solid, the fullness of the valence bands and the magnitude of the energy gap between full and empty bands. A simplified band structure diagram can be seen in *Figure 2.3*.

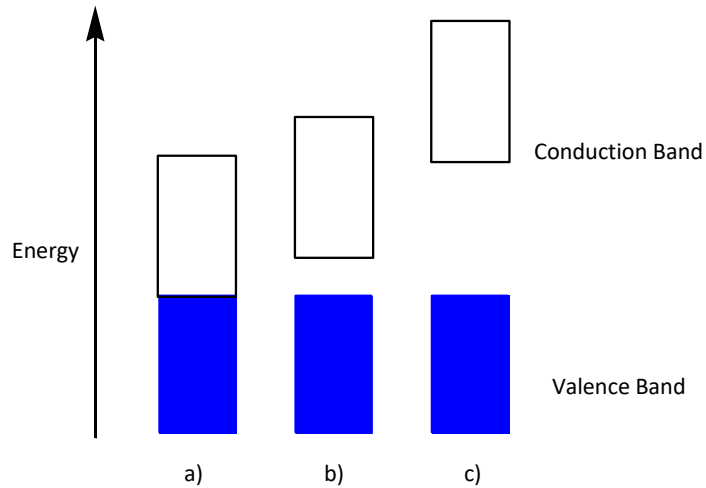


Figure 2.3 - A simplified band-structure diagram of a) a metallic conductor, b) a semiconductor and c) an insulator. For clarity, the blue colour depicts a 'filled' band.

2.1.3 Insulators

Materials regarded as *insulators* are those in which the flow of localised electrons is restricted due to the *valence* band being full.¹⁰ The energy gap between the *valence* and *conduction* bands is considerable and often termed a 'forbidden gap'. Due to the size of the band gap, electrons are not able to make the 'jump' from the occupied band to the unoccupied band at room temperature. Diamond is considered an excellent example of an *insulator*, with a band gap of *ca.* 6 eV. Very few electrons have sufficient thermal energy to reach the conduction band and therefore the conductivity is negligible. The origin of this band gap is down to the covalent bonding between the individual carbon atoms within its structure and their stereochemical arrangement; each atom is bonded in a tetrahedral manner to four other carbon atoms.⁹ It is noted that when the conductivity of an insulating solid can be measured, it is found to increase as temperature increases. In these cases, it is possible to regard all solids as either *semiconductors* or *metallic conductors*.^{8,11}

2.1.4 Semiconductors

As a general definition, a *semiconducting* material is one in which its conductivity increases with an increase in applied temperature. The band structure of *semiconducting* materials is similar to that of *insulating* materials except the size of the band gap is considerably smaller, in the range 0.5 – 3.0 eV. Due to this observed decrease in band gap, valence electrons are able to move more freely between the *valence* and *conduction* bands and thus, markedly better conduction is observed than that relating to those considered *insulators*. Materials of this type include transition metal compounds (with the exception of metallic ones) and silicon.

Semiconductors can be sub-divided into two categories, intrinsic and extrinsic. In intrinsic conductors, the solid is regarded as pure and the band gap is so small that application of thermal energy promotes some electrons from the *valence* band to the *conduction* band, introducing positive 'holes' in the absence of said electrons from the lower bands. Conduction occurs as a result of both the holes and electrons acting as charge carriers within the solid. Conversely, the conductivity of extrinsic semiconductors is attributed to the presence of intentional impurities within the solid. Doping is used to either increase or decrease the number of electron carriers *via* use of atoms with more or less valence electrons. This sub-category of *semiconductors* can be further distinguished into two additional categories, *n-type* and *p-type*. Simply put, *n-type* conductors are those which have negative charge carriers (electrons) in the lower bands by doping of impurities with more valence electrons, and *p-type* conductors are those which have positive charge carriers (holes) in the lower bands by doping of impurities with less valence electrons.¹¹ The ability to dope *semiconductors* gives rise to many applications and is the basis of the microelectronics industry.

2.1.5 Metallic conductors

A *metallic conductor* is defined as a material with an electrical conductivity that decreases as temperature increases. As discussed previously, the band structure of a metal has no gap between the *conduction* and *valence* bands owing to the partial filling of said *valence* band. Being the highest occupied band, the *Fermi level* therefore lies within the *valence* band rather than between the two bands and electrons can be easily promoted to nearby empty orbitals. Metals have delocalised electrons which allows for near-free movement within the crystal structure of the material and gives rise to markedly higher conductivity than *semiconductors*. The key difference between the two types of conductors is their opposing relationships between conductivity and temperature, *Figure 2.4*. Despite the presence of delocalised electrons improving conductivity at lower temperatures when compared to *semiconductors*, the amplitude of vibrational energy of *metallic* atoms increases as temperature is increased, resulting in greater collisions between atoms and electrons, and therefore increasing resistance.

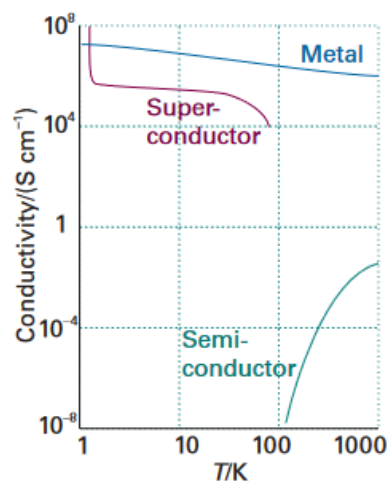


Figure 2.4 - Variation of electrical conductivity as a function of varying temperature for solids classified as a metallic conductor, a semiconductor and a superconductor.¹¹

Although typical examples of *metallic conductors* include metals and alloys, the property can also be observed in organic metals and polymers. Synthesis of such materials has allowed the fabrication of thin films with high conductivity usually reserved for pure metals. Conducting organic materials can be considered in two forms, those exhibiting conjugated systems, and those expressed as charge-transfer complexes.¹²

2.2 Conductivity in Organic Materials

Organic solids are widely considered as *insulators* owing to the restricted movement of electrons both within individual molecules and between molecules. Any electrical conduction observed within these materials, often as a result of loosely bound ions, was long-viewed as undesirable.¹³ Despite examples being synthesised over a century before,¹⁴ breakthrough interest in these materials did not occur until the 1970's, when Heeger, MacDiarmid and Shirakawa discovered and developed Nobel Prize-worthy electronically conductive polymers.^{15–17} These polymers belong to the aforementioned conjugated category of organic conductors.

2.2.1 Conducting Polymers: Conjugated Systems

This new class of conducting polymers rely on conjugation to achieve their expression of electrical activity. Polyethylene for example, is an *insulator* as a result of the saturated single carbon-carbon bonds throughout its skeletal structure. However, polyacetylene was discovered to be conducting owing to its alternating double and single carbon-carbon bonds which allow movement of electrons through the conjugated π -system. Despite only showing modest conductivity in relation to pure Si *semiconductors*, research gained traction when Heeger *et al.*

introduced the idea of doping said materials with suitable inorganic compounds. Upon introduction of electron accepting and donating dopants, these conductive polymers display a markedly increased conductivity comparable to many metals, launching the new field of interest.¹⁸

2.2.2 Charge-Transfer Complexes

Organic complexes with two components whereby one component is a π -electron donor and the other a π -electron acceptor are known as charge-transfer (CT) salts; one notes that these salts are also referred to as charge-transfer complexes and radical-cation salts, but for ease of understanding and consistency, one will refer to all salts simply as *charge-transfer salts*. Some of these materials behave as highly conducting organic metals, the most interesting of which are those where the donors and acceptors form separate and alternating stacks within the crystal structure. In this case, donor stacks transfer charge to the acceptor stacks to yield a partially filled π -electron band and therefore delocalisation across the entire structure.¹² Examples of well-investigated π -electron donors include *p*-phenylenediamine (TMPD), tetrathiafulvalene (TTF) and bis(ethylenedithio)tetrathiafulvalene (BEDT-TTF), *Figure 2.5*. TTF is of interested due to its highly symmetric structure, as well as high polarisability from the presence of the sulphur atoms, thus lowering any destabilising electron repulsions from neighbouring π -electron acceptor sites when compared to nitrogen-containing heterocyclic counterparts.^{19,20}

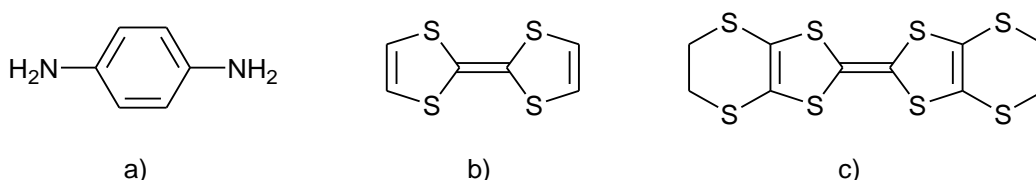


Figure 2.5 – Electron donating molecules; a) p-phenylenediamine (TMPD), b) tetrathiafulvalene (TTF) and c) bis(ethylenedithio)tetrathiafulvalene (BEDT-TTF).

Conversely, examples of good π -electron acceptors include tetracyanoquinodimethane (TCNQ) and chloranil, *Figure 2.6*. Much interest was initially based upon the semiconducting character of *p*-phenylenediamine/chloranil complexes until *Melby et al.* reported a variety of new conducting organic compounds using TCNQ as the acceptor in 1962.^{21,22} Since then, TCNQ has been one of the most widely studied and highly regarded acceptors to date owing to its planar, conjugated system with strongly electron withdrawing CN groups.^{12,22–26}

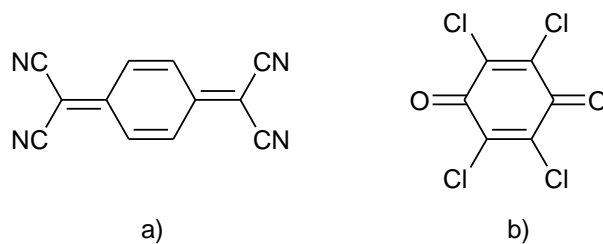


Figure 2.6 - Electron accepting molecules; a) tetracyanoquinodimethane (TCNQ) and b) chloranil.

It would be within a decade of research into these new TCNQ systems that the first organic metal was discovered by *Ferraris et al.* in 1973.²⁷ This complex was a 1:1 charge-transfer salt of TTF/TCNQ, where TTF is the donor and TCNQ is the acceptor. Not only did this new salt express metallic character from room temperature down to 54 K, it also demonstrated the largest maximum electrical conductivity of any known organic compound up until this point. It became clear that for high conductivity along the donor/acceptor stacks, the donors and acceptors must form unique, separate stacks, and electron transfer between said stacks must be partial to achieve the desired partially occupied π -electron systems. Mixing of stacks allows for localised electron transfer as opposed to the desired delocalisation for long-range conductivity.¹² The next dramatic advancement in the search for highly conducting organic solids came with the discovery of a *superconducting* charge-transfer salt of $(\text{TMTSF})_2\text{PF}_6$ in 1980 by *Bechgaard et al.* (TMTSF = tetramethyltetraselenafulvalene).²⁸

2.3 A Brief History of Superconductors

Three years after liquefying helium for the first time in 1908,²⁹ Kamerlingh-Onnes discovered the first expression of *superconductivity* in metallic mercury.^{30,31} Here, he observed that the electrical resistance of pure mercury disappeared rather abruptly below a critical temperature (T_c) of 4.2 K, *Figure 2.7*. This historic discovery paved the way for scientists across the globe to study this exciting new type of conduction, and is still one of the most hotly researched areas in the race to find a near-room temperature T_c *superconductor*.

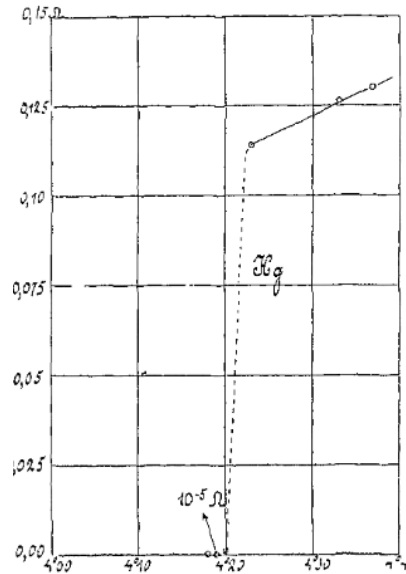


Figure 2.7 - Kamerlingh-Onnes' original plot of resistance (ohms, Ω) against absolute temperature (K) marking the discovery of superconductivity in mercury at 4.2K.³⁰

Materials possessing this property have the ability to conduct large electrical currents with zero resistance indefinitely, as well as displaying perfect diamagnetism. Like all electronically conducting materials, *superconductivity* is reliant upon temperature, as graphically demonstrated earlier in Figure 2.4. At a temperature coined the *critical temperature* (T_c), the material in question undergoes a phase transition from the state of normal resistance to a *superconducting* state. Here, electrons are able to flow indefinitely with zero resistance and therefore, zero loss of energy. Bardeen, Cooper and Schrieffer proposed a quantum theory to model the origin of this zero-resistance arising in materials of these types.³² However, the first major advancement in understanding *superconductivity* occurred when Walther Meissner and Robert Ochsenfeld put forward a theory for the second distinct *superconducting* property of perfect diamagnetism, known as the Meissner effect, in 1933.³³

2.3.1 The Meissner Effect

Simply defined, the Meissner effect is an observed expulsion of an applied magnetic field upon activation of the *superconducting* state of a material. When the bulk material is cooled down in the presence of a weak magnetic field through to the T_c , an ejection of said field is observed once the sample enters the *superconducting* state, Figure 2.8. This observation of flux expulsion and exclusion when cooled through T_c implied that *superconductivity* can be destroyed by increasing the applied magnetic field above a critical value, H_c . The general theory of electromagnetism governed by Maxwell's equations did not sufficiently account for the expulsive behaviour of *superconducting* materials; the most they could account for is with

regard to perfect conduction (zero resistance), in that the magnetic field cannot vary with time.^{34,35} This however, does not apply to a perfect diamagnet since the field is expelled *via* the Meissner effect.

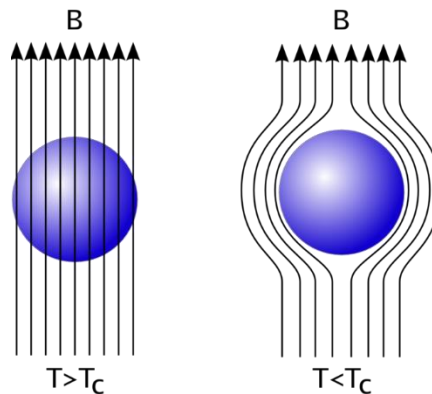


Figure 2.8 - Visual representation of the Meissner effect when a superconducting sample is cooled below T_c , where B is the applied magnetic field.

The fundamental difference between a perfect conductor and a *superconductor* can be seen in Figure 2.9; when a perfect conductor is exposed to a magnetic field and cooled below T_c , if the magnetic field is then turned off, the originally applied field becomes ‘trapped’ within the sample to oppose any changes. In a *superconducting* sample, the Meissner effect is observed under the same conditions until the field is turned off, whereby the field vanishes entirely (i.e. is not trapped). The magnetic state therefore is dependent upon its history for a perfect conductor, but not for a *superconductor*.³⁶

	$B^0 \neq 0$ $T > T_c$	$B^0 \neq 0$ $T < T_c$	$B^0 = 0$ $T < T_c$
normal/perfect conductor transition		(a)	(b)
normal/superconductor transition		(c)	(d)

Figure 2.9 - Comparison of the magnetic behaviour of a perfect conductor and a superconductor cooled under an applied magnetic field (B^0), before the field is turned off (a and c) and after the field is removed (b and d).³⁶

Modifications of Maxwell's equations were put forward by F. and H. London in 1935, with the aim to satisfy these new electrodynamic properties exhibited by *superconducting* samples.³⁷ Gorter and Casimir introduced a 'two-fluid' model to account for the electrons involved in the *superconducting* state; at $T = 0$ K, all free electrons can be considered as *superconducting*, but at non-zero temperatures, not all appear to be involved.³⁸ Thus, the model denotes that the free electrons with density n are equal to the sum of superconducting electrons of density n_s and normal electrons of density n_n . The phenomenological thermodynamic theory proffered by London and London is based upon this two-fluid model, following the logic that if electrons within *superconductors* do not encounter resistance, they will continue to accelerate in an applied electric field. The theory describes the relationship between the current in a *superconducting* material and the electromagnetic fields within and around it, and the second equation specifically yields the perfect diamagnetism, and therefore predicting the Meissner effect. The London duo proposed the fundamental *London penetration depth*, λ_L , as a means to explain the observed exponential suppression of the magnetic field inside the material. The derived equations revealed that despite the complete expulsion upon reaching and below T_c , to a small extent it is possible for the magnetic field to penetrate the surface of said sample up until the aforementioned London depth, with typical values ranging between 50 and 500 nm.

London theory is limited by its vectoral locality and assumption that n_s (and therefore n_n) remains constant; this is not the case when considering a material being cooled below T_c in a non-zero applied field. Despite providing an explanation for both properties of *superconductors*, one must take the super-electron density along with their effective charge and mass into account. In 1950, Ginzburg and Landau arose to account for these parameters by introducing the *coherence length*, ξ , which is a measure of the distance within which the super-electron concentration cannot drastically change in a magnetic field, expressed as a wave function.³⁹ From this, they proposed the *Ginzburg-Landau parameter*, κ , which is the roughly temperature-independent dimensionless ratio of λ_L to ξ , and remains a very important parameter for the behaviour of superconductors in an applied magnetic field. It is important to mention that numerical values for the *penetration depth* that aligned with experimental values were not realised until Pippard generalised London's equations to include non-local effects, which lead to a renormalisation of the *London penetration depth*, referred to simply as *penetration depth*, λ .⁴⁰ For typical metallic *superconductors*, λ is much smaller than ξ , thus the ratio (κ) is less than 1. The value of κ is used to distinguish between two classes of

superconductor, Type I and Type II (section 2.3.3). For a type I *superconductor*, κ is less than $1/\sqrt{2}$ and for type II, κ is greater than $1/\sqrt{2}$; therefore, *ca.* 0.707 is the dividing line between the two types.

2.3.2 BCS Theory: Cooper Pairs

In the same year the above theories were proposed, Emmanuel Maxwell studied the effect of isotopes of mercury (Hg) upon *superconductivity*; here, it was concluded that the transition temperature (T_c) varied depending upon the average atomic mass of the sample.⁴¹ Samples of Hg¹⁹⁸ were cooled alongside pure Hg to their transitional temperatures and he concluded that the point of activation of the *superconducting* state is indeed a function of the nuclear mass. This was confirmed in the same year by Serin and Reynolds, who performed similar isotopic experiments using Hg¹⁹⁹, Hg²⁰² and Hg²⁰⁴, observing that lighter isotopes have higher transition temperatures than their heavier counterparts.^{42,43} Since this discovery and subsequent work by Fröhlich,⁴⁴ it became clear that *superconductivity* arises from the interaction between electrons and lattice vibrations (phonons), but difficulty in formulating a route for which this interaction occurs led to *Bardeen et al.* proposing the Bardeen-Cooper-Schrieffer (BCS) microscopic theory.³²

Work published by Cooper in 1956 presented the idea that even a weak attraction can bind a pair of electrons within a *superconductor*.⁴⁵ Here, he postulated that the *Fermi-sea* of electrons is unstable against the attractive formation of at least one bound pair, no matter how weak the interaction may be. The phenomenon is odd, since electrons would not usually interact as a result of repulsive Coulombic forces. The filled *Fermi-sea* is the ground-state, and the electrons occupying it are non-interacting. An excitation can occur from the *Fermi level* to just above said level, forming a *BCS ground state* where *superconductivity* is activated and hereby forming an energy gap between said ground states. The BCS ground state contains mixtures of one-electron orbitals from above the *Fermi energy*, and appears to have a higher energy than the *Fermi-state*, but the attractive potential energy of the BCS state outweighs the kinetic energy and acts to lower the total energy of said state with respect to the *Fermi state*. Known as Cooper pairs, the theory submits that an electron of positive momentum and spin up, $+K\uparrow$, and an electron of equal but opposite momentum and spin, $-K\downarrow$, are coupled by a weak attraction at $T = 0$ (i.e. no thermal energy) and as a bound pair, are of lower energy than as a separated pair in the presence of the *Fermi-sea*. This occurs *via* electron-phonon interactions; an electron moving within a material leaves a

net positive charge in its vicinity as a result of the Coulombic attraction between the electron and positive ions within the lattice (phonons), and causes a localised structure distortion. It is thereby favourable for a second electron to join the first as a result of this rich positive charge, causing a virtual attraction between the two electrons and indirectly forming a Cooper pair. This pair undergoes less scattering than their unpaired counterparts since the distortion caused by one electron attracts the second back towards its path, should either electron undergo a scattering collision with the lattice. This resistance to scattering allows said electrons to carry charge freely through the solid, hence giving rise to *superconductivity*.

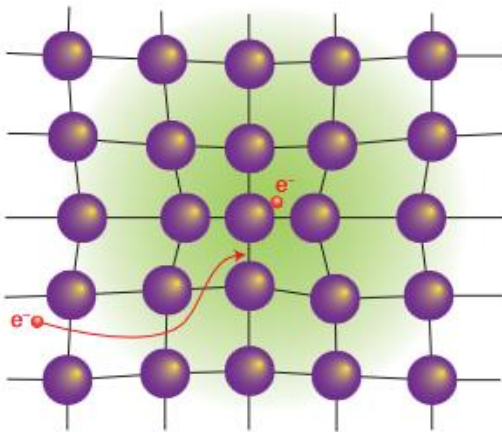


Figure 2.10 - The formation of a Cooper pair; one electron distorts the lattice attracting a second electron, forming a lower energy pair as a result of this electron-lattice interaction.¹¹

Bardeen, Cooper and Schrieffer extended Cooper's theory to bulk systems, proposing that at the critical temperature (T_c) these loosely-associated Cooper pairs don't just exist as single pairs, rather, that all the pairs of electrons within the system act as one large electron-pair superfluid. This aforementioned BCS state has incredibly low energy and is reliant on the co-dependence of all Cooper pairs within the solid, such that if one pair was to interact with the lattice, all pairs would undergo said interaction, and, at such low temperatures required to activate said superfluid, there is not enough energy for this collective interaction to occur. Therefore, as long as the temperature remains below the T_c for the *superconducting* material in question, the paired electrons will carry charge indefinitely with zero resistance. BCS theory proposed a wavefunction by which mathematical quantification for which the energy required to separate the Cooper pairs into their individual electrons could be measured experimentally. Here, the criterion for the transition temperature was proposed to involve the electron density of orbitals of one spin at the *Fermi level* and the electron-lattice interaction. In doing so, a paradoxical observation was made; the higher the resistivity at room temperature (and therefore the higher the electron-lattice interaction), the more likely

the material will be *superconducting* when cooled. The previously proposed *penetration depth* and *coherence length* emerge as natural consequences of this theory, since both are dependent upon the electron mean free path (l) measured in the normal state, moreover positively reinforcing the theory of the Meissner effect.

2.3.3 Type I and Type II Superconductors

Superconductivity can be destroyed by one of three important limiting parameters that exist within a material; the aforementioned critical temperature, T_c , the critical field, H_c , and the critical current, J_c .^{46,47} All three are interlinked, in that at the T_c , the critical field is very small but increases as temperature decreases. The value of the critical temperature impacts the application for materials that rely on zero resistance properties, whereas the critical field determines whether or not a *superconductor* can withstand an applied magnetic field. The critical current parameter impacts the application of such materials in power transmission, whereby high currents are applied to *superconducting* wires or devices.

In 1956, the same year that BCS theory was proposed, Alexei Abrikosov published very significant work based upon the theories previously put forward by Ginzburg and Landau (G-L).⁴⁸ The G-L parameter, κ , which one recalls as the ratio between the *penetration depth* λ and *coherence length* ξ ; $\kappa = \lambda / \xi$, was the most important basis of this work. For a pure *superconductor*, the parameter has a value much less than 1, whereby λ and ξ have values of *ca.* 500 Å and *ca.* 3000 Å respectively; in the case of mercury, $\kappa = 0.16$.^{48,49} Abrikosov investigated the consequence to G-L theory if κ was large rather than small, in other words $\xi < \lambda$, rather than the classically observed reverse scenario. At this point, all calculations performed by Ginzburg and Landau were done with up until a critical value of $\kappa = 1/\sqrt{2}$. By solving the Ginzburg-Landau equations, he showed that the κ parameter essentially determines the surface tension between the normal and *superconducting* states in an applied magnetic field. The classic scenario results in a positive surface tension, whereas the proposal by Abrikosov would result in a negative surface tension, which had previously been considered as completely unphysical. Since this is radically different from the earlier described *superconducting* materials, he proposed a simple definition for each type; a type I *superconductor* has $\kappa < 1/\sqrt{2}$ and type II has $\kappa > 1/\sqrt{2}$; thus, *ca.* 0.707 is the dividing line between the two types.

Abrikosov then became curious as to the properties of bulk type II *superconductors* and since the surface energy of these materials was negative, it became apparent that the phase transition

from the normal state to the *superconducting* state in a magnetic field was of second order. Type I materials observe first order transitions, whereby at the critical field value, H_c , the phase change is uniformly instantaneous and *superconductivity* is immediately lost. Conversely, the second order phase change displays an initial critical point, H_{c1} , at which the properties of *superconductivity* decrease in an orderly fashion up until a second critical point, H_{c2} , by which the phase change occurs. As a result of this second order phase transition, a *mixed state* emerges, where the external magnetic field gradually penetrates the material, *Figure 2.11*. In this mixed state, the formation of so-called *vortices* was observed, where the magnetic field is concentrated around particular points within the material surrounded by a circular current, coined the *quantum vortex*, ϕ .⁵⁰

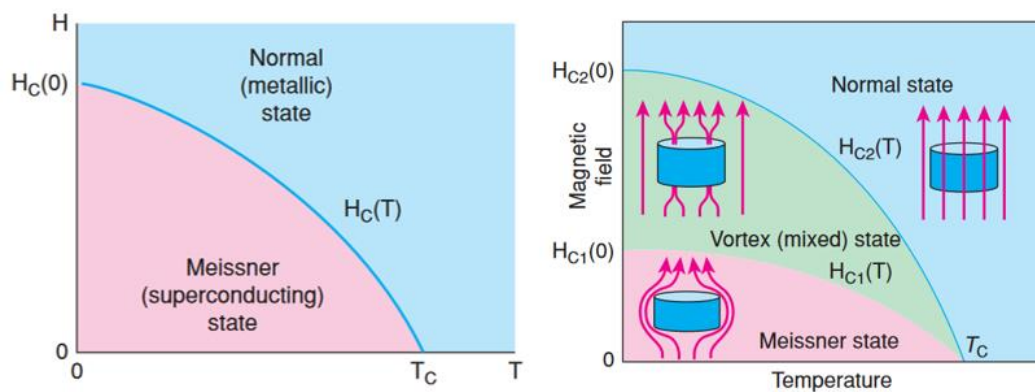


Figure 2.11 - A magnetic field (H) vs temperature (T) diagram for a type I superconductor (left) and a type II superconductor (right), allowing visual representation between the two different phase transitions.¹²

The quantum vortex is described to have an order parameter, $|\psi|$, with a value that increases from zero to a maximum in absence of a magnetic field at the *coherence length* ξ . As per the parameters of the Meissner effect, the magnetic field decreases exponentially from its maximum to zero at the *penetration depth*, λ . The field where the vortices first appear is H_{c1} , and increasing this value increases the number of vortices present to form a regular lattice. One notes that an important difference between the two types of *superconductors* is that a type II undergoes a differing Meissner effect than that of its type I counterpart. Abrikosov commented that instead of travelling smoothly through the material, the flux appears in regular arrays of flux tubes, taking the appearance of triangular or quadratic arrays, *Figure 2.12*.⁵⁰ It would be later confirmed and visualised in 1967 by Essmann and Träuble that the vortices indeed form the lower-energy triangular lattice structure, as opposed to the miscalculated quadratic structure.⁵¹

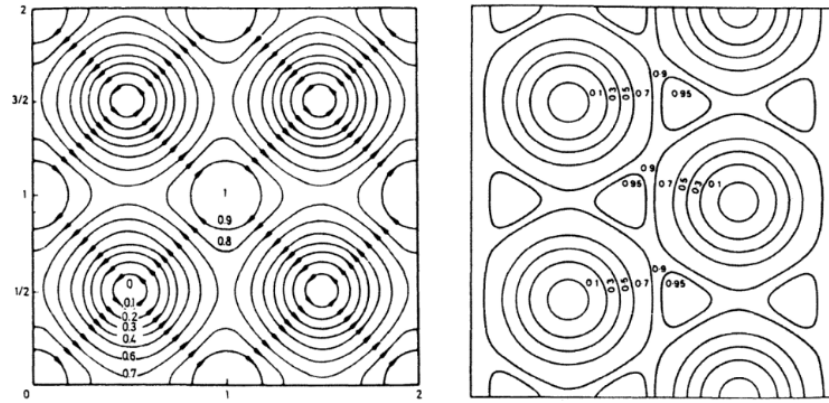


Figure 2.12 – Simultaneous lines of fields and currents in a vortex lattice in the vicinity of H_{c2} , giving rise to quadratic arrays of vortices (left) and triangular arrays of vortices (right).⁵⁰

It should be noted that the presence of two critical magnetic fields in *superconducting* alloys was first reported as early as 1935 by Haas and Casimir-Jonker,⁵² which was then confirmed by Rjabinin & Shubnikov,⁵³ and then by Mendelssohn & Moore.⁵⁴ The first definitive investigations into type II superconductors was by *Shubnikov et al.* in 1937, the experimental data of which provided Abrikosov a thorough and compelling comparison for his theory.⁵⁵ These vortex lattices allow a *levitation* effect to be observed, whereby under the *mixed state* of a type II *superconductor*, the material may be seen to be suspended above or below a magnet by means of trapped lines of flux, *Figure 2.13*. This flux pinning effect appears to centre itself around defects in the crystal or where impurities arise.

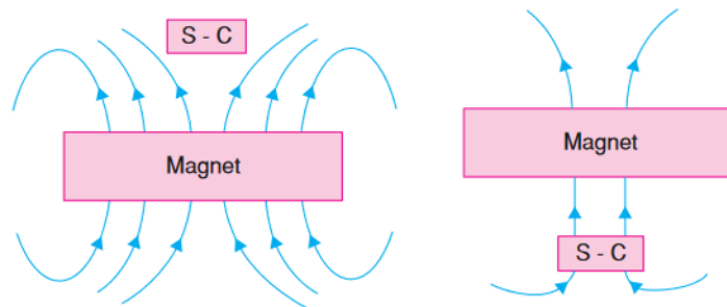


Figure 2.13 - Vortex pinning giving rise to levitation of a superconductor above a magnet (left) and suspension of a superconductor below a magnetic (right) as a result of these flux lines.¹²

In 1959, Gor'kov published a remarkable paper which would confirm that, in following the BCS *superconductivity* theory put forward by *Bardeen et al.*, close to the T_c , the behaviour of a pure superconductor in a magnetic field is indeed described by the equations of Ginzburg-Landau's phenomenological equations.^{56,57} This gave rise to the Ginzburg-Landau-Abrikosov-Gor'kov (GLAG) theory which would allow one to explain the properties of all sorts of *superconductors* from first principles. However, this theory did not garner much attention nor appreciation until

Kunzler et al. studied the Nb_3Sn type II *superconductor*, whereby very high critical fields, H_c , in combination with high critical currents, J_c , were observed.⁵⁸ Further study into these materials allowed the observation that as well as having differing Meissner states, these secondary types of *superconductor* hold differing Cooper pairing; type I materials have pairs with opposing spins and momentum such that their net spin and momentum is zero, known as *s-wave singlet superconductors*. An applied magnetic field can easily decouple the electron pairs so that the spins align with the field and *superconductivity* is lost. In type II counterparts, the Cooper pairs have parallel spins such that a *triplet state* forms that cannot so easily be decoupled on application of an external field. This appears to be the mechanism for which these materials are stable in higher currents and fields without losing their *superconductivity*, the discovery of which would kickstart the era of large-scale applications of *superconductivity*.¹²

2.3.4 The Josephson Effect

Prior to Josephson's 1962 discovery of electron-pair tunnelling, a young scientist named Ivar Giaever was studying tunnelling effects of thin metal films of lead separated by insulating layers of aluminium oxide.⁵⁹ The insulator normally acts as a barrier to the flow of conduction from one metal to the other. Provided that the barrier is sufficiently thin, in this case less than 20 Å, there is a significant probability that an electron may pass from one metal to the other, hence the electrons may undergo a *tunnelling effect*.⁶⁰ When using normal conductors, the current is directly proportional to the voltage, such that a linear relationship is observed. Giaever postulated that the probability of tunnelling between *superconducting* materials was directly proportional to the aforementioned density of states within the *superconductor*, and that the effect should give rise to a negative resistance characteristic. He very quickly proved his own theory to be experimentally correct and when one of the metals becomes *superconducting*, the current-voltage relationship observed is no longer linear, but appears as a curve.

Not long after these experiments, Josephson predicted that Cooper pairs of electrons should be able to tunnel between two *superconductors* under suitable conditions. In these experiments, two *superconductors* separated by a thin insulating barrier were prepared and a DC *supercurrent* was observed up until a critical current, J_c . Once this value is reached and exceeded, a new voltage develops across the junction, and an AC current is observed. As a result, two types of Josephson junctions arise; when the current is below that of the critical current, the observed voltage is zero and a DC Josephson effect is observed, whereas above this critical value, the voltage oscillates over time, giving rise to the AC Josephson effect.^{61–63} The presence

of magnetic fields near these junctions influences the observed Josephson effect, allowing this phenomenon to be used in the measurement of weak magnetic fields. Josephson derived equations to calculate this new effect using those postulated by Ginzburg and Landau in terms of phase differences, with regard to the relationship between the potential difference across the junction and the wave functions of the Cooper pairs in each individual *superconductor*. To this day, Josephson junction technology represents the basis of promising *superconducting* electronics.

2.4 High Temperature Superconductivity

After Onnes' initial discovery of *superconductivity* in mercury in 1911, he went on to observe the same effect in samples of tin and lead.⁶⁴ Most metallic elements have since been found to be *superconducting* at very low temperatures, having critical temperatures of the order of a few Kelvins; amongst these, niobium has the highest elemental T_c of 9.5 K. There is yet to be a definitive reason as to which metals become *superconductors* and which do not, though it has been noted that it is important to eliminate even trace quantities of foreign paramagnetic elements from metallic *superconductors* with ultra-low transition temperatures, because they can lower the transition temperature more severely. A number of materials have been known to *superconduct* only under high pressure, such as Si which undergoes the transition at 165 kbar and T_c of 8.3 K. Much of the interest in these materials throughout the sixties and seventies has focused on transition metal alloys and intermetallic compounds, such as the aforementioned Nb_3Sn type II *superconductor*, as a result of the very high critical fields and currents observed.⁵⁸ A wide range of alloys have been found to *superconduct*, the highest T_c of which belongs to Nb_3Ge at 23.2 K.⁶⁵ Materials of this type have since been developed technologically and implemented as *superconducting* magnets in devices such a magnetic resonance imaging (MRI).

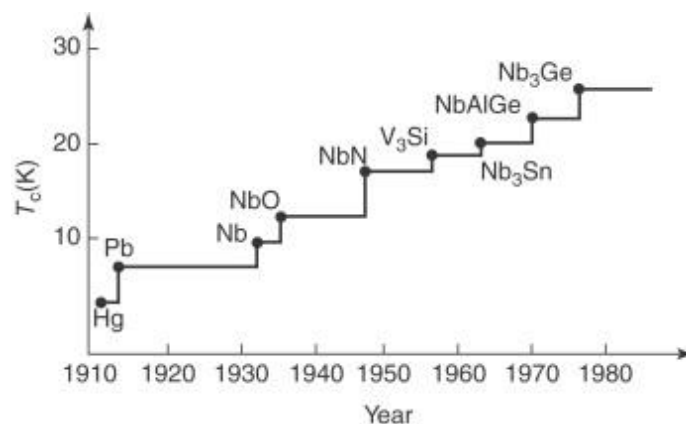


Figure 2.14 - Discovery of low temperature elemental and intermetallic superconductors from 1911 until 1980.⁶⁶

A significant and exciting breakthrough in 1986 marked the beginning of the *high temperature superconductor* era and reignited interest in materials of these types for scientists across the globe. Bednorz and Müller synthesised the first *superconductor* in this high temperature category with a T_c of *ca.* 30 K in the form of a $\text{La}_{2-x}\text{Ba}_x\text{CuO}_{4-\delta}$ cuprate oxide.⁶⁷ After some initial scepticism surrounding this discovery, further ceramic cuprates were synthesised within a year, not only confirming the existence of these new types of *superconductors*, but further improving upon the critical temperatures observed. In 1987, *Bednorz et al.* synthesised a cuprate oxide substituted with strontium with a T_c of *ca.* 36 K, as well as those with barium and calcium with slightly lower T_c 's.⁶⁸ In the same year, joint research groups lead by Wu and Chu synthesised the first ceramic *superconductor* to break the liquid nitrogen threshold of 77 K, starting a new family of cuprates.⁶⁹ With a T_c of 93 K, $\text{YBa}_2\text{Cu}_3\text{O}_7$ was an important discovery as it was the first time a *superconductor* had been observed using liquid nitrogen rather than liquid helium, and provided much hope towards technological advances since these ceramics are relatively easy to fabricate into wires and tapes. To date, the highest T_c observed in the YBCO family is the $\text{Y}_3\text{Ba}_5\text{Cu}_8\text{O}_{18-\delta}$ compound, at 105 K.⁷⁰ Extensions to the general ceramic cuprate group include bismuth- and thallium-calcium-cuprate oxides (BBCO and TBCO families), each having higher still T_c 's of 110 K and 125 K respectively.^{71,72}

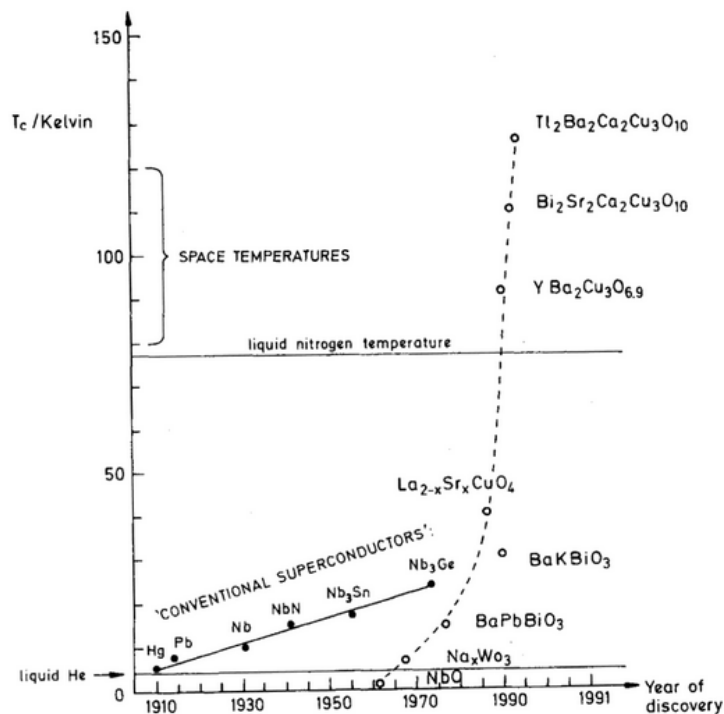


Figure 2.15 - Evolution of superconducting critical temperatures, with the high temperature era stating from the 1980's.⁷³

Since the eighties, a number of cuprate families have been discovered and expanded, the most recent of which is a mercury-based ceramic, $\text{HgBa}_2\text{Ca}_2\text{Cu}_3\text{O}_{8+\delta}$, which happens to have the highest observed T_c of 134 K at ambient pressure.⁷⁴ It is interesting to note that those discovered to have the highest critical temperatures are comprised of increasingly unstable and toxic elements, such that they are impractical for wide-scale application. A number of other notable families of *superconductors* have been studied, including that of the hydride family, though one notes that these only exhibit this property at very high pressures above 150 GPa. In order of increasing critical temperature, these include H_3S at 203 K,⁷⁵ LaH_{10} at 250 K, and YH_{10} at 320 K.⁷⁶ This family too has its limitations in industrial applications owing to the impracticality of the conditions to which they undergo the transition into the *superconducting* state. Other notable materials include alkali metal fullerenes (C_{60}) and MgB_2 ; the former are 3D *superconductors* in contrast to the 2D cuprates,⁷⁷ and the latter shows a strong isotope effect which in turn shows the importance of lattice vibrations, consistent with BCS theory.⁷⁸

The physical mechanism for which these high-temperature-type materials are able to *superconduct* is still very much unclear. BCS theory covers the low temperature counterparts very well and thorough peer-review has solidified the microscopic theory for these materials, with no perceived upper limit for values of T_c . Although it is clear a two-electron Cooper-style pairing is involved in these higher temperature materials, the nature of the pairing remains relatively controversial; type I superconductors are known to have *s-wave* pairings, whereas theories surrounding *p-* and *d-wave* pairings have been hypothesised for these type II materials.⁴⁹ In order to elucidate the true mechanisms at play, research continues to search for more high-temperature-ambient-pressure *superconductors* in the hopes of one day achieving a room temperature (and ambient pressure) *superconductor*. Though there is still much to discover, organic-type materials offer an alternative route towards this, having much fewer toxicity and instability issues than materials studied thus far.

2.5 Organic Superconductivity

Superconductivity arising from organic systems is a novel and exciting area of materials research. Prior to the discovery of organic polymeric conductors in the 1970's,¹⁵⁻¹⁷ the general consensus was that these materials have insulating properties and were therefore deemed uninteresting.¹³ The field of molecular conductors based upon charge-transfer systems began when *Ferraris et al.* discovered the first organic metal in 1972, a 1:1 charge-transfer salt of TTF/TCNQ, with TTF

as the donor and TCNQ as the acceptor.²⁷ The most interesting result of this discovery was that it demonstrated the largest maximum electrical conductivity of any known organic compound up until this point in time. This led research into salts with unique donor-acceptor *stack* motifs, observing that high conductivity along the donor/acceptor stacks arises from the separation of said stacks, as well as partial electron transfer between them to achieve the desired partially occupied π -electron systems. Mixing of stacks allows for localised electron transfer as opposed to the desired delocalisation for long-range conductivity.¹²

As mentioned previously, the next dramatic advancement in the search for highly conducting organic solids came with the discovery of a *superconducting* charge-transfer salt of $(\text{TMTSF})_2\text{PF}_6$ in 1980 by *Bechgaard et al.* (TMTSF = tetramethyltetraselenafulvalene).²⁸ This was the first observation of a *quasi*-one-dimensional organic *superconductor*, with a critical temperature of 1.2 K at 9 kbar pressure. Like TCNQ, TMTSF is planar and forms stacks along which the electrons are most conducting as a result of the orbital overlap between said stacks, with PF_6^- anions forming unique stacks either side, *Figure 2.16*. Two molecules of TMTSF donate one electron to the PF_6^- anion, forming a charge-transfer salt. The orbitals of the TMTSF valence electrons overlap along the stack, giving rise to anisotropic conductivity parallel to the stacks vs other directions.

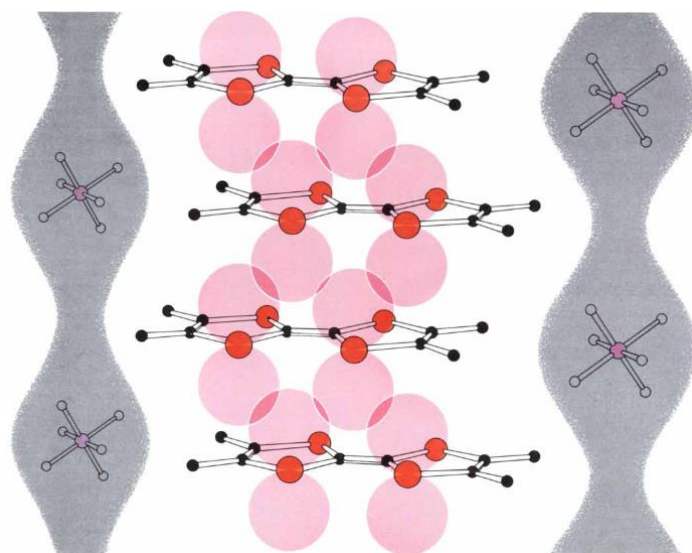


Figure 2.16 - Crystalline lattice structure of $(\text{TMTSF})_2\text{PF}_6$, where P atoms are pink, C atoms are black, F atoms are white and Se atoms are orange. Regions of negative charge lie along the vertical stacks of PF_6^- (grey shading), and regions of positive charge lie along the vertical stacks of TMTSF (pink shading).⁷⁹

A small family of these salts have since been synthesised, including $(\text{TMTSF})_2\text{ReO}_4$ and $(\text{TMTSF})_2\text{ClO}_4$, with T_c 's of 1.4 K and 1.2 K respectively.⁸⁰ It should be noted however, that the ClO_4 salt is the only material in this family to *superconduct* at ambient pressure; the ReO_4 salt

requires a pressure of 9.5 kbar for the property to be observed.⁷³ Interest towards these materials diminished when it became apparent that this family is relatively limited; owing to both their *quasi*-1D nature as well as pressure-dependent conductivity and observed low-temperature metal-insulator transitions as a result of low dimensionality, attempts to extend the number of *superconductors* within the family were subsequently unsuccessful after the initial establishment of said family. The appeal of TTF-based conductors was renewed when the second generation of organic *superconductors* were discovered, being those of the BEDT-TTF family (BEDT-TTF = bis(ethylenedithio)tetrathiafulvalene).

2.5.1 BEDT-TTF-based Materials

The aforementioned tetrathiafulvalene (TTF) and its derivatives have been studied extensively over the last fifty years owing to their unique π -electron donor properties. Synonymous with the development of molecular organic metals mentioned above, as well as recent developments within supramolecular chemistry, they were originally developed for the synthesis of materials expressing electrical conduction properties and have thus been instrumental in the vast expansion of the research area. This expansion led to *Mizuno et al.* synthesising a BEDT-TTF salt in 1978 as part of their research into TTF derivatives.²⁶ Here, they yielded a 1:1 BEDT-TTF/TCNQ charge-transfer salt which displayed no sufficiently interesting electroconducting properties in comparison to the original 1:1 TTF/TCNQ salt. However, it was noted that the π -electron donation ability of BEDT-TTF is smaller than TTF, which leads to smaller charge-transfer with TCNQ, and therefore decreases the band occupancy.

The molecular structure of BEDT-TTF as opposed to TTF is characterised by the presence of additional sulphur-containing rings as well as terminal ethylene groups which lie out of the plane of the rest of the molecule. These terminal groups afford some steric hinderance for face-to-face intermolecular π -interactions, which leads to the reduction in observed conductivity compared to TTF. Alternatively, the S-atoms show a strong tendency to form multiple S...S intermolecular contacts along the side-to-side direction, increasing the electronic dimensionality within the salts, which in turn supresses the Peierls distortion observed in the aforementioned TMTSF material which causes the metal-insulator transition at low temperatures.

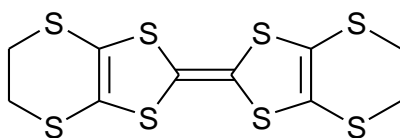


Figure 2.17 - Structure of BEDT-TTF (bis(ethylenedithio)tetrathiafulvalene).

Due to the lack of interesting electrical properties of the BEDT-TTF/TCNQ salt, interest divulged into other TTF derivatives until 1982, when *Saito et al.* synthesised a $(\text{BEDT-TTF})_2\text{ClO}_4(1,1,2\text{-trichloroethane})_{0.5}$ salt. This new BEDT-TTF charge transfer salt marked the first observation of an organic sulphur donor complex to retain its metallic conductivity down to 1.4 K and, in contrast to the *quasi*-1D TMTSF salts, demonstrated *quasi*-2D metallic conductivity.⁸¹

The first *superconducting* BEDT-TTF salt was discovered by *Parkin et al.* in the form of $(\text{BEDT-TTF})_4(\text{ReO}_4)_2$ with a critical temperature of 2 K at *ca.* 4-6 kbar.⁸² Unlike the perchlorate salt, this material shows more similarity in structure and electrical properties to the *quasi*-1D TMTSF family of *superconductors*, since it exhibits the familiar metal-insulator transition which is suppressed under pressure to allow the transition into the *superconducting* state.⁸³ The discovery of the *quasi*-two-dimensional metal (perchlorate salt) along with the finding of a *superconducting* BEDT-TTF salt (perrhenate salt) stimulated the subsequent research into continuing the formulation of this new family. Many *superconducting* BEDT-TTF salts have since been synthesised, one of which contained linear anions of iodine, giving rise to the $(\text{BEDT-TTF})_2\text{I}_3$ family. These 2:1 salts were found to hold a number of different polymorphic phases, including α - (alpha), β - (beta), δ - (delta), κ - (kappa) and θ - (theta). *Yagubskii et al.* performed the synthesis of the first $(\text{BEDT-TTF})_2\text{I}_3$ salt in 1984 holding the β -phase; this β - $(\text{BEDT-TTF})_2\text{I}_3$ salt was observed to undergo a *superconducting* transition at ambient pressure with a T_c of *ca.* 1.4 K.⁸⁴ This salt proved interesting as a result of a pressure study; it was found that the β -phase can exist in two *superconducting* states, one at low temperature ambient pressure, β_L ($T_c = \text{ca. } 1.4 \text{ K}$), and one at high temperature under applied pressure, β_H ($T_c = \text{ca. } 8 \text{ K}$).^{85,86} In the same year, *Bender et al.* discovered the α -phase, α - $(\text{BEDT-TTF})_2\text{I}_3$, which is metallic down to 135 K, at which it exhibits a metal-insulator transition.⁸⁷ The final two polymorphous phases of κ - $(\text{BEDT-TTF})_2\text{I}_3$ and θ - $(\text{BEDT-TTF})_2\text{I}_3$ both undergo an ambient pressure *superconducting* transition at *ca.* 3.6 K, completing this polymorphic family of BEDT-TTF charge-transfer salts.^{88,89} Further studies using linear iodide-based anions have led to the synthesis of IBr_2^- and AuI_2^- salts, with T_c 's of 2.7 K and 4.2 K respectively.^{90,91}

Subsequent work in the search for high temperature *superconductors* has included those with transition metal-containing acceptors. This led to the publishing of breakthrough research by *Urayama et al.*, who synthesised the first stable organic *superconductor* with a critical temperature above 10 K; κ -(BEDT-TTF)₂Cu(SCN)₂.⁹² Compared to the I₃ counterparts, it was observed that the increased length of the Cu(SCN)₂⁻ anion leads to an increase in T_c , being 10.4 K at ambient pressure for this new salt. It was also noted that the use of asymmetric anions has a tendency to destroy *superconductivity*, resulting in *insulating* and *semiconducting* phases. *Urayama et al.* therefore postulated that salts exploiting longer linear anions would be a natural next step, leading *Aravinda et al.* to synthesise κ -(BEDT-TTF)₂Cu[N(CN)₂]Br, which currently holds the record for the highest observed T_c among the organic *superconductors* obtained at ambient pressure so far, at 11.6 K.⁹³

Following the successful syntheses of BEDT-TTF salts with their ever-improving critical temperatures at ambient pressure, *Takehiko Mori* undertook a series of three studies into the structural genealogy of the polymorphic BEDT-TTF salts to provide a systematic nomenclature for identifying the individual phases of α -, β -, δ -, κ - and θ -.⁹⁴⁻⁹⁶ Here, he noted two essential building blocks when analysing the crystal structures of these materials; *ring-over-bond* (RB) and *ring-over-atom* (RA) overlap modes between two BEDT-TTF molecules, *Figure 2.18*. As well as this, dislocations were noted as a result of anion packing and steric hinderance arising from the donor molecules which also contribute to the resulting phase observed. The *ring-over-bond* overlap mode is a 90° interaction better known as the face-to-face stacking, which leads to closest S-S contacts within the BEDT-TTF stacks and optimal overlap for conduction. Conversely, the *ring-over-atom* overlap mode is a 60° interaction, labelled *pseudo stacking* as a result of its unfamiliar stacking motif compared to conventional 1D conductors.

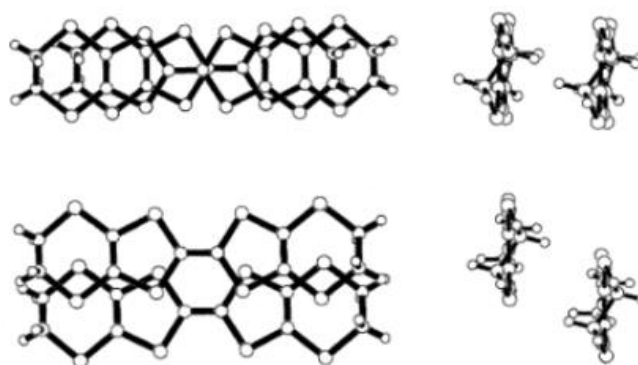


*Figure 2.18 - Ring-over-bond (RB) stacking motif, top, and ring-over-atom (RA) stacking motif, bottom. Overlap modes viewed from two planes; left is perpendicular to the molecular plane and right is along the long axis.*⁹⁴

In terms of the genealogy of these stacking motifs, *Mori* proposed that the β -phase arises from one-directional repeating modes of the *ring-over-bond* (RB) type, such that the usual *face-to-face* stack arises. When the *ring-over-atom* (RA) mode is repeated and *pseudo*-stacks form constructed from directionally inclined BEDT-TTF molecules, such that when the inclination is the same (parallel), the β'' -phase arises. A third β -phase is observed, named the β' -phase, arising from alternating parallel RA and RB stacking modes. *Figure 2.19* provides visual clarity for the aforementioned β -type phases.

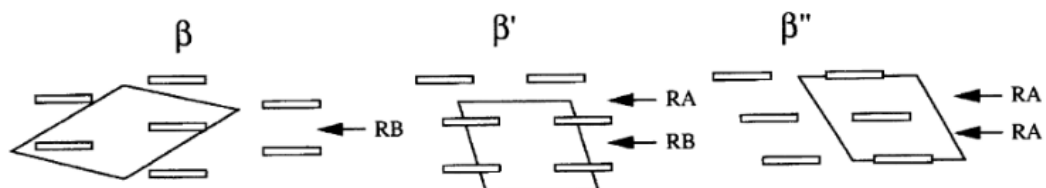


*Figure 2.19 - B-type phases arising from RA and RB stacking motifs.*⁹⁴

Within the RA overlapping mode, there are three further observed phases, α -, α'' - and θ -. The θ -phase arises similarly to the β'' -phase, with the exception of oppositely alternating inclinations in separate stacks. A helpful analogy to discern the two types is to assign the inclined stacks as upward (+) and downward (-), whereby the β'' -phase is comprised of repeating upward stacks (+++...), and the θ -phase is comprised of alternating upward and downward stacks (+-+...). The α -phase is the same as the θ -phase, with weak dimerization along the stack direction causing the phase difference. Finally, the α'' -phase is a hybrid of the θ - and β'' -phases; two discrete chains of parallel-inclined BEDT-TTF appear such that the stacks repeat in a +-+-+ fashion.⁹⁴

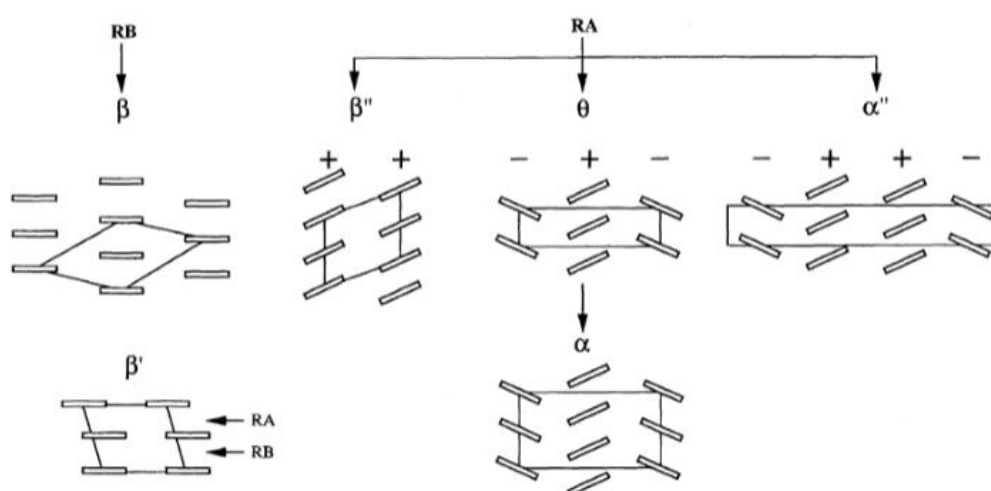


*Figure 2.20 – A visual representation of the α -, β - and θ -type stacking motifs based upon RA and RB overlap and their relevant inclinations; + indicates an upward inclination and – indicates a downward inclination of the BEDT-TTF molecules.*⁹⁴

Mori goes on to describe the δ -, δ' - and α' -phases, which display an interesting *twisting* motif whereby the BEDT-TTF long axes are no longer parallel, but the molecular planes are.⁹⁶ The δ -, δ' -types are discerned by the type of overlapping present alongside the twisting motifs, be it RA or RB; those with RA are denoted δ -, and those with RB are denoted δ' , both having parallel layers in between. The α' -type arises when all overlap modes in the BEDT-TTF stacks are twisted alternately in opposite directions and the parallel layers cease to exist.

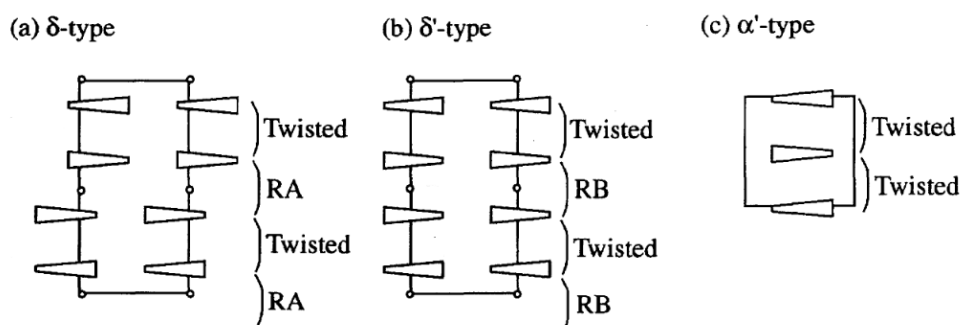


Figure 2.21 - A visual representation of the δ -, δ' - and α' -phases and their relevant twisting and RA/RB overlapping motifs.⁹⁶

Finally, Mori *et al.* categorised the κ -phase, with this stacking motif appearing to be the most unique. This phase is composed *ring-over-bond* dimers located on four *corners* surrounding a central dimer, with the corner dimers having the opposite inclination to the centre one.⁹⁵

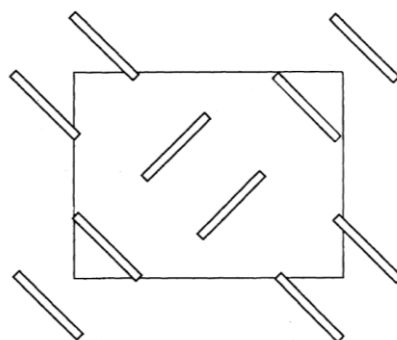


Figure 2.22 - A visual representation of the κ -phase.⁹⁵

Mori *et al.* also noted a general rule based upon the anion used; the β'' -phase appeared to be prevalent when the included anion is small, with a volume $<100 \text{ \AA}^3$. Conversely, when the anion is larger (*i.e.* $>100 \text{ \AA}^3$), the α -, β -, κ - and θ - phases arise. The anion packing is therefore to be considered as well as the overlapping modes of the donor, since both appear to give rise to the observed dislocations and subsequent arising of multiple phases.⁹⁴

It is clear that the BEDT-TTF family of *superconductors* synthesised thus far provide a strong motivation to continue research in this area in the search for high-temperature-ambient-pressure materials given the wide scope of phases available. *Superconducting, metallic, semiconducting* and *insulating* materials of this type have been studied thus far, with small structural changes being directly correlated to the changing physical properties and phases observed.^{94,97} A large range of acceptor molecules/anions can be used to potentially tailor the properties of the charge-transfer salts synthesised, combining multiple properties within the same materials. In the use of metal trisoxalate-based anions and metal halides, one may study the influence upon conduction with the magnetic properties induced by variation of the identity of the central metal ion.⁹⁸ Further to this, metal trisoxalate and spiroborate complexes, as well as alterations to the BEDT-TTF donor itself may be used to introduce the property of chirality within the (*super*)conducting system, a combination which is not seen in nature.^{5,99} Synthesis of multifunctional materials that combine conductivity with chirality is an area of major interest to global researchers as a result of the ever-tantalising possibility of generating novel physical properties, like that of electrical magneto-chiral anisotropy (eMChA) discovered by *Rikken et al.* in 2002.¹⁰⁰

2.5.2 Chiral Molecular Conductors

Chirality naturally manifests itself in nature, where materials hold two conformations, much like human hands hold a left and right conformation, such that they are non-superimposable mirror images of one another. Structurally, they are identical and have the same physical and chemical properties; a common example of this is thalidomide, whereby the *R*-enantiomer gives rise to sedative effects whereas the *S*-enantiomer is responsible for immunomodulatory effects, *Figure 2.23*.

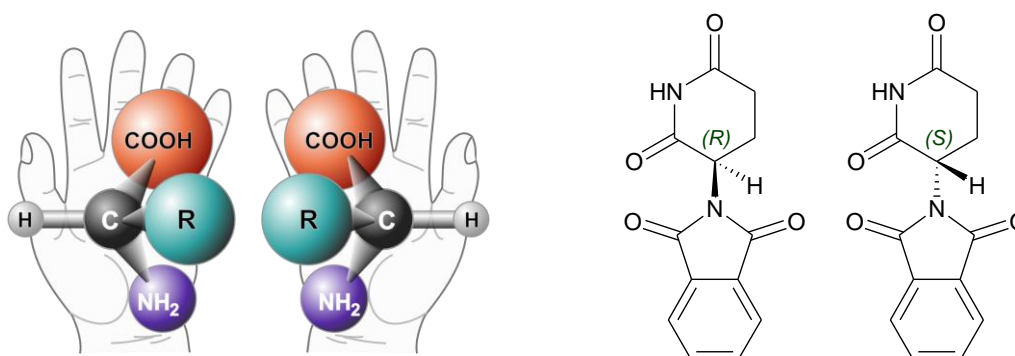


Figure 2.23 - a) Visual illustration of chirality with its left and right-handed nature, and b) R-(+)- & S-(-)-Thalidomide. The single enantiomers and the racemic form may differ in their dosages, efficacies, side effect profiles, or indicated use.

Chirality is largely based upon a centre of rotation, which give rise to a number of observed forms of the property, the most prominent of which being around a stereogenic centre. Rotation can follow in a R/ Δ (clockwise) or S/ Λ (anticlockwise) manner around a central atom, usually carbon. As well as being a molecular property, chirality can be found in the crystallisation modes of materials such that the separate molecules may stack in a helical manner, clockwise or anti-clockwise. For example, two enantiomers may crystallise in opposite modes, giving rise not only to enantiomeric molecules but also enantiomorphic crystal structures. This structural property has been observed to produce an optical activity of materials containing chiral building blocks; in the case of chiral magnets, a new property known as magneto-chiral dichroism occurs as a result of the interplay between the two properties.¹⁰¹ In the case of chiral conductors, differences in conducting properties in a magnetic field have been observed; this effect is known as electrical magnetochiral anisotropy (eMChA).¹⁰⁰ The origin of eMChA remains relatively unknown owing to a lack of chiral conducting materials available for study and as a result, the quantitative theory behind this property in bulk materials is yet to be discovered. This effect has been observed in single-walled carbon nanotubes,¹⁰⁰ bismuth helices,¹⁰² bulk organic conductors,¹⁰³ chiral magnets,¹⁰⁴ and *superconducting* nanotubes.¹⁰⁵

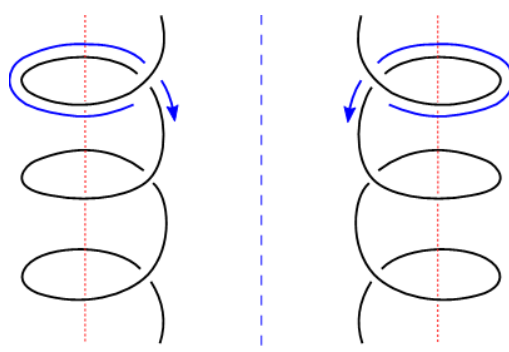


Figure 2.24 - A simple diagram to demonstrate eMChA and how chirality can affect the direction of electrical transport. In simple terms, the 'left-handed' material may direct the electrical current in a clockwise fashion, whereas the 'right-handed' material directs it in an anti-clockwise fashion.

The first experimental evidence for the effect of chirality upon electrical conductivity was reported in 2014 by Pop *et al.*, where a bulk chiral molecular conductor based on an enantiopure tetrathiafulvalene (TTF) derivative was synthesised; $(\text{DM-EDT-TTF})_2\text{ClO}_4$, where DM-EDT-TTF = dimethyl-ethylenedithio tetrathiafulvalene.¹⁰³ Single crystals of both the (S,S) and (R,R) donors were used to make perchlorate salts yielding both (S,S)- and (R,R)- $(\text{DM-EDT-TTF})_2\text{ClO}_4$. Pop noted that the resultant salts crystallised in enantiomorphic hexagonal space groups of $P6_222$ in the case of (S,S)-salt and $P6_422$ in the case of the (R,R)-salt; this represented the first

enantiomeric pair of charge-transfer salts crystallising in enantiomorphic space groups. Here, the magnetic field and current dependencies of each salt were observed to be of equal magnitude but opposite in sign, and both showed metallic behavior down to 40 K. Though not *superconducting*, this research allowed the unique observation of the eMChA effect in the case of bulk metallic chiral conductors, and provides a solid foundation for the continuation into charge-transfer salts comprised of TTF-based derivatives. The study of eMChA is an extremely intriguing and of utmost importance, since the degeneracy between electrons associated with $+k$ and $-k$ wave vectors is broken under magnetic field because of the electrical magnetochiral anisotropy; *i.e.* bringing into question the essential components of Cooper pairs and therefore the basis of BCS theory.¹⁰⁶ Moreover, this produces an interesting apparent paradox between the mechanisms at play in the (high temperature) *superconducting* state, such that an adjusted theory may need to be proposed to account for this loss of degeneracy, should a chiral *superconducting* charge-transfer salt be synthesised and eMChA is simultaneously observed.

2.6 Combining Magnetism, Chirality and Superconductivity

The first occurrence of chirality and superconductivity in the same material was reported in 2017 within a nanotube of tungsten disulphide.¹⁰⁵ In this material, the forward and backward flow of electric current was inequivalent in the presence of an applied magnetic field. The origin of this antisymmetric observation is unknown and has never been studied in terms of the interplay between chirality and superconductivity, and therefore provides the basis of this research. Combination of the properties of (*super*)conductivity with chirality in the same lattice can be achieved using both organic and organic-inorganic hybrid materials, opening the door for the study of chiral molecular metals, as well as the potential to synthesise the first ever chiral molecular superconductor. Crystal engineering of materials of this type allows for a multitude of new property combinations to be studied, examples of those synthesised thus far include ferromagnetic conductors,¹⁰⁷ paramagnetic superconductors,¹⁰⁸ antiferromagnetic semiconductors,¹⁰⁹ and metallic proton conductors.¹¹⁰

Three routes by which chirality can be introduced into charge-transfer salts are currently being studied; using a chiral donor, use of chiral anions or by the use of a chiral solvent. Although the first chiral TTF-based donor TMET was synthesised in 1986,¹¹¹ only recently has an increasing interest in the introduction of chiral information in TTF derivatives been observed, mainly motivated by the potential to study the eMChA effect. Since then, a range of enantiopure donors have been reported, including hydroxyalkyl-BEDT-TTF derivatives,¹¹²

oxazoline-TTF derivatives,¹¹³ pyrrolo-TTF derivatives,¹¹⁴ and TTF-sulphoxides containing chiral sulphur atoms,¹¹⁵ as well as several simple TTF derivatives with chiral side chains.¹¹⁶ A chiral molecular conductor of (1'*R*,5*S*)-*N*-(1'-phenylethyl)(BEDT-TTF)acetamide with TCNQ was reported very recently, which remains metallic down to 4.2 K and exhibits room-temperature switching capabilities with a transition to an insulating state above 10 °C.²

Many chiral and racemic anions have been used thus far to synthesise an extensive family of *insulating, semiconducting, metallic and superconducting* charge-transfer salts with BEDT-TTF, including Fe(chloranilate)₃,¹¹⁷ Fe(croconate)₃,¹¹⁸ Cr(oxalate)₂(2,2'-bipyridine),¹¹⁹ Sb₂(2*R*,3*R*)-(+)-Tartrate)₂,¹²⁰ TRISPHAT,¹²¹ and B(malate)₂.⁷ The use of metal trisoxalate anions in BEDT-TTF salts offers the potential to synthesise chiral conductors, since these anions are themselves chiral and crystallise in Λ (lambda) or Δ (delta) forms; a number of chiral semiconductors have already been synthesised *via* chiral induction by using the chiral solvents (*R*)-(-)-carvone,^{122–126} and (*S*)-*sec*-phenethyl alcohol.¹²⁷ As well as this, novel packing arrangements of Δ - and Λ - metal trisoxalate enantiomers have been observed in racemic salts. Further to this, enantiopure and racemic charge-transfer salts of BEDT-TTF with spiroborate anions have very recently been reported for the first time.⁶

2.7 Aims of this Body of Work

Since the origin of high temperature superconductivity and the ideal conditions required for a material to enter this state are not yet fully understood, this project aims to aid in providing theoretical information to allow explanation of this strange phenomenon. In this, materials will be synthesised which possess both (*super*)*conducting* properties, as well as chirality and magnetism; a combination that is not observed in nature, and therefore in doing so, it may be possible to understand the mechanism of superconductivity as well as that of eMChA. Two main types of conducting material will be synthesised during this project; those of hybrid organic-inorganic metal trisoxalate-based types and those of functionalised BEDT-TTF/TCNQ charge-transfer salts. The resistivity measurements for a third type of charge-transfer material, the spiroborate salts, has been included from other students within the research group as a result of the characterisation studies the author performed during this PhD work.

2.7.1 BEDT-TTF-Based Donors with TCNQ

The first objective of this project was to synthesise charge-transfer salts of functionalised BEDT-TTF with TCNQ. Here, the BEDT-TTF donor can be modified *via* addition of chiral side

chains, which gives a total of two chiral centres, using synthetic methods reported by *Wallis et al.*³ These materials are highly sought-after by physicists as they allow the study of electrical conduction within bulk chiral conductors *via* exhibition of eMChA, which may therefore allow theoretical modelling of *superconductivity*. The synthesis of BEDT-TTF allows for easy modification to introduce functionalised side chains, such that *Wallis et al.* successfully synthesised a chiral donor molecule based on BEDT-TTF in 2013, *Figure 2.25*.³ This new donor was later reacted with TCNQ to form a new charge-transfer salt in 2020, θ -((1'*R*,5*S*)-N-(1'-phenylethyl)(BEDT-TTF)acetamide)₄TCNQ; though not superconducting, this salt showed an insulator-to-metal transition at 10 °C, giving potential for applications in molecular switching, as well as remaining a stable chiral metal down to 4.2 K.²

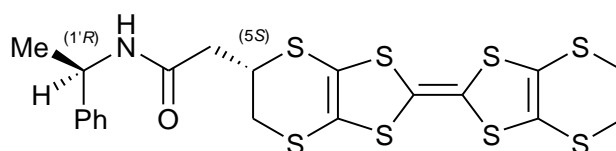


*Figure 2.25 - Novel donor molecule based on BEDT-TTF, synthesised by Wallis et al.*³

Synthesis of new donors of this type began *via* the use of *R*-(+)- α -methylbenzylamine in order to reproduce the salt above (1'*R*, 5*S*), as well as its diastereoisomer (1'*R*, 5*R*), and subsequently using *S*-(+)- α -methylbenzylamine to produce (1'*S*, 5*R*), as well as its diastereoisomer (1'*S*, 5*S*). These novel materials will allow the first study of the effect of chirality upon conductivity between chiral enantiomers and diastereomers. Further functionalisation of this donor is possible which is likely to give a large family of materials for a study of the aforementioned dual-properties and to formulate a model of eMChA. This can be done using derivatives of the above amine, such that the methyl group may be substituted for ethyl, or an additional group may be present on the phenyl ring. Atom-at-a-time changes to the donor will allow study of changes in the crystal structure of the CT salt, as well as differences in conduction and any new properties arising as a result. Several new donors have been synthesised during this work, which will form the basis of future work in the synthesis of charge-transfer salts with TCNQ and other suitable anions. These can then be used to study the relative effects of chirality upon conductivity when suitable crystals are yielded.

2.7.2 BEDT-TTF salts with Metal Trisoxalate Anions

Conducting charge-transfer salts of BEDT-TTF with metal trisoxalates were first synthesised by Peter Day *et al.* in 1995.¹⁰⁸ These materials are composed of alternating layers of conducting organic BEDT-TTF and insulating inorganic metal trisoxalate enantiomers, which are chiral and can have two conformations, Δ (D) or Λ (L). The spatial arrangement of these opposing enantiomers influences the packing arrangement of the conducting layers of BEDT-TTF, which in turn determines the conducting behaviour. Synthesis of materials of this type allows the opportunity for one to combine chirality, conductivity and magnetism within the same lattice.¹²⁸ The oxalate layers form a hexagonal network of 2D sheets between the BEDT-TTF donors, and chirality can be introduced through the inclusion of a guest solvent, which sits in the hexagonal cavity of the trisoxalate layer, *Figure 2.26*. As a result, salts of the form β'' -(BEDT-TTF)₄[(H₃O)M(C₂O₄)₃].guest have been reported, which display superconducting properties as a result of close contacts between the BEDT-TTF donors.¹²⁹ By employing ammonium iron trisoxalate with various guest molecules, the idea is to increase the *b* axis length of the cavity to >19.96 Å, a value which was suggested to be the ideal length for overlap of the donor orbitals for superconductivity in 2019.¹³⁰ Use of benzonitrile or nitrobenzene as the guest has produced materials with the longest *b* axis length and the highest *superconducting* temperatures. The second objective of this project was to synthesise materials of this type, employing slightly larger guests with similar structures to benzonitrile to increase the *b* axis and the superconducting temperature, *T_c*. One also reports some salts arising from employment of non-magnetic metal oxalates, focussing on the interplay between chirality and conductivity as an initial point of interest.

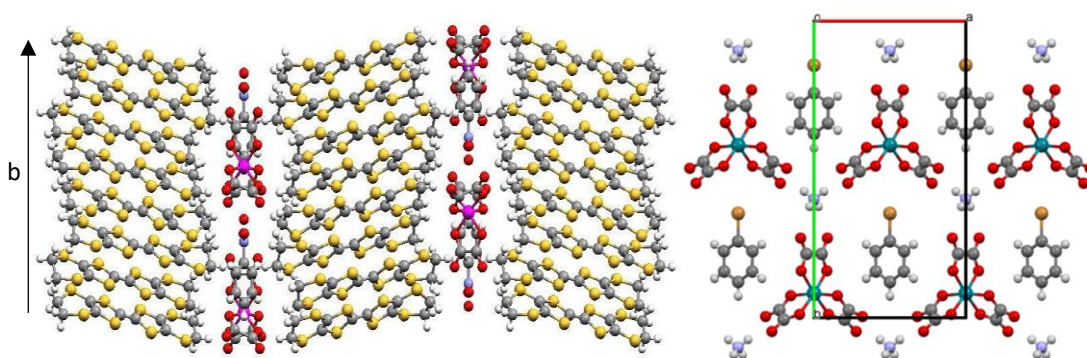


*Figure 2.26 - a) 4:1 β'' -(BEDT-TTF)₄[(H₃O)Fe(C₂O₄)₃].PhBr with alternating layers of BEDT-TTF donors and metal trisoxalate, and b) the hexagonal cavity arising in these 4:1 salts, with bromobenzene as a cavity guest.*¹²⁹

2.7.3 BEDT-TTF salts with Spiroborate Anions

Although the most widely reported family of chiral anions with BEDT-TTF salts is that of the metal trisoxalate family, spiroborate anions have recently been postulated as a promising novel route in the search for a larger pool of chiral conducting materials that allow for study of the interplay between multiple properties within one material and more specifically, eMChA. The employment of bis-chelated spiroborate anions in BEDT-TTF charge-transfer salts yields complexes with multiple stereogenic centres. The chirality of the bidentate chelated ligand is retained but diastereomers are produced through two possible stereochemical configurations at the boron centre. Dependent upon whether one employs enantiopure or racemic bidentate ligands, one may synthesise up to six diastereomers. In the case of the former with enantiopure bidentate ligands with S chirality, a pair of diastereomeric anions result; B_SSS and B_RSS. In the latter case, when using racemic bidentate ligands, four further diastereomers are obtained: B_SRR & B_RRR, and B_SRS & B_RRS. Owing to the high lability of chiral boron centres, and therefore likely racemisation, reliance upon suitable ligand-based chirality is necessary when synthesising these materials.

Martin et al. reported the first examples of charge-transfer salts of BEDT-TTF with chiral borate anions of malic acid, [B(malate)₂]⁻, in 2016.⁷ Using enantiopure *R*-(-)-malic acid, two spiroborate anions, B_SRR and B_RRR, were synthesised before electrochemical crystallisation with BEDT-TTF. This yielded a charge-transfer salt for which only the B_SRR anion was incorporated into the structure. When using a mixture of the six possible diastereomeric spiroborate anions prepared from racemic malic acid, a racemic salt was obtained, but only two of the six diastereomeric anions were present in the crystal; B_SRS and B_RRS. Since the first example was reported, *Martin et al.* have continued this new avenue of research and multiple BEDT-TTF salts with spiroborate anions have materialised.⁶ Alongside, a spiroborate salt with an alternative donor, BDH-TTP, has also been demonstrated.⁵ A number of novel salts synthesised by other members within the authors research group were taken to Japan for characterisation during the authors awarded JSPS fellowship in 2022; these measurements are reported in the final chapter.

3. BEDT-TTF-Based Donors with TCNQ

3.1 Introduction

After the observation of the first charge-transfer salt of TTF-TCNQ in 1973, interest in organic salts was initiated.²⁷ Not only did this new salt express metallic character from room temperature down to 54 K, it also demonstrated the largest maximum electrical conductivity of any known organic compound up until this point. Early examples of these materials had a tendency to undergo Peierls distortion, such that a metal-insulator transition occurs at low temperatures as a result of low dimensionality. Increasing material dimensionality postulated a means to which one may avoid this distortion. One method with which to achieve this, was by increasing the number of sulphur-sulphur interactions within the stacks of donor molecules. BEDT-TTF-based salts gained traction in this way, since the donor holds more sulphur atoms than TTF, and these atoms show a strong tendency to form multiple S...S intermolecular contacts along the side-to-side direction, increasing the electronic dimensionality within the salts, which in turn suppresses the Peierls distortion observed.

Mizuno et al. synthesised a BEDT-TTF salt in 1978 as part of their research into TTF derivatives,²⁶ though it wasn't until *Saito et al.* synthesised the (BEDT-TTF)₂ClO₄(1,1,2-trichloroethane)_{0.5} salt that prompted an increase in research into these new materials. This new BEDT-TTF charge transfer salt marked the first observation of an organic sulphur donor complex to retain its metallic conductivity down to 1.4 K as well as demonstrating *quasi*-2D metallic conductivity.⁸¹ Many *superconducting* BEDT-TTF salts have since been synthesised, including the (BEDT-TTF)₂I₃ family,^{84–89,131} the κ-(BEDT-TTF)-copper systems,^{92,93} and the Peter Day family of metal trisoxalate BEDT-TTF salts.^{97,108,129,132,133}

Chemical modification of the BEDT-TTF motif is one of the most important and exciting directions in the search for new donors to synthesise further charge-transfer salts. A number of publications by *Wallis et al.* detail the synthesis of BEDT-TTF-based donor molecules with hydrogen bonding functionality.³ In doing so, a wide variety of novel donor molecules have been realised, including those containing a number of hydroxyl groups, esters, carboxylic acids, and materials with additional ring systems as well as metal-binding sites.^{3,134–138} Following this, further derivatives have been synthesised including alkyls,^{139,140} as well as incorporation of carboxylic ester and amide functionalities.¹⁴¹

Since the successful synthesis of a BEDT-TTF-derived donor by *Wallis et al.* in 2013,³ and subsequent realisation of an interesting charge-transfer salt with TCNQ in 2020,² focus

of the Martin research group has been to study this family of BEDT-TTF-based motifs and explore the properties of the diastereoisomeric and enantiomeric counterparts. The CT salt synthesised was that of θ -((1'R,5S)-N-(1'-phenylethyl)(BEDT-TTF)acetamide)₄TCNQ; though not *superconducting*, the salt showed an *insulator-to-metal* transition at 10 °C, giving potential for applications in molecular switching, as well as remaining a stable chiral metal down to 4.2 K.

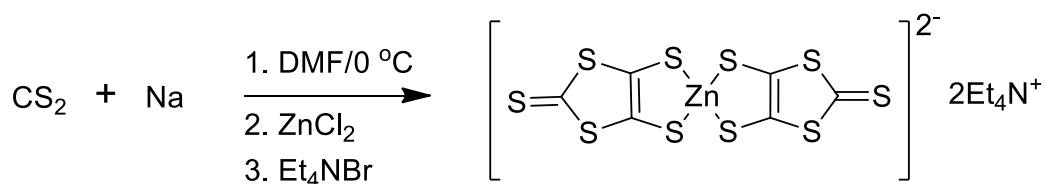
Theta (θ)-type salts are of interest owing to their variation in electronic properties in materials synthesised thus far; (θ -BEDT-TTF₂Cu₂(CN)[N(CN)₂]₂) is an *insulator*,¹⁴² whereas θ -BEDT-TTF₂I₃ is a *superconductor*.¹³¹ During the aforementioned structural genealogy studies performed by *Mori et al.*, it was noted that an interesting and intricate relationship exists between the dihedral angle of a θ -type salt and the bandwidth of the material, such that the latter is regulated by the former, and therefore dictates the conducting properties of said material.¹⁴³ *Mori* observes that as the dihedral angle is decreased, the θ -salts vary from *insulators to metals*, and in some cases, *superconductors* as a result of changing orbital overlap of sulphur atoms.¹⁴³

Since the synthesis of BEDT-TTF allows for easy modification such that one may introduce and make atom-at-a-time changes to functionalised side chains, it is possible to yield charge-transfer salts with varying dihedral angles. This will allow one to study the effect of individual atom changes on the conducting properties of new salts as a result of dihedral angle variations, and observe resultant fluctuations of their transition temperatures. Since the Martin group have yielded a molecular switch, one would be vastly interested in the conduction properties observed of the enantiomeric θ -((1'S,5R)-N-(1'-phenylethyl)(BEDT-TTF)acetamide)₄TCNQ, should one be able to synthesise this counterpart. A family of diastereomeric molecular switching salts may then be synthesised in the hope to observe the effect of changing chirality, and therefore eMChA, alongside (*super*)conductivity. These syntheses follow those proposed by *Wallis et al.*, though one notes a small alteration to the proposed method in the use of T₃P (propyl phosphonic anhydride solution (≥ 50 wt. % in ethyl acetate)) as opposed to the use of ethyl chloroformate.³ Not only does it have markedly lower toxicity and volatility, T₃P has been successfully implemented in large-scale amid synthesis and has since been found to be an efficient activating agent for carboxylic acids, such that it is ideal for the condensation of an acid and amine, like those employed in this research.^{144,145}

3.2 Experimental

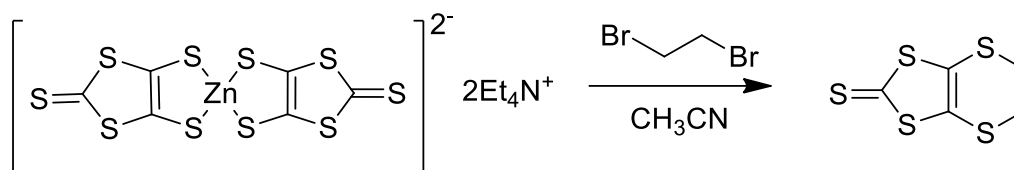
All reagents and solvents were purchased from Alfa Aesar, Fischer Scientific, Fluorochem, Merck or TCI chemicals and used as provided. Chemical manipulations were carried out in oven-dried glassware and in an atmosphere of air unless otherwise stated. Flash column chromatography was performed manually on silica gel (Fluorochem silica gel 60 Å particle size 40-63 µm). Thin layer chromatography was carried out on glass-backed silica gel plates (2.5 x 7.5 cm; Merck, TLC silica gel 60 Å).

3.2.1 Synthesis of Bis(tetraethylammonium)bis(1,3-dithiol-2-thione-4,5-dithiol)zincate



Degassed DMF (480 ml) was added to CS₂ (240 ml, 3.99 mol) and the mixture was cooled to 0 °C under N₂ using an ice-bath. Na metal (14.50 g, 0.63 mol) was cut into fine pieces under cyclohexane and added gradually to the cooled solution. The colourless mixture was stirred for 8 hours until all sodium was consumed. After stirring, MeOH (50 ml) was added to the solution to destroy any undissolved Na. After 30 minutes, separate solutions of ZnCl₂ (21.30 g, 0.16 mol) in 35% NH₃ (360 ml) and H₂O (100 ml), and Et₄NBr (66.00 g, 0.31 mol) in distilled H₂O (500 ml) were added consecutively in roughly equivolume portions over 20 minutes. A red precipitate formed during addition of these solutions and the mixture was stirred at room temperature overnight. The product was isolated *via* filtration under vacuum and washed sequentially with isopropanol (3 x 250 ml) and ether (250 ml). This afforded the product as a bright raspberry red powdered solid (75.03 g, 65 %); m.p. 205 – 207 °C.

3.2.2 Synthesis of 4,5-Ethylenedithio-1,3-dithiole-2-thione

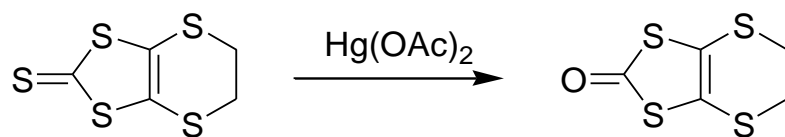


Zinc complex (20.00 g, 27.8 mmol) was dissolved in dry CH_3CN (125 ml), affording an opaque deep raspberry pink solution before 1,2-dibromoethane (5.00 ml, 57.8 mmol) was added with no visible change. The mixture was degassed and refluxed under N_2 for 5 hours, after which the solution was deep orange/brown. The solution was filtered under vacuum and washed with CHCl_3 and CH_3OH , yielding a deep green solid and an opaque red/orange filtrate. The green solid was redissolved in DCM (*ca.* 2000 ml) and decoloured with activated charcoal while heating to boiling with stirring for 20 minutes. After stirring and allowing to cool, the deep forest green solution was filtered again under vacuum to remove the charcoal and undissolved impurity. This afforded a black solid and a translucent orange/yellow solution. The filtrate was collected and the solvent removed *via* rotary evaporation to yield the product as a golden honeycomb crystalline solid (9.34 g, 75 %); m.p. 122-124 °C;

δ_{H} (400 MHz, CDCl_3) 3.40 (4H, s, 5-, 6- CH_2);

δ_{C} (100 MHz, CDCl_3) 208.0 (C=S), 122.9 (3 α -, 7 α -C), 29.7 (5-, 6-C).

3.2.3 Synthesis of 4,5-Ethylenedithio-1,3-dithiole-2-one

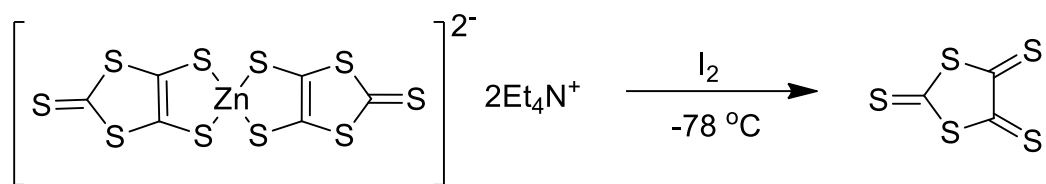


Thione (5.20 g, 23.0 mmol) was dissolved in CHCl₃ (150 ml), affording an opaque deep brown/green solution with undissolved thione. Mercury (II) acetate (10.99 g, 34.5 mmol) was added yielding a milky caramel viscous suspension which was stirred for 1.5 hours at room temperature. After stirring, the mixture was filtered under vacuum, affording a bright orange solution filtrate and pale-yellow solid. The solid was washed with CHCl₃ and the filtrate was transferred into a separating funnel before washing with distilled H₂O (3 x 100 ml). The orange organic layer was dried over MgSO₄ and filtered under gravity before the solvent was removed *via* rotary evaporation to afford the product as a peach crystalline solid (3.78 g, 79 %); m.p. 127-129 °C;

δ_{H} (400 MHz, CDCl₃) 3.42 (4H, s, 5-, 6-CH₂);

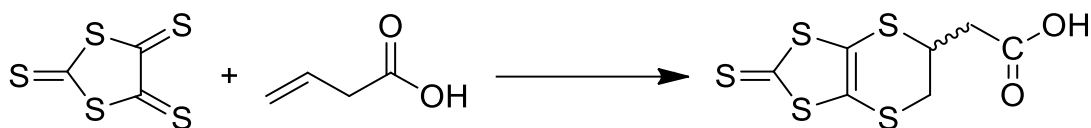
δ_{C} (100.5 MHz, CDCl₃): 189.0 (C=O), 113.4 (3 α -, 7 α -C), 31.1 (5-, 6-C).

3.2.4 Synthesis of 1,3-Dithiolane-2,4,5-trithione



Zinc salt (20.00 g, 27.8 mmol) was dissolved in acetone (140 ml), affording an opaque raspberry pink solution which was cooled to -78°C. A solution of I₂ (14.50 g, 57.1 mmol) in EtOH (150 ml) was prepared before dropwise addition to the zinc solution, yielding an opaque orange paint-like solution which was stirred for 1.5 hours. After leaving to warm to room temperature, an orange precipitate formed within the deep yellow solution. The mixture was filtered under vacuum and washed with acetone (50 ml), distilled H₂O (50 ml), EtOH (50 ml) and Et₂O (50 ml). The solid was left to dry *in vacuo*, yielding the product as a bright orange powder (11.85 g, 109 %). The high yield was likely due to zinc iodide impurities; however, the product was used without further purification.

3.2.5 Synthesis of 2-(2-Thioxo-5,6-dihydro-[1,3]dithiolo[4,5-b][1,4]dithiin-5-yl)acetic acid



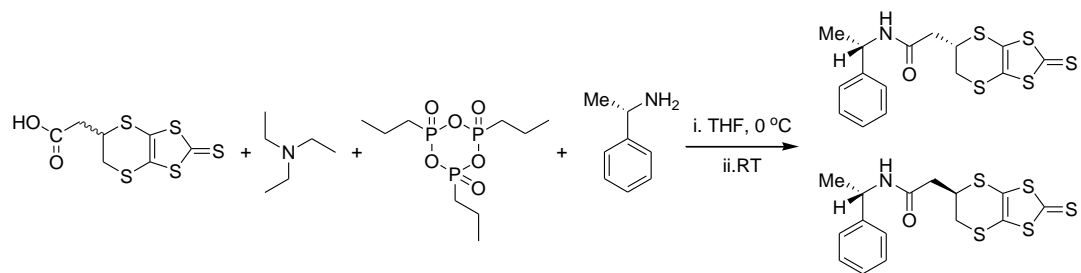
Trithione (5.50 g, 28.0 mmol) was dissolved in toluene (500 ml), affording an opaque bright orange solution. Vinyl acetic acid (4.83 ml, 56.8 mmol) was added with no visible change before the mixture was degassed and refluxed with stirring under N₂ for 5 hours. Once cool, the deep red suspension with visible black solid was filtered under vacuum, resulting in a translucent orange/red filtrate and a black solid. The filtrate was collected and put aside before the solid was stirred in more hot toluene (*ca.* 200 ml) for 1 hour, after which the solution was re-filtered and the resulting filtrate combined with initial filtrate. The solvent was removed *via* rotary evaporation to yield a brown putrid-smelling solid, which was subsequently stirred in cyclohexane (*ca.* 200 ml) for 1 hour as an opaque chocolate-brown suspension. The mixture was filtered under vacuum to yield a bright orange solution and a pale brown solid. The resulting solid was stirred in hexane (*ca.* 200 ml) for 2 hours as a milky-brown suspension, after which it was filtered under vacuum to yield the product as a fine brown powder (4.64 g, 59 %);

δ_{H} (400 MHz, CDCl₃): 4.20 (1H, m, 5-H), 3.40 (2H, m, (C=O)CH₂), 2.90 (1H, dd, J = 17.4, 5.5 Hz, 6-H _{α}), 2.75 (1H, dd, J = 17.2, 8.9 Hz, 6-H _{β});

δ_{C} (100.5 MHz, CDCl₃): *product too insoluble for a clear and representative* ¹³C NMR;

ν_{max} /cm⁻¹: 2914 br (OH), 1697 (C=O), 1483, 1432, 1414, 1396, 1347, 1299, 1253, 1202, 1057 (C=S), 1017, 924, 885, 791, 644, 519, 482, 461.

3.2.6 Synthesis of the *S,S* & *S,R*-Diastereoisomers of *N*-(1'-phenyl-ethyl)-2-thioxo-5,6-dihydro-[1,3]dithiolo[4,5-*b*][1,4]dithiin-5-yl-acetamide



Carboxy-thione (3.32 g, 11.72 mmol) in dry THF (100 ml) afforded a deep red suspension, to which *S*-α-methylbenzylamine (2.37 ml, 18.40 mmol) was added to yield a milky opaque red suspension. Addition of NEt₃ (12.0 ml) yielded a deep red/orange solution in which all solid had dissolved, followed by T₃P (15.0 ml, 50.4 mmol) to yield a deep cherry red mixture which was warm to the touch. The mixture was degassed and stirred under N₂ overnight at room temperature to yield an opaque deep red/brown solution. The solvent was removed *via* rotary evaporation to afford a chocolate brown oil which was subsequently washed with DCM (*ca.* 100 ml) and distilled H₂O (*ca.* 100 ml). The organic layer was dried over MgSO₄ and filtered under gravity to yield a chocolate brown opaque solution. The solvent was again removed *via* rotary evaporation to yield the crude product as an orange/brown viscous oil (3.58 g).

Product purified *via* column chromatography using SiO₂:CHCl₃ to elute the non-product, then SiO₂:CHCl₃/EtOAc 10:1; oil re-dissolved in minimal amount of CHCl₃ and column wet-loaded. After elution of the unreacted chiral amine, two bright yellow fractions were yielded after subsequent solvent evaporation; fraction *first* (*S,S*) and fraction *second* (*S,R*) respectively, in order of elution. *One notes that the first fraction is assumed to be the S,S-diastereoisomer and second is the S,R-diastereoisomer following the order for which those synthesised by Wallis et al. eluted in. This assumption is carried forward throughout this chapter.*³

First (*S,S*) as a golden-yellow crystalline solid (1.29 g, 30 %), m.p. 132-133 °C; R_f (CHCl₃/EtOAc 10:1) 0.29;

δ_{H} (400 MHz, CDCl_3): 7.35-7.25 (5H, m, Ar- H_5), 5.78 (1H, d, $J = 7.6$ Hz, N- H), 5.04 (1H, quin, $J = 7.2$ Hz, N- CH), 4.11-4.16 (1H, m, 5- H), 3.36 (1H, dd, $J = 13.6, 2.8$ Hz, 6- H_{α}), 3.08 (1H, dd, $J = 13.6, 5.2$ Hz, 6- H_{β}), 2.68 (2H, d, $J = 7.2$ Hz, (O=C) CH_2), 1.45 (3H, d, $J = 6.8$ Hz, CH_3);

δ_{C} (100 MHz, CDCl_3): 207.64 (C=S), 167.59 (C=O), 142.66, 128.82, 127.65 & 126.03 (Ar- C_6), 122.39 & 120.79 (3a-,7a- C), 49.35 (N- CH), 41.51 (O=C- CH_2), 38.13 (5- C), 33.85 (6- C), 21.76 (CH_3);

$\nu_{\text{max}}/\text{cm}^{-1}$: 3332 & 3279 (N-H), 2977, 2923, 1646 & 1634 (C=O), 1539, 1531, 1487, 1447, 1417, 1410, 1402, 1367, 1324, 1246, 1228, 1167, 1059, 1038, 1014, 964, 921, 903, 865, 761, 703, 604, 596, 564, 546, 523, 470, 463;

HRMS (ASAP): Found: 385.9823 $[M+1]^+$, $[C_{15}H_{15}NOS_5 + H]^+$ requires: 385.9830;

$[\alpha]_D^{17} = -116$ ($c = 0.45$, CHCl_3).

Second (*S,R*) as a honeycomb-yellow crystalline solid (1.27 g, 29 %), m.p. 158-160 °C; R_f ($\text{CHCl}_3/\text{EtOAc}$ 10:1) 0.18;

δ_{H} (400 MHz, CDCl_3): 7.26-7.36 (5H, m, Ar- H_5), 5.77 (1H, d, $J = 7.6$ Hz, N- H), 5.06 (1H, quin, $J = 7.2$ Hz, N- CH), 4.10-4.16 (1H, m, 5- H), 3.45 (1H, dd, $J = 13.2, 2.8$ Hz, 6- H_{α}), 3.21 (1H, dd, $J = 13.2, 5.2$ Hz, 6- H_{β}), 2.72 (1H, dd, $J = 15.4, 7.0$ Hz, (O=C) CH_{α}), 2.64 (1H, dd, $J = 15.4, 7.0$ Hz, (O=C) CH_{β}), 1.44 (3H, d, $J = 6.8$ Hz, CH_3);

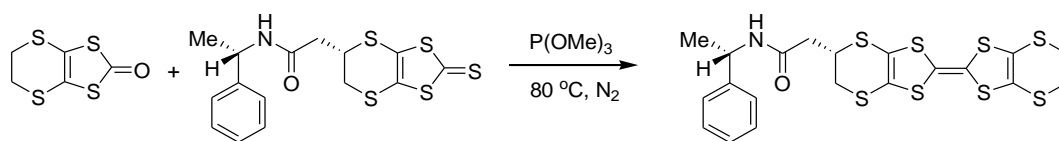
δ_{C} (100 MHz, CDCl_3): 207.61 (C=S), 167.65 (C=O), 142.41, 128.79, 127.66 & 126.10 (Ar- C_6), 122.27 & 120.90 (3a-,7a- C), 49.24 (N- CH), 41.40 (O=C- CH_2), 38.10 (5- C), 34.00 (6- C), 21.66 (CH_3);

$\nu_{\text{max}}/\text{cm}^{-1}$: 3328 (N-H), 3058, 3029, 2981, 2932, 1651 (C=O), 1634, 1538, 1487, 1446, 1417, 1408, 1366, 1324, 1259, 1226, 1208, 1165, 1132, 1063, 1049, 1025, 1011 (C=S), 950, 926, 900, 878, 873, 753, 696, 674, 654, 614, 571, 550, 520, 468;

HRMS (ASAP): Found: 385.9825 $[M+1]^+$, $[C_{15}H_{15}NOS_5 + H]^+$ requires: 385.9830;

$[\alpha]_D^{17} = +151$ ($c = 0.49$, CHCl_3).

3.2.7 Synthesis of the *S,S*-Diastereoisomer of *N*-(1'-phenylethyl)-(BEDT-TTF)-acetamide



Oxo-compound (1.09 g, 5.00 mmol) and *S,S*-thione (0.771 g, 2.00 mmol) in $\text{P}(\text{OMe})_3$ (30 ml) yielded a translucent orange solution. The mixture was degassed and refluxed with stirring under N_2 overnight to yield an opaque paint-like orange solution after cooling. The solvent was removed *via* rotary evaporation to afford a bright orange powdered solid which was dissolved in CHCl_3 (*ca.* 30-60 ml) and stirred for 10 minutes. The mixture was filtered under vacuum and the filtrate collected as a translucent red/orange solution. The solvent was again removed *via* rotary evaporation to yield the crude product as a red powdered solid (2.34 g).

Product purified *via* column chromatography using $\text{SiO}_2:\text{CHCl}_3$ to elute the non-product, then $\text{SiO}_2:\text{CHCl}_3/\text{EtOAc}$ 20:1; powder re-dissolved in minimal amount of CHCl_3 and column wet-loaded. After elution of BEDT-TTF, the cross-coupled/self-coupled mixture was yielded after solvent evaporation. Mixture re-columned using $\text{SiO}_2:\text{C}_6\text{H}_{12}/\text{EtOAc}$ 2:1; solid loaded onto silica before wet-loading of the column. After secondary elution, the mixture was separated to yield the donor as an orange-pink powder (0.29 g, 27 %), m.p. 129-130 °C; R_f ($\text{C}_6\text{H}_{12}/\text{EtOAc}$ 2:1) 0.25;

δ_{H} (400 MHz, CDCl_3): 7.18-7.28 (5H, m, Ar- H_5), 6.04 (1H, d, $J = 8.0$ Hz, N- H), 5.01 (1H, quin, $J = 7.2$ Hz, N- CH), 3.99-4.04 (1H, m, 5- H), 3.20-3.24 (1H, m (signal obscured), 6- H_{α}), 3.21 (4H, s, 5'-,6'- H_2), 2.93 (1H, dd, $J = 4.9, 13.4$ Hz, 6- H_{β}), 2.57 (2H, ABX system, $J_{a,b} = 12.8, J_{a,x} = 3.0, J_{b,x} = 2.4$ Hz, (O=C) CH_2), 1.41 (3H, d, $J = 6.8$ Hz, CH_3);

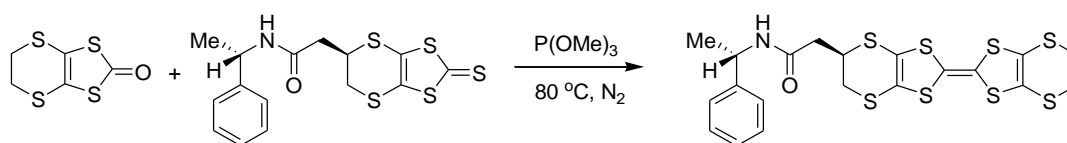
δ_{C} (100 MHz, CDCl_3): 168.14 (C=O), 142.87, 128.67, 127.42 & 126.02 (Ar- C_6), 113.77, 113.71, 112.73, 111.98 & 111.20 (2-,2'-,3a-, 3a'-,7a-, 7a'-C), 49.15 (N- CH), 41.57 (O=C- CH_2), 38.50 (5-C), 34.53 (6-C), 30.09 (5'-,6'-C), 21.84 (CH_3);

$\nu_{\text{max}}/\text{cm}^{-1}$: 3276, 2964, 2920, 2849, 1635, 1539, 1518, 1494, 1447, 1408, 1285, 1249, 906, 887, 772, 698, 610, 541, 506;

HRMS (ASAP): Found: 545.9313 $[\text{M}+\text{H}]^+$, $[\text{C}_{20}\text{H}_{19}\text{NOS}_8 + \text{H}]^+$ requires: 545.9311;

$[\alpha]_{\text{D}}^{20} = +39.8$ ($c = 1.63, \text{CHCl}_3$).

3.2.8 Synthesis of the *S,R*-Diastereoisomer of *N*-(1'-phenylethyl)-(BEDT-TTF)-acetamide



Oxo-compound (1.09 g, 5.00 mmol) and *S,R*-thione (0.771 g, 2.00 mmol) in P(OMe)₃ (30 ml) yielded an iridescent mustard-yellow solution. The mixture was degassed and refluxed with stirring under N₂ overnight to yield an opaque paint-like orange solution after cooling. The solvent was removed *via* rotary evaporation to afford a bright orange powdered solid which was dissolved in CHCl₃ (*ca.* 30-60 ml) and stirred for 10 minutes. The mixture was filtered under vacuum and the filtrate was collected as a translucent red/orange solution. The solvent was again removed *via* rotary evaporation to yield the crude product as a red powdered solid (2.63 g).

Product purified *via* column chromatography using SiO₂:CHCl₃ to elute the non-product, then SiO₂:CHCl₃/EtOAc 20:1; solid loaded onto silica before wet-loading of the column. Purification yielded the donor as a peach solid (0.29 g, 27 %), m.p. 148-152 °C; *R_f* (CHCl₃/EtOAc 20:1) 0.53;

δ_{H} (400 MHz, CDCl₃): 7.25-7.35 (5H, m, Ar-H₅), 5.87 (1H, d, *J* = 7.6 Hz, N-H), 5.08 (1H, quin, *J* = 7.2 Hz, N-CH), 3.99-4.05 (1H, m, 5-H), 3.35 (1H, dd, *J* = 13.3, 3.0 Hz, 6-H_{*a*}), 3.26 (4H, s, 5'-,6'-H₂), 3.13 (1H, dd, *J* = 13.3, 4.8 Hz, 6-H_{*b*}), 2.66 (1H, dd, *J* = 15.1, 6.8 Hz, (O=C)CH_{*a*}), 2.59 (1H, dd, *J* = 15.1, 7.4 Hz, (O=C)CH_{*b*}), 1.46 (3H, d, *J* = 6.8 Hz, CH₃);

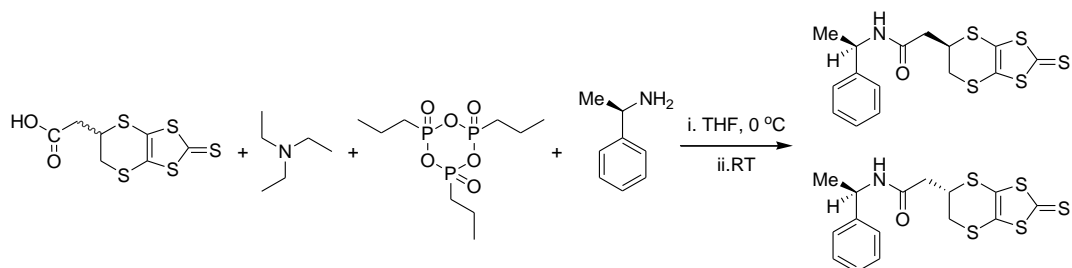
δ_{C} (100 MHz, CDCl₃): 168.19 (C=O), 142.54, 128.72, 127.52 & 126.13 (Ar-C₆), 113.81, 113.74, 112.51, 112.05, 111.94 & 111.27 (2-,2'-,3a-, 3a'-,7a-, 7a'-C), 49.10 (N-CH), 41.52 (O=C-CH₂), 38.35 (5-C), 34.70 (6-C), 30.13 (5'-,6'-C), 21.72 (CH₃);

ν_{max} /cm⁻¹: 3259, 3035, 3003, 2973, 2919, 1634, 1548, 1496, 1447, 1408, 1373, 1329, 1284, 1261, 1168, 968, 919, 884, 775, 746, 691, 616, 586, 522, 512, 484;

HRMS (ASAP): Found: 545.9308 [M+1]⁺, [C₂₀H₁₉NOS₈ + H]⁺ requires: 545.9311;

$[\alpha]_{\text{D}}^{22} = +56.1$ (*c* = 1.23, CHCl₃).

3.2.9 Synthesis of the *R,R* & *R,S*-Diastereoisomers of *N*-(1'-phenyl-ethyl)-2-thioxo-5,6-dihydro-[1,3]dithiolo[4,5-*b*][1,4]dithiin-5-yl-acetamide



Carboxythione (3.32 g, 11.72 mmol) in dry THF (100 ml) afforded a deep opaque brown/yellow solution, to which *R*- α -methylbenzylamine (2.37 ml, 18.40 mmol) and NEt_3 (12.0 ml) were added with no visible change. Following this, T_3P (15.0 ml, 50.4 mmol) was added to yield a deep brown/red mixture which was warm to the touch. The mixture was degassed and stirred under N_2 overnight at room temperature to yield an opaque deep opaque yellow/brown solution. The solvent was removed *via* rotary evaporation to afford a viscous brown oil which was subsequently washed with DCM (*ca.* 100 ml) and distilled H_2O (*ca.* 100 ml). The organic layer was dried over MgSO_4 and filtered under gravity to yield a deep brown/yellow solution. The solvent was again removed *via* rotary evaporation to yield the crude product as a dark brown viscous oil (3.27 g).

Product purified *via* column chromatography using $\text{SiO}_2:\text{CHCl}_3$ to elute the non-product, then $\text{SiO}_2:\text{CHCl}_3/\text{EtOAc}$ 10:1; oil re-dissolved in minimal amount of CHCl_3 and column wet-loaded. After elution of the unreacted chiral amine, two bright yellow fractions were yielded after subsequent solvent evaporation; fraction *first* (*R,R*) and fraction *second* (*R,S*) respectively, in order of elution.

First (*R,R*) as a golden-yellow crystalline solid (1.39 g, 32 %), m.p. 134-137 °C; R_f ($\text{CHCl}_3/\text{EtOAc}$ 10:1) 0.35;

δ_{H} (400 MHz, CDCl_3): 7.21-7.31 (5H, m, Ar- H_5), 5.88 (1H, d, $J = 7.6$ Hz, N- H), 5.04 (1H, quin, $J = 7.2$ Hz, N- CH), 4.09-4.15 (1H, m, 5- H), 3.36 (1H, dd, $J = 13.6, 2.8$ Hz, 6- H_α), 3.08 (1H, dd, $J = 13.6, 5.4$ Hz, 6- H_β), 2.68 (2H, d, $J = 7.2$ Hz, (O=C) CH_2), 1.45 (3H, d, $J = 6.8$ Hz, CH_3);

δ_{C} (100 MHz, CDCl_3): 207.64 (C=S), 167.69 (C=O), 142.56, 128.82, 127.68 & 126.03 (Ar- C_6), 122.49 & 120.89 (3a-,7a-C), 49.35 (N- CH), 41.41 (O=C- CH_2), 38.14 (5-C), 33.95 (6-C), 21.76 (CH_3);

$[\alpha]_D^{26.3} + 114.2$ (c 1.02, CH₂Cl₂).

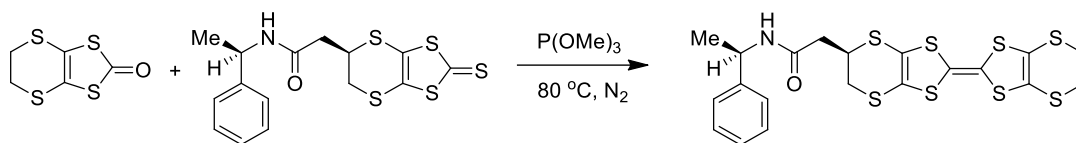
Second (R,S) as a honeycomb-yellow crystalline solid (1.37 g, 32 %), m.p. 162-165 °C; R_f (CHCl₃/EtOAc 10:1) 0.22;

δ_H (400 MHz, CDCl₃): 7.26-7.38 (5H, m, Ar-H₅), 5.90 (1H, d, $J = 8.0$ Hz, N-H), 5.12 (1H, quin, $J = 7.2$ Hz, N-CH), 4.16-4.22 (1H, m, 5-H), 3.48 (1H, dd, $J = 13.2, 2.4$ Hz, 6-H _{α}), 3.28 (1H, dd, $J = 13.2, 5.2$ Hz, 6-H _{β}), 2.79 (1H, dd, $J = 15.2, 7.2$ Hz, (O=C)CH _{α}), 2.71 (1H, dd, $J = 15.2, 7.2$ Hz, (O=C)CH _{β}), 1.51 (3H, d, $J = 7.2$ Hz, CH₃);

δ_C (100 MHz, CDCl₃): 207.65 (C=S), 167.66 (C=O). 142.43, 128.76, 127.63 & 126.09 (Ar-C₆), 122.31 & 120.94 (3a-,7a-C), 49.21 (N-CH), 41.38 (O=C-CH₂), 38.12 (5-C), 34.00 (6-C), 21.65 (CH₃);

$[\alpha]_D^{18} = -138$ (c = 0.45, CHCl₃).

3.2.10 Synthesis of the *R,R*-Diastereoisomer of *N*-(1'-phenylethyl)-(BEDT-TTF)-acetamide



Oxo-compound (1.09 g, 5.00 mmol) and *R,R*-thione (0.771 g, 2.00 mmol) in $\text{P}(\text{OMe})_3$ (30 ml) yielded a translucent orange/red solution. The mixture was degassed and refluxed with stirring under N_2 overnight to yield a viscous deep orange suspension after cooling. The solvent was removed *via* rotary evaporation to afford a deep orange powdered solid which was dissolved in CHCl_3 (*ca.* 30-60 ml) and stirred for 10 minutes. The mixture was filtered under vacuum and filtrate collected as a translucent deep red/orange solution. The solvent was again removed *via* rotary evaporation to yield the crude product as a red powdered solid (3.13 g).

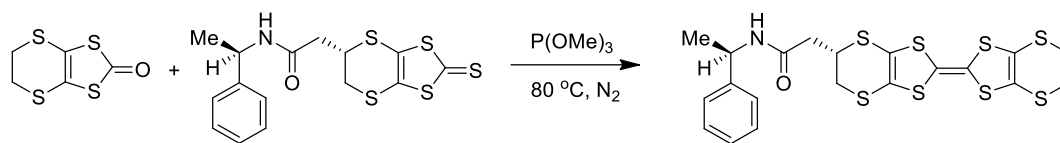
Product purified *via* column chromatography using $\text{SiO}_2:\text{CHCl}_3$ to elute the non-product, then $\text{SiO}_2:\text{CHCl}_3/\text{EtOAc}$ 20:1; powder loaded onto silica and column wet-loaded. After elution of the BEDT-TTF, mixture separated and subsequent solvent removal from fractions *via* rotary evaporation yielded the donor as beautiful orange flaky crystals (0.30 g, 28 %), m.p. 137-142 °C; R_f ($\text{CHCl}_3/\text{EtOAc}$ 20:1) 0.43;

δ_{H} (400 MHz, CDCl_3): 7.18-7.30 (5H, m, *Ar-H*₅), 5.79 (1H, d, $J = 7.6$ Hz, *N-H*), 5.06 (1H, quin, $J = 7.2$ Hz, *N-CH*), 4.01-4.07 (1H, m, 5-*H*), 3.27 (1H, dd, $J = 3.0, 13.2$ Hz, 6-*H* _{α}), 3.23 (4H, s, 5'-,6'-*H*₂), 2.97 (1H, dd, $J = 4.8, 13.2$ Hz, 6-*H* _{β}), 2.59 (2H, d, $J = 7.2$ Hz, (*O=C*)*CH*₂), 1.44 (3H, d, $J = 6.8$ Hz, *CH*₃);

δ_{C} (100 MHz, CDCl_3): 168.11 (*C=O*), 142.80, 128.76, 127.34 & 126.14 (*Ar-C*₆), 113.81, 113.20, 112.53, 111.98 & 111.21 (2-,2'-,3a-, 3a'-,7a-, 7a'-*C*), 49.24 (*N-CH*), 41.64 (*O=C-CH*₂), 38.36 (5-*C*), 34.53 (6-*C*), 30.14 (5'-,6'-*C*), 21.82 (*CH*₃);

$[\alpha]_{\text{D}}^{23} = -23.4$ ($c = 1.65$, CHCl_3).

3.2.11 Synthesis of the *R,S*-Diastereoisomer of *N*-(1'-phenylethyl)-(BEDT-TTF)-acetamide



Oxo-compound (1.09 g, 5.00 mmol) and *R,S*-thione (0.771 g, 2.00 mmol) in P(OMe)₃ (30 ml) yielded a semi-translucent deep yellow/orange suspension. The mixture was degassed and refluxed with stirring under N₂ overnight to yield an opaque milky orange solution after cooling. The solvent was removed *via* rotary evaporation to afford a deep orange powdered solid which was dissolved in CHCl₃ (*ca.* 30-60 ml) and stirred for 10 minutes. The mixture was filtered under vacuum and the filtrate was collected as a translucent deep red/orange solution. The solvent was again removed *via* rotary evaporation to yield the crude product as a red powdered solid (3.09 g).

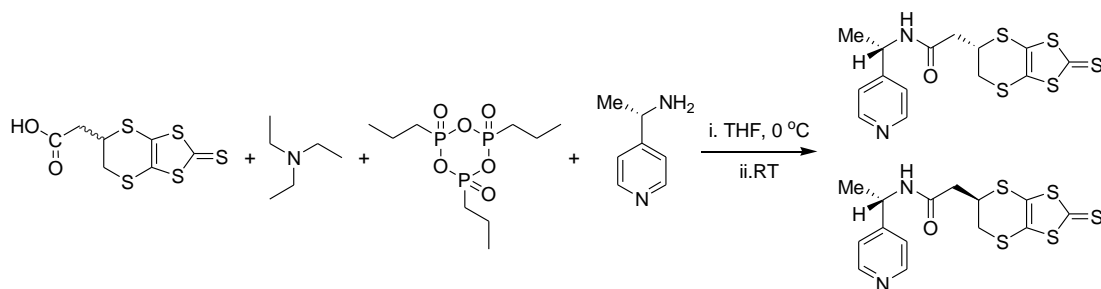
Product purified *via* column chromatography using SiO₂:CHCl₃ to elute the non-product, then SiO₂:CHCl₃/EtOAc 20:1; powder loaded onto silica and column wet-loaded. After elution of the BEDT-TTF, mixture separated and subsequent solvent removal from fractions *via* rotary evaporation yielded the donor as beautiful orange flaky crystals (0.37 g, 34 %), m.p. 156-159 °C; R_f (CHCl₃/EtOAc 20:1) 0.27;

δ_{H} (400 MHz, CDCl₃): 7.21-7.31 (5H, m, Ar-H₅), 5.74 (1H, d, J = 8.0 Hz, N-H), 5.05 (1H, quin, J = 7.2 Hz, N-CH), 4.03-4.06 (1H, m, 5-H), 3.35 (1H, dd, J = 13.2, 3.0 Hz, 6-H _{α}), 3.23 (4H, s, 5',6'-H₂), 3.10 (1H, dd, J = 13.2, 4.8 Hz, 6-H _{β}), 2.63 (1H, dd, J = 15.0, 6.8 Hz, (O=C)CH _{α}), 2.56 (1H, dd, J = 15.0, 7.6 Hz, (O=C)CH _{β}), 1.43 (3H, d, J = 6.8 Hz, CH₃);

δ_{C} (100 MHz, CDCl₃): 168.15 (C=O), 142.52, 128.74, 127.55 & 126.14 (Ar-C₆), 113.83, 113.76, 112.46, 112.08, 111.79 & 111.25 (2-,2'-,3a-, 3a'-,7a-, 7a'-C), 49.12 (N-CH), 41.55 (O=C-CH₂), 38.31 (5-C), 34.70 (6-C), 30.13 (5'-,6'-C), 21.71 (CH₃);

$[\alpha]_{\text{D}}^{23} = -40.6$ (c = 1.60, CHCl₃).

3.2.12 Synthesis of the *S,S* & *S,R*-Diastereoisomers of *N*-(1'-(2'-Pyridyl)-ethyl)-2-thioxo-5,6-dihydro-[1,3]dithiolo[4,5-*b*][1,4]dithiin-5-yl-acetamide



Carboxy-thione (3.32 g, 11.72 mmol) in dry THF (100 ml) afforded a deep red opaque suspension, to which (*S*)-1-(pyridin-2-yl)-ethylamine (2.20 ml, 16.41 mmol) was added to yield a viscous opaque red suspension. Addition of NEt_3 (12.0 ml) yielded no visible change, followed by T_3P (15.0 ml, 50.4 mmol) to yield a deep brown/red mixture which was warm to the touch. The mixture was degassed and stirred under N_2 overnight at room temperature to yield an opaque deep red/brown solution. The solvent was removed *via* rotary evaporation to afford a deep brown viscous oil which was subsequently washed with DCM (*ca.* 100 ml) and distilled H_2O (*ca.* 100 ml). The organic layer was dried over MgSO_4 and filtered under gravity to yield a chocolate brown opaque solution. The solvent was again removed *via* rotary evaporation to yield the crude product as chocolate brown viscous oil (3.85 g).

Product purified *via* column chromatography using $\text{SiO}_2:\text{CHCl}_3$ to elute the non-product, then $\text{SiO}_2:10\% \text{ MeOH/EtOAc}$; oil re-dissolved in minimal amount of CHCl_3 and column wet-loaded. After elution of the unreacted chiral amine, a mixture was yielded of the two products. The column was re-attempted using $\text{SiO}_2:\text{EtOAc}/0.5\% \text{ TEA}$ with which two bright yellow fractions were yielded after subsequent solvent evaporation; fraction *first* (*S,S*) and fraction *second* (*S,R*) respectively, in order of elution.

First (*S,S*) as a golden powdered solid (0.90 g, 20%), m.p. 96-98 °C; R_f (EtOAc/0.5% TEA) 0.25;

δ_{H} (400 MHz, CDCl_3): 8.50 (1H, ddd, $J = 4.8, 1.6, 1.2$ Hz, 6'-*H*), 7.67 (1H, dt, $J = 7.6, 1.6$ Hz, 4'-*H*), 7.18-7.24 (3H, m, 3'-, 5'-*H*, N-*H*), 5.11 (1H, pent, $J = 7.0$ Hz, NCH), 4.17-4.23 (1H, m, 5-*H*), 3.40 (1H, dd, $J = 13.6, 2.8$ Hz, 6- H_{α}), 3.20 (1H, dd, $J = 13.6, 5.6$ Hz, 6- H_{β}), 2.81 (2H, d, $J = 7.2$ Hz, (O=C) CH_2), 1.46 (3H, d, $J = 6.4$ Hz, CH_3);

δ_c (100 MHz, CDCl₃): 207.77 (C=S), 167.80 (C=O), 160.21 (2'-C), 148.78 (6'-C), 137.17 (4'-C), 123.00 & 121.10 (3a-,7a-C), 122.59 & 121.52 (3'-,5'-C), 49.90 (N-CH), 41.53 (5-C), 38.70 (O=C)CH₂, 34.00 (6-C), 22.71 (CH₃);

$\nu_{\max}/\text{cm}^{-1}$: 3332 (N-H), 3041, 2964, 2925, 2897, 1635 (C=O), 1590, 1569, 1526, 1483, 1472, 1432, 1409, 1362, 1253, 1147, 1051(C=S), 1033, 1012, 992, 946, 887, 785, 749, 667, 636, 608, 550, 514, 461;

HRMS (ASAP): Found: 386.9779 [M+1]⁺, [C₁₄H₁₅N₂OS₅]⁺ requires: 386.9782;

$[\alpha]_D^{18} = -60.5$ (c = 0.43, CHCl₃).

Second (*S,R*) as a yellow powdered solid (1.00 g, 22 %), m.p. 99-101 °C; R_f (EtOAc/0.5% TEA) 0.20;

δ_H (400 MHz, CDCl₃): 8.51 (1H, ddd, *J* = 4.8, 1.6, 0.9 Hz, 6'-H), 7.67 (1H, dt, *J* = 7.6, 1.8 Hz, 4'-H), 7.19 – 7.23 (3H, m, 3'-,5'-H, N-H), 5.11 (1H, pent, *J* = 6.9 Hz, N-CH), 4.16-4.22 (1H, m, 5-H), 3.45 (1H, dd, *J* = 13.62 2.8 Hz, 6-H_α), 3.26 (1H, dd, *J* = 13.2, 5.8 Hz, 6-H_β), 2.83 (1H, dd, *J* = 15.6, 7.2 Hz, (O=C)CH_α), 2.77 (1H, dd, *J* = 15.6, 6.8 Hz, (O=C)CH_β), 1.46 (3H, d, *J* = 6.8 Hz, CH₃);

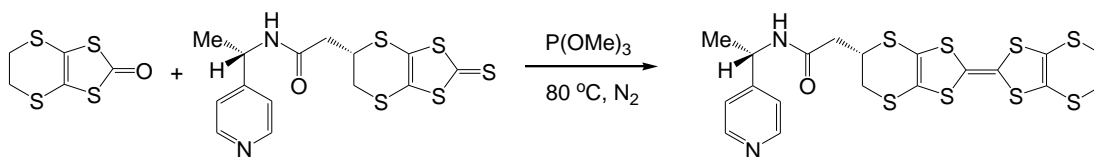
δ_c (100 MHz, CDCl₃): 207.79 (C=S), 167.78 (C=O), 160.07 (2'-C), 148.78 (6'-C), 137.21 (4'-C), 122.87 & 121.16 (3a-,7a-C), 122.62 & 121.54 (3'-,5'-C), 49.90 (N-CH), 41.38 (5-CH₂), 38.55 (5-C), 34.11 (6-C), 22.76 (CH₃);

$\nu_{\max}/\text{cm}^{-1}$: 3264 (N-H), 3063, 2985, 2964, 2917, 1634 (C=O), 1589, 1569, 1548, 1490, 1473, 1444, 1431, 1414, 1367, 1323, 1261, 1237, 1164, 1147, 1126,1059, 1054 (C=S), 1021, 994, 964, 923, 906, 885, 790, 768, 746, 706, 654, 616, 595, 539, 515, 490, 462;

HRMS (ASAP): Found: 386.9772 [M+1]⁺, [C₁₄H₁₅N₂OS₅]⁺ requires: 386.9782;

$[\alpha]_D^{18} = +134.9$ (c = 0.43, CHCl₃).

3.2.13 Synthesis of the *S,S*-Diastereoisomer of *N*-(1'-(2'-Pyridyl)-ethyl)-(BEDT-TTF)-acetamide

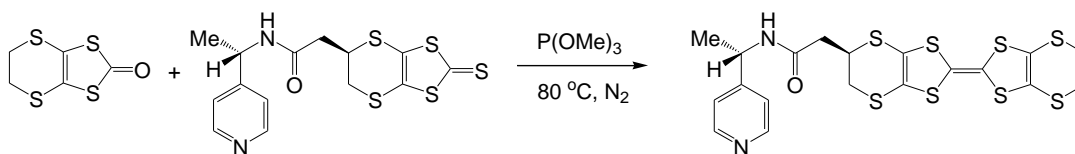


Oxo-compound (1.09 g, 5.00 mmol) and *S,S*-thione (0.771 g, 2.00 mmol) in $\text{P}(\text{OMe})_3$ (30 ml) yielded a translucent orange solution. The mixture was degassed and refluxed with stirring under N_2 overnight to yield an opaque ruby red solution with visible red solid after cooling. The solvent was removed *via* rotary evaporation to afford a bright orange/red powdered solid which was dissolved in CHCl_3 (ca. 30-60 ml) and stirred for 10 minutes. The mixture was filtered under vacuum and the filtrate was collected as a deep wine-red solution and a bright red/orange solid. The solvent was again removed *via* rotary evaporation to yield the crude product as a red powdered solid (2.96 g).

Product purified *via* column chromatography using $\text{SiO}_2:\text{CHCl}_3$ to elute the non-product, then $\text{SiO}_2:\text{EtOAc}/0.5\% \text{ TEA}$; powder re-dissolved in minimal amount of CHCl_3 and column wet-loaded. After elution of the BEDT-TTF, mixture separated and subsequent solvent removal from fractions *via* rotary evaporation yielded the donor as a bright orange/red solid (0.70 g, 64 %), m.p. 96-100 °C; R_f (EtOAc/0.5% TEA) 0.29.

No pure material could be obtained, despite TLC studies suggesting the new donor had formed. In the presence of the pyridyl group on the chiral sidechain, the donors move more slowly on the column and appear to elute with substances derived from trimethyl phosphite.

3.2.14 Synthesis of the *S,R*-Diastereoisomer of *N*-(1'-(2'-Pyridyl)-ethyl)-(BEDT-TTF)-acetamide

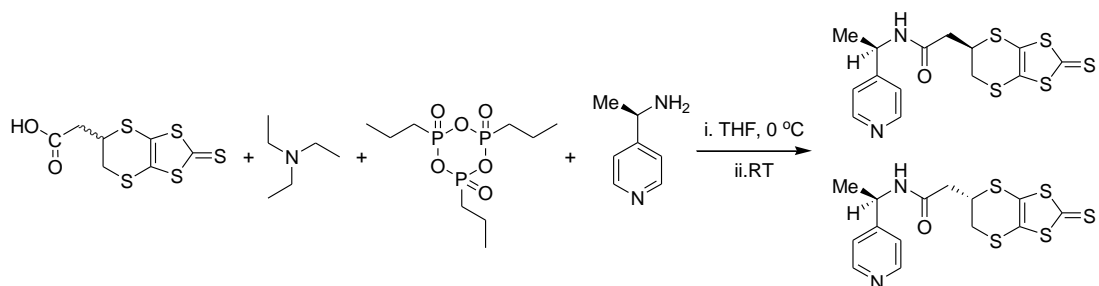


Oxo-compound (1.09 g, 5.00 mmol) and *S,R*-thione (0.771 g, 2.00 mmol) in P(OMe)_3 (30 ml) yielded an iridescent mustard-yellow solution. The mixture was degassed and refluxed with stirring under N_2 overnight to yield an opaque paint-like orange solution after cooling. The solvent was removed *via* rotary evaporation to afford a bright orange powdered solid which was dissolved in CHCl_3 (*ca.* 30-60 ml) and stirred for 10 minutes. The mixture was filtered under vacuum and the filtrate was collected as a translucent red/orange solution. The solvent was again removed *via* rotary evaporation to yield the crude product as a red powdered solid (2.69 g).

Product purified *via* column chromatography using $\text{SiO}_2:\text{CHCl}_3$ to elute the non-product, then $\text{SiO}_2:\text{EtOAc}/0.5\%$ TEA; powder re-dissolved in minimal amount of CHCl_3 and column wet-loaded. After elution of the BEDT-TTF, mixture separated and subsequent solvent removal from fractions *via* rotary evaporation yielded the donor as a deep red solid (0.85 g, 78 %), m.p. $105\text{-}108\text{ }^\circ\text{C}$; R_f ($\text{CHCl}_3/\text{EtOAc}/0.5\%$ TEA) 0.22.

No pure material could be obtained, despite TLC studies suggesting the new donor had formed. In the presence of the pyridyl group on the chiral sidechain, the donors move more slowly on the column and appear to elute with substances derived from trimethyl phosphite.

3.2.15 Synthesis of the *R,R* & *R,S*-Diastereoisomers of *N*-(1'-(2'-Pyridyl)-ethyl)-2-thioxo-5,6-dihydro-[1,3]dithiolo[4,5-*b*][1,4]dithiin-5-yl-acetamide



Carboxy-thione (3.32 g, 11.72 mmol) in dry THF (100 ml) afforded a deep red opaque suspension, to which (*R*)-1-(pyridin-2-yl)-ethylamine (2.20 ml, 16.41 mmol) was added to yield a viscous opaque red/brown suspension. Addition of NEt₃ (12.0 ml) yielded no visible change, followed by T₃P (15.0 ml, 50.4 mmol) to yield no visible change but solution was warm to the touch. The mixture was degassed and stirred under N₂ overnight at room temperature to yield an opaque deep orange/brown solution. The solvent was removed *via* rotary evaporation to afford a deep chocolate brown viscous oil which was subsequently washed with DCM (*ca.* 100 ml) and distilled H₂O (*ca.* 100 ml). The organic layer was dried over MgSO₄ and filtered under gravity to yield a chocolate brown opaque solution. The solvent was again removed *via* rotary evaporation to yield the crude product as chocolate brown viscous oil (3.68 g).

Product purified *via* column chromatography using SiO₂:CHCl₃ to elute the non-product, then SiO₂:EtOAc/0.5% TEA; oil re-dissolved in minimal amount of CHCl₃ and column wet-loaded. After elution of the unreacted chiral amine, two bright yellow fractions were yielded after subsequent solvent evaporation; fraction *first* (*R,R*) and fraction *second* (*R,S*) respectively, in order of elution.

First (*R,R*) as a golden/orange shiny solid (1.01 g, 22 %), m.p. 100-102 °C; R_f (EtOAc/0.5% TEA) 0.38;

δ_{H} (400 MHz, CDCl₃): 8.52 (1H, ddd, *J* = 4.8, 1.6, 1.2 Hz, 6'-*H*), 7.68 (1H, dt, *J* = 7.6, 1.6 Hz, 4'-*H*), 7.20-7.23 (2H, m, 3'-, 5'-*H*), 7.15 (1H, d, *J* = 7.6 Hz, N-*H*), 5.13 (1H, pent, *J* = 7.0 Hz, NCH), 4.19-4.25 (1H, m, 5-*H*), 3.42 (1H, dd, *J* = 13.6, 2.8 Hz, 6-*H*_α), 3.22 (1H, dd, *J* = 13.6, 5.6 Hz, 6-*H*_β), 2.82 (2H, d, *J* = 7.2 Hz, (O=C)CH₂), 1.47 (3H, d, *J* = 6.8 Hz, CH₃);

δ_c (100 MHz, CDCl₃): 207.81 (C=S), 167.77 (C=O), 160.22 (2'-C), 148.92 (6'-C), 137.07 (4'-C), 122.94 & 121.07 (3a-,7a-C), 122.58 & 121.48 (3'-,5'-C), 49.94 (N-CH), 41.59 (5-CH₂), 38.66 (5-C), 34.00 (6-C), 22.82 (CH₃);

$\nu_{\max}/\text{cm}^{-1}$: 3273 (N-H), 3069, 2964, 2923, 2893, 1639 (C=O), 1588, 1573, 1546, 1480, 1472, 1432, 1407, 1297, 1255, 1147, 1054 (C=S), 1033, 1012, 992, 949, 905, 891, 765, 745, 625, 607, 566, 545, 518, 471;

HRMS (ASAP): Found: 386.9774 [M+1]⁺, [C₁₄H₁₅N₂OS₅]⁺ requires: 386.9782;

$[\alpha]_D^{21} = +85.7$ (c = 1.26, CHCl₃).

Second (*R,S*) as a golden solid (0.95 g, 22 %), m.p. 104-106 °C; R_f (EtOAc/0.5% TEA) 0.30;

δ_H (400 MHz, CDCl₃): 8.53 (1H, ddd, *J* = 4.8, 1.6, 1.2 Hz, 6'-H), 7.69 (1H, dt, *J* = 7.6, 2.0 Hz, 4'-H), 7.19 – 7.27 (2H, m, 3'-,5'-H), 7.18 (1H, br, N-H), 5.12 (1H, pent, *J* = 6.8 Hz, N-CH), 4.18-4.24 (1H, m, 5-H), 3.47 (1H, dd, *J* = 13.6, 2.8 Hz, 6-H_α), 3.28 (1H, dd, *J* = 13.6, 5.6 Hz, 6-H_β), 2.85 (1H, dd, *J* = 15.4, 7.3 Hz, (O=C)CH_α), 2.79 (1H, dd, *J* = 15.4, 7.0 Hz, (O=C)CH_β), 1.47 (3H, d, *J* = 6.8 Hz, CH₃);

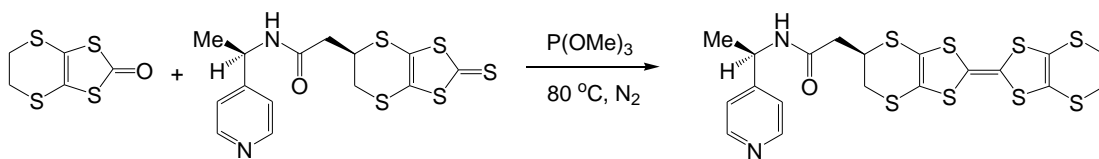
δ_c (100 MHz, CDCl₃): 207.82 (C=S), 167.76 (C=O). 160.09 (2'-C), 148.90 (6'-C), 137.1 (4'-C), 122.84 & 121.14 (3a-,7a-C), 122.61 & 121.49 (3'-,5'-C), 49.91 (N-CH), 41.42 (5-CH₂), 38.52 (5-C), 34.11 (6-C), 22.85 (CH₃);

$\nu_{\max}/\text{cm}^{-1}$: 3265 (N-H), 3065, 2988, 2914, 1634 (C=O), 1588, 1569, 1548, 1489, 1473, 1444, 1431, 1416, 1367, 1322, 1289, 1261, 1237, 1164, 1147, 1127, 1054 (C=S), 1021, 995, 964, 906, 884, 768, 746, 706, 654, 616, 595, 539, 515, 490, 468;

HRMS (ASAP): Found: 386.9777 [M+1]⁺, [C₁₄H₁₅N₂OS₅]⁺ requires: 386.9782;

$[\alpha]_D^{21} = -125.2$ (c = 1.47, CHCl₃).

3.2.16 Synthesis of the *R,R*-Diastereoisomer of *N*-(1'-(2'-Pyridyl)-ethyl)-(BEDT-TTF)-acetamide

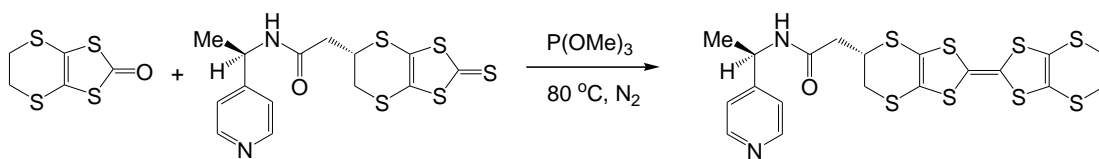


Oxo-compound (1.09 g, 5.00 mmol) and *R,R*-thione (0.770 g, 2.00 mmol) in P(OMe)_3 (30 ml) yielded a translucent orange solution with visible undissolved solid. The mixture was degassed and refluxed with stirring under N_2 overnight to yield an opaque paint-like orange solution after cooling. The solvent was removed *via* rotary evaporation to afford a bright orange clay-like solid which was dissolved in CHCl_3 (*ca.* 30-60 ml) and stirred for 10 minutes. The mixture was filtered under vacuum and the filtrate was collected as a translucent red/orange solution. The solvent was again removed *via* rotary evaporation to yield the crude product as a red/orange powdered solid (3.68 g).

Product purified *via* column chromatography using $\text{SiO}_2:\text{CHCl}_3$ to elute the non-product, then $\text{SiO}_2:\text{EtOAc}/0.5\% \text{ TEA}$; powder loaded onto silica and column wet-loaded. After elution of the BEDT-TTF, mixture separated and subsequent solvent removal from fractions *via* rotary evaporation yielded the donor as a bright red/orange solid (0.60 g, 55 %), m.p. 105-108 $^\circ\text{C}$; R_f (EtOAc/0.5% TEA) 0.40.

No pure material could be obtained, despite TLC studies suggesting the new donor had formed. In the presence of the pyridyl group on the chiral sidechain, the donors move more slowly on the column and appear to elute with substances derived from trimethyl phosphite.

3.2.17 Synthesis of the *R,S*-Diastereoisomer of *N*-(1'-(2'-Pyridyl)-ethyl)-(BEDT-TTF)-acetamide

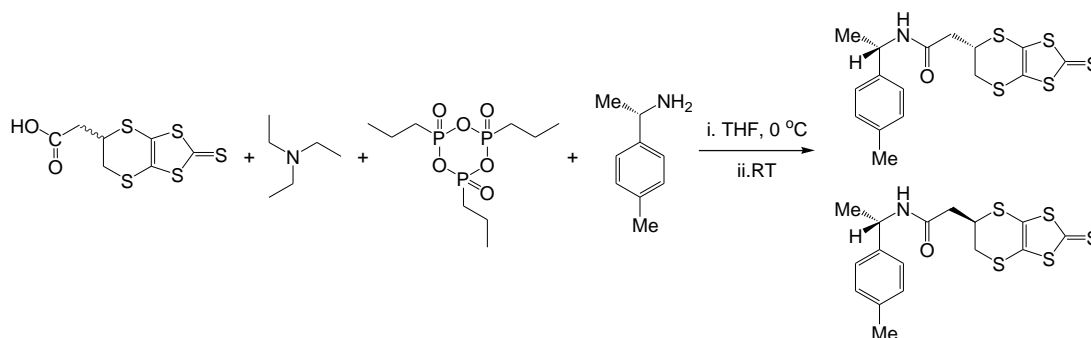


Oxo-compound (1.09 g, 5.00 mmol) and *R,S*-thione (0.770 g, 2.00 mmol) in P(OMe)_3 (30 ml) yielded a translucent deep orange/red solution with visible undissolved solid. The mixture was degassed and refluxed with stirring under N_2 overnight to yield a deep red solution after cooling. The solvent was removed *via* rotary evaporation to afford a bright orange clay-like solid which was dissolved in CHCl_3 (*ca.* 30-60 ml) and stirred for 10 minutes. The mixture was filtered under vacuum and filtrate collected as a translucent red/orange solution. The solvent was again removed *via* rotary evaporation to yield the crude product as an orange/red powdered solid (3.35 g).

Product purified *via* column chromatography using $\text{SiO}_2:\text{CHCl}_3$ to elute the non-product, then $\text{SiO}_2:\text{EtOAc}/0.5\% \text{ TEA}$; powder loaded onto silica and column wet-loaded. After elution of the BEDT-TTF, mixture separated and subsequent solvent removal from fractions *via* rotary evaporation yielded the donor as a bright red powdered solid (0.87 g, 80 %), m.p. $105\text{-}108\text{ }^\circ\text{C}$; R_f ($\text{EtOAc}/0.5\% \text{ TEA}$) 0.30.

No pure material could be obtained, despite TLC studies suggesting the new donor had formed. In the presence of the pyridyl group on the chiral sidechain, the donors move more slowly on the column and appear to elute with substances derived from trimethyl phosphite.

3.2.18 Synthesis of the *S,S* & *S,R*-Diastereoisomers of *N*-(1'-(4''-Methylphenyl)-ethyl)-2-thioxo-5,6-dihydro-[1,3]dithiolo[4,5-*b*][1,4]dithiin-5-yl-acetamide



Carboxy-thione (3.32 g, 11.72 mmol) in dry THF (100 ml) afforded a deep red suspension, to which *S*-1-(*p*-tolyl)ethanamine (2.67 ml, 18.11 mmol) was added to yield a deep burgundy suspension. Addition of NEt_3 (12.0 ml) yielded no visible change, followed by T_3P (15.0 ml, 50.4 mmol) to yield a deep cherry red mixture which was warm to the touch. The mixture was degassed and stirred under N_2 overnight at room temperature to yield an opaque deep chocolate-brown solution. The solvent was removed *via* rotary evaporation to afford a chocolate brown oil which was subsequently washed with DCM (*ca.* 100 ml) and distilled H_2O (*ca.* 100 ml). The organic layer was dried over MgSO_4 and filtered under gravity to yield a chocolate brown opaque solution. The solvent was again removed *via* rotary evaporation to yield the crude product as a brown viscous oil (3.65 g).

Product purified *via* column chromatography using $\text{SiO}_2:\text{CHCl}_3$ to elute the non-product, then $\text{SiO}_2:\text{CHCl}_3/\text{EtOAc}$ 10:1; oil re-dissolved in minimal amount of CHCl_3 and column wet-loaded. After elution of the unreacted chiral amine, two bright yellow fractions were yielded after subsequent solvent evaporation; fraction *first* (*S,S*) and fraction *second* (*S,R*) respectively, in order of elution.

First (*S,S*) as a golden crystalline solid (1.20 g, 26 %), m.p 212-214 °C; R_f ($\text{CHCl}_3/\text{EtOAc}$ 10:1) 0.70;

δ_{H} (400 MHz, CDCl_3) 7.16 (4H, AB system, $J = 8.0$ Hz, Ar- H_4), 5.78 (1H, d, $J = 7.8$ Hz, N- H), 5.08 (1H, pent, $J = 7.1$ Hz, N- CH), 4.15 – 4.25 (1H, m, 5- H), 3.43 (1H, dd, $J = 13.6, 2.7$ Hz, 6- H_α), 3.16 (1H, dd, $J = 13.6, 5.2$ Hz, 6- H_β), 2.73 (2H, d, $J = 7.1$ Hz, (O=C) CH_2), 2.34 (3H, s, Ar- CH_3), 1.50 (3H, d, $J = 6.9$ Hz, CH_3);

δ_c (100 MHz, CDCl₃): 207.67 (C=S), 167.54 (C=O), 139.70 (1''-C), 136.37 (4''-C), 129.45 & 125.96 (2''-,3''-,5''-,6''-C), 122.47 & 120.94 (3a-,7a-C), 49.09 (N-CH), 41.53 (5-CH₂), 38.22 (5-C), 33.88 (6-C), 21.76 (-CH₃), 21.06 (Ar-CH₃);

$\nu_{\max}/\text{cm}^{-1}$: 3264 (N-H), 2969, 2937, 1641 (C=O), 1550, 1514, 1486, 1446, 1391, 1365, 1292, 1052 (C=S), 1029, 1012, 962, 947, 905, 889, 864, 814, 722, 642, 570, 515, 482, 464.

HRMS (ASAP): Found: 399.9991 [M+1]⁺, [C₁₆H₁₈NOS₅]⁺ requires: 399.9992;

$[\alpha]_D^{22} = -130$ (c = 0.43, CHCl₃).

Second (*S,R*) as an orange crystalline solid (1.30 g, 28 %), m.p. 180-182 °C; *R_f* (CHCl₃/EtOAc 10:1) 0.46;

δ_H (400 MHz, CDCl₃): 7.18 (4H, AB system, *J* = 8.0 Hz, Ar-*H_a*), 5.79 (1H, d, *J* = 7.8 Hz, N-*H*), 5.08 (1H, pent, *J* = 7.1 Hz, N-*CH*), 4.11-4.14 (1H, m, 5-*H*), 3.48 (1H, dd, *J* = 13.5, 2.8 Hz, 6-*H_α*), 3.27 (1 H, dd, *J* = 13.5, 5.2 Hz, 6-*H_β*), 2.77 (1H, dd, *J* = 7.2, 15.2 Hz, (O=C)CH_α), 2.69 (1H, dd, *J* = 7.0, 15.2 Hz, (O=C)CH_β), 2.33 (3H, s, Ar-CH₃), 1.48 (3H, d, *J* = 6.9 Hz, CH₃);

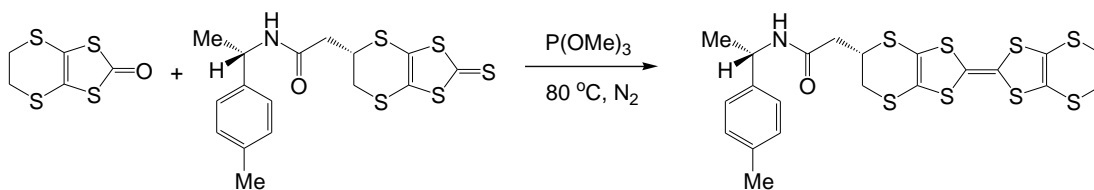
δ_c (100 MHz, CDCl₃): 207.81 (C=S), 167.72 (C=O), 139.60, 137.53 (*ipso* and *para*-C), 129.57, 126.16 (*ortho* and *meta*-C), 122.46, 121.03 (3a-,7a-C), 49.13 (N-CH), 41.56 (5-C), 38.27 (5-CH₂), 34.14 (6-C), 21.79 (-CH₃), 21.19 (Ar-CH₃);

$\nu_{\max}/\text{cm}^{-1}$: 3323 (N-H), 2981, 1649 (C=O), 1536, 1513, 1486, 1324, 1258, 1061, 1050, 1032 (C=S), 1012, 949, 926, 902, 812, 719, 693, 655, 587, 567, 545, 523, 510, 467;

HRMS (ASAP): Found: 399.9991 [M+1]⁺, [C₁₆H₁₈NOS₅]⁺ requires: 399.9992;

$[\alpha]_D^{22} = +188$ (c = 0.54, CHCl₃).

3.2.19 Synthesis of the *S,S*-Diastereoisomer of *N*-((4''-Methylphenyl)-ethyl)-(BEDT-TTF)-acetamide



Oxo-compound (1.09 g, 5.00 mmol) and *S,S*-thione (0.798 g, 2.00 mmol) in P(OMe)₃ (30 ml) yielded a translucent deep orange/red solution with visible undissolved solid which dissolved upon reflux. The mixture was degassed and refluxed with stirring under N₂ overnight to yield an opaque paint-like orange solution after cooling. The solvent was removed *via* rotary evaporation to afford a bright orange powdered solid which was dissolved in CHCl₃ (*ca.* 30-60 ml) and stirred for 10 minutes. The mixture was filtered under vacuum and the filtrate was collected as a translucent red/orange solution with a visible orange solid. The solvent was again removed *via* rotary evaporation to yield the crude product as an orange powdered solid (3.90 g).

Product purified *via* column chromatography using SiO₂:CHCl₃ to elute the non-product, then SiO₂:CHCl₃/EtOAc 20:1; powder loaded onto silica and column wet-loaded. After elution of the BEDT-TTF, the cross-coupled donor was yielded as a bright orange powder (0.30 g, 28 %), m.p. 168-170 °C; R_f (CHCl₃/EtOAc 20:1) 0.40;

δ_{H} (400 MHz, CDCl₃): 7.12 (4H, AB system, $J = 8.1$ Hz, Ar- H_4), 5.74 (1H, d, $J = 7.6$ Hz, N- H), 5.05 (1H, quin, $J = 7.2$ Hz, N- CH), 4.07-4.13 (1H, m, 5- H), 3.30 (1H, dd, $J = 3.0, 13.4$ Hz, 6- H_{α}), 3.28 (4H, s, 5'-,6'- H_2), 3.02 (1H, dd, $J = 5.0, 13.4$ Hz, 6- H_{β}), 2.62 (2H, d, $J = 7.2$ Hz, (O=C) CH_2), 2.31 (3H, s, Ar- CH_3), 1.49 (3H, d, $J = 6.8$ Hz, CH_3);

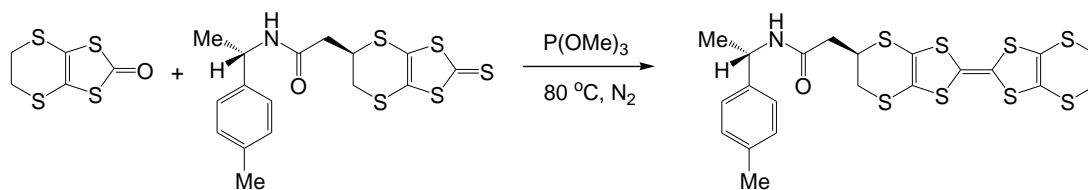
δ_{C} (100 MHz, CDCl₃): 168.04 (C=O), 139.83 & 137.24 (1'''-,4'''-C), 129.41 & 125.98 (2'''-,3'''-,5'''-,6'''-C), 113.82, 113.78, 112.57, 112.00 & 111.24 (2-,2'-3a-,3a'-,7a-,7a'-C), 48.98 (N-CH), 41.67 (O=C- CH_2), 38.40 (5-C), 34.56 (6-C), 30.14 (5'-,6'-C), 21.80 (CH_3), 21.05 (Ar- CH_3);

ν_{max} /cm⁻¹: 3281 (N-H), 2977, 2920, 2904, 1627 (C=O), 1539, 1515, 1447, 1414, 1370, 1318, 1282, 1255, 1228, 1167, 1107, 1084, 1017, 964, 891, 877, 812, 804, 776, 687, 594, 563, 509, 500, 467, 451;

HRMS (ASAP): Found: 559.9466 [M+1]⁺, [C₂₁H₂₂NOS₈]⁺ requires: 559.9467. (Peaks: 559.9466 (28%), 472.0026 (85%) [M + 1 - C₂S₂]⁺, 399.9987 (100%) [M - 159]⁺, 384.8467 (90%) [M - 174]⁺ [BEDT-TTF+H]⁺);

$[\alpha]_D^{20} = +49.8$ (c = 1.70, CHCl₃).

3.2.20 Synthesis of the *S,R*-Diastereoisomer of *N*-((4''-Methylphenyl)-ethyl)-(BEDT-TTF)-acetamide



Oxo-compound (1.09 g, 5.00 mmol) and *S,R*-thione (0.798 g, 2.00 mmol) in $P(OMe)_3$ (30 ml) yielded a translucent orange/red solution with visible undissolved solid which dissolved upon reflux. The mixture was degassed and refluxed with stirring under N_2 overnight to yield an opaque bright orange solution after cooling. The solvent was removed *via* rotary evaporation to afford a bright orange powdered solid which was dissolved in $CHCl_3$ (*ca.* 30-60 ml) and stirred for 10 minutes. The mixture was filtered under vacuum and the filtrate was collected as a translucent red/orange solution. The solvent was again removed *via* rotary evaporation to yield the crude product as an orange powdered solid (3.18 g).

Product purified *via* column chromatography using $SiO_2:CHCl_3$ to elute the non-product, then $SiO_2:CHCl_3/EtOAc$ 20:1; powder loaded onto silica and column wet-loaded. After elution of the BEDT-TTF, the cross-coupled donor was yielded as a bright orange-pink powder (0.30 g, 28 %), m.p. 165-167 °C; R_f ($CHCl_3/EtOAc$ 20:1) 0.25;

δ_H (400 MHz, $CDCl_3$): 7.16 (4H, AB system, $J = 8.4$ Hz, *Ar-H*₄), 5.74 (1H, d, $J = 7.2$ Hz, *N-H*), 5.06 (1H, quin, $J = 7.4$ Hz, *N-CH*), 4.06-4.11 (1H, m, 5-*H*), 3.38 (1H, dd, $J = 5.0, 13.2$ Hz, 6-*H*_α), 3.28 (4H, s, 5'-,6'-*H*₂), 3.15 (1H, dd, $J = 4.8, 13.2$ Hz, 6-*H*_β), 2.67 (1H, dd, $J = 7.0, 15.0$ Hz, (O=C)*CH*_α), 2.59 (1H, dd, $J = 7.2, 15.0$ Hz, (O=C)*CH*_β), 2.33 (3H, s, *Ar-CH*₃), 1.46 (3H, d, $J = 6.8$ Hz, *CH*₃);

δ_C (100 MHz, $CDCl_3$): 168.10 (C=O), 139.59, & 137.16 (1'''-,4'''-C), 129.36 & 126.05 (2'''-,3'''-5'''-,6'''-C), 113.89, 113.74, 112.60, 112.06, 111.85 & 111.32 (2-,2'-3a-,3a'-,7a-,7a'-C), 48.84 (*N-CH*), 41.54 (O=C-*CH*₂), 38.41 (5-C), 34.71 (6-C), 30.12 (5'-,6'-C), 21.69 (*CH*₃), 21.07 (*Ar-CH*₃);

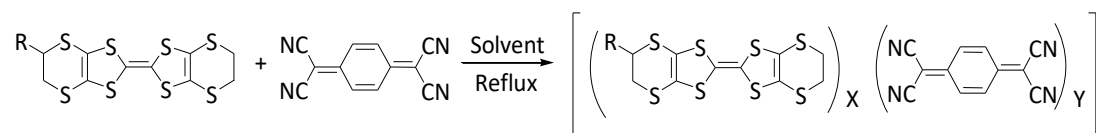
ν_{max}/cm^{-1} : 3268 (*N-H*), 2979, 2970, 2914, 1634 (C=O), 1557, 1549, 1539, 1516, 1447, 1413, 1369, 1291, 1252, 1165, 1107, 1082, 1018, 964, 919, 891, 814, 775, 731, 702, 614, 594, 566, 502, 480, 467;

HRMS (ASAP): Found: 559.9467 [M+1]⁺, [C₂₁H₂₂NOS₈]⁺ requires: 559.9467. (Peaks 559.9467 (60%) [M+1]⁺, 472.0024 (40%) [M+1 - C₂S₂]⁺, 399.9988 (50%) [M - 159]⁺, 384.8466 (100%) [M - 174]⁺ [BEDT- TTF+H]⁺);

$[\alpha]_D^{20} = + 86.4$ (c = 1.37, CHCl₃).

3.2.21 Synthesis of Charge-Transfer Salts from Novel Donor Molecules with TCNQ

Following the synthesis of the novel donor molecules, syntheses of charge-transfer salts with TCNQ were then attempted for each donor *via* reflux on a 4:1 molar ratio. One notes that in the case of the pyridyl-derivatives of the donors, further syntheses were not performed due to the lack of donor purity.



3.2.21.1 *S,S*-*N*-(1'-phenylethyl)-(BEDT-TTF)-acetamide

The *S,S*-donor (54.6 mg, 0.1 mmol) and TCNQ (5.1 mg, 0.025 mmol) were dissolved in DCM (15 ml); this afforded a translucent bright orange solution. The mixture was heated under reflux at 50 °C for 3 hours before leaving to cool and subsequent sealing with a rubber stopper equipped with a small needle to allow slow solvent evaporation for crystallisation. After four weeks, the solvent had evaporated to yield an amorphous black solid which was re-crystallised in a minimal amount of hot CHCl₃ and re-sealed to allow slow solvent evaporation. Despite multiple recrystallisation attempts using a number of different solvents, a black amorphous solid was continuously yielded with some green TCNQ crystals.

3.2.21.2 *S,R*-*N*-(1'-phenylethyl)-(BEDT-TTF)-acetamide

The *S,R*-donor (54.6 mg, 0.1 mmol) and TCNQ (5.1 mg, 0.025 mmol) were dissolved in DCM (15 ml); this afforded a translucent bright orange solution. The mixture was heated under reflux at 50 °C for 3 hours before leaving to cool and sealing with a rubber stopper equipped with a small needle to allow slow solvent evaporation for crystallisation. After four weeks, the solvent had evaporated to yield a black clustered-crystalline solid with some green TCNQ crystals.

3.2.21.3 *R,R*-*N*-(1'-phenylethyl)-(BEDT-TTF)-acetamide

The *R,R*-donor (54.6 mg, 0.1 mmol) and TCNQ (5.1 mg, 0.025 mmol) were dissolved in DCM (15 ml); this afforded a translucent bright orange solution. The mixture was heated under reflux at 50 °C for 3 hours before leaving to cool and sealing with a rubber stopper equipped with a small needle to allow slow solvent evaporation for crystallisation. After four weeks, the solvent had evaporated to yield a black amorphous solid which was re-crystallised in a minimal amount of hot CHCl₃ and re-sealed to allow slow solvent evaporation. Despite multiple

recrystallisation attempts using a number of different solvents, a black amorphous solid was continuously yielded with some green TCNQ crystals.

3.2.21.4 *R,S-N-(1'-phenylethyl)-(BEDT-TTF)-acetamide*

The *R,S-donor* (54.6 mg, 0.1 mmol) and TCNQ (5.1 mg, 0.025 mmol) were dissolved in DCM (15 ml); this afforded a translucent bright orange solution. The mixture was heated under reflux at 50 °C for 3 hours before leaving to cool and sealing with a rubber stopper equipped with a small needle to allow slow solvent evaporation for crystallisation. After four weeks, the solvent had evaporated to yield a black amorphous solid with some green TCNQ crystals which were re-crystallised in a minimal amount of hot CHCl₃ and re-sealed to allow slow solvent evaporation, after which beautiful black crystals were yielded.

3.2.21.5 *S,S-N-(4''-methylphenyl)-ethyl)-(BEDT-TTF)-acetamide*

The *S,S-donor* (54.6 mg, 0.1 mmol) and TCNQ (5.1 mg, 0.025 mmol) were dissolved in DCM (15 ml); this afforded a translucent bright orange solution. The mixture was heated under reflux at 50 °C for 3 hours before leaving to cool and sealing with a rubber stopper equipped with a small needle to allow slow solvent evaporation for crystallisation. After four weeks, the solvent had evaporated to yield a black amorphous solid which was re-crystallised in a minimal amount of hot CHCl₃ and re-sealed to allow slow solvent evaporation. Further recrystallisation could not be performed due to time constraints.

3.2.21.6 *S,R-N-(4''-methylphenyl)-ethyl)-(BEDT-TTF)-acetamide*

The *S,R-donor* (54.6 mg, 0.1 mmol) and TCNQ (5.1 mg, 0.025 mmol) were dissolved in DCM (15 ml); this afforded a translucent bright orange solution. The mixture was heated under reflux at 50 °C for 3 hours before leaving to cool and subsequent sealing with a rubber stopper equipped with a small needle to allow slow solvent evaporation for crystallisation. After four weeks, the solvent had evaporated to yield a black amorphous solid which was re-crystallised in a minimal amount of hot CHCl₃ and re-sealed to allow slow solvent evaporation. Further recrystallisation could not be performed due to time constraints.

3.2.22 Characterisation Techniques

3.2.22.1 NMR

NMR spectra were recorded on a JEOL ECX or ECZ 400 Spectrometer at 298K at a frequency of 400 MHz for ^1H and 100.6 MHz for ^{13}C . All chemical shifts (δ) are quoted in ppm and coupling constants (J) are measured in Hertz. Residual signals from the solvents were used as an internal reference. The samples were then run, for both ^1H and ^{13}C , every sample used the same parameters for ^1H NMR however, some samples required more scans and longer relaxation times for ^{13}C due to weak peak signals. In some cases, it proved useful to use ^1H - ^1H COSY, ^1H - ^{13}C HMQC and ^1H - ^{13}C HMBC 2D NMR experiments in order to aid assignments. After data had been collected, the spectra were analysed using ACD/Labs Spectral Processor software, which proved to be a useful technique for attaining the ratio of diastereomers present in solution.

3.2.22.2 Infra-Red Spectroscopy

All products yielded from the syntheses in this project, crystalline or otherwise, were subject to attenuated total reflection fourier-transform infra-red (ATR FT-IR) spectroscopy as an initial method of characterisation. This analysis was performed using an Agilent Technologies Cary 630 Attenuated FT-IR spectrometer and wavenumbers are reported to the nearest whole number, in cm^{-1} .

3.2.22.3 Melting Point Determination

All synthesised thiones and subsequent donors were analysed to determine the melting points of each compound, these were obtained using a Stuart SMP10 melting point apparatus and reported in $^{\circ}\text{C}$.

3.2.22.4 X-ray Crystallography

Several structures presented in this thesis were analysed at room and low temperatures at NTU, Osaka University in Japan and the National Crystallographic Service (NCS) in Southampton. Data was collected in Osaka by Professor Hiroki Akutsu on a Rigaku R-AXIS VII imaging plate system with FR-E SuperBright High-Brilliance Rotating Anode Generator with confocal mono-chromated $\text{MoK}\alpha$ radiation, using Rapid Auto software for control and processing. Structures were solved *via* programs from the SHELX family by direct methods and refined on F2 full-matrix least squares using all unique data. Data was collected at the NCS on a Rigaku AFC12 diffractometer with Mo rotating anode, using standard control and

processing software. Structures were solved *via* programs from the SHELX family by direct methods and refined on F2 full-matrix least squares using all unique data. Data was collected at NTU on both a Rigaku Oxford Xcalibur, Sapphire3, Gemini four-circle diffractometer with a graphite monochromator using monochromatic Molybdenum K α radiation ($\lambda = 0.7107 \text{ \AA}$) or Copper K α radiation ($\lambda = 1.5406 \text{ \AA}$) at either room temperature or a constant temperature of 150.00(10) K. This diffractometer was subsequently replaced by a Rigaku Rotating Anode XtalLAB Synergy-DW equipped with Cu/Mo radiation. Structures were solved using programs from the SHELX family within OLEX2 by direct methods and refined on F2 full matrix least squares using all unique data. Molecular illustrations included in this body of work were made with Mercury using POV-Ray.¹⁴⁶

3.2.22.5 Cyclic Voltammetry

Cyclic voltammetry was performed to determine the oxidation and reduction potentials of all *full donors*. Measurements were conducted using a typical three electrode system connected to a Metrohm μ Autolab Type II potentiostat/galvanostat. Potentials were measured in dry CH₂Cl₂ containing 0.1 M *n*-Bu₄NPF₆ as the electrolyte at room temperature and under N₂ relative to an Ag/AgCl reference electrode and a platinum electrode using a 100 mV s⁻¹ scan and reported in V. After dissolution of the sample in dry DCM containing 0.1 M *n*-Bu₄NPF₆, each electrode was then connected to the potentiostat and a potential was applied across the electrodes between a range of 0.00 V and 1.1 V at a scan rate of 100 mV s⁻¹. The oxidation potential was measured first, followed by the reduction potential; this yielded a plot which displayed the forward sweep (oxidation) and the backward sweep (reduction), and allowed identification of redox-switchability within the complex. This cycle was repeated 3 times and resulted in a graph that contains two peaks on the forward oxidative sweep and a further two peaks from the reverse reductive sweep. *Figure 3.1* serves as an example of a typical CV graph for each donor synthesised, using data resulting from the study of the *S,R*-N-(1'-phenylethyl)-(BEDT-TTF)-acetamide donor.

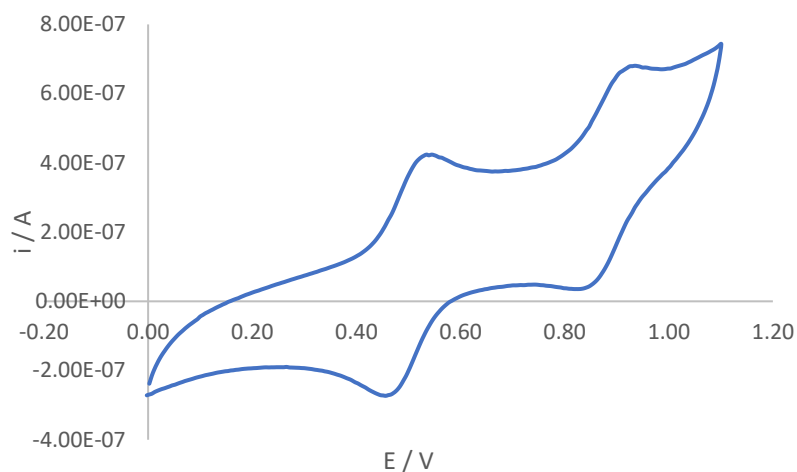


Figure 3.1 – A general cyclic voltammetry plot to visualise those yielded by all donors (with the exception of the pyridyl-type donors due to purity issues). Data used for this graph was that of *S,R-N*-(1'-phenylethyl)-(BEDT-TTF)-acetamide.

3.2.22.6 High-resolution Mass Spectrometry

High-resolution mass spectrometry was obtained from the EPSRC UK National Mass Spectrometry Facility at Swansea University on an LTQ Orbitrap XL 1, using positive electrospray ionisation (ESI+).

3.2.22.7 Optical Rotation

Optical rotation measurements were conducted on all synthesised thiones and subsequent donors using a Bellingham and Stanley ADP 440 polarimeter, with a D-line of sodium, $\lambda = 589$ nm and a reading accuracy of $\pm 0.010^\circ$. The temperature of the analyses was between 17 and 26.3 °C and concentrations of samples ranged from 0.43 – 1.70 g / 100 ml in CHCl_3 . Values of the observed rotation, α° , were recorded for each sample, except for those of the *full-pyridyl*-type donors due to purity issues. After measurements were performed, one is able to determine the specific rotation ($[\alpha]_D^T$) of each sample using the following equation (T is the temperature of the analysis in this case 26.3 ° and D is the wavelength of light used, in this case 589 nm), the following equation was used:

$$[\alpha]_D^T = \frac{100 * \alpha}{l * c}$$

α = observed rotation (°)

T = temperature of analysis

D = wavelength of light (589 nm)

l = path length of the cell (0.5 dm)

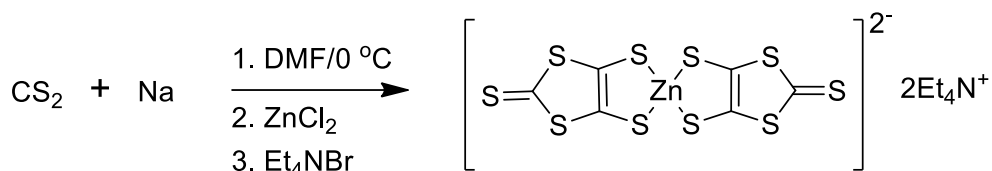
c = sample concentration (g / 100 ml).

3.3 Results and Discussion

3.3.1 Analysis of Synthesised Novel Organic Donor Molecules and their Precursors

3.3.1.1 Synthesis of Bis(tetraethylammonium)bis(1,3-dithiol-2-thione-4,5-dithiol)zincate

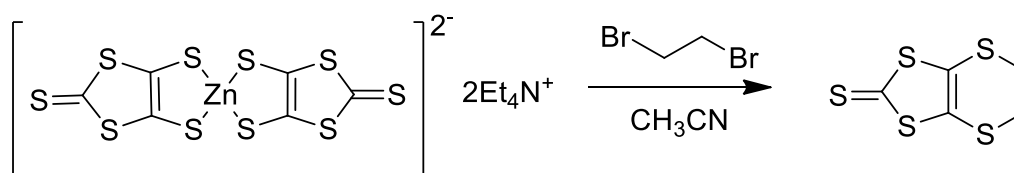
In order for one to synthesise a new BEDT-TTF-based donor molecule, one must first synthesise the building blocks of BEDT-TTF; starting with the zinc salt. The method followed in this synthesis is that of the self-assembly mechanism reported by Wang *et al.* in 1998.¹⁴⁷ CS₂ and sodium metal were stirred in DMF to initially form the sodium salt of the desired product, after which ZnCl₂ and Et₄NBr were added to afford the desired zinc salt as bright raspberry red powdered solid (65 %), Scheme 3.1. The melting point of the zinc salt was measured at 205-207°C; perfectly matching that which is reported in literature.¹⁴⁸ The complex was carried forward with no further purification.



Scheme 3.1 - Self-assembly reaction for the synthesis of the zinc salt, using methods reported by Wang *et al.*¹⁴⁷

3.3.1.2 Synthesis of 4,5-ethylenedithio-1,3-dithiole-2-thione

Once the zinc salt has been synthesised, one may then synthesise the unsubstituted bicyclic thione, which is referred to simply as *thione*. To do so, methods reported by Varma *et al.* are employed; the zinc salt is reacted with 1,2-dibromoethane *via* reflux under N₂ for 5 hours before decolouring with charcoal to yield a golden honeycomb crystalline solid (75%), Scheme 3.2.¹⁴⁹

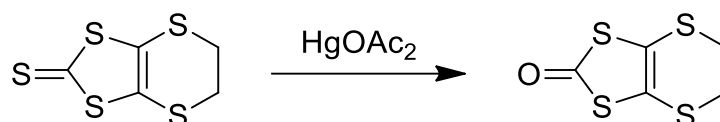


Scheme 3.2 - Synthesis of the thione, using methods reported by Varma *et al.*¹⁴⁹

When analysing the data collected for the *thione* and comparing it to literature,^{149,150} one can say with a sufficient level of confidence that the synthesis was successful; the ¹H NMR spectra displayed the expected single singlet peak at 3.40 ppm, the ¹³C NMR showed the thione carbon shift (C=S) at 208 ppm and the observed melting point of the thione was measured at 122-124°C. The complex was carried forward with no further purification.

3.3.1.3 Synthesis of 4,5-ethylenedithio-1,3-dithiole-2-one

Following the synthesis of the unsubstituted thione, one can synthesise the *oxo-compound* using the *Varma et al.* methodology once more; the *thione* was stirred with mercury acetate to yield a peach crystalline solid (79%), *Scheme 3.3*.

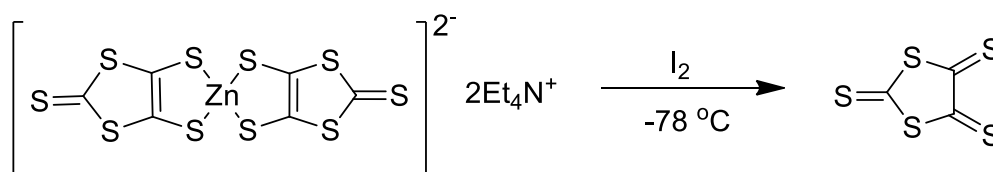


Scheme 3.3 - Synthesis of the oxo-compound.

Similar to the above reaction, when analysing the data collected for the *oxo-compound* and comparing it to literature as well as that collected for the *thione*, it is apparent that the conversion from the *thione* to the *oxo-compound* was successful.^{149–152} Although the ¹H NMR spectra displayed the same singlet peak at 3.42 ppm as expected, the most important differences in the ¹³C NMR spectra were apparent; the thione carbon shift (C=S) at 208 ppm is no longer present and instead the carbonyl carbon shift presents itself at 189.0 ppm. Owing to the increased electronegativity of the oxygen atom as opposed to the previous sulphur atom, the rest of the carbon signals are shifted slightly. The observed melting point of the thione was measured at 122–124 °C and the complex was carried forward with no further purification.

3.3.1.4 Synthesis of 1,3-dithiolane-2,4,5-trithione

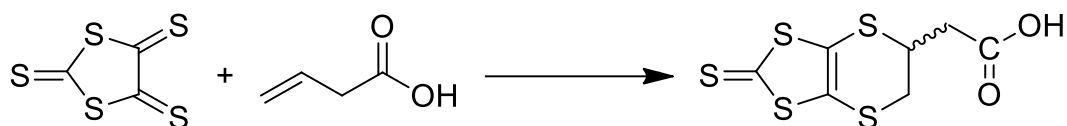
A secondary reaction involving the aforementioned zinc salt is in the synthesis of the *trithione*, which provides the key to further synthesis of the novel donor molecules. Utilising literature methodology, the zinc salt is reacted with iodine in a dry ice/acetone bath (-78 °C) before work-up to yield the product as a bright orange powder (109%), *Scheme 3.4*.^{147,148,153} The author notes that the high yield is likely as a result of zinc iodide impurities, though the product was used without further purification.



Scheme 3.4 - Synthesis of the trithione.

3.3.1.5 Synthesis of 2-(2-thioxo-5,6-dihydro-[1,3]dithiolo[4,5-b][1,4]dithiin-5-yl)acetic acid

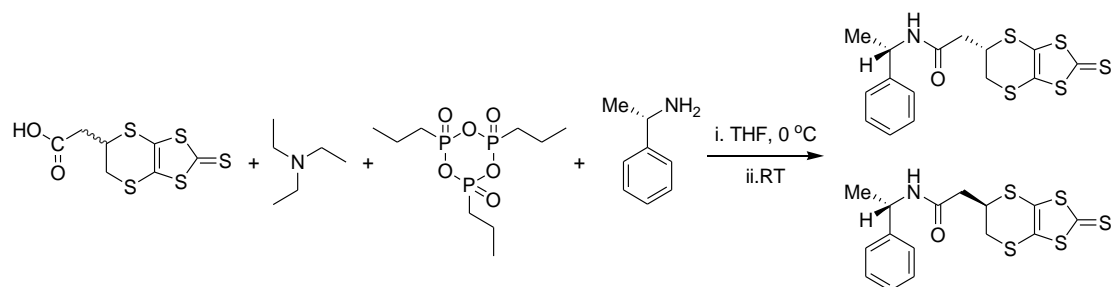
The final important building block prior to synthesising novel BEDT-TTF-based donors is in that of the *carboxy*-thione. In the method reported by *Neiland et al.*, the synthesised *trithione* undergoes a Diels-Alder-type reaction with vinyl acetic acid to yield a racemic mixture of *S*- and *R*- *carboxy*-thione after work-up as a fine brown powder (59%), *Scheme 3.5*.¹⁵⁴



Scheme 3.5 - Synthesis of carboxy-thione.

The NMR produced clean spectra. In the ¹H NMR it can be seen that the side chain methylene group appeared as a multiplet at 3.40 ppm and the methylene group in the dithiin ring next to the chiral centre was split into two signals, both as double doublets at 2.90 and 2.75 ppm. A clear ¹³C NMR could not be obtained.

3.3.1.6 Synthesis of the *S,S* & *S,R*-Diastereoisomers of *N*-(1'-phenyl-ethyl)-2-thioxo-5,6-dihydro-[1,3]dithiolo[4,5-b][1,4]dithiin-5-yl-acetamide



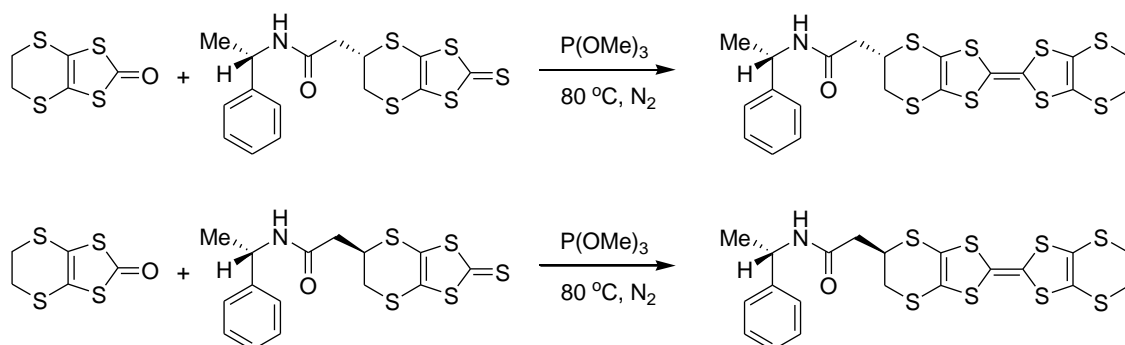
*Scheme 3.6 - Synthesis of the half *S,S*- and *S,R*- diastereomeric acetamides using *S*- α -methylbenzylamine.*

Following the successful synthesis of novel BEDT-TTF donors using *R*- α -methylbenzylamine reported by *Wallis et al.* in 2013,³ the natural next step was to synthesise the *S,S*- and *S,R*- counterparts using the same methods, with the exception of the use of propyl phosphonic anhydride solution (T3P) in place of ethyl chloroformate as a coupling agent. The two isomeric acetamides were separated by chromatography and obtained in similar yields of *ca.* 30 % as golden/yellow crystalline solids. The main difference in their ¹H NMR spectra is between the signals from the side chain methylene groups, which in *first* (*S,S*) appears as a doublet at δ : 2.68 ppm, but in *second* (*S,R*) appears as two doublet doublets at δ : 2.72 and 2.64 ppm. The thione groups for both isomers appear in ¹³C NMR with signals at δ : 207.6

ppm. Currently, the stereochemistry is unassigned until crystalline material of either diastereoisomer can be obtained and confirmed *via* x-ray crystallography. However, their assigned chirality is assumed based upon the order for which the literature proposes the pair elute in along with their subsequently reported x-ray structures,^{2,3} as well as the XRD study for the full donors in *section 3.1.7*. Moreover, further evidence to indicate the successful synthesis of diastereoisomers as opposed to a racemic mixture can be obtained from the specific rotation values for each *half-donor*; with thiones *first* and *second* having specific rotation values of $[\alpha]_D^{17} = -166$ and $+151$ respectively. One notes that since these values are not the same (and of opposite sign), one can be confident that the pair are indeed diastereoisomers.

3.3.1.7 Synthesis of Enantiopure *S,S*- and *S,R*-Diastereoisomers of *N*-(1'-phenylethyl)-(BEDT-TTF)-acetamide

Following the synthesis of the two *half-donors*, each thione was then cross-coupled with the unsubstituted *oxo-compound* in trimethyl phosphite at 80 °C separately, to give their corresponding chiral donors in 27 % yields, *Scheme 3.7*.



Scheme 3.7 - Synthesis of the full *S,S*- and *S,R*-diastereomeric acetamides using *S*- α -methylbenzylamine.

The structure of *first* eluted *full-donor* was confirmed *via* x-ray crystallography to hold the (*S*)-configuration at 5-C, to yield the full stereochemistry as (*1''S*, *5S*)-, and therefore the latter is assumed as (*1''S*, *5R*)-, fitting nicely with the reported literature for the *R*-counterparts synthesised by *Wallis et al.*³

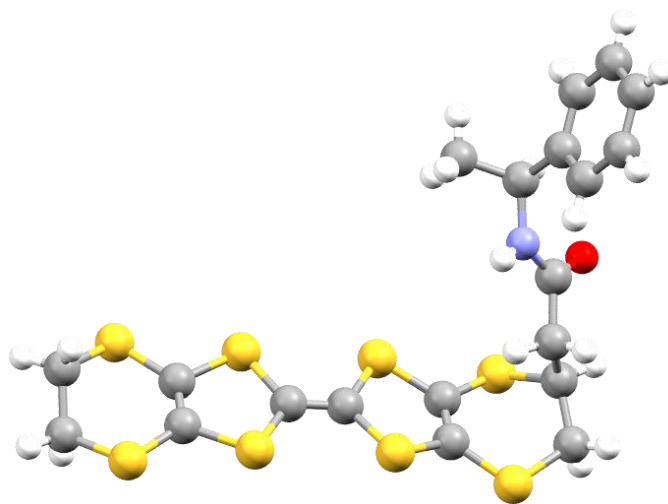


Figure 3.2 - Molecular structure of first (S,S)-full donor, showing the (S)-stereochemistry at 5-C on the dithiin ring. Acetone solvent molecule omitted for clarity.

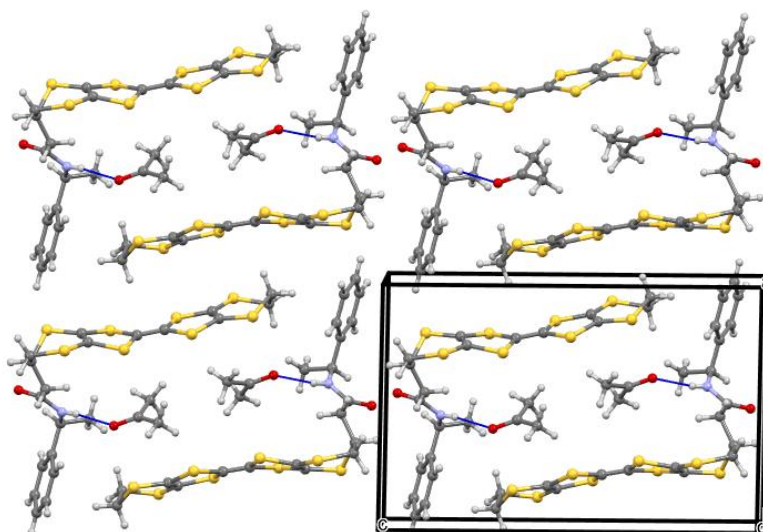


Figure 3.3 – Packing of the donor molecules within the crystal structure of the (S,S)-full donor; one observes interesting hydrogen bonding interactions between the acetone solvent and donors, as opposed to the usual donor-donor H-bonding motifs observed in previously published materials.

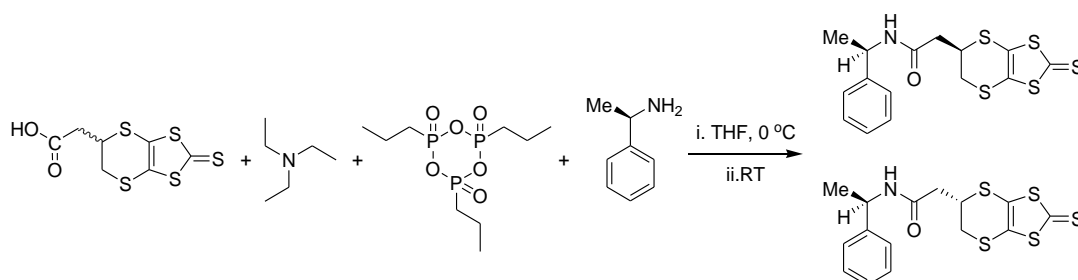
Crystal data at 150K: $C_{20}H_{19}NOS_8 \cdot C_3H_6O$, $M = 603.92$, yellow plate, Monoclinic, $a = 11.50077(14)$, $b = 6.56772(7)$, $c = 17.7096(2)$ Å, $\beta = 90.9201(12)^\circ$, $U = 1337.50(3)$ Å³, $T = 150$ K, space group $P2_1$, $Z = 2$, reflections collected = 5172, independent reflections = 4905, $R1 = 0.0369$, $wR2 = 0.0884$ [$F^2 > 2\sigma(F^2)$], Flack parameter = $-0.010(17)$, Residual electron density = 0.36 and -0.33 eÅ⁻³.

Aside from the XRD, one can measure the success of the synthesis of these donors in the loss of the thione signal from ¹³C NMR, which was previously observed at δ : 207.6 ppm. In the ¹H

NMR spectra, the signals for the methylene group in the dithiin ring at 6-C displays one multiplet and one doublet doublets for the *S,S-donor* at δ : 3.20-3.24 and 2.93 ppm, whereas the assumed *S,R-donor* displays two doublet doublets at δ : 3.35 and 3.13 ppm. When looking at the proton signals for the methylene groups on the chiral side-chain, one observes an ABX system at δ : 2.57 ppm for the *S,S-donor*, and two set of doublet doublets at δ : 2.66 and 2.59 ppm for the *S,R-donor*. One can measure the specific rotation of each donor for further evidence to indicate that these products are diastereoisomers as opposed to a racemate. The *S,S-donor* had a specific rotation value of $[\alpha]_D^{20} = +39.8$, and the *S,R-donor* had a specific rotation value of $[\alpha]_D^{20} = +56.1$; these values are not the same suggesting a successful diastereoisomeric donor synthesis.

3.3.1.8 Synthesis of the *R,R* & *R,S*-Diastereoisomers of *N*-(1'-phenyl-ethyl)-2-thioxo-5,6-dihydro-[1,3]dithiolo[4,5-*b*][1,4]dithiin-5-yl-acetamide

Using the same method as above, another set of functionalised chiral acetamides were synthesised, this time of the *R*-type isomers using *R*- α -methylbenzylamine. The two isomeric *R*-type acetamides were separated by chromatography and obtained in yields of *ca.* 32 % as golden/yellow crystalline solids, *Scheme 3.8*.



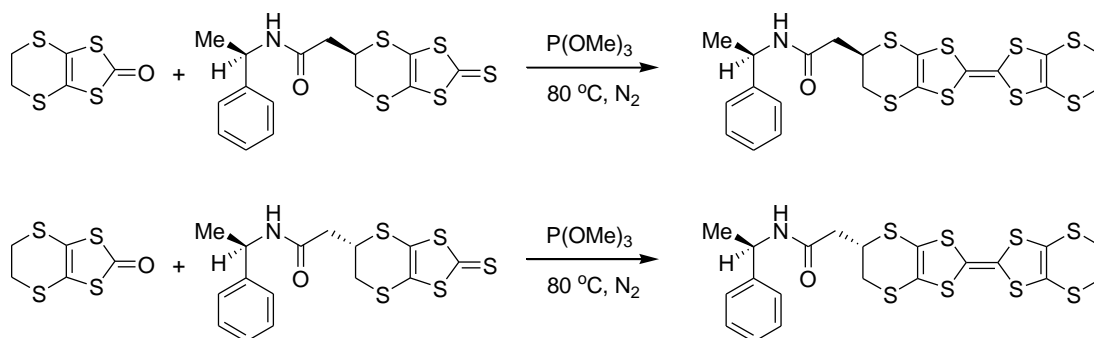
Scheme 3.8 - Synthesis of the half *R,R*- and *R,S*-diastereoisomeric acetamides using *R*- α -methylbenzylamine.

Both sets of methylene groups display differences with the ^1H NMR of each *half-donor*; for the side chain methylene group in *first (R,R)*, the signal appears as a doublet at δ : 2.68 ppm, but in *second (R,S)* it appears as two doublet doublets at δ : 2.79 and 2.71 ppm. The methylene group on the dithiin ring adjacent to the chiral centre was split into two separate doublet of doublets signals for each isomer, at δ : 3.36 and 3.08 ppm for the *RR-half donor* and δ : 3.48 and 3.28 ppm for the *R,S-half*. The thione groups for both isomers appear in ^{13}C NMR with signals at δ : 207.6 ppm. Since these structures have been previously reported by *Wallis et al.*, the assigned chirality is assumed to be that which the literature proposes for the pair.^{2,3} Once again, further evidence to indicate the successful synthesis of diastereoisomers as opposed to a racemic mixture can be obtained from the specific rotation values for each *half-donor*;

having specific rotation values of $[\alpha]_D^{26.3} = +114.2$ and -138 respectively, for the thiones *first* and *second*. One notes that since these values are not the same (and of opposite sign), one can be confident that the pair are indeed diastereoisomers.

3.3.1.9 Synthesis of Enantiopure *R,R* & *R,S*-Diastereoisomers of *N*-(1'-phenylethyl)-(BEDT-TTF)-acetamide

Following the synthesis of the two *half-donors*, each thione was then cross-coupled with the unsubstituted *oxo-compound* in trimethyl phosphite at 80 °C separately, to give their corresponding chiral donors in 28 and 34 % yields respectively, *Scheme 3.9*.



*Scheme 3.9 - Synthesis of the full *R,R*- and *R,S*-diastereomeric acetamides using *R*- α -methylbenzylamine.*

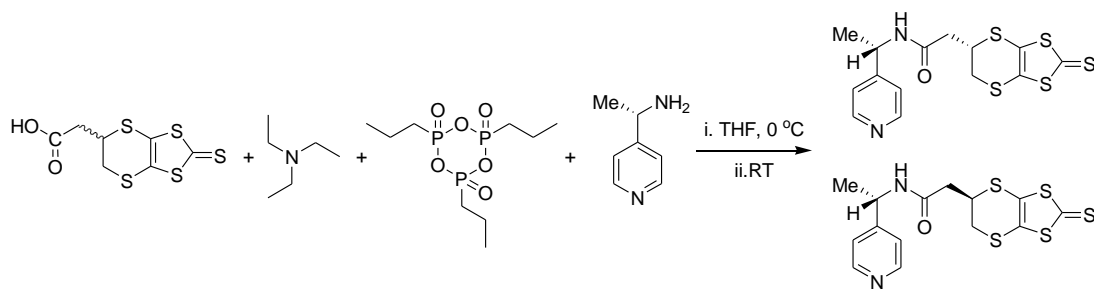
Despite being previously reported, these *R-donors* were synthesised in order to study the effects of chirality within the *R,R-donor* and the *R,S-donor* if one can indeed synthesise the *R,R-charge-transfer* salt counterpart to the *R,S-salt* published recently.² Although orange flaky crystals arose from both syntheses, they were not suitable for XRD. As a result, the absolute stereochemistry of these *full-donors* is assumed based upon the published data for these donors.³

In lieu of XRD data, one comments upon the relative success of the synthesis of these donors using the ^1H and ^{13}C data collected, as well as specific rotation. Once again, the loss of the thione signal from ^{13}C NMR which was previously observed at δ : 207.6 ppm, is noted for these *full-donors*. In the ^1H NMR spectra, the signals for the methylene group in the dithiin ring at 6-C displays two pairs of doublet doublets at δ : 3.27 and 2.97 ppm for the assumed *RR-donor*, and two pairs of doublet doublets at δ : 3.35 and 3.10 ppm for the assumed *R,S-donor*. When looking at the proton signals for the methylene groups on the chiral side-chain, one observes a doublet at δ : 2.59 ppm for the *R,R-donor*, and a pair of doublet doublets at δ : 2.63 and 2.56 ppm for the *R,S-donor*. One then measures the specific rotation of each donor for further evidence to indicate that these products are diastereoisomers as opposed

to a racemate. The *R,R-donor* had a specific rotation value of $[\alpha]_D^{20} = -23.4$, and the *R,S-donor* had a specific rotation value of $[\alpha]_D^{20} = -40.6$; these values are not the same suggesting a successful diastereoisomeric donor synthesis.

3.3.1.10 Synthesis of the *S,S* & *S,R*-Diastereoisomers of *N*-(1'-(2'-Pyridyl)-ethyl)-2-thioxo-5,6-dihydro-[1,3]dithiolo[4,5-*b*][1,4]dithiin-5-yl-acetamide

Following the full synthesis of the *N*- α -methylbenzylamine family of four diastereomeric isomers, a new family of functionalised chiral acetamides were synthesised, this time of *N*-1-pyridin-2-yl-ethylamine, beginning with the *S*-type pair. (*S*)-1-pyridin-2-yl-ethylamine was reacted with carboxy-thione using T3P as a coupling agent, after which the two isomeric acetamides were separated by chromatography and obtained in yields of *ca.* 20 % and 22% respectively as golden/yellow powdered solids, *Scheme 3.10*.

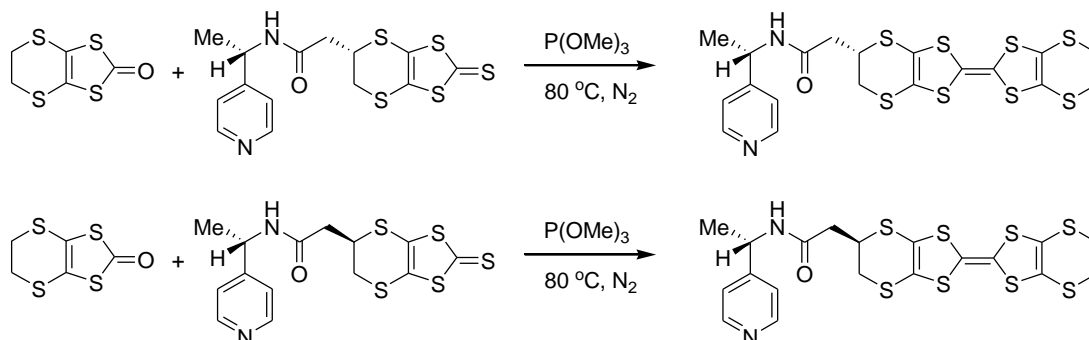


Scheme 3.10 - Synthesis of the half *S,S*- and *S,R*- diastereoisomeric acetamides using (*S*)-1-pyridin-2-yl-ethylamine.

Both sets of methylene groups display differences with the ^1H NMR of each *half-donor*; for the side chain methylene group in the *first (S,S) half-donor*, the signal appears as a doublet at δ : 2.81 ppm, but in the *second (S,R) half-donor*, it appears as two doublet doublets at δ : 2.83 and 2.77 ppm. The methylene group on the dithiin ring adjacent to the chiral centre was split into two separate doublet of doublets signals for each isomer, at δ : 3.40 and 3.20 ppm for the *SS-half donor* and δ : 3.45 and 3.26 ppm for the *S,R-half donor*. The thione groups for both isomers appear in ^{13}C NMR with signals at δ : 207.8 ppm. Neither *half donor* yielded suitable crystals for x-ray crystallography despite multiple recrystallisation attempts, and thus the chirality is assumed following the previous system of *first* being *S,S*- and *second* being *S,R*. Once again, further evidence to indicate the successful synthesis of diastereoisomers as opposed to a racemic mixture can be obtained from the specific rotation values for each *half-donor*; having specific rotation values of $[\alpha]_D^{26.3} = -60.5$ and $+134.9$ respectively, for the thiones *first* and *second*. One notes that since these values are not the same (and of opposite sign), one can be confident that the pair are indeed diastereoisomers.

3.3.1.11 Synthesis of Enantiopure *S,S* & *S,R*-Diastereoisomers of *N*-(1'-(2'-Pyridyl)-ethyl)-(BEDT-TTF)-acetamide

Following the synthesis of the two *half-donors*, each thione was then cross-coupled with the unsubstituted *oxo-compound* in trimethyl phosphite at 80 °C separately, to give impure chiral donors in 64 and 78 % yields respectively, *Scheme 3.11*.

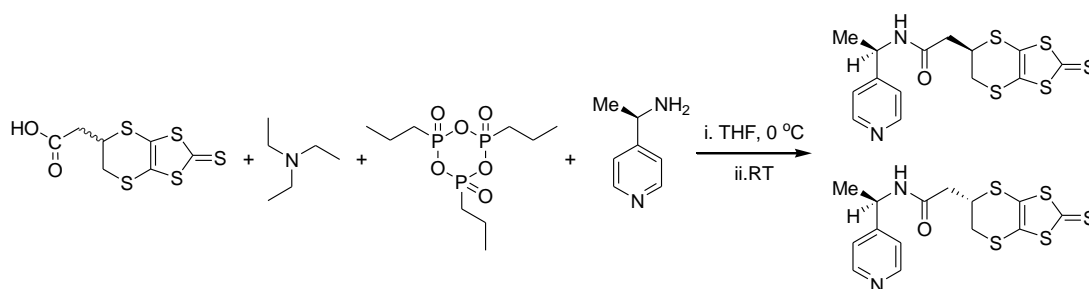


Scheme 3.11 - Synthesis of the full *S,S*- and *S,R*-diastereoisomeric acetamides using (*S*)-1-pyridin-2-yl-ethylamine.

Currently, characterisation data for these *full donors* has been relatively inconclusive and does not allow one to make comparative comments. It would appear that perhaps the cross-coupled enantiomers have not been separated fully from the initial BEDT-TTF product and trimethyl phosphite material, such that they are very impure. The melting points recorded for both R-type donors are the same for each *full donor*; 105-108°C. One notes that the yield of both donors is over 50% higher than all other donors synthesised, indicating the presence of impurities. The lack of reported data points towards a further purification being needed for these donors. As such, it was not possible to isolate pure full-donors of this type and they are not carried further at this time.

3.3.1.12 Synthesis of the *R,R* & *R,S*-Diastereoisomers of *N*-(1'-(2'-Pyridyl)-ethyl)-2-thioxo-5,6-dihydro-[1,3]dithiolo[4,5-*b*][1,4]dithiin-5-yl-acetamide

To complete the *N*-1-pyridin-2-yl-ethylamine family of donors, the *R-type* pair were synthesised; (*R*)-1-pyridin-2-yl-ethylamine was reacted with carboxy-thione using T3P as a coupling agent, after which the two isomeric acetamides were separated by chromatography and obtained in yields of *ca.* 22 % as golden/orange shiny solids, *Scheme 3.12*.

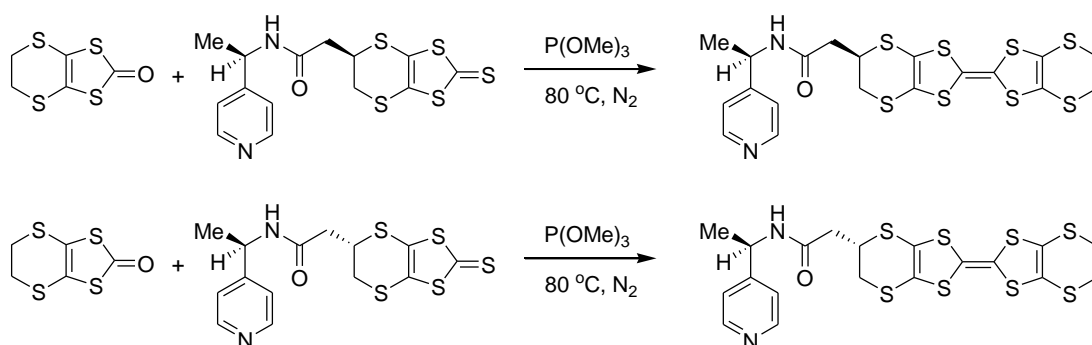


Scheme 3.12 - Synthesis of the half *R,R*- and *R,S*- diastereomeric acetamides using (*R*)-1-pyridin-2-yl-ethylamine.

Both sets of methylene groups display differences with the ^1H NMR of each *half*-donor; for the side chain methylene group in the *first* (*R,R*) *half*-donor, the signal appears as a doublet at δ : 2.82 ppm, but in the *second* (*S,R*) *half*-donor, it appears as two doublet doublets at δ : 2.85 and 2.79 ppm. The methylene group on the dithiine ring adjacent to the chiral centre was split into two separate doublet of doublets signals for each isomer, at δ : 3.42 and 3.22 ppm for the *R,R*-*half* donor and δ : 3.47 and 3.28 ppm for the *R,S*-*half* donor. The thione groups for both isomers appear in ^{13}C NMR with signals at δ : 207.8 ppm. Neither *half* donor yielded suitable crystals for x-ray crystallography despite multiple recrystallisation attempts, and thus the chirality is assumed following the previous system of *first* being *R,R*- and *second* being *R,S*-. Once again, further evidence to indicate the successful synthesis of diastereoisomers as opposed to a racemic mixture can be obtained from the specific rotation values for each *half*-donor; having specific rotation values of $[\alpha]_D^{21} = +85.7$ and -125.2 respectively, for the thiones *first* and *second*. One notes that since these values are not the same (and of opposite sign), one can be confident that the pair are indeed diastereoisomers.

3.3.1.13 Synthesis of Enantiopure *R,R* & *R,S*-Diastereoisomers of *N*-(1'-(2'-Pyridyl)-ethyl)-(BEDT-TTF)-acetamide

Following the synthesis of the two *half*-donors, each thione was then cross-coupled with the unsubstituted *oxo*-compound in trimethyl phosphite at 80 °C separately, to give impure chiral donors in 55 and 80 % yields respectively, Scheme 3.13.

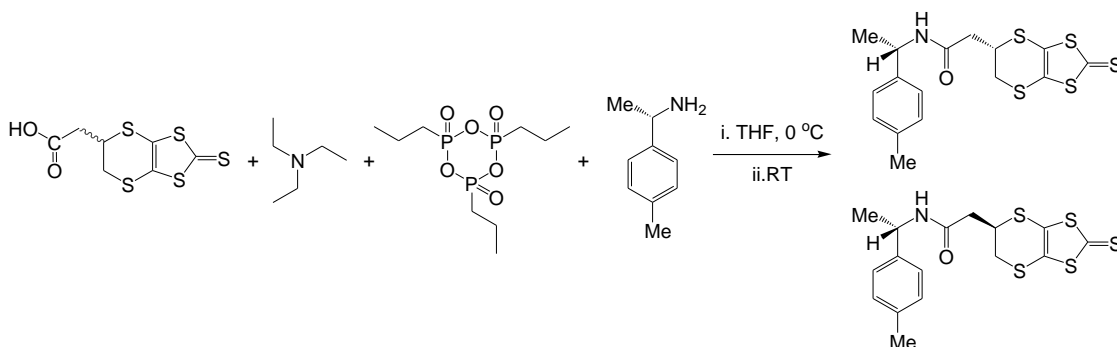


Scheme 3.13 - Synthesis of the full *R,R*- and *R,S*-diastereoisomeric acetamides using (*R*)-1-pyridin-2-yl-ethylamine.

Currently, characterisation data for these *full donors* has been relatively inconclusive and does not allow one to make comparative comments. It would appear that perhaps the cross-coupled enantiomers have not been separated fully from the initial BEDT-TTF product and trimethyl phosphite material, such that they are very impure. The melting points recorded for both *R*-type donors are the same for each *full donor*; 105-108°C. One notes that the yield of both donors is over 50% higher than all other donors synthesised, indicating the presence of impurities. The lack of reported data points towards a further purification being needed for these donors. As such, it was not possible to isolate pure full-donors of this type and they are not carried further at this time.

3.3.1.14 Synthesis of the *S,S* & *S,R*-Diastereoisomers of *N*-(1'-(4''-Methylphenyl)-ethyl)-2-thioxo-5,6-dihydro-[1,3]dithiolo[4,5-*b*][1,4]dithiin-5-yl-acetamide

Finally, following the full synthesis of the *N*-1-pyridin-2-yl-ethylamine family of four diastereomeric isomers, a one further synthesis of a third family functionalised chiral acetamides was performed using *S*-1-(*p*-tolyl)ethanamine. After reaction with the *carboxythione* in the presence of T3P, the two isomeric acetamides were separated by chromatography and obtained in yields of *ca.* 26 % and 28 % respectively as golden/orange crystalline solids, *Scheme 3.14*.



Scheme 3.14 - Synthesis of the half *S,S*- and *S,R*- diastereoisomeric acetamides using *S*-1-(*p*-tolyl)ethanamine.

The structure of *first* eluted *half-donor* was confirmed *via* x-ray crystallography to hold the (*S*)-configuration at 5-C, to yield the full stereochemistry as (*1''S*, *5S*)-, and therefore the latter is assumed as (*1''S*, *5R*)-, following the system adhered to throughout based upon the reported literature for the *R*- α -methylbenzylamine donors synthesised by *Wallis et al.*³

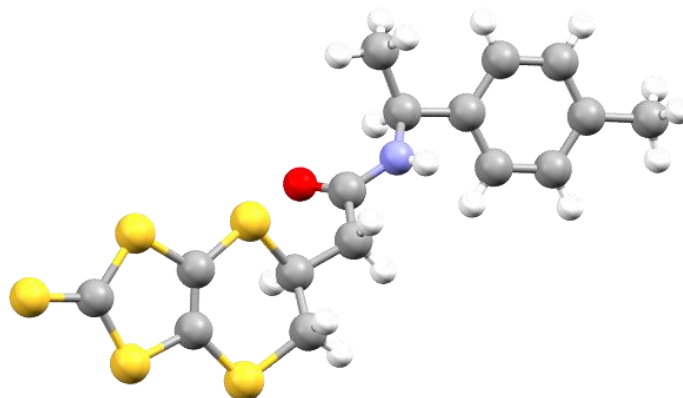


Figure 3.4 - Molecular structure of the first (*S,S*)-half donor, showing the (*S*)-stereochemistry at 5-C on the dithiophene ring. No solvent appears in this structure.

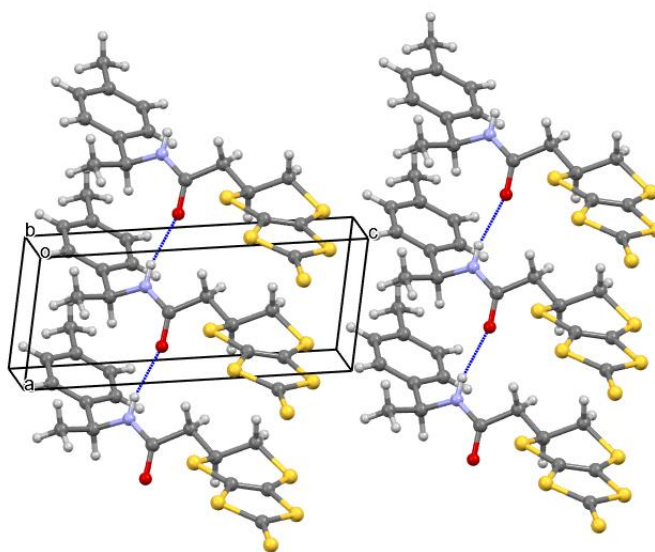


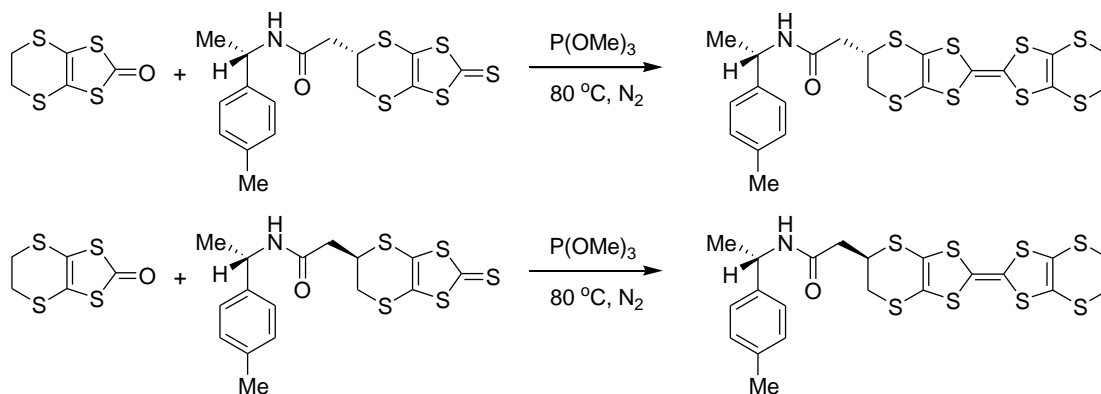
Figure 3.5 – Packing of the donor molecules within the crystal structure of the *S,S*-half donor. For clarity, the acetone solvent molecules are not displayed.

Crystal data at 120K: C₁₆H₁₇NOS₅, *M* = 399.650, golden needle, Triclinic, *a* = 4.7188(1), *b* = 8.5874(1), *c* = 11.6175(2) Å, α = 100.029(1), β = 99.597(2), γ = 100.468(2)°, *U* = 446.191(14) Å³, *T* = 120 K, space group *P1*, *Z* = 1, reflections collected = 3513, independent reflections = 3426, *R1* = 0.0360, *wR2* = 0.0975 [*F*² > 2 σ (*F*²)], Flack parameter = -0.008(6), Residual electron density = 0.36 and -0.32 eÅ⁻³.

Aside from XRD, both sets of methylene groups display differences with the ^1H NMR of each *half-donor*; for the side chain methylene group in the *first (S,S) half-donor*, the signal appears as a doublet at δ : 2.73 ppm, but in the *second (S,R) half-donor*, it appears as two doublet doublets at δ : 2.77 and 2.69 ppm. The methylene group on the dithiin ring adjacent to the chiral centre was split into two separate doublet of doublets signals for each isomer, at δ : 3.43 and 3.16 ppm for the *S,S-half donor* and δ : 3.48 and 3.27 ppm for the *S,R-half donor*. The thione groups for both isomers appear in ^{13}C NMR with signals at δ : 207.8 ppm. Once again, further evidence to indicate the successful synthesis of diastereoisomers as opposed to a racemic mixture can be obtained from the specific rotation values for each *half-donor*; having specific rotation values of $[\alpha]_D^{22} = -130$ and $+188$ respectively, for the thiones *first* and *second*. One notes that since these values are not the same (and of opposite sign), one can be confident that the pair are indeed diastereoisomers.

3.3.1.15 Synthesis of Enantiopure *S,S-* and *S,R-Diastereoisomers* of *N*-((4''-Methylphenyl)-ethyl)-(BEDT-TTF)-acetamide

Following the synthesis of the two *half-donors*, each thione was then cross-coupled with the unsubstituted *oxo-compound* in trimethyl phosphite at 80 °C separately, to give their corresponding chiral donors in 28 % yields, *Scheme 3.15*.



Scheme 3.15 - Synthesis of the full *S,S-* and *S,R-diastereomeric acetamides* using *S*-1-(*p*-tolyl)ethanamine.

In lieu of XRD data for the *full donors*, one assumes the chirality remains the same for the above synthesis and comments upon the relative success of these donors using the ^1H and ^{13}C data collected, as well as specific rotation. Once again, the loss of the thione signal from ^{13}C NMR which was previously observed at δ : 207.6 ppm, is noted for these *full-donors*. In the ^1H NMR spectra, the signals for the methylene group in the dithiin ring at 6-C displays two pairs of doublet doublets at δ : 3.30 and 3.02 ppm for the assumed *SS-donor*, and two

pairs of doublet doublets at δ : 3.38 and 3.15 ppm for the assumed *S,R-donor*. When looking at the proton signals for the methylene groups on the chiral side-chain, one observes a doublet at δ : 2.62 ppm for the *S,S-donor*, and a pair of doublet doublets at δ : 2.67 and 2.59 ppm for the *S,R-donor*. One then measures the specific rotation of each donor for further evidence to indicate that these products are diastereoisomers as opposed to a racemate. The *S,S-donor* had a specific rotation value of $[\alpha]_D^{20} = + 49.8$, and the *S,R-donor* had a specific rotation value of $[\alpha]_D^{20} = + 86.4$; these values are not the same suggesting a successful diastereoisomeric donor synthesis.

One notes that the *R*-counterparts have not yet been synthesised owing to cost of the *R*-1-(*p*-tolyl)ethanamine starting material as well as time constraints, though this is a natural next step for future syntheses.

3.3.2 Cyclic Voltammetry

Cyclic voltammetry measurements were performed on all successfully synthesised full donor molecules (with the exception of the full N-pyridyl-type donors as a result of purity issues) to determine their relative oxidation potentials, *Table 3.1*. The cyclic voltammograms were measured in a 0.1 M solution of *n*-Bu₄NPF₆ in dichloromethane using a scan rate of 100 mV s⁻¹. All six donors showed the expected two reversible oxidation potentials, with potentials relative to the Ag/AgCl reference electrode of 0.51-0.55 V and 0.90-0.93 V.

Table 3.1 - Cyclic voltammetry data for synthesised donors, giving oxidation potentials for each donor molecule, measured relative to Ag/AgCl, with n-Bu₄NPF₆ in CH₂Cl₂ as the charge-carrier using a scan rate of 100 mV s⁻¹.

Donor	E ₁ / V	E ₂ / V
<i>S,S-N</i> -(1'-phenylethyl)-(BEDT-TTF)-acetamide	0.51	0.90
<i>S,R-N</i> -(1'-phenylethyl)-(BEDT-TTF)-acetamide	0.53	0.93
<i>R,R-N</i> -(1'-phenylethyl)-(BEDT-TTF)-acetamide	0.55	0.91
<i>R,S-N</i> -(1'-phenylethyl)-(BEDT-TTF)-acetamide	0.52	0.91
<i>S,S-N</i> -((4''-Methylphenyl)-ethyl)-(BEDT-TTF)-acetamide	0.52	0.91
<i>S,R-N</i> -((4''-Methylphenyl)-ethyl)-(BEDT-TTF)-acetamide	0.54	0.93

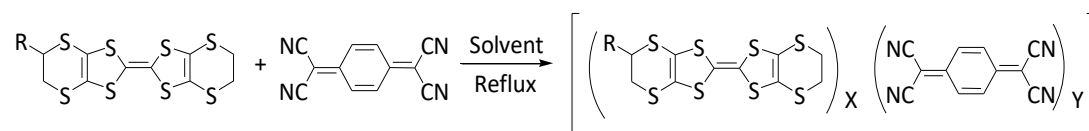
According to *Table 1*, the synthesised donors show two oxidation potentials which are similar to those of BEDT-TTF; (E₁ = 0.500 V and E₂ = 0.910 V).¹⁵⁵ Results for the *R,R*- and *R,S*- α -methyl donors match those reported by *Wallis et al.* relatively well; *R,R-donor* (E₁ = 0.560 V and E₂ = 0.950 V) and *R,S-donor* (E₁ = 0.520 V and E₂ = 0.910 V).³ Owing to the vast success of charge-

transfer salts synthesised in literature thus far with BEDT-TTF and different acceptor molecules including TCNQ,^{2,12} and I₂,¹⁵⁶ one suggests that the novel families of donors synthesised by the author in this body of work will also be able to produce salts with similar acceptors since their oxidation potentials are similar to those observed for BEDT-TTF. Moreover, this comparison allows one to propose that the BEDT-TTF motif is present and fully intact for charge-transfer salt synthesis. Salts with TCNQ are currently the most desired as a result of the previously published ϑ -(1'R,5S)-N-(1'-phenylethyl)(BEDT-TTF)acetamide)₄TCNQ by the research group in 2020.² One is hopeful that all donors (including the *pyridyl*-types when purified further) will achieve similar salts and allow the study of eMChA and other chirality-induced properties, should they be observed.

3.3.3 Analysis of the Synthesis of Charge-Transfer Salts Under Reflux Conditions

3.3.3.1 Synthesis of Charge-Transfer Salts from Novel Donor Molecules with TCNQ

Following the successful synthesis of novel donor families of diastereoisomers, one was hopeful in the synthesis of charge-transfer salts with TCNQ so that comparisons between the recently reported ϑ -(1'R,5S)-N-(1'-phenylethyl)(BEDT-TTF)acetamide)₄.TCNQ salt and subsequent novel salts using novel donors synthesised in this body of work.² Reactions of the BEDT-TTF-based donors and the TCNQ-acceptor were conducted under reflux conditions all reactions followed the same basic approach, *Scheme 3.16*. To an RBF, a 4:1 molar ratio of donor molecule and TCNQ were dissolved in DCM. This reaction mixture was subsequently refluxed, and the resulting solution was sealed with a rubber stopper equipped with a fine needle to allow the slow evaporation of the solvent. Once the solvent had evaporated, each sample was checked for crystallinity and a number of recrystallisations using several different solvents (CHCl₃, DCM, EtOH, MeOH *etc.*) were performed where necessary. *Table 3.2* reports the observations arising from these refluxes.



Scheme 3.16 - General reaction scheme for the synthesis of charge-transfer salts with new donors and TCNQ.

Table 3.2 – Results of the reflux reactions between novel donor molecules and TCNQ.

Donor	Result
<i>S,S,N-(1'-phenylethyl)-(BEDT-TTF)-acetamide</i>	Slow evaporation of solvent followed by recrystallisation in CH ₂ Cl ₂ yielded a black amorphous solid and green TCNQ crystals.
<i>S,R,N-(1'-phenylethyl)-(BEDT-TTF)-acetamide</i>	Slow evaporation of solvent produced a beautiful black clustered-crystalline solid with some green TCNQ crystals.
<i>R,R,N-(1'-phenylethyl)-(BEDT-TTF)-acetamide</i>	Slow evaporation of solvent followed by recrystallisation in CH ₂ Cl ₂ yielded a black amorphous solid and green TCNQ crystals.
<i>R,S,N-(1'-phenylethyl)-(BEDT-TTF)-acetamide</i>	Slow evaporation of solvent followed by recrystallisation in CH ₂ Cl ₂ yielded black crystals.
<i>S,S,N-(4'-Methylphenyl)-ethyl)-(BEDT-TTF)-acetamide</i>	Slow evaporation of solvent followed by recrystallisation in CH ₂ Cl ₂ yielded a black amorphous solid and green TCNQ crystals. Further recrystallisation could not be performed due to time constraints.
<i>S,R,N-(4''-Methylphenyl)-ethyl)-(BEDT-TTF)-acetamide</i>	Slow evaporation of solvent followed by recrystallisation in CH ₂ Cl ₂ yielded a black amorphous solid and green TCNQ crystals. Further recrystallisation could not be performed due to time constraints.

When one analyses the table above, one notes that there are a number of different results arising from all reactions; with each yielding at the very least, black amorphous solids. Although not crystalline, the vast array of amorphous solids yielded are positive indicators that the reaction between each donor and TCNQ have been a success, one just needs to find the optimal recrystallisation solvent to yield the highly desired black crystals. Moreover, it indicates that these simple reflux reactions are a fruitful method for synthesising charge-transfer salts, one just needs to refine the recrystallisation process. Those which yielded some green crystalline solid was assumed to be excess TCNQ, Those which appeared to be crystalline material were extracted from the flask and studied *via* XRD for their structures, of

which were *S,R-N-(1'-phenylethyl)-(BEDT-TTF)-acetamide* and *R,S-N-(1'-phenylethyl)-(BEDT-TTF)-acetamide*.

3.3.3.2 Crystallographic Data for Charge-Transfer salts of Donors with TCNQ

The first reaction to yield crystalline solid was that involving the *S,R-N-(1'-phenylethyl)-(BEDT-TTF)-acetamide*, whereby a beautiful black clustered-crystalline solid was observed. This result was particularly exciting since it is the enantiomeric counterpart to the previously published charge-transfer salt of the *R,S-N-(1'-phenylethyl)-(BEDT-TTF)-acetamide*. Prior to NTU purchasing the rotating-anode diffractometer, the crystals could not be measured using the Rigaku Oxford Xcalibur diffractometer due to sensitivity incompatibilities with the crystal size; these crystals were therefore sent to Southampton University for measurement by the National Crystallographic Service (NCS). Rather anti-climactically, results for these crystals were inconclusive and further recrystallisation proves necessary. However, a unit cell determination supported that the same structure had been obtained for the *S,R* that was obtained for the published *R,S*, but the crystals were too small for a full data collection at neither NTU, nor Southampton University. One then comments on the unsuitability of said crystals for physical property measurements, in that the crystals are simply too small.

The second reaction to yield crystalline solid was that employing the *R,S-N-(1'-phenylethyl)-(BEDT-TTF)-acetamide* in the form of black crystals. This charge-transfer salt is the same as that reported by *Short et al.* from 2018 and therefore structures are not reported having been previously published by the research group. Despite this, it did allow one to observe the proof of concept for future donors.

Those which were amorphous black powders require recrystallisation refinement, though one did observe that the round-bottomed flask appeared to give the most success, as well as using CHCl_3 as a solvent. Other solvents consistently yielded powders, whereas some crystalline material was yielded using chloroform.

3.4 Conclusion

Following the successful synthesis of a chiral charge-transfer salt displaying molecular switching capabilities around ambient temperatures by previous members of the research group in 2020,² focus upon synthesis of similar BEDT-TTF-based donor/TCNQ salts has been unwavering. Using the methodologies reported by *Wallis et al.*,³ a range of eight new unsymmetrically substituted enantiopure donors are now available, as well as two previously-synthesised donors. These novel donors are in the form of four pairs of diastereoisomers, with varying constituents around the chiral amine centre. The slight modifications made to the newly synthesised donor molecules compared were designed to add steric bulk and hinderance in different manners to the chiral portion of the sidechain. Going forward, the challenge pertains to the successful preparation of conducting systems from them in the form of crystalline charge-transfer salts. This will subsequently allow one to study how their chirality moderates their electromagnetic properties by a comparison of the properties of products prepared from opposite enantiomers.

The relative success of each synthesis was followed *via* ¹H and ¹³C NMR, as well as cyclic voltammetry, specific rotation and in some cases, HRMS. The cyclic voltammetry studies of six of the synthesised donor molecules was collected and each resulted in similar oxidation potentials of *ca.* 0.500 V and 0.900 V relative to an Ag/AgCl reference electrode. Each donor appears to undergo two reversible oxidation potentials similar to those of BEDT-TTF,¹⁵⁵ allowing one to propose that the BEDT-TTF motif is present and fully intact for charge-transfer salt synthesis.

During the aforementioned syntheses of these novel thiones and donors, one was able to yield two x-ray structures to aid in the theory for which the order of the products elute in; for the synthesis of the *S,S*- and *S,R*-*N*-(1'-phenylethyl)-(BEDT-TTF)-acetamide diastereoisomers, the *first* eluting donor product yielded orange/pink crystals after recrystallisation which allowed confirmation that the 5-C chiral centre holds the *S*-configuration, such that the donor is of the *S,S*-type. Secondly, in the synthesis of the *S,S* & *S,R*-diastereoisomers of *N*-(1'-(4''-Methylphenyl)-ethyl)-2-thioxo-5,6-dihydro-[1,3]dithiolo[4,5-*b*][1,4]dithiin-5-yl-acetamide, the *first* eluting *half-donor* was confirmed to hold the *S*-configuration at 5-C. In both instances, the assumed stereochemistry agreed with that reported by *Wallis et al.* for the *R*-type thiones and donors.³ One has therefore followed

these assumptions throughout in lieu of XRD data to confirm the absolute stereochemistry for those yielding solids that were unsuitable for study using this technique.

It can be noted that the *pyridyl*-type *full-donors* were notoriously difficult to separate as a result of the presence of a tertiary amine within the benzene ring. Column conditions were altered to increase the basicity of the system using 0.5 % triethylamine to allow separation of the two diastereoisomeric *half-* and *full-donors*. Given that one obtained well-matching data for the *half-thiones*, it would appear that the problem of purity appears to arise in the synthesis of the *full-donor* motifs for both the *R*- and *S*-types. Of all ten syntheses, these four *full-donors* appear to be the least successful and require further purification to comment fully. Due to time constraints, one was not able to complete this step, however, one remains positive that the *full-donors* can be yielded with satisfactory data to support in future, and therefore allow further synthesis of charge-transfer salts for this new family of donors.

It is with some frustration that one could not synthesise suitable crystalline charge-transfer salts during this project, although one is confident that they have been successful, just as powders/amorphous solids. Once the ideal crystallisation parameters have been discovered, these new donors could be fundamental in the study of chirality-induced differences in electrical and physical properties of (*super*)conducting charge-transfer salts. Should similar θ -type TCNQ salts of these new donor molecules be yielded, one proposes that the added steric bulk of the *p-tolyl* and *pyridyl* systems will force subtle changes in the packing arrangement of the donor molecules, which in turn may lead to changes in the electronic properties of the salts when compared to those observed for the θ -(1'*R*,5*S*)-N-(1'-phenylethyl)(BEDT-TTF)acetamide)₄.TCNQ salt.² As it stands, not only has the aim of synthesising novel families of chiral donor molecules been successful, this research provides a clear synthetic pathway for further synthesis of similar donor molecules and their relative studies.

4. BEDT-TTF salts with Metal Trisoxalate Anions

4.1 Introduction

Extensive research has been performed in the field of molecular conductors with TTF-based systems ever since the first observation the charge-transfer salt of TTF-TCNQ in 1973.²⁷ Many (*super*)conducting BEDT-TTF salts have since been synthesised, including the (BEDT-TTF)₂I₃ family,^{84–89,131} the κ-(BEDT-TTF)-copper systems,^{92,93} and the Peter Day family of metal trisoxalate BEDT-TTF salts.^{97,108,129,132,133}

Transition-metal complexes have been extensively used in charge-transfer salts of BEDT-TTF since they offer a unique opportunity to combine a di-and trifecta of properties within the same lattice, utilising two or more from chirality, conductivity and magnetism. The most extensively studied family of these salts are those with metal trisoxalate anions, examples synthesised thus far include ferromagnetic conductors,¹⁰⁷ paramagnetic superconductors,¹⁰⁸ antiferromagnetic semiconductors,¹⁰⁹ and metallic proton conductors.¹¹⁰ Owing to the unique ability of the metal trisoxalate anion [M(C₂O₄)₃]³⁻ to form infinite 2D sheets in a hexagonal network, making subtle changes to the crystal structure is possible in a number of ways including changing the metal centre, the counter cation, or the guest solvent molecule located within the hexagonal cavities of the 2D sheet. Small changes such as these can impart a drastic effect upon the crystal structure and thus the physical properties arising from the material.

A number of different types of charge-transfer salts of BEDT-TTF with metal trisoxalate anions have been studied thus far, including 4:1, 3:1,^{122–124,126} 2:1,^{110,157,158} as well as other interesting phases. The 4:1 family was established by *Day et al.* in 1995, whereby the synthesis of the first molecular paramagnetic *superconductor* was performed to yield the salt β''-(BEDT-TTF)₄[(H₃O)Fe(C₂O₄)₃]·PhCN.^{108,133,159,160} This important discovery still holds the record for the highest *T_c* of all known BEDT-TTF/metal trisoxalate superconductors to date, at 8.5 K. Twenty-nine *superconductors* of the monoclinic β'' salts have since been prepared with the same formula, making these salts the most widely-studied of all BEDT-TTF/metal trisoxalate charge-transfer salts. Marked effects upon the conductivity of salts of this type appear to arise when the size and shape of the guest solvent molecule is altered, as opposed to changes to the metal centre or counter cation.¹⁶¹ The highest *superconducting T_c's* are observed when larger guest molecules occupy the hexagonal cavity of the 2D sheets. Specific

interest lies with those which increase the *b* axis length of the hexagonal cavity; benzonitrile appears to extend this axis length the furthest.

Within this 4:1 family of salts, one may yield the *superconducting* β'' C2/c salt, or the *semiconducting pseudo- κ* Pbcn salt, depending on the way in which the BEDT-TTF donor molecules pack within the crystal structure. The chemical formula remains the same as before, but the packing arrangement leads to changes in the anion layers of the salts. Though they look almost identical, the β'' salts have alternating layers of enantiopure metal trisoxalate anions, such that one layer holds the Λ (L) conformation and the next holds the Δ (D) conformation, repeating in this manner throughout the crystal lattice. In the case of the *pseudo- κ* salts, each anion layer contains a racemic 50:50 mixture of the D and L enantiomers.

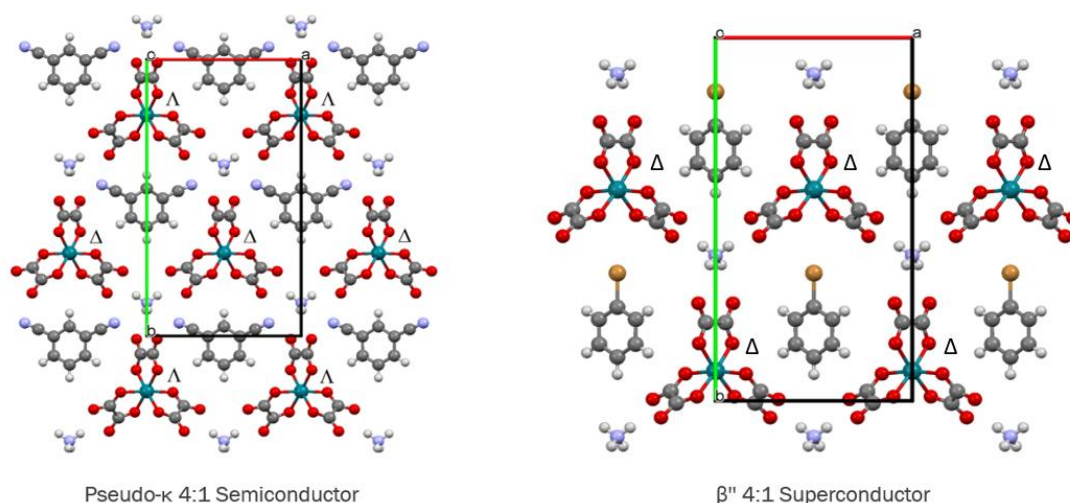


Figure 4.1 - Packing arrangements of the anion layer within the 4:1 salts; the pseudo- κ phase on the left shows alternating enantiomers within the same layer, whereas the β'' phase on right shows the singly-enantiomeric layer.

The use of metal trisoxalate anions in BEDT-TTF salts offers the potential to synthesise chiral conductors, since these anions are themselves chiral and crystallise in Λ or Δ forms; a number of chiral semiconductors have already been synthesised *via* chiral induction by using the chiral solvents (*R*)-(-)-carvone,^{122–126} and (*S*)-*sec*-phenethyl alcohol.¹²⁷ The diversity of packing arrangements of the metal trisoxalate anions with BEDT-TTF donor molecules has led to an extensive family of *insulators, semiconductors, metals and superconductors*. Although there have been no novel effects upon the bulk physical properties observed, the inclusion of other components such as guest solvent molecules, cations and crown ethers have produced a wealth of multifunctional materials with properties such as proton conductivity.¹¹⁰ The synthesis of materials combining chirality and conductivity are important to explore the

aforementioned electrical magneto-chiral anisotropy (eMChA). A vast array of novel guest molecules have been employed in this body of work, in the hope to synthesise the desired 4:1 β'' salts, which will in turn allow one to investigate the proposed relationship between the increasing of the b axis length of the cavity upon conductivity.

4.2 Experimental

All reagents and solvents were purchased from Alfa Aesar, Fischer Scientific, Fluorochem, Merck or TCI chemicals and used as provided. Chemical manipulations were carried out in oven-dried glassware and in an atmosphere of air unless otherwise stated.

4.2.1 BEDT-TTF salts with Metal Trisoxalates and Benzonitrile

Since salts having the formula $(\text{BEDT-TTF})_4[(\text{H}_3\text{O})\text{M}(\text{C}_2\text{O}_4)_3]\cdot\text{benzonitrile}$ give a *superconducting* β'' M = Fe or Cr, with the iron salt having the second highest T_c in the series, there has been interest in obtaining the β'' salt of benzonitrile with other metal trisoxalates.^{108,129,132,133} Japanese collaborators of the Martin research group are particularly interested in obtaining a non-magnetic series of salts using the metals M = Al, Ga, Co, Ir and Rh. This formulated the first focus of this secondary project aim. All metal trisoxalates employed in this section had been synthesised and recrystallised by previous members of the Martin research group, such that they are not reported here.

Synthesis of these non-magnetic salts were attempted using three published literature methods referred to here as pyridine,⁹⁷ methanol,^{161,162} and 1,2,4-trichlorobenzene methods.^{160,163} The conditions which each method employs are detailed below.

4.2.1.1 The Pyridine Method⁹⁷

Metal trisoxalate (120 mg) and 18-crown-6 ether (200 mg) were added to benzonitrile (40 ml) and pyridine (1 ml). The mixture was stirred overnight before gravitational filtration into two clean H-cells. BEDT-TTF (10 mg) was added to the anode side of each H-cell before sealing of each cell with two platinum electrodes and connection to a circuit to allow crystal growth at 0.5 μA for a number of weeks undisturbed.

4.2.1.2 The Methanol Method^{161,162}

Metal trisoxalate (90 mg) and 18-crown-6 ether (180 mg) were added to a 10:1 benzonitrile/methanol solvent system (40 ml). The mixture was stirred overnight before gravitational filtration into two clean H-cells. BEDT-TTF (10 mg) was added to the anode side of each H-cell before sealing of each cell with two platinum electrodes and connection to a circuit to allow crystal growth at a) 0.5 μA for one cell and b) 3 μA for the second cell, for a number of weeks undisturbed.

4.2.1.3 *The 1,2,4-Trichlorobenzene Method*^{160,163}

Metal trisoxalate (100 mg) and 18-crown-6 ether (200 mg) were added to 1,2,4-trichlorobenzene (10 ml), benzonitrile (10 ml) and ethanol (2 ml). The mixture was stirred overnight before gravitational filtration into two clean H-cells. BEDT-TTF (10 mg) was added to the anode side of each H-cell before sealing of each cell with two platinum electrodes and connection to a circuit to allow crystal growth at 0.5 μ A for a number of weeks undisturbed.

4.2.2 *BEDT-TTF salts with Metal Trisoxalates and New Guest Molecules*

Metal trisoxalate (100 mg), 18-crown-6 ether (250 mg) and guest (100 mg) were added to 1,2,4-trichlorobenzene (15 ml) and ethanol (3 ml). The mixture was stirred overnight before gravitational filtration into two clean H-cells. BEDT-TTF (10 mg) was added to the anode side of each H-cell before sealing of each cell with two platinum electrodes and connection to a circuit to allow crystal growth at 0.5 μ A for a number of weeks undisturbed.

A variety of guest concentrations were employed during these syntheses, ranging from 100 mg up to 10 g of guest to allow one to observe any increase in crystal quality and/or success of salt growth in changing this parameter. One found this variation relatively inconclusive, since no real trend was observed in salt growth success as a function of guest concentration, and indeed it appears that a larger number of publishable structures were yielded from syntheses employing the former milligram scale. The chosen guest molecules studied ranging in size, shape and chirality were as follows:

4.2.2.1 *Iron Trisoxalate Syntheses*

Salicylaldehyde, imidazole, 2-chloro-6-hydroxybenzoic acid, phthalic acid, 2,6-pyridinedicarboxylic acid, p-benzoquinone, 4-methylcatechol, chelidonic acid, 2-aminophenol, chloroanilic acid, squaric acid, R-(-)-mandelic acid, L-valine, L-alanine, D-alanine, m-toluic acid, o-toluic acid, 2,5-pyridinedicarboxylic acid, chlorobenzene, benzaldehyde, benzoic acid, L-carvone, picolinic acid, aniline, o-chloranil, 1-hydroxy-2-naphthoic acid, L-(+)-tartaric acid, 3-hydroxy-2-naphthoic acid, 2-aminopyrimidine, D-(-)-quinic acid, L-(-)-phenyl-lactic acid, kojic acid, D-(-)-tartaric acid, S-(+)-mandelic acid, meso-hydrobenzoin, bromobenzene, fluorobenzene, toluene, D-camphor, cyclohexane, thiobenzoic acid, α -methylbenzylamine, sodium-rhodizonate, 2-hydroxypyridine, o-xylene, m-xylene, p-xylene, S-(+)- & R-(-)-cyclohexylethylamine, benzenesulphonic acid,

phenylboronic acid, TBA-thiophenolate, 4H-pyran-4-one, anisole, picolinic acid, TBA-p-nitro-phenoxide, TBA-p-toluenesulphonate, cumene.

4.2.2.2 *Chromium Trisoxalate Syntheses*

2-Aminopyrimidine, benzenesulphonic acid, thiobenzoic acid, phenylboronic acid, TBR-thiophenolate, aniline, benzaldehyde, benzoic acid, 4H-pyran-4-one, toluene, anisole, picolinic acid, TBA-p-nitro-phenoxide, TBA-p-toluenesulphonate, cumene.

4.2.3 *Electrocrystallisation using H-cells*

To ensure optimal growth conditions and prevention of contamination, both the H-cells and the electrodes were thoroughly cleaned prior to operation. The electrodes were cleaned by applying a small current whilst submerged in 1M H₂SO₄. Terminals are then swapped multiple times to change direction of the current, giving rise to effervescence at the surface of the electrode which indicates the evolution of H₂ and O₂. Following this, the electrodes are washed with distilled water and ethanol before drying thoroughly. The H-cells were cleaned by addition of acetone to one compartment and leaving to diffuse through a glass frit. This was repeated multiple times, after which distilled water was employed in the same manner. Once each cell had been cleaned, they were left to dry in a glassware oven, at *ca.* 80 °C.

After dissolution of the metal trisoxalate with appropriate guest in solvent, the mixture was filtered into a clean and dry H-cell. BEDT-TTF donor was placed into the front compartment of the cell and a platinum electrode is placed into either side, separated by a porous glass frit to prevent contamination between the anodic and cathodic solutions. All joints present on electrodes and H-cells were sealed tightly with paraffin film. The front electrode is connected to the anode and the back electrode is connected to the cathode, such that a current may flow as a result of the circuit. The cells are then left at constant current to allow for electro-crystallisation under vibration free conditions at constant temperature. Crystals of the charge-transfer salt slowly form on the platinum anode, with crystal size and quality depending on the growth conditions such as current, solvent combination, quality of reactants and environmental surroundings. The cells were fixed firmly in place within black-out boxes on a vibration free table and kept at a constant temperature of 293K. Currents used during this project ranged between 0.5 and 3.0 μ A, depending on the method employed.

After a number of weeks, any cells which showed crystal growth were detached from the current source and the crystals were harvested. The electrode was carefully removed and rinsed with acetone to remove single crystals onto a piece of filter paper. Crystals that remained within the cell solution were obtained *via* filtration of said solution and washing with acetone. It has previously been observed that the second and third crystal batches obtained from a single solution are markedly better quality as a result of higher cation concentration influencing higher nucleation uniformity and therefore enhanced growth. As such, after removal of the first crystals, the remaining solution was filtered into a freshly cleaned and dried H-cell containing donor and electrocrystallisation was re-attempted under the same conditions as before. This method may be repeated up to *ca.* three times.

4.2.4 X-ray Crystallography

Several structures presented in this thesis were analysed at room and low temperatures at NTU, Osaka University in Japan and the National Crystallographic Service (NCS) in Southampton. Data was collected in Osaka by Professor Hiroki Akutsu on a Rigaku R-AXIS VII imaging plate system with FR-E SuperBright High-Brilliance Rotating Anode Generator with confocal mono-chromated MoK α radiation, using Rapid Auto software for control and processing. Structures were solved *via* programs from the SHELX family by direct methods and refined on F2 full-matrix least squares using all unique data. Data was collected at the NCS on a Rigaku AFC12 diffractometer with Mo rotating anode, using standard control and processing software. Structures were solved *via* programs from the SHELX family by direct methods and refined on F2 full-matrix least squares using all unique data. Data was collected at NTU on both a Rigaku Oxford Xcalibur, Sapphire3, Gemini four-circle diffractometer with a graphite monochromator using monochromatic Molybdenum K α radiation ($\lambda = 0.7107 \text{ \AA}$) or Copper K α radiation ($\lambda = 1.5406 \text{ \AA}$) at either room temperature or a constant temperature of 150.00(10) K. This diffractometer was subsequently replaced by a Rigaku Rotating Anode XtalLAB Synergy-DW equipped with Cu/Mo radiation. Structures were solved using programs from the SHELX family within OLEX2 by direct methods and refined on F2 full matrix least squares using all unique data. Molecular illustrations included in this body of work were made with Mercury using POV-Ray.¹⁴⁶

4.2.5 Resistivity Measurements

Four-probe DC transport measurements were made on crystals using a HUSO HECS 994C multi-channel conductometer. Gold wires (*ca.* 15 μm diameter) were attached to the crystal,

and the attached wires were connected to an integrated circuit plug with carbon conductive cement.

4.3 Results and Discussion

This section reports the crystal structures and electrical resistivity measurements of six new BEDT-TTF salts with metal trisoxalate anions. Firstly, one explores the inclusion of benzonitrile as guest when using iridium trisoxalate, since the β'' salt of iron trisoxalate was the first, and is still one of the highest *superconducting* T_c salts in this family. Secondly, one attempts to introduce new guest molecules for the first time; ethanol, toluene, 2-phenoxirane, kojic acid & tartaric acid, which has produced a variety of new BEDT-TTF packing arrangements, giving both *semiconductors* and *metals*.

4.3.1 BEDT-TTF salts with Metal Trisoxalates and Benzonitrile

The first, and also the most extensively used guest molecule in the BEDT-TTF-metal trisoxalate series of salts is benzonitrile. Salts having the formula $(\text{BEDT-TTF})_4[(\text{A})\text{M}(\text{C}_2\text{O}_4)_3]\cdot\text{benzonitrile}$ give a *superconducting* β'' salt ($\text{A} = \text{H}_3\text{O}^+$) and a *semiconducting pseudo- κ* salt ($\text{A} = \text{K}^+$ and NH_4^+) when $\text{M} = \text{Fe}$ or Cr .^{108,129,132,133} As well as being the first guest molecule used, the *superconducting* T_c of the $\text{M} = \text{Fe}$ β'' salt with benzonitrile is the second highest in the series, such that there has been interest in obtaining the β'' salt of benzonitrile with other metal trisoxalates. Despite the ease with which the $\text{M} = \text{Fe}$ or Cr produces the β'' salt it has not been possible to obtain this phase when $\text{M} = \text{Ga}$, Rh , Mn , Al , Co , Ru , or Ru , which produce only the *semiconducting pseudo- κ* phase. This *pseudo- κ* phase is only obtained when using benzonitrile as a guest molecule despite the extensive range of guest sizes and shapes that have been employed.^{129,132}

4.3.1.1 *pseudo- κ* -(BEDT-TTF)₄[(H₃O)Ir(C₂O₄)₃].PhCN⁴

Similarly to the $\text{M} = \text{Mn}$, Al , Co , Rh , or Ru cases when using benzonitrile, only crystals of the *pseudo- κ* phase $(\text{BEDT-TTF})_4[(\text{H}_3\text{O})\text{Ir}(\text{C}_2\text{O}_4)_3]\cdot\text{benzonitrile}$ can be obtained. This is despite numerous attempts using all previously reported methods of obtaining the β'' phase. Better quality crystals were obtained when using the crystal growth method which includes 1,2,4-trichlorobenzene,¹⁶⁴ compared to the original method which was used to prepare β'' crystals where $\text{M} = \text{Fe}$.^{108,133}

The crystal structure of *pseudo- κ* -(BEDT-TTF)₄[(H₃O)Ir(C₂O₄)₃].PhCN is the same as the previously published salts with $\text{M} = \text{Fe}$, Cr , Mn , Al , Co , Rh , or Ru .⁴ It crystallises in orthorhombic space group *Pbcn* with two independent donor molecules, half an iridium metal trisoxalate anion, half a benzonitrile and half a H_3O^+ .

Figure 4.2 shows the layered packing, whilst the *pseudo-κ* donor packing is shown in Figure 4.3 and the honeycombed packing of the anion layer in Figure 4.4.

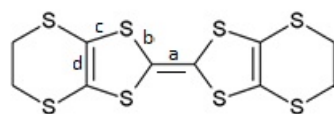
Table 4.1 gives the short S...S contacts between the donors and Table 4.2 provides the estimated charges on the donor molecules. These confirm the *pseudo-κ* arrangement where (BEDT-TTF⁺)₂ dimers are surrounded by six BEDT-TTF⁰ monomers in the donor layer. The electrical resistivity measurements (Figure 4.5) show that *pseudo-κ*-(BEDT-TTF)₄[(H₃O)Ir(C₂O₄)₃].benzotrile is a *semiconducting* salt with an activation energy of 116 meV, which is slightly smaller than observed previously in *pseudo-κ*-(BEDT-TTF)₄[M³⁺(C₂O₄)₃].benzotrile salts, where values are between 140 and 245 meV.^{129,132}

Crystal data: C₅₃H₃₉O₁₃S₃₂N₁Ir₁, *M* = 2115.99, black block, *a* = 10.38140(14), *b* = 19.6057(3), *c* = 35.5790(5) Å, *U* = 7241.56(18) Å³, *T* = 150.00(10) K, space group *Pbcn*, *Z* = 4, *μ* = 12.724 mm⁻¹, reflections collected = 30911, independent reflections = 6344, *R1* = 0.0454, *wR2* = 0.1171 [*F*² > 2σ(*F*²)], *R1* = 0.0503, *wR2* = 0.1200 (all data).

Table 4.1 - Short S...S contacts (>sum VdW radii) in *pseudo-κ*-(BEDT-TTF)₄[(H₃O)Ir(C₂O₄)₃].benzotrile.⁴

S atom 1...	Contact/ Å
S atom 2	
S1...S14	3.2190(17)
S1...S16	3.4418(19)
S7...S10	3.4384(18)
S2...S15	3.5170(19)
S8...S9	3.5214(18)
S2...S11	3.4333(17)
S6...S15	3.5106(18)
S11...S14	3.4460(17)
S12...S13	3.4768(17)

Table 4.2 - Approximation of the charge of BEDT-TTF molecules in pseudo- κ -(BEDT-TTF)₄[(H₃O)Ir(C₂O₄)₃].benzointrile from bond lengths (Å): $\delta = (b + c) - (a + d)$, $Q = 6.347 - 7.463\delta$.⁴



Donor	a	b	c	d	δ	Q
A	1.381	1.725	1.743	1.3505	0.736	0.85+
B	1.343	1.756	1.758	1.340	0.831	0.15+

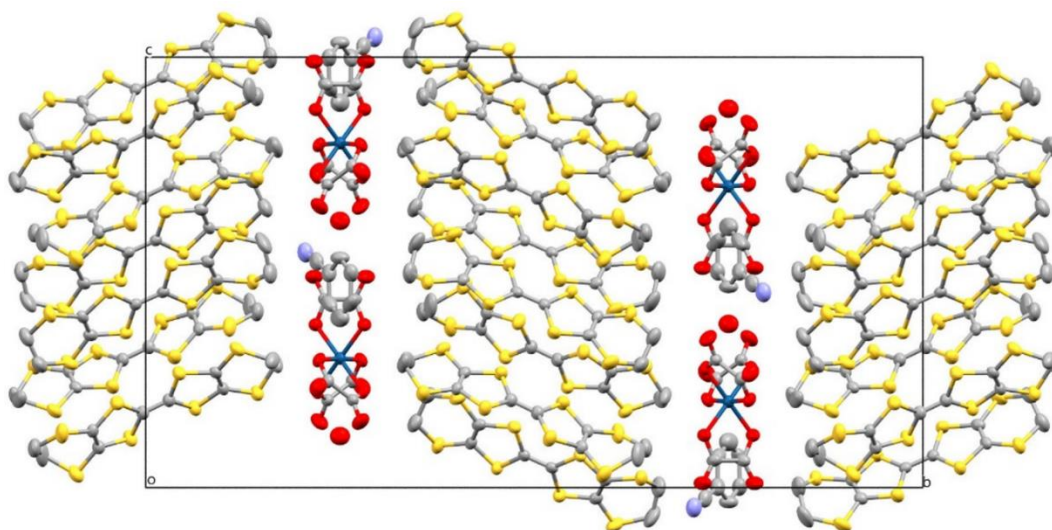


Figure 4.2 - Pseudo- κ -(BEDT-TTF)₄[(H₃O)Ir(C₂O₄)₃].benzointrile viewed down the a axis. Hydrogen atoms and disorder of terminal ethylene groups of BEDT-TTF omitted for clarity.⁴

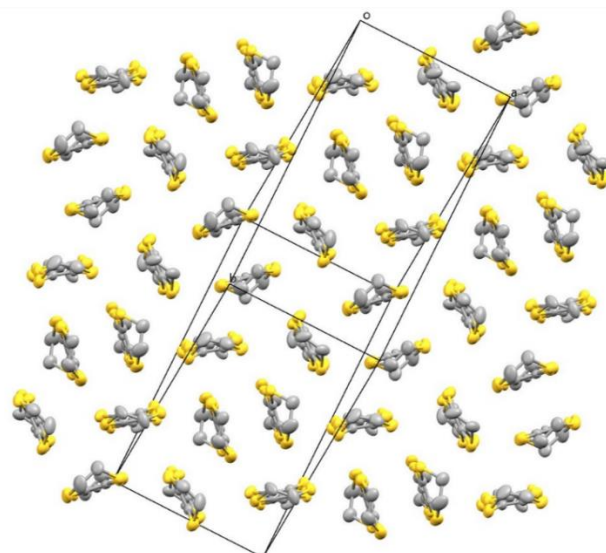


Figure 4.3 - Pseudo- κ -(BEDT-TTF)₄[(H₃O)Ir(C₂O₄)₃].benzotrile donor layer. Hydrogen atoms and disorder of terminal ethylenes of BEDT-TTF omitted for clarity. Distinct donors are clarified in terms of charge in figure 4.7. ⁴

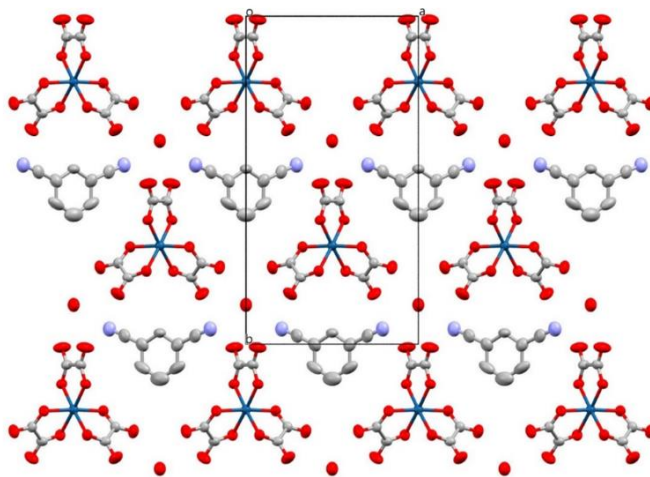


Figure 4.4 - Pseudo- κ -(BEDT-TTF)₄[(H₃O)Ir(C₂O₄)₃].benzotrile anion layer viewed down the *c* axis. Hydrogen atoms omitted for clarity. ⁴

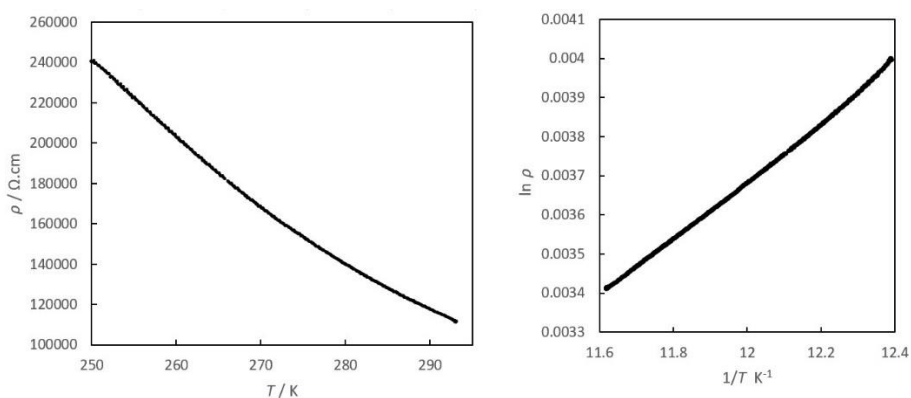


Figure 4.5 - Pseudo- κ -(BEDT-TTF)₄[(H₃O)Ir(C₂O₄)₃].benzotrile electrical resistivity. ⁴

4.3.2 BEDT-TTF salts with Metal Trisoxalate and New Guest Molecules

The aim was to introduce new guest molecules into the hexagonal cavity of *superconducting* salts of β'' -(BEDT-TTF)₄[(A)M(C₂O₄)₃] \cdot guest.^{108,129,132,133} The introduction of guest molecules which increase the *b* axis length of the crystal structure have been found to increase the *superconducting* *T_c*, with benzonitrile and nitrobenzene giving the highest *T_c*'s.¹³⁰

The desired 4:1 β'' -(BEDT-TTF)₄[(A)M(C₂O₄)₃] \cdot guest has been obtained when using toluene as the guest molecule. Novel structures have been obtained with other guests including 5:1 salts with ethanol or tartaric acid as guest, and a 4:1 superstructure having two crystallographically independent β'' layers with 2-phenoxirane as guest. Using D-kojic acid led to the kojic acid replacing one of the oxalate bidentate ligands of the anion which produced a novel 4:1 salt with BEDT-TTF.

Table 4.3 - Details of other guests that were tried but gave no crystals or crystals of phases that are already published or undesired phases.

Structure	Guest
Proton-conducting metal β'' -(BEDT-TTF) ₄ [(A)M(C ₂ O ₄) ₃] ₂ [(H ₃ O ⁺) ₂ 18-crown-6](H ₂ O) ₅ (M = Cr or Ga) ¹¹⁰	Benzaldehyde, Anisole, Picolinic acid, 4H-pyran-4-one, Benzoic acid & Thiophenol.
α'' -(BEDT-TTF) ₅ [M(C ₂ O ₄) ₃] \cdot (H ₂ O) _{3,4} \cdot (EtOH) _{0,6} ¹⁶⁵	Toluic acid & Cumene
P-1 β'' 5:1 phase – similar have been published by Zhang et al. ¹⁶⁶	Aniline
No metal trisoxalate in the charge-transfer salts; anion only	2,5-Pyridinedicarboxylic acid & Benzenesulphonic acid
No crystals/suitable crystals could not be obtained	Mandelic acid, Salicylaldehyde, Imidazole, L-Carvone, D-(-)-Quinic acid, D-Alanine, L-Valine, L-(-)-Phenyllactic acid, Phthalic acid, 4-Methylcatechol, Squaric acid, Sodium rhodizonate, Xylene, 2-Hydroxypyridine, D-camphor, S/R-(-)-cyclohexylethylamine, Thiobenzoic acid, Phenylboronic acid

4.3.2.1 β'' -(BEDT-TTF)₅[Ir(C₂O₄)₃].ethanol

Using acetophenone with ethanol as the electrocrystallisation medium has produced a 5:1 salt β'' -(BEDT-TTF)₅[Ir(C₂O₄)₃].ethanol.⁴ Crystals of this radical-cation salt are obtained when using either the ammonium or potassium salt of tris(oxalato)iridate, and also when changing the solvent to a mixture of 1,2,4-trichlorobenzene:ethanol (10:2). Two semiconducting 5:1 salts of BEDT-TTF salts with metal trisoxalate anions have been published previously: (BEDT-TTF)₅[Fe(C₂O₄)₃].(H₂O)₂.CH₂Cl₂ and α'' -(BEDT-TTF)₅[Ga(C₂O₄)₃].(H₂O)_{3.4}.(EtOH)_{0.6}.¹¹⁰ The salt reported here (*Figure 4.6*) differs from both of these with having β'' donor packing (*Figure 4.7*) and a novel packing of iridium trisoxalate in the anion layers with included ethanol molecules (*Figure 4.8*).

β'' -(BEDT-TTF)₅[Ir(C₂O₄)₃].ethanol crystallises in the monoclinic space group C2/c, with 2.5 independent BEDT-TTF donors, 0.5 of an iridium trisoxalate anion, and an ethanol molecule. Each anion layer is made up of only a single enantiomer of iridium trisoxalate, with adjacent anion layers containing opposing enantiomers to give a racemic structure overall.

The independent donor molecules A, B and C (yellow, blue and red respectively, in *Figure 4.7* and *Figure 4.8*) adopt an ...AABCBAABC... pattern within a stack. Short side-to-side S...S interactions between donor stacks are given in *Table 4.4*. There are no face-to-face interactions within a single stack. Donor A forms a dimer (*Figure 4.7*, circled) which is twisted by 2.6° with respect to the B-C-B trimer (*Figure 4.7*, dashed circled). The estimations of the donor charges based on bond lengths (

Table 4.5) give a total of 3+ charge across the five donors which balances with that expected for a single 3- iridium trisoxalate anion.

Figure 4.10 shows that the electrical resistivity of β'' -(BEDT-TTF)₅[Ir(C₂O₄)₃].ethanol is metallic down to 50 K at which point there is a change to insulating behaviour. Upon rewarming there is a similar transition temperature but a weak semiconducting/semi-metallic region from 50 K up to 225 K followed by metallic behaviour again above 225 K. Band calculations have been performed by Professor Hiroki Akutsu of Osaka University and reported in *Reference 4*. A charge-density wave along the side-by-side direction is the most suitable explanation, although it is merely speculative.

Crystal data: at 100K: C₅₈H₄₆IrO₁₃S₄₀, *M* = 2425.56, black prism, *a* = 18.37840(10), *b* = 13.17680(10), *c* = 33.6413(3) Å, β = 94.0750(10)°, *U* = 8126.27(11) Å³, *T* = 100(2) K, space group C2/c, *Z* = 4, μ = 13.310 mm⁻¹, reflections collected = 38584, independent reflections = 7628, *R*₁ = 0.0314, *wR*₂ = 0.0820 [*F*² > 2σ(*F*²)], *R*₁ = 0.0322, *wR*₂ = 0.0824 (all data).

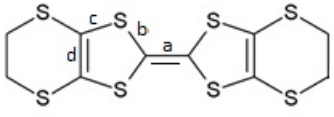
Crystal data: at 150K: C₅₈H₄₆IrO₁₃S₄₀, *M* = 2425.56, black prism, *a* = 18.4349(2), *b* = 13.18390(10), *c* = 33.6063(2) Å, β = 94.1340(10)°, *U* = 8146.55(12) Å³, *T* = 150.01(10) K, space group *C2/c*, *Z* = 4, μ = 13.276 mm⁻¹, reflections collected = 15759, independent reflections = 7803, *R*₁ = 0.0350, *wR*₂ = 0.0876 [*F*² > 2σ(*F*²)], *R*₁ = 0.0383, *wR*₂ = 0.0899 (all data).

Crystal data: at 290K: C₅₆H₄₀IrO₁₂S₄₀ + solvent, *M* = 2379.50, black prism, *a* = 18.6386(15), *b* = 13.2500(8), *c* = 33.689(2) Å, β = 94.474(6)°, *U* = 8294.5(10) Å³, *T* = 290.03(10) K, space group *C2/c*, *Z* = 4, μ = 13.016 mm⁻¹, reflections collected = 7329, independent reflections = 5332, *R*₁ = 0.0964, *wR*₂ = 0.2453 [*F*² > 2σ(*F*²)], *R*₁ = 0.1199, *wR*₂ = 0.2645 (all data).

Table 4.4 - Short S...S contacts (>sum VdW radii) in β''-(BEDT-TTF)₅[Ir(C₂O₄)₃].ethanol in Å. ⁴

S atom 1...	S atom 2	100K	150K	298K
Contact/	Å			
S1...S3		3.4725(11)	3.4745(11)	3.521(6)
S1...S11		3.4159(12)	3.4273(11)	3.469(5)
S1...S12		3.4122(11)	3.4285(11)	3.490(5)
S3...S9		3.5057(11)	3.5167(11)	3.558(5)
S4...S9		3.5775(11)	3.5893(11)	3.634(5)
S5...S16		3.5337(13)	3.5400(12)	3.607(7)
S6...S8		3.5810(11)	3.5854(11)	3.615(5)
S6...S16		3.4319(12)	3.4442(12)	3.526(6)
S8...S13		3.5046(10)	3.5138(10)	3.560(6)
S9...S17		3.3585(10)	3.3701(10)	3.417(5)
S9...S18		3.4240(12)	3.4356(12)	3.495(5)
S13...S18		3.5533(12)	3.5661(11)	3.581(5)
S14...S18		3.3542(11)	3.3648(11)	3.413(5)
S16...S19		3.3860(11)	3.4022(11)	3.457(5)
S16...S20		3.3683(11)	3.3792(11)	3.431(5)

Table 4.5 - Approximation of the charge of BEDT-TTF molecules in β'' -(BEDT-TTF)₅[Ir(C₂O₄)₃].ethanol from bond lengths (Å): $\delta = (b + c) - (a + d)$, $Q = 6.347 - 7.463\delta$.¹⁶⁴ *1 Normalised by the total charge. *2 Normalised charges of dimers and trimers.

										
	Donor	a	b	c	d	δ	Q	Q_n^{*1}		Q_m^{*2}
100K	A	1.375	1.736	1.750	1.352	0.759	0.68+	0.60+	A-A dimer	1.20+
	B	1.371	1.737	1.750	1.353	0.763	0.65+	0.58+	B-C-B trimer	1.81+
	C	1.376	1.734	1.753	1.358	0.753	0.73+	0.65+		
150K	A	1.362	1.737	1.751	1.347	0.779	0.53+	0.57+	A-A dimer	1.14+
	B	1.360	1.738	1.750	1.343	0.785	0.49+	0.53+	B-C-B trimer	1.85+
	C	1.375	1.732	1.752	1.357	0.752	0.73+	0.79+		
290K	A	1.374	1.730	1.756	1.324	0.788	0.47+	0.90+	A-A dimer	1.80+
	B	1.347	1.735	1.747	1.323	0.812	0.29+	0.55+	B-C-B trimer	1.20+
	C	1.312	1.747	1.751	1.329	0.857	0.05+	0.10+		

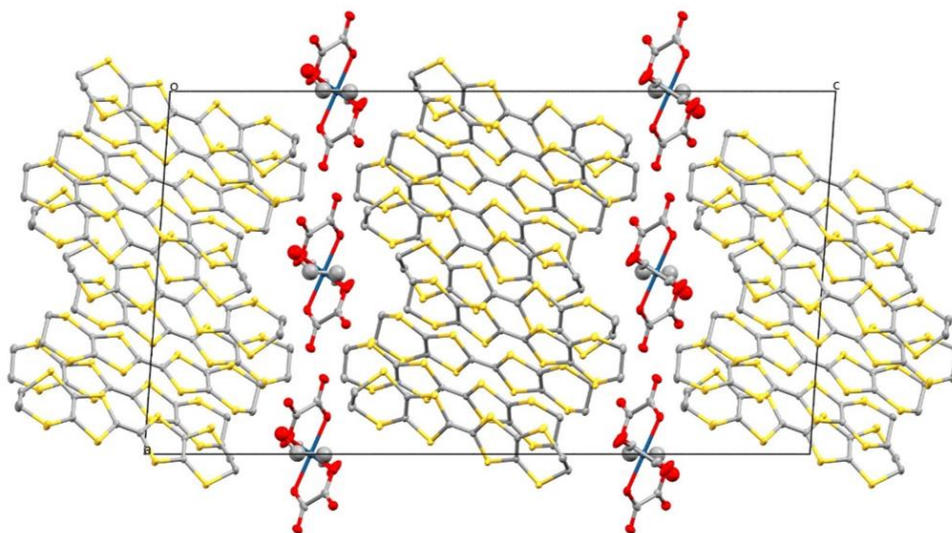


Figure 4.6 - β'' -(BEDT-TTF)₅[Ir(C₂O₄)₃].ethanol viewed down the b axis. Hydrogen atoms and disorder of terminal ethylenes of BEDT-TTF omitted for clarity.⁴

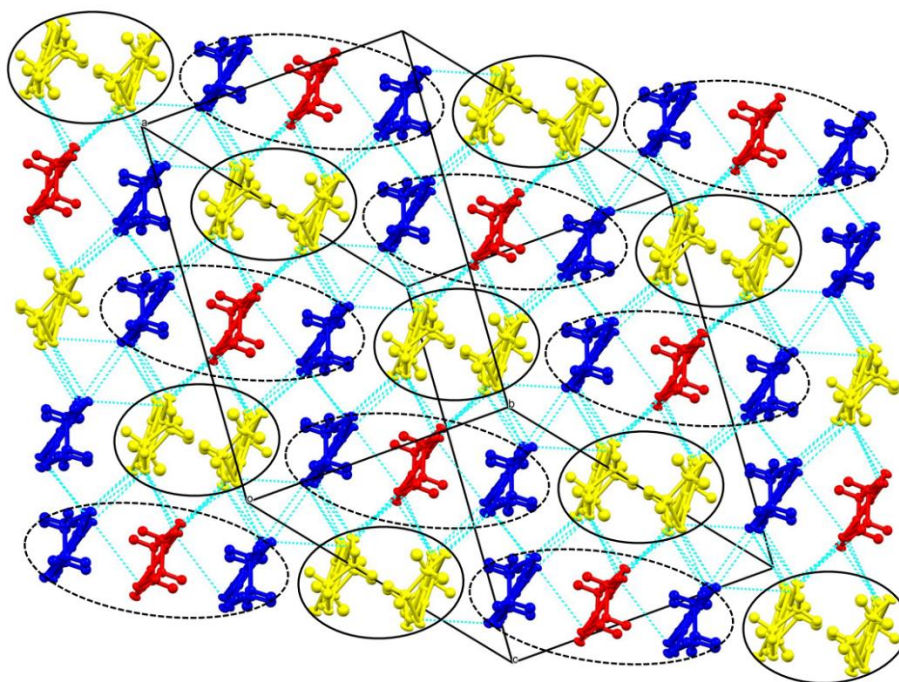


Figure 4.7 - β'' -(BEDT-TTF)₅[Ir(C₂O₄)₃].ethanol donor layer. Donor A = Yellow, B = Blue, C = Red. Donor A forms a dimer (circled), whereas donors B and C form a B-C-B trimer (dashed circled).⁴

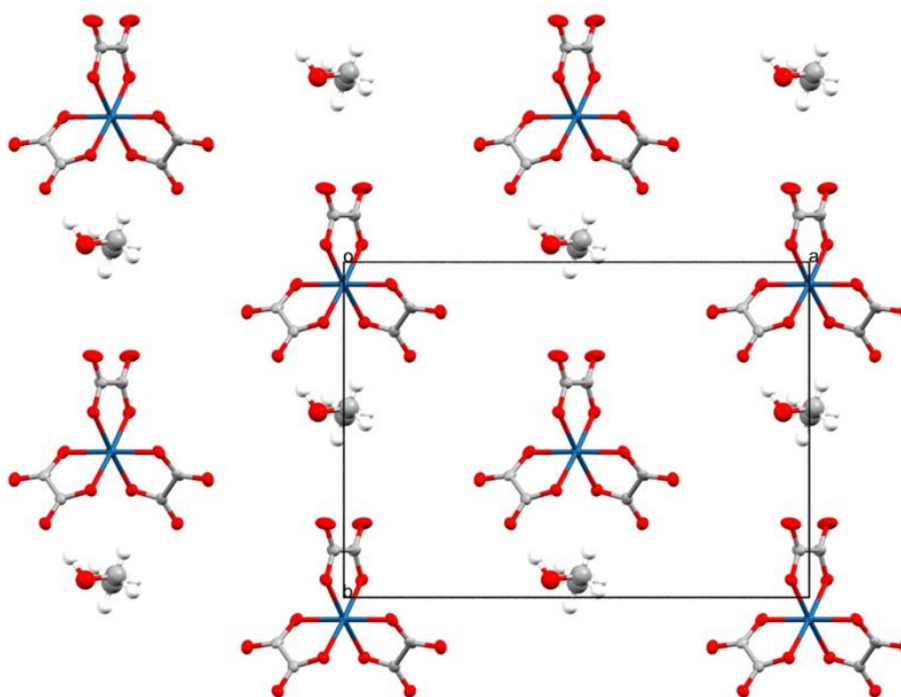


Figure 4.8 - β'' -(BEDT-TTF)₅[Ir(C₂O₄)₃].ethanol anion layer viewed down the c axis.⁴

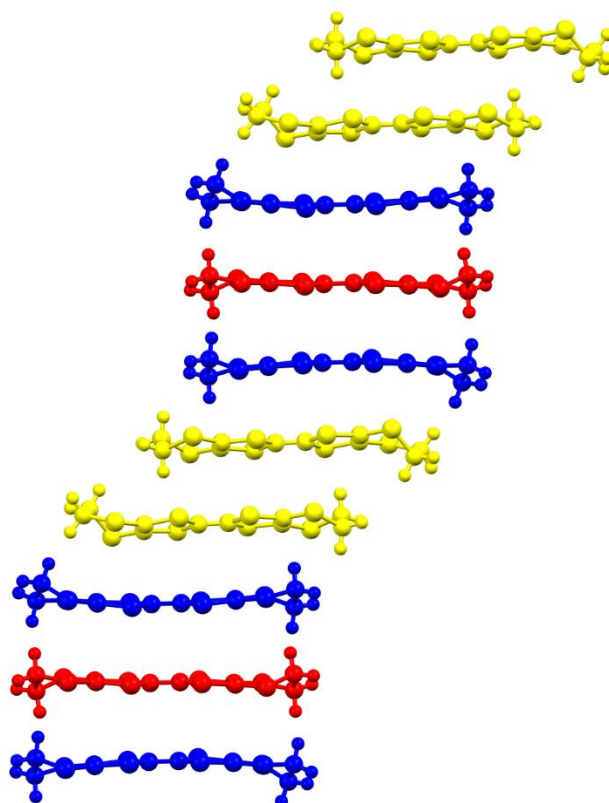


Figure 4.9 - Packing arrangement of donor layer for β'' -(BEDT-TTF)₅[Ir(C₂O₄)₃].ethanol. A = Yellow, B = Blue, C = Red.⁴

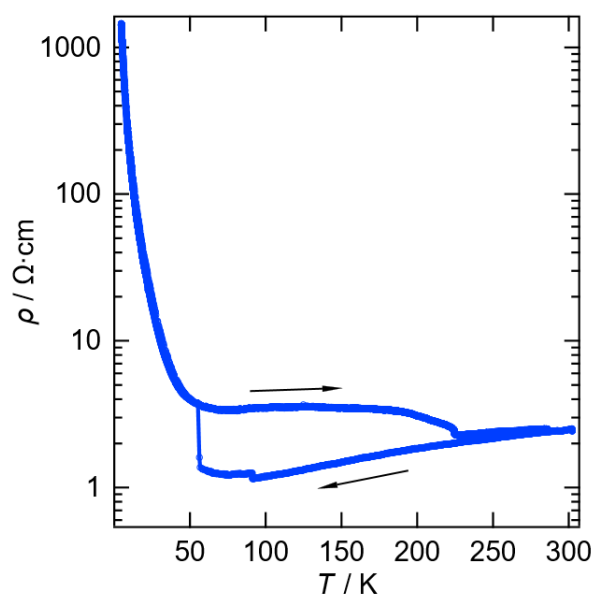
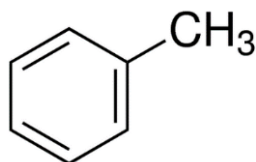


Figure 4.10 - β'' -(BEDT-TTF)₅[Ir(C₂O₄)₃].ethanol electrical resistivity.⁴

4.3.2.2 β'' -(BEDT-TTF)₄[(H₃O)M(C₂O₄)₃].toluene (M = Cr or Fe)

The use of toluene (below) as the guest achieved the aim of introducing a new guest molecule into the hexagonal cavity of a salt of formula β'' -(BEDT-TTF)₄[(A)M(C₂O₄)₃].guest.^{108,129,132,133}



β'' -(BEDT-TTF)₄[(H₃O)M(C₂O₄)₃].toluene (M = Cr or Fe) crystallises in monoclinic space group C2/c and has an asymmetric unit of two crystallographically independent BEDT-TTF donor molecules, 0.5 of a metal trisoxalate anion, 0.5 of a toluene molecule and 0.5 of a H₃O cation.

The donors and anions form segregated stacks (*Figure 4.11*) with the BEDT-TTF donors having a β'' packing arrangement with the two crystallographically independent donors adopting an ...AABBAA... packing order within a stack (*Figure 4.12*). *Table 4.6* shows the S...S close contacts and *Table 4.7* shows the estimation of charge on the donor molecules for the Fe/toluene salt, which has the better X-ray data compared to the Cr/toluene salt. The S...S contacts (*Table 4.6*) are similar to other salts in this series of 4:1 salts, as are the donor charges (*Table 4.7*) which are close to the 0.5⁺ expected for these salts.¹²⁹ The anion layer (*Figure 4.13*) is a hexagonal arrangement of metal trisoxalate anions and H₃O cation with a toluene guest in the hexagonal cavity with the -CH₃ group directed along the *b* axis.

The highest *superconducting* T_c 's in this series of salts are found when the *b* axis length of the crystal structure is elongated by the inclusion of solvents such as benzonitrile and nitrobenzene.¹³⁰ The desired 4:1 β'' -(BEDT-TTF)₄[(A)M(C₂O₄)₃].guest has been obtained when using toluene as the guest molecule, though the *b* axis length is shorter (19.9069 Å at 150 K in Fe/toluene, 19.8966 Å at 120 K in Cr/toluene) compared to the isostructural Fe/benzonitrile (20.04 Å at 120 K) and Fe/nitrobenzene (19.949 Å at 120 K) salts.^{108,133} The *superconducting* T_c would therefore be expected to be lower than the Fe/benzonitrile and Fe/nitrobenzene salts if superconductivity is present. *Figure 4.14* shows the electrical resistivity measurements for both β'' -(BEDT-TTF)₄[(H₃O)M(C₂O₄)₃].toluene (M = Cr (*top*) and Fe (*bottom*)). Both M = Cr and Fe show metallic behaviour from room temperature down to 4.2 K with no transition to the *superconducting* state. SQUID magnetometry was performed on a polycrystalline sample of both down to 1.8 K but no Meissner signal was observed

(Figure 4.14). This is similar to salts such as Fe/fluorobenzene and Fe/chlorobenzene which remain metallic down to 1.8 K without a *superconducting* transition, whilst larger guests such as Fe/bromobenzene shows a T_c of 4 K.¹⁶¹

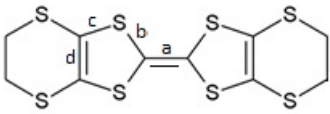
M = Fe Crystal data: at 150K: $C_{53}H_{44}FeO_{13}S_{32}$, $M = 1970.65$, black needle, $a = 10.2478(6)$, $b = 19.9069(14)$, $c = 35.264(2)$ Å, $\beta = 94.106(5)^\circ$, $U = 7175.5(8)$ Å³, $T = 150.15$ K, space group $C2/c$, $Z = 4$, $\mu = 10.914$ mm⁻¹, reflections collected = 14834, independent reflections = 6875, $R1 = 0.0865$, $wR2 = 0.2084$ [$F^2 > 2\sigma(F^2)$], $R1 = 0.1221$, $wR2 = 0.2439$ (all data).

M = Cr Crystal data: at 120K: $C_{53}H_{44}CrO_{13}S_{32}$, $M = 1970.65$, black needle, $a = 10.2411(2)$, $b = 19.8966(3)$, $c = 35.4830(7)$ Å, $\beta = 94.275(2)^\circ$, $U = 7210.0(2)$ Å³, $T = 120(2)$ K, space group $C2/c$, $Z = 4$, $\mu = 10.456$ mm⁻¹, reflections collected = 14909, independent reflections = 13303, $R1 = 0.1054$, $wR2 = 0.3016$ [$F^2 > 2\sigma(F^2)$], $R1 = 0.1136$, $wR2 = 0.3144$ (all data).

Table 4.6 - Short S...S contacts (>sum VdW radii) in β'' -(BEDT-TTF)₄[(H₃O)M(C₂O₄)₃].toluene; here, M= Fe.

S atom 1...	Contact/ Å, M = Fe
S1...S7	3.404
S2...S9	3.299
S2...S11	3.350
S3...S7	3.469
S6...S15	3.475
S8...S15	3.501
S8...S10	3.566

Table 4.7 - Approximation of the charge of BEDT-TTF molecules in β'' -(BEDT-TTF)₄[(H₃O)M(C₂O₄)₃].toluene from bond lengths (Å): $\delta = (b + c) - (a + d)$, $Q = 6.347 - 7.463\delta$; here M=Fe.¹⁶⁴



Donor	a	b	c	d	δ	Q
A M=Fe	1.369	1.730	1.757	1.341	0.777	0.55+
B M=Fe	1.361	1.729	1.748	1.350	0.766	0.63+

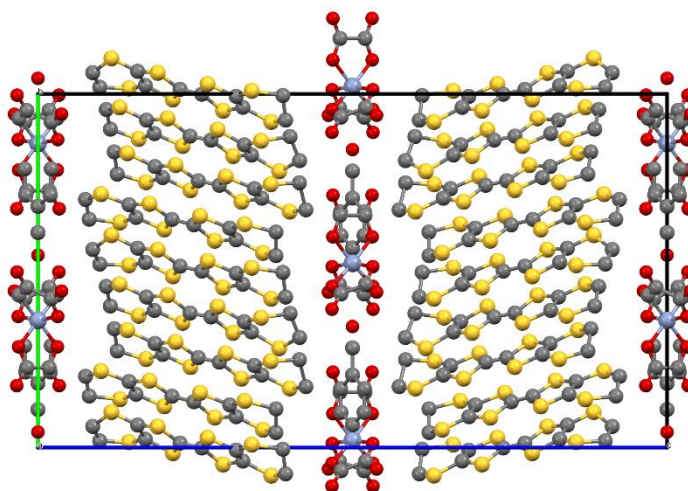


Figure 4.11 - β'' -(BEDT-TTF)₄[(H₃O)M(C₂O₄)₃].toluene viewed down the a axis. Hydrogen atoms and disorder of terminal ethylenes of BEDT-TTF omitted for clarity.

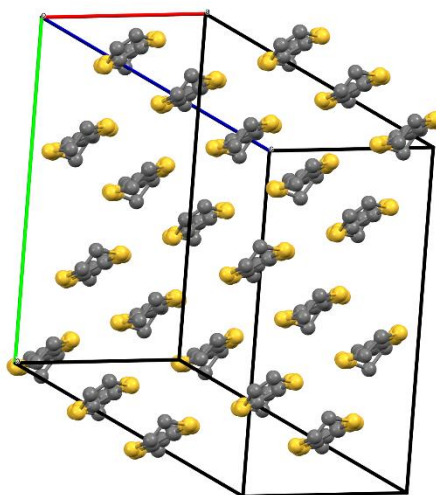


Figure 4.12 - β'' -(BEDT-TTF)₄[(H₃O)M(C₂O₄)₃].toluene donor layer. Hydrogen atoms and disorder of terminal ethylene groups of BEDT-TTF groups omitted for clarity.

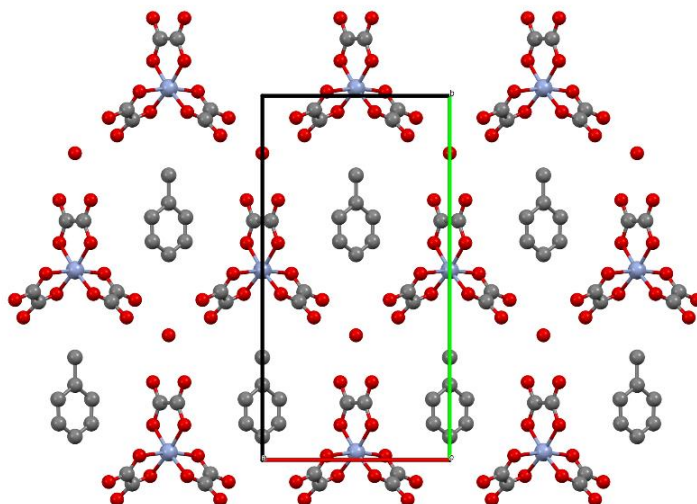


Figure 4.13 - β'' -(BEDT-TTF)₄[(H₃O)M(C₂O₄)₃].toluene anion layer viewed down the *c* axis. Hydrogen atoms omitted for clarity.

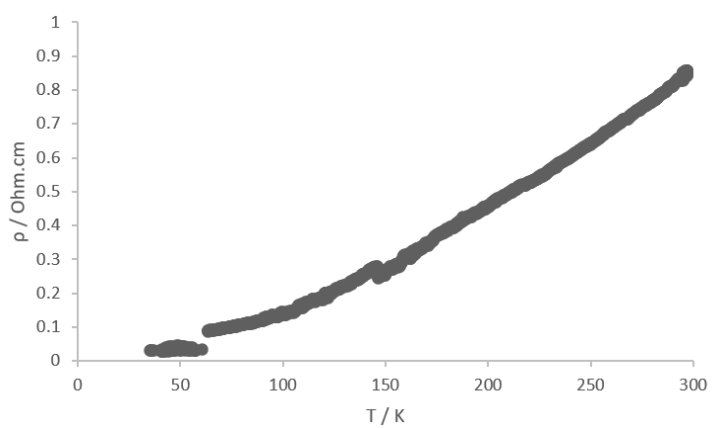
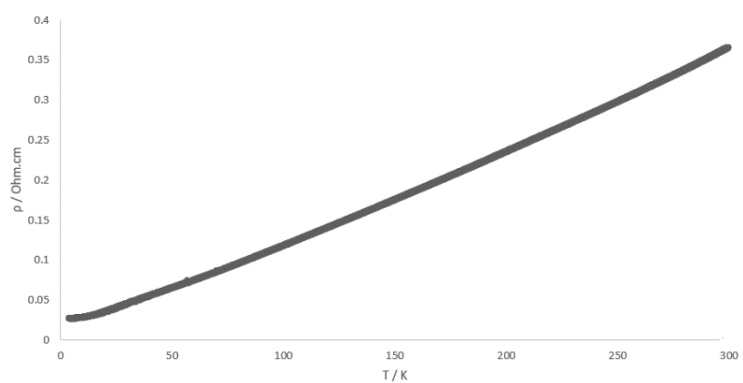
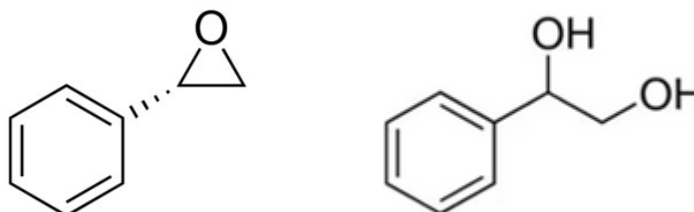


Figure 4.14 - β'' -(BEDT-TTF)₄[(H₃O)M(C₂O₄)₃].toluene electrical resistivity. *M* = Cr (top) and Fe (bottom).

4.3.2.3 β'' - β'' -(BEDT-TTF)₄[(H₂O/H₃O)Fe(C₂O₄)₃].1-phenylethane-1,2-diol

The use of chiral (S)-phenyloxirane as the guest has produced a new type of salt, β'' - β'' -(BEDT-TTF)₄[(H₂O/H₃O)Fe(C₂O₄)₃].1-phenylethane-1,2-diol. Under the conditions of electrocrystallisation, the (S)-phenyloxirane guest molecule (*below left*) has undergone ring opening to produce 1-phenylethane-1,2-diol (*below right*).



β'' - β'' -(BEDT-TTF)₄[(H₂O/H₃O)Fe(C₂O₄)₃].1-phenylethane-1,2-diol crystallises in space group P-1 and has an asymmetric unit of four crystallographically independent BEDT-TTF donor molecules, an iron trisoxalate anion, a 1-phenylethane-1,2-diol molecule, and a H₂O or H₃O.

The donors and anions form segregated stacks (*Figure 4.15*) with the BEDT-TTF donors having a β'' packing arrangement with the two crystallographically independent donors within each β'' layer adopting an ...AABBAA... packing order within a stack (*Figure 4.16*). The two donor layers show different β'' packing arrangements (*Figure 4.16*). Donor layer 1 has only side-to-side S...S contacts, whilst donor layer 2 also has diagonal S...S interactions between them (*Table 4.8*). Donor layer 1 (*Figure 4.16 left*) is on the edge of the unit cell (*c* axis) docking into anion layers facing the R-group of the guest molecule. Donor layer 2 (*Figure 4.16 right*) is in the centre of the unit cell (*c* axis) docking into anion layers facing the phenyl groups of the guest molecule. This type of bilayered 4:1 salt has been seen before when large non-symmetrical guest molecules have been used which protrude more on one side of the anion layer than the other side.

The anion layer (*Figure 4.17*) is a hexagonal arrangement of iron trisoxalate anions and H₂O/H₃O with a 1-phenylethane-1,2-diol guest in the hexagonal cavity. *Figure 4.15* shows how the guest is sited within the anion layer presenting a different part of the guest molecule to each of donor layers 1 and 2. These two different faces of the anion layer lead to two different donor packing arrangements on either side of the anion layer. This has previously produced alpha-beta'' and kappa-beta'' salts before, but this is the first example of a beta''-beta'' salt.¹²⁹

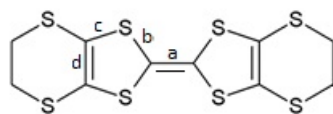
The BEDT-TTF donor charges (*Table 4.9*) have been estimated as 0.76+ and 0.76+ in Donor layer 1, and 0.59+ and 0.65+ in Donor layer 2. All four crystallographically independent donors would be expected to be 0.5+ if the cation was H_3O^+ ; similar to other salts in this series. This suggests an overall charge on the 4 donors of 2.76+ balanced by $\text{H}_2\text{O}:\text{H}_3\text{O}^+$ 75:25. Electrical resistivity has been measured on single crystals of this salt which shows *metallic* behaviour from room temperature down to 160 K below which there is transition to the *insulating* state (*Figure 4.18*). SQUID magnetometry was performed on a polycrystalline sample down to 1.8 K but no Meissner signal was observed.

Crystal data: at 120K: $\text{C}_{54}\text{H}_{44}\text{FeO}_{15}\text{S}_{32}$, $M = 2014.66$, black prism, $a = 9.6581(2)$, $b = 10.9638(3)$, $c = 38.0447(8)$ Å, $\alpha = 89.295(2)$ $\beta = 82.890(2)$, $\gamma = 66.880(2)^\circ$, $U = 3673.58(16)$ Å³, $T = 120.00(10)$ K, space group $P-1$, $Z = 2$, $\mu = 10.697$ mm⁻¹, reflections collected = 82840, independent reflections = 15110, $R1 = 0.0883$, $wR2 = 0.2352$ [$F^2 > 2\sigma(F^2)$], $R1 = 0.1078$, $wR2 = 0.2544$ (all data).

Table 4.8 - Short S...S contacts (>sum VdW radii) in $\beta''\text{-}\beta''\text{-(BEDT-TTF)}_4[(\text{H}_2\text{O}/\text{H}_3\text{O})\text{Fe}(\text{C}_2\text{O}_4)_3]$.1-phenylethane-1,2-diol.

S atom 1...	Contact / Å
S atom 2	
S14...S10	3.479
S11...S7	3.457
S9...S7	3.346
S1...S15	3.270
S3...S15	3.370
S2...S6	3.439
S2...S8	3.465
S18...S24	3.514
S24...S29	3.528
S24...S31	3.586
S19...S31	3.474
S23...S25	3.553
S17...S31	3.346
S26...S30	3.504

Table 4.9 - Approximation of the charge of BEDT-TTF molecules in β'' - β'' -(BEDT-TTF)₄[(H₂O/H₃O)Fe(C₂O₄)₃].1-phenylethane-1,2-diol from bond lengths (Å): $\delta = (b + c) - (a + d)$, $Q = 6.347 - 7.463\delta$.¹⁶⁴



Donor	a	b	c	d	δ	Q
A	1.376	1.7378	1.7468	1.3595	0.749	0.76+
B	1.369	1.7398	1.7513	1.3625	0.760	0.76+
C	1.369	1.7435	1.7540	1.3570	0.772	0.59+
D	1.366	1.7385	1.7478	1.3565	0.764	0.65+

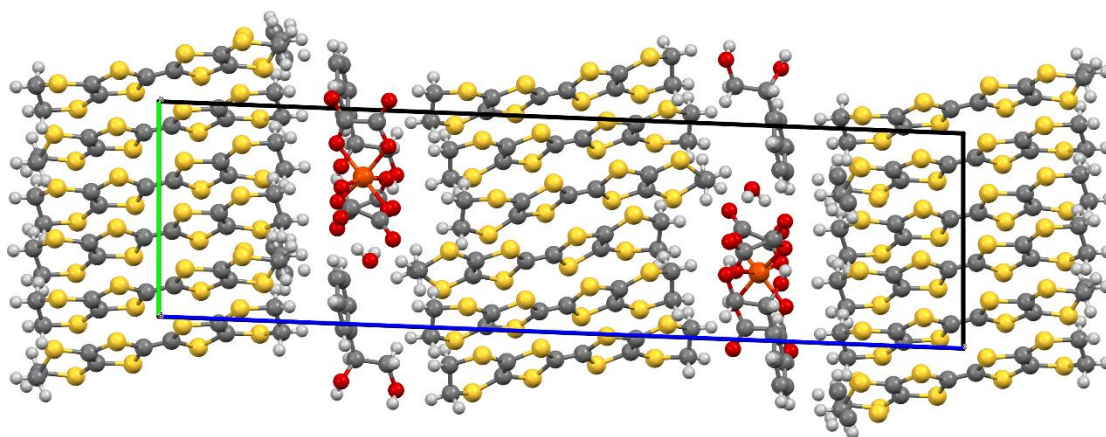


Figure 4.15 - β'' - β'' -(BEDT-TTF)₄[(H₂O/H₃O)Fe(C₂O₄)₃].1-phenylethane-1,2-diol viewed down the a axis.

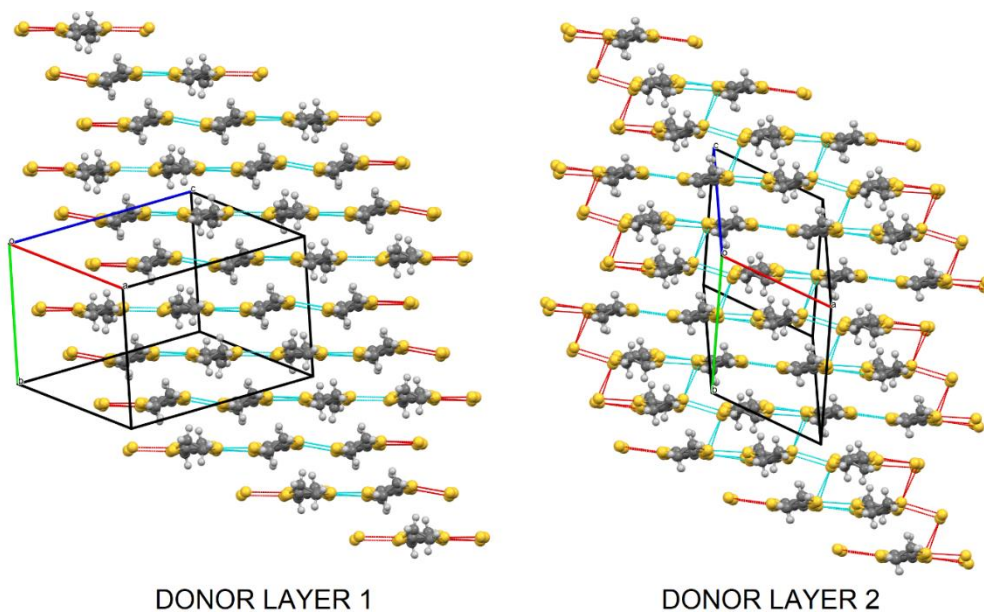


Figure 4.16 - β'' - β'' -(BEDT-TTF)₄[(H₂O/H₃O)Fe(C₂O₄)₃].1-phenylethane-1,2-diol donor layers. Donor layer 1 (left) is on the edge of the unit cell (c axis) docking into anion layers facing the R group of the guest molecule. Donor layer 2 (right) is in the centre of the unit cell (c axis) docking into anion layers facing the phenyl groups of the guest molecule.

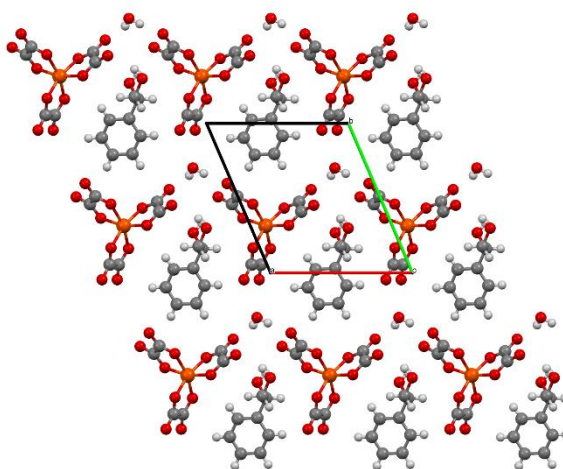


Figure 4.17 - β'' - β'' -(BEDT-TTF)₄[(H₂O/H₃O)Fe(C₂O₄)₃].1-phenylethane-1,2-diol anion layer viewed down the c axis.

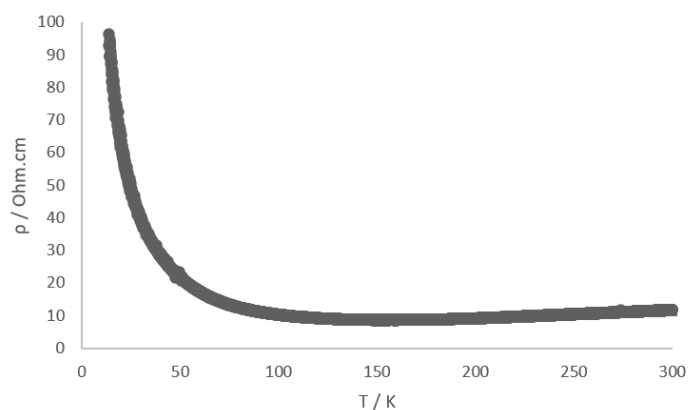
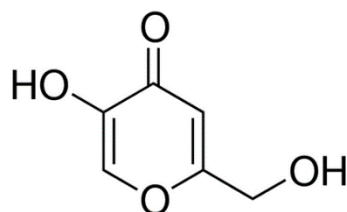


Figure 4.18 - β'' - β'' -(BEDT-TTF)₄[(H₂O/H₃O)Fe(C₂O₄)₃].1-phenylethane-1,2-diol electrical resistivity.

4.3.2.4 α''' -(BEDT-TTF)₄[Fe(C₂O₄)₂(kojate)]

The use of kojic acid (below) as a guest has produced a new salt of formula α''' -(BEDT-TTF)₄[Fe(C₂O₄)₂(kojate)].



α''' -(BEDT-TTF)₄[Fe(C₂O₄)₂(kojate)] crystallises in space group P2/n and has an asymmetric unit of eight crystallographically independent BEDT-TTF donor molecules and two Fe(C₂O₄)₂(kojate) anions. Under the conditions of electrocrystallisation one of the oxalate ligands on metal trisoxalate has been replaced with a kojate.

The donors and anions form segregated stacks (*Figure 4.19*) with the BEDT-TTF donors having a packing not previously observed which, following convention, has been called α''' packing (*Figure 4.20*). *Table 4.10* shows the S...S close contacts which are all side-to-side between adjacent stacks with no face-to-face S...S contacts.

Table 4.11 shows the estimation of charge on the eight crystallographically independent BEDT-TTF donor molecules. The overall charge for the eight BEDT-TTF molecules is estimated as 5.6+. There is charge localisation in this structure at room temperature with the donor stack which is tilted at an angle to the others (claret and light blue donors in *Figure 4.20*) having BEDT-TTF^{0.32+} and BEDT-TTF^{0.49+} whilst BEDT-TTFs in the other layers have higher charges of between 0.67+ and 0.91+ (*Table 4.11*). The anion layer (*Figure 4.21*) consists of

only $\text{Fe}(\text{C}_2\text{O}_4)_2$ (kojate) anions which alternate in each stack between the delta and the lambda enantiomers to give a racemic structure.

Electrical resistivity has been measured on single crystals of this salt which shows metallic behaviour from room temperature down to 100K below which there is transition to the insulating state (*Figure 4.22*). SQUID magnetometry was performed on a polycrystalline sample down to 1.8K but no Meissner signal was observed.

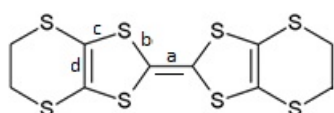
Crystal data: at 293K: $\text{C}_{50}\text{H}_{37}\text{FeO}_{12}\text{S}_{32}$, $M = 1911.56$, black prism, $a = 24.9368(6)$, $b = 19.4833(3)$, $c = 31.827(10)$ Å, $\beta = 108.849(3)^\circ$, $U = 14634.6(7)$ Å³, $T = 293(2)$ K, space group $P2/n$, $Z = 8$, $\mu = 10.671$ mm⁻¹, reflections collected = 100711, independent reflections = 28105, $R1 = 0.0707$, $wR2 = 0.1793$ [$F^2 > 2\sigma(F^2)$], $R1 = 0.1528$, $wR2 = 0.2308$ (all data).

Table 4.10 - Short S...S contacts (>sum VdW radii) in $\alpha''''-(\text{BEDT-TTF})_4[\text{Fe}(\text{C}_2\text{O}_4)_2(\text{kojate})]$

S atom 1	S atom 2	Contact/ Å
S01T	S00S	3.583
S003	S009	3.506
S01A	S009	3.386
S01U	S019	3.549
S01U	S01G	3.418
S008	S00W	3.455
S00I	S00W	3.581
S00L	S00D	3.467
S00L	S00R	3.547
S00P	S00S	3.426
S004	S007	3.596
S00L	S00T	3.583
S00B	S01P	3.573
S01N	S01P	3.394
S01S	S00U	3.404
S01S	S015	3.482
S00B	S01O	3.568

S01D	S018	3.552
S01J	S00F	3.475
S01J	S017	3.434
S01K	S018	3.460
S006	S00W	3.582
S010	S01C	3.568
S01Q	S00W	3.575
S006	S011	3.536
S010	S00Z	3.537
S007	S00X	3.597
S007	S01E	3.479
S00E	S01B	3.546
S00T	S01B	3.558
S00V	S01I	3.455
S01H	S01I	3.491
S01O	S00J	3.535
S01O	S01R	3.399

Table 4.11 - Approximation of the charge of BEDT-TTF molecules in $\alpha''''-(\text{BEDT-TTF})_4[\text{Fe}(\text{C}_2\text{O}_4)_2(\text{kojate})]$ from bond lengths (\AA): $\delta = (b + c) - (a + d)$, $Q = 6.347 - 7.463\delta$.¹⁶⁴



Donor	a	b	c	d	δ	Q
White	1.385	1.73075	1.747	1.351	0.742	0.81+
Green	1.374	1.73475	1.74275	1.3515	0.752	0.74+
Magenta	1.386	1.7295	1.74525	1.3515	0.737	0.85+
Red	1.375	1.7335	1.7305	1.360	0.729	0.91+
Yellow	1.378	1.73525	1.7505	1.3515	0.756	0.70+
Dark Blue	1.3575	1.738	1.746	1.366	0.761	0.67+
Claret	1.356	1.74125	1.75725	1.335	0.808	0.32+
Light Blue	1.352	1.73775	1.7505	1.351	0.785	0.49+

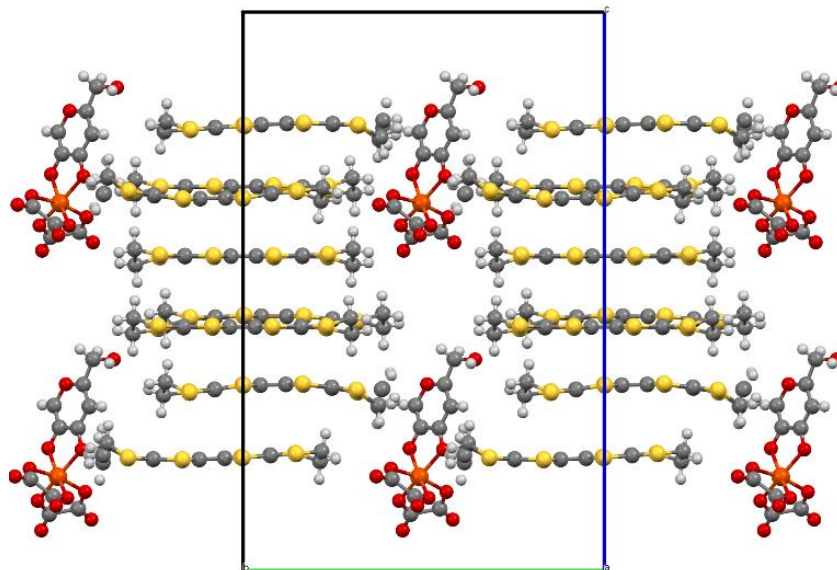


Figure 4.19 - α''' -(BEDT-TTF)₄[Fe(C₂O₄)₂(kojate)] viewed down the *a* axis.

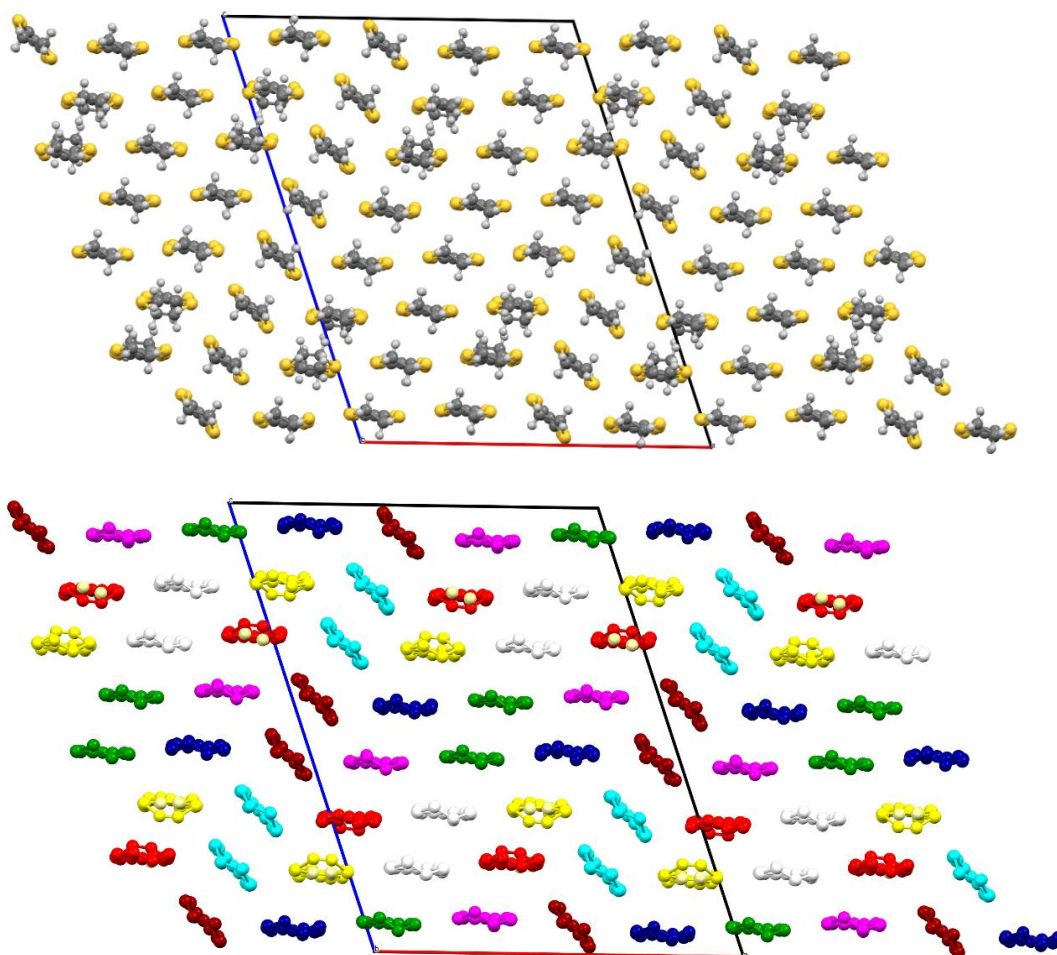


Figure 4.20 - α''' -(BEDT-TTF)₄[Fe(C₂O₄)₂(kojate)] donor layer; the top figure displays the donor layer in a simple view, whereas the bottom figure highlights the differently charged donors, distinguished by colours. Respective

charges are as follows; white = 0.81+, green = 0.74+, magenta = 0.85+, red = 0.91+, yellow = 0.70+, dark blue = 0.67+, claret = 0.32+ and light blue = 0.49+.

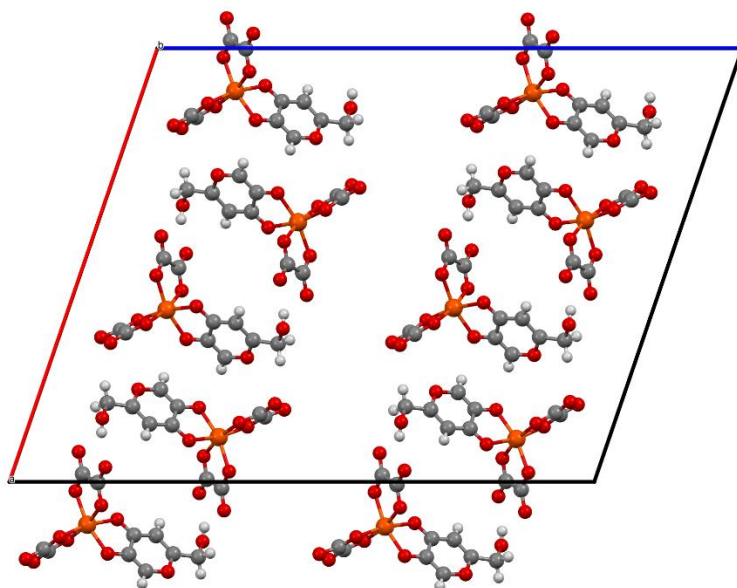


Figure 4.21 - α'''' -(BEDT-TTF)₄[Fe(C₂O₄)₂(kojate)] anion layer viewed down the c axis.

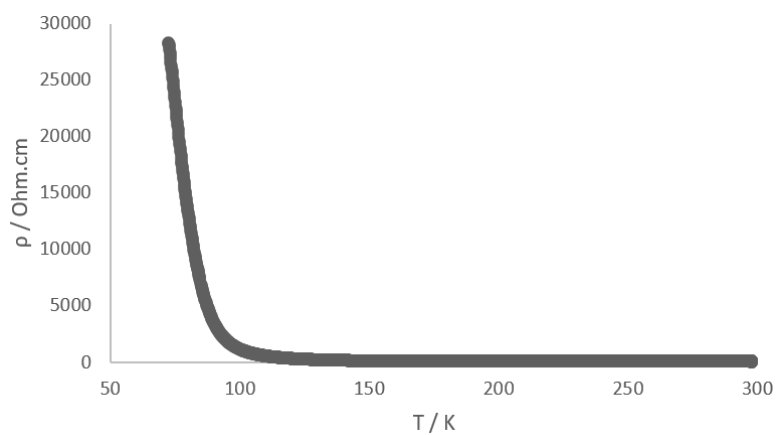
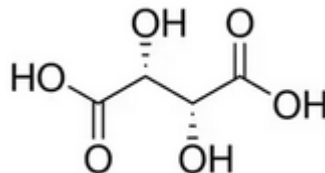


Figure 4.22 - α'''' -(BEDT-TTF)₄[Fe(C₂O₄)₂(kojate)] electrical resistivity.

4.3.2.5 α -(BEDT-TTF)₅[Fe(C₂O₄)₃].(tartaric acid)₂

The use of L-(+)-tartaric acid (below) as the guest has produced a new salt of formula α -(BEDT-TTF)₅[Fe(C₂O₄)₃].L-(+)-tartaric acid.



α -(BEDT-TTF)₅[Fe(C₂O₄)₃].(tartaric acid)₂ crystallises in space group C2 with a Flack parameter of -0.25(3). This charge-transfer salt has an asymmetric unit of ten crystallographically independent BEDT-TTF donor molecules, two Fe(C₂O₄)₃ anions, and four L-(+)-tartaric acid molecules. The donors and anions form segregated stacks (*Figure 4.23*) with the BEDT-TTF donors having alpha packing (*Figure 4.24*).

The anion layer (*Figure 4.25*) consists of a novel packing of only Fe(C₂O₄)₃ anions with L-(+)-tartaric acid molecules. Spontaneous resolution of the Fe(C₂O₄)₃ anions has occurred with only the delta enantiomers of Fe(C₂O₄)₃ present in the crystal despite starting from a racemic solution of labile Fe(C₂O₄)₃.

S...S close contacts and BEDT-TTF charge calculations have not been calculated owing to the poor quality of the X-ray data on these crystals and the sheer size of the unit cell containing 40 donor molecules.

Electrical resistivity has been measured on single crystals of this salt which shows metallic behaviour from room temperature down to 150 K, below which there is transition to the insulating state (*Figure 4.26*). SQUID magnetometry was performed on a polycrystalline sample down to 1.8 K but no Meissner signal was observed.

Crystal data: at **150K**: C₁₀H₁₀FeO₆S₈, $M = 566.54$, black block, $a = 77.090(4)$, $b = 11.2809(13)$, $c = 20.872(2)$ Å, $\beta = 92.076(7)^\circ$, $U = 18139(3)$ Å³, $T = 150.00(10)$ K, Flack parameter -0.25(3), space group C2, $Z = 38$, $\mu = 14.840$ mm⁻¹, reflections collected = 50814, independent reflections = 28069, $R1 = 0.01614$, $wR2 = 0.4131$ [$F^2 > 2\sigma(F^2)$], $R1 = 0.2323$, $wR2 = 0.4906$ (all data).

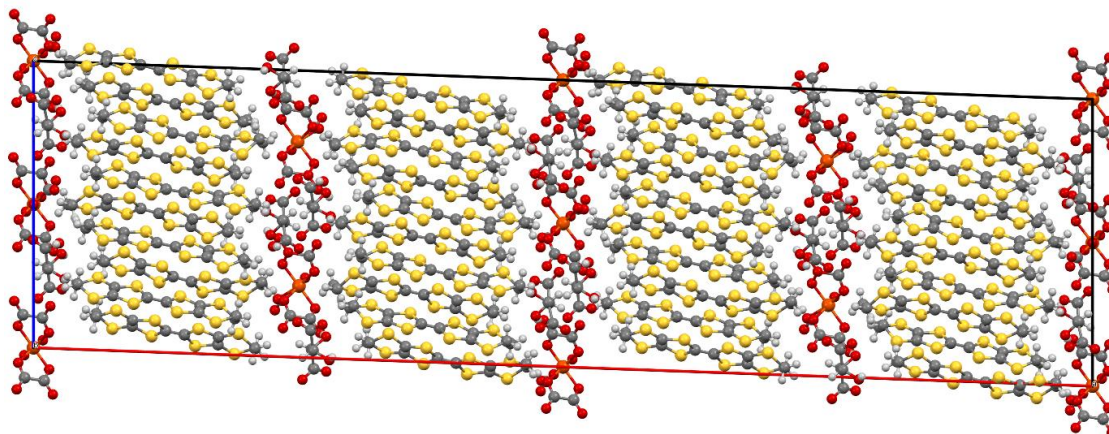


Figure 4.23 - α -(BEDT-TTF)₅[Fe(C₂O₄)₃].(tartaric acid)₂ viewed down the a axis.

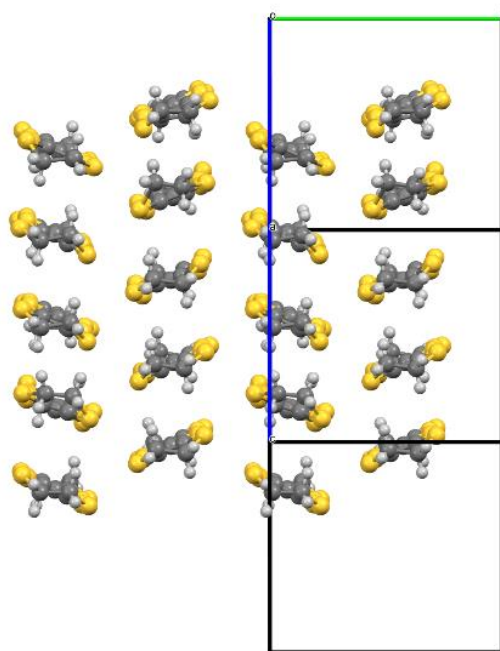


Figure 4.24 - α -(BEDT-TTF)₅[Fe(C₂O₄)₃].(tartaric acid)₂ donor layer.

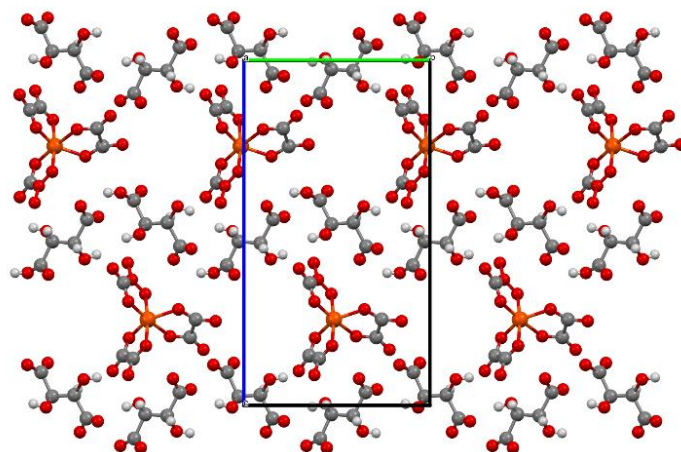


Figure 4.25 - α -(BEDT-TTF)₅[Fe(C₂O₄)₃].(tartaric acid)₂ anion layer viewed down the *c* axis.

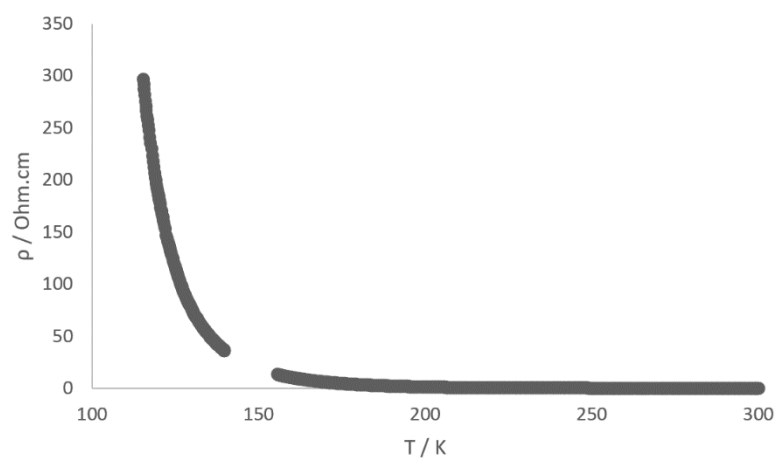


Figure 4.26 - α -(BEDT-TTF)₅[Fe(C₂O₄)₃].(tartaric acid)₂ electrical resistivity.

4.4 Conclusions

4.4.1 BEDT-TTF salts with Metal Trisoxalate and Benzonitrile

The first salts in this family grown from a 5d metal trisoxalate are reported. The iridate anion gave a *pseudo-κ* semiconducting *Pbcn* salt exclusively and a *superconducting C2/c* salt could not be obtained. Unfortunately, suitable crystals of the other non-magnetic salts could not be obtained despite extensive multiple attempts for each synthetic method and metal trisoxalate.

4.4.2 BEDT-TTF salts with Metal Trisoxalate and New Guest Molecules

With several guests, the 5d iridium trisoxalate gave a new 5:1 salt that has not been obtained in the large family of BEDT-TTF salts with 3d metal trisoxalates.

A salt with toluene as the guest has given a *b* axis length that is not as long as that found in the benzonitrile or nitrobenzene salts, and no *superconductivity* is observed down to 1.8 K. In contrast, a guest molecule that is larger, (*S*)-(-)-phenyloxirane, underwent ring-opening to give 1-phenylethane-1,2-diol as the guest in a bilayered 4:1 *metal-insulating* salt. The new β''-β'' salt from guest molecule 1-phenylethane-1,2-diol opens the possibility for future work using the chiral guest molecules (*R*)-(-)-1-phenylethane-1,2-diol and (*S*)-(+)-1-phenylethane-1,2-diol to prepare isostructural chiral metals. Whilst the salt reported here was grown from chiral (*S*)-(-)-phenyloxirane, the diol produced *via* ring opening was racemic.

A new anion has been synthesised where an oxalate ligand of an iron trisoxalate has been replaced by kojic acid to give [Fe(C₂O₄)₂(kojate)] which has produced a charge-transfer salt with BEDT-TTF having a novel α'''' packing motif.

A new charge-transfer salt containing enantiopure L-(+)-tartaric acid has led to spontaneous resolution of the [Fe(C₂O₄)₃]³⁻ anion to produce a chiral conductor. This salt introduces the possibility of using L-(+)-tartaric acid to obtain spontaneous resolution of other anions in chiral charge-transfer salts, and also employing D-(-)-tartaric acid to produce the opposite enantiomer.

5. BEDT-TTF salts with Spiroborate Anions

5.1 Introduction

Charge-transfer salts of BEDT-TTF have been studied extensively following the discovery of a large number of organic metals and superconductors. These salts have the ability to combine multiple physical properties *via* crystal engineering of both the conducting BEDT-TTF layers and the insulating anion layers. The synthesis of radical-cation salts of this type offers a promising approach to producing crystalline materials which combine the properties of chirality and conductivity.¹⁶⁷ Electrical magneto-chiral anisotropy was first observed in bismuth helices,^{101,102} as well as carbon nanotubes,¹⁰⁰ where differences in resistivity along nanotubes of opposing chirality is observed in a coaxial magnetic field. Of the previously discussed three routes through which chirality can be introduced into charge-transfer salts, chiral anions are the mostly extensively reported in the form of metal trisoxalates.¹⁰⁸

Similarly, spiroborate anions have recently been postulated as a promising novel route for synthesis of multifunctional materials. As mentioned in the *Section 2.7.3*, the employment of bis-chelated spiroborate anions in BEDT-TTF charge-transfer salts yields complexes with multiple stereogenic centres. The chirality of the bidentate chelated ligand is retained but diastereomers are produced through two possible stereochemical configurations at the boron centre. Dependent upon whether one employs enantiopure or racemic bidentate ligands, one may synthesise up to six diastereomers. In the case of the former with enantiopure bidentate ligands with S chirality, a pair of diastereomeric anions result; B_SSS and B_RSS. In the latter case, when using racemic bidentate ligands, four further diastereomers are obtained: B_SRR & B_RRR, and B_SRS & B_RRS. Owing to the high lability of chiral boron centres, and therefore likely racemisation, reliance upon suitable ligand-based chirality is necessary when synthesising these materials.

Wong et al. proposed the use of spiroborate anions as chiral resolving agents, such that they appeared to be widely effective in the resolution of chiral cations.¹⁶⁸ Here, they reported three examples to successfully demonstrate their scope as resolving agents with tetrahydropalmatine, diaminopropane and the metal–organic complex [Co(phen)₃]³⁺. Later, *Wong et al.* reported a chiral spiroborate anion from diphenyl-L-tartramide in the form of [B(L-Tar(NHPh)₂)]⁻ as an alternative resolving agent.¹⁶⁹

Martin et al. were the first, and remain the only current researchers, to report examples of these charge-transfer salts of BEDT-TTF with chiral borate anions. Initial studies employed the borate anions of malic acid, $[B(\text{malate})_2]^-$, in 2016.⁷ Using B_SRR and B_RRR anions, a charge-transfer salt was yielded whereby only B_SRR anion was incorporated into the structure. When using a mixture of the six possible diastereomeric spiroborate anions prepared from racemic malic acid, a racemic radical-cation salt was obtained but only two of the six diastereomeric anions were present in the crystal (B_SRS and B_RRS). Since the first example was reported, *Martin et al.* have continued this new avenue of research and multiple BEDT-TTF salts with spiroborate anions have materialised, including those utilising $B(\text{mandelate})_2^-$ and $B(2\text{-chloromandelate})_2^-$ anions.⁶ Alongside, a spiroborate salt with an alternative donor, BDH-TTP, has also been demonstrated with the $B(2\text{-chloromandelate})_2^-$ anion.⁵

This chapter reports the resistivity measurements of two novel charge-transfer salts of BEDT-TTF with spiroborate anions; $\beta''\text{-(BEDT-TTF)}_2B(4\text{-chlorosalicylate})_2$ and $\beta''\text{-(BEDT-TTF)}_2B(\text{glycolate})_2$.

5.2 Experimental

5.2.1 X-ray Crystallography

Several structures presented in this thesis were analysed at room and low temperatures at NTU, Osaka University in Japan and the National Crystallographic Service (NCS) in Southampton. Data was collected in Osaka by Professor Hiroki Akutsu on a Rigaku R-Axis VII imaging plate system with FR-E SuperBright High-Brilliance Rotating Anode Generator with confocal mono-chromated MoK α radiation, using Rapid Auto software for control and processing. Structures were solved *via* programs from the SHELX family by direct methods and refined on F2 full-matrix least squares using all unique data. Data was collected at the NCS on a Rigaku AFC12 diffractometer with Mo rotating anode, using standard control and processing software. Structures were solved *via* programs from the SHELX family by direct methods and refined on F2 full-matrix least squares using all unique data. Data was collected at NTU on both a Rigaku Oxford Xcalibur, Sapphire3, Gemini four-circle diffractometer with a graphite monochromator using monochromatic Molybdenum K α radiation ($\lambda = 0.7107 \text{ \AA}$) or Copper K α radiation ($\lambda = 1.5406 \text{ \AA}$) at either room temperature or a constant temperature of 150.00(10) K. This diffractometer was subsequently replaced by a Rigaku Rotating Anode XtaLAB Synergy-DW equipped with Cu/Mo radiation. Structures were solved using programs from the SHELX family within OLEX2 by direct methods and refined on F2 full matrix least squares using all unique data. Molecular illustrations included in this body of work were made with Mercury using POVray.¹⁴⁶

5.2.2 Resistivity Measurements

Four-probe DC transport measurements were made on crystals using a HUSO HECS 994C multi-channel conductometer. Gold wires (*ca.* 15 μm diameter) were attached to the crystal, and the attached wires were connected to an integrated circuit plug with carbon conductive cement.

5.3 Results and Discussion

As outlined in the introduction section, the Martin research group has successfully employed spiroborate anions in charge-transfer salts of both BDH-TTP⁵ and BEDT-TTF.^{6,7} These salts have made use of readily available chiral bidentate ligands malate, mandelate, or 2-chloromandelate to produce spiroborate anions which have chiral centres on the ligands and also a racemic boron centre. Using a mixture of enantiomers/diastereomers in the H-cell during electrocrystallisation produces crystals of the radical-cation salt containing only a single preferred enantiomer or diastereomer. The Martin group has continued to investigate the use of spiroborate anions with a variety of different sized and shaped bidentate ligands which has produced a wide variety of donor packing motifs. This section reports the electrical resistivity of two new BEDT-TTF radical-cation salts with B(4-chlorosalicylate)₂⁻ and B(glycolate)₂⁻, which are both 2:1 salts with β'' donor packings. The crystal structures will not be reported in full here because these salts were synthesized and structurally characterised by other members of the Martin research group, however, the electrical resistivity was measured as part of the authors JSPS fellowship at Osaka University.

5.3.1 β''-(BEDT-TTF)₂B(4-chlorosalicylate)₂⁻

The spiroborate anion B(4-chlorosalicylate)₂⁻ (*Figure 5.1*) is slightly smaller than B(chloromandelate)₂⁻ which has previously been used in BEDT-TTF and BDH-TTP salts, and lacking the chiral carbon. 4-Chlorosalicylate forms an asymmetrical bidentate ligand when a pair of these ligands attached to boron making the labile boron centre racemic with both R and S forms.

B(4-chlorosalicylate)₂⁻ produces a 2:1 β'' salt with BEDT-TTF, crystallising in the space group P-1 with the B_R and B_S present in a 50:50 ratio alternating ...RSRSRSRS... in the b direction within each anion layer as shown in *Figure 5.2*. Electrical resistivity shows semiconducting behaviour with an activation energy, E_a = 0.141eV.

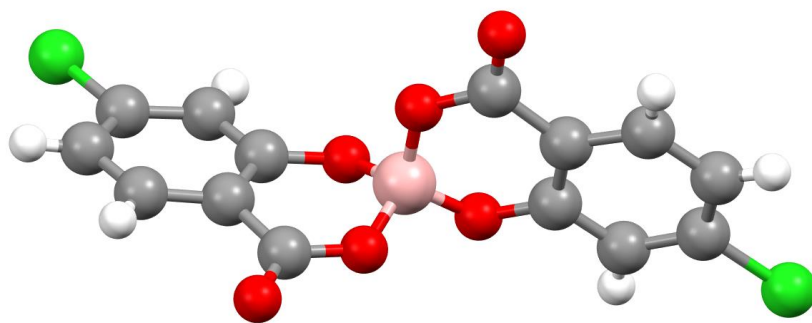


Figure 5.1 - Spiroborate anion $B(4\text{-chlorosalicylate})_2^-$.

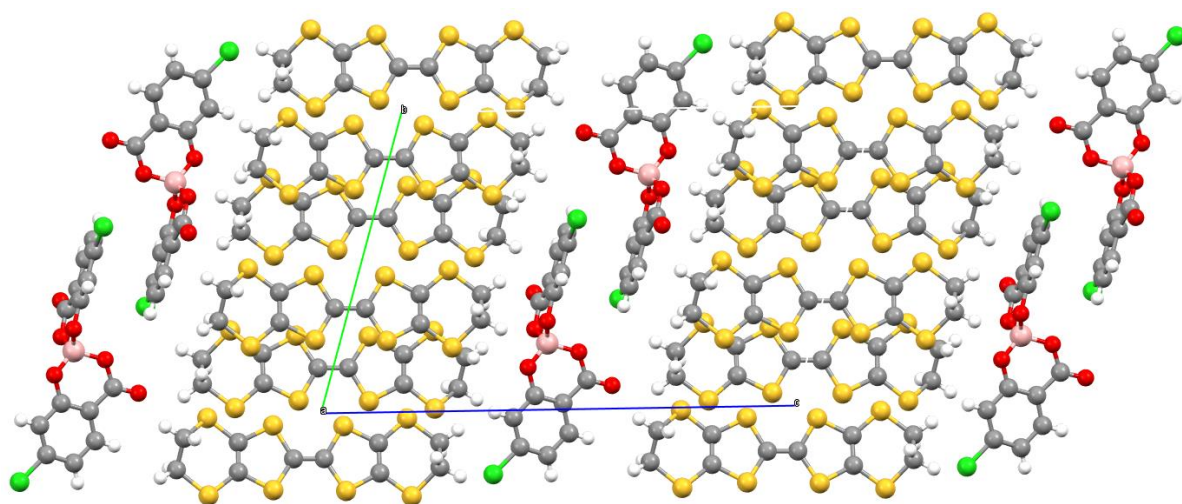


Figure 5.2 - $\beta''\text{-(BEDT-TTF)}_2B(4\text{-chlorosalicylate})_2$ viewed down the a axis.

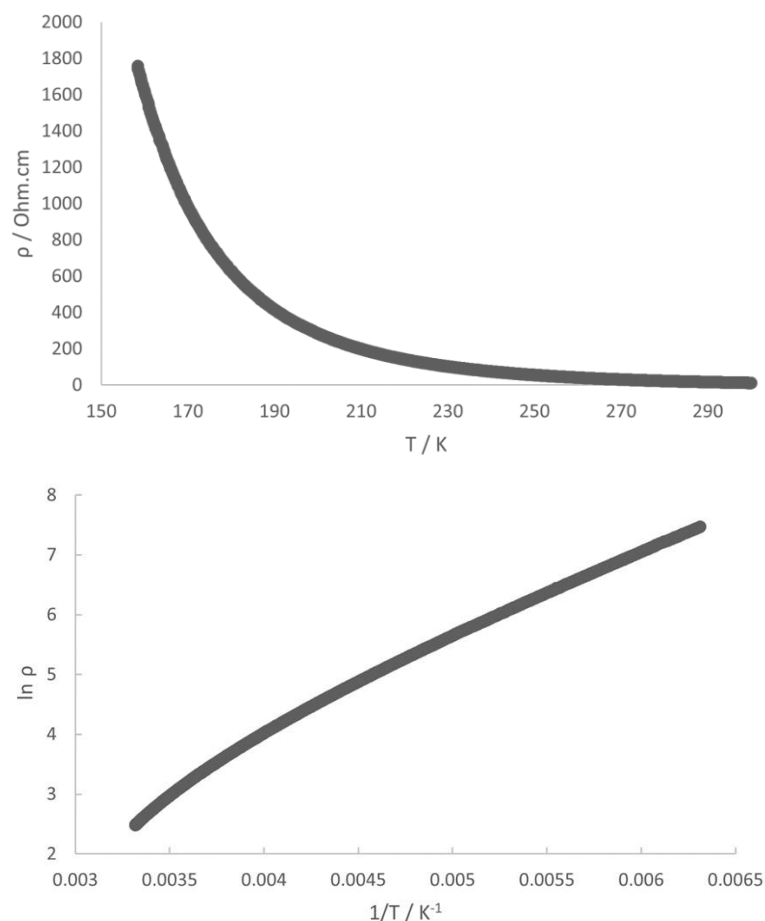


Figure 5.3 - β'' -(BEDT-TTF)₂B(4-chlorosalicylate)₂ electrical resistivity.

5.3.2 β'' -(BEDT-TTF)₂[B(glycolate)₂]

The spiroborate anion B(glycolate)₂⁻ (Figure 5.4) is smaller than the B(malate)₂⁻ and B(mandelate)₂⁻ anions which have previously been used in BEDT-TTF salts. Glycolic acid is not chiral like malic and mandelic acid, but since glycolate forms an asymmetrical bidentate ligand when a pair of glycolates are attached to boron, the labile boron centre is racemic.

B(glycolate)₂⁻ produces a 2:1 β'' salt with BEDT-TTF with the BR and BS present in a 50:50 ratio and alternating ...RSRSRSRS... in the c direction within each anion layer as shown in Figure 5.5. Electrical resistivity shows metallic behaviour down to 170 K where there is a metal-insulator transition and a sharp increase in resistivity below 140 K.

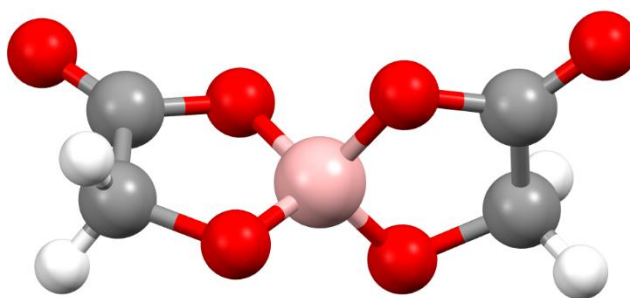


Figure 5.4 - Spiroborate anion $B(\text{glycolate})_2^-$.

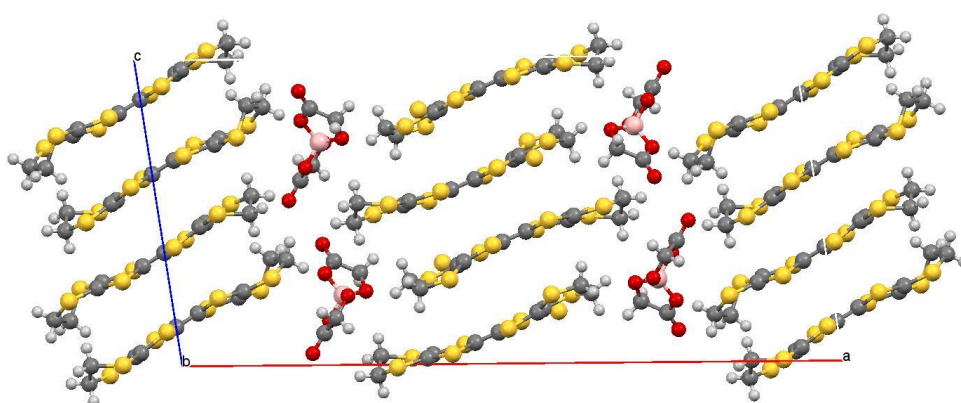


Figure 5.5 - $\beta''\text{-(BEDT-TTF)}_2[B(\text{glycolate})_2]$ viewed down the b axis.

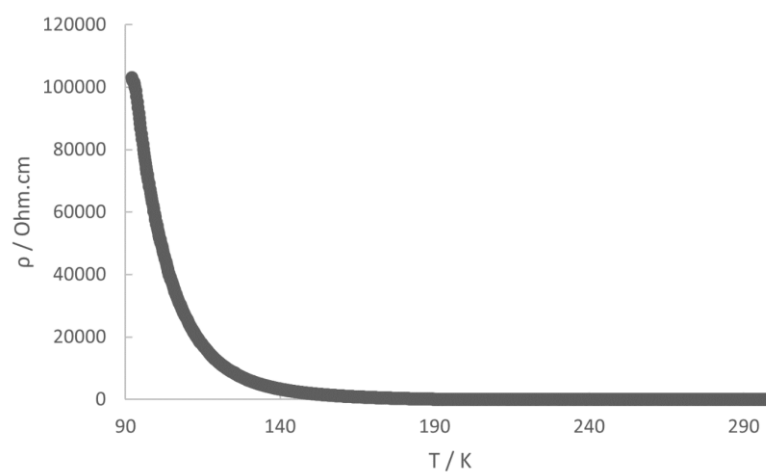


Figure 5.6 - $\beta''\text{-(BEDT-TTF)}_2[B(\text{glycolate})_2]$ electrical resistivity.

5.4 Conclusions

Electrical resistivity measurements have been used to characterise the conducting properties of two new BEDT-TTF charge-transfer salts with spiroborate anions. Both salts have β'' donor packing arrangements but one shows semiconducting behaviour, whilst the other a metal-insulator transition. The large pool of potential bidentate ligands available will make it possible to produce an extensive library of spiroborate anions with great variety in their size and shape which will undoubtedly lead to a multitude of BEDT-TTF charge-transfer salts with different properties and potentially interesting behaviour from the chirality which can be induced into these conducting salts.

6. Final Conclusions and Future Work

6.1 BEDT-TTF-Based Donors with TCNQ

Following successful implementation of methods proposed by *Wallis et al.*,³ eight novel unsymmetrically substituted enantiopure donors are now available for further chemical manipulation. The first and most important step to take is that of recrystallisation and subsequent purification of these new donors such that one may yield suitable crystalline material to allow full elucidation of their chiral structures as well as absolute certainty of the perceived stereochemistry at the chiral centres. Once this is completed, one may then take the second important step and attempt to synthesise charge-transfer salts with TCNQ to allow full characterisation of the electronic properties and study the effect of chirality upon these physical properties. Comparison not only to diastereoisomers, but also to their enantiomers for observation of the interplay of multiple properties within each material and therefore allow potential postulation for not only eMChA, but also some insight into the very workings of (high-temperature) *superconductivity*, should they display such properties.

The functionalisation work carried out in this project has focussed mainly upon increasing the steric bulk/hinderance of the chiral sidechain, where it may in fact prove even more interesting to instead decrease the steric bulk of the chiral sidechain. In such cases, one would then grasp the opportunity to employ chiral amines with smaller heterocyclic motifs such as that of thiophene or furan. The pyridyl-amine employed is one example of this potential future work already, though one notes once again that there appeared to be increased difficulty in yielding the pure full-donor diastereoisomers. The half-donors have been successfully synthesised, such that if one wishes to study these smaller heterocyclic sidechains further, one need only work to find a better purification method for these half-motifs as a starting point. The possibilities for alternative amine sidechains are relatively wide-open, since one may also look to alter the alkyl substituent with smaller derivatives. The limiting factor for these future syntheses will depend on the availability and related cost of amines of these types.

This work has focussed on salts with TCNQ, whereby an alternative route of future study may be to employ other TCNQ-derivatives as well as other acceptors entirely. One may also be tempted to the use of more complex chiral anions, such as the metal trisoxalate anions with chiral guests that have been studied in the second aim of this PhD work, since they have proven to be excellent counter-anions with BEDT-TTF. One may then yield another

opportunity to study the effects of dual-chirality, since both the donor and acceptor contain chiral centres, as well as magnetism and conductivity within the same material; another excellent opportunity to study eMChA and synthesise further multifunctional molecular materials.

6.2 BEDT-TTF salts with Metal Trisoxalate Anions

A number of novel charge-transfer salts of BEDT-TTF with metal trisoxalate anions have been realised, with varying magnetic and conductivity properties. Using the iridium trisoxalate anion, one has yielded and published a 5:1 racemic molecular *metal-insulator* salt, β'' -(BEDT-TTF)₅Ir(C₂O₄)₃.ethanol, as well as the pseudo- κ -(BEDT-TTF)₄[(H₃O)Ir(C₂O₄)₃].benzotrile salt observed by the research group previously.⁴ In further work for these salts, isostructural derivatives of the 5:1 *metal-insulating* phase could be synthesised by replacing the metal centre with Al, Co, Ga and Ru to allow a systematic study of the effect the metal centre has upon the (*super*)conducting properties. One notes that this salt was synthesised rather serendipitously, since the 4:1 β'' salt was the goal during this project, however, one would be interested to re-attempt synthesis of the 5:1 salt with the other non-metallic trisoxalate employed to allow such comparisons. One would also postulate that re-attempting synthesis of the non-magnetic salts may prove fruitful if one can alter the synthetic conditions to yield more consistent results.

The use of toluene as a guest in the second part of the aforementioned syntheses yielded salts of β'' -(BEDT-TTF)₄[(H₃O)M(C₂O₄)₃].toluene with both Fe and Cr metal trisoxalate anions. Despite being the desired 4:1 β'' phase, no *superconductivity* is observed and instead the salts are metallic down to 4.2 K. Previously published occurrences of this include the Fe/fluorobenzene and Fe/chlorobenzene salts which display the same conducting behaviour down to 1.8 K. As such, one postulates that larger guests allow for observation of *superconductivity*, since the larger Fe/bromobenzene counterpart shows a T_c of 4 K.¹⁶¹

Following this postulation, one has yielded a β'' - β'' salt using the larger guest molecule (*S*)-(-)-phenyloxirane, which underwent an interesting and unexpected ring-opening to give 1-phenylethane-1,2-diol as the guest. The racemic 4:1 salt of β'' - β'' -(BEDT-TTF)₄[(H₂O/H₃O)Fe(C₂O₄)₃].1-phenylethane-1,2-diol displays a *metal-insulator* transition and is the first example of a salt with this type of donor packing, since previously observed salts of this type have been of α - β'' and κ - β'' types.¹²⁹ This new β'' - β'' salt leads one towards

synthesis of isostructural chiral metals using (*R*)-(-)-1-phenylethane-1,2-diol and (*S*)-(+)-1-phenylethane-1,2-diol. One would be very interested in the observed changes to *metallic* conductivity of these salts, should any arise.

Once again, serendipity has led to another surprising salt synthesis using kojic acid as a guest; a novel salt of α'''' -(BEDT-TTF)₄[Fe(C₂O₄)₂(kojate)] has been realised. Here, one notes that rather than inclusion of the acid as a guest molecule within the salt, instead one observes the replacement of one oxalate ligand with the kojate ligand. Once again, a *metal-insulating* transition is observed, this time at 100 K and unfortunately no Meissner signal was yielded. Despite this, the salt yielded provides the first example of an α'''' packing motif.

Finally, when employing L-(+)-tartaric acid, one yields the novel salt of formula α -(BEDT-TTF)₅[Fe(C₂O₄)₃].L-(+)-tartaric acid. Despite being another example of a *metal-insulating* salt, this guest leads to the spontaneous chiral resolution of the iron trisoxalate anion, such that only the delta (Δ) enantiomers of the trisoxalate being present in the crystal, despite starting from a racemic solution. Not only does this allow one to perform future syntheses using D-(-)-tartaric acid to yield the opposite enantiomer and study any changes in properties arising as a result, one may also use these guest to spontaneously resolve other anions in chiral charge-transfer salts.

6.3 BEDT-TTF salts with Spiroborate Anions

Novel BEDT-TTF charge-transfer salts with spiroborate anions B(4-chlorosalicylate)₂ and B(glycolate)₂ have been characterised *via* electrical resistivity measurements. These salts are further examples of the recently established family of BEDT-TTF charge-transfer salts containing chiral and racemic four-coordinate borate anions.⁵⁻⁷ β'' -(BEDT-TTF)₂B(4-chlorosalicylate)₂ and β'' -(BEDT-TTF)₂B(glycolate)₂ are both racemic 2:1 salts, with the former exhibiting *semiconducting* behaviour compared to the latter, which shows *metallic* behaviour down to 170 K, at which the salts becomes an *insulator*.

The potential of this novel family of spiroborate salts is still relatively unknown, owing to its only very recent discovery. The extensive availability of potential bidentate ligands opens the door to the synthesis of an expansive array of yet more novel charge-transfer salts with variation in anion size and shape, which may allow one to closely examine the effect of chirality upon the physical properties exhibited by such materials. The Martin group have also

postulated the use of chiral hydroxyalkyl-BEDT-TTF derivatives with the aim of transmitting the chirality between anion and conducting donor layers through hydrogen-bonding interactions. Moreover, following the success of these experiments, perhaps one may also be able to employ the functionalised-BEDT-TTF donors synthesised in this PhD work for even further novel families of spiroborate salts. It is clear that the study of these materials is in its early stages, but much excitement may come in the very near future through the realisation of further *(super)conducting* spiroborate salts with BEDT-TTF and its derivatives.

In conclusion, one has performed extensive syntheses throughout this PhD work, which have yielded many novel materials that may be studied further, with some successfully published and others being prepared for publication. One hopes that this work may provide the basis for synthesising further chiral molecular *(super)conductors* with interesting arrays of novel properties arising from the interplay between chirality, magnetism and conductivity. One is excited for the future of materials of these types and their successful employment in revolutionary real-world molecular electronics.

References

- 1 H. K. Onnes, Disappearance of the electrical resistance of mercury at helium temperatures, *Proc K Ned Akad Wet*, 1911, **14**, 113–115.
- 2 J. I. Short, T. J. Blundell, S. J. Krivickas, S. Yang, J. D. Wallis, H. Akutsu, Y. Nakazawa and L. Martin, Chiral molecular conductor with an insulator–metal transition close to room temperature, *Chem Commun*, 2020, **56**, 9497.
- 3 I. Awgheda, S. J. Krivickas, S. Yang, L. Martin, M. A. Guziak, A. C. Brooks, F. Pelletier, M. Le Kerneau, P. Day, P. N. Horton, H. Akutsu and J. D. Wallis, Synthesis of new chiral organosulfur donors with hydrogen bonding functionality and their first charge transfer salts, *Tetrahedron*, 2013, **69**, 8738–8750.
- 4 T. J. Blundell, A. L. Morritt, E. K. Rusbridge, L. Quibell, J. Oakes, H. Akutsu, Y. Nakazawa, S. Imajo, T. Kadoya, J. I. Yamada, S. J. Coles, J. Christensen and L. Martin, Molecular conductors from bis(ethylenedithio)tetrathiafulvalene with tris(oxalato)gallate and tris(oxalato)iridate, *Mater Adv*, 2022, **3**, 4724–4735.
- 5 T. J. Blundell, M. Brannan, H. Nishimoto, T. Kadoya, J. I. Yamada, H. Akutsu, Y. Nakazawa and L. Martin, Chiral metal down to 4.2 K - a BDH-TTP radical-cation salt with spiroboronate anion B(2-chloromandelate)₂⁻, *Chem Commun*, 2021, **57**, 5406–5409.
- 6 T. J. Blundell, J. R. Lopez, K. Sneade, J. D. Wallis, H. Akutsu, Y. Nakazawa, S. J. Coles, C. Wilson and L. Martin, Enantiopure and racemic radical-cation salts of B(mandelate)⁻ and B(2-chloromandelate)₂⁻ anions with BEDT-TTF, *Dalt Trans*, 2022, **51**, 4843–4852.
- 7 J. R. Lopez, L. Martin, J. D. Wallis, H. Akutsu, Y. Nakazawa, J. I. Yamada, T. Kadoya, S. J. Coles and C. Wilson, Enantiopure and racemic radical-cation salts of B(malate)₂⁻ anions with BEDT-TTF, *Dalt Trans*, 2016, **45**, 9285–9293.
- 8 M. Weller, T. Overton, J. Rourke and F. Armstrong, in *Inorganic Chemistry*, Oxford University Press, 6th edn, 2014, pp. 107–112.
- 9 A. R. West, in *Solid State Chemistry and its Applications*, 2012, vol. 2nd Edition, pp. 173–181.
- 10 W. Kohn, Theory of the Insulating State, *PhRv*, 1964, **133**, 171–181.
- 11 P. Atkins and J. De Paula, in *Elements of Physical Chemistry*, Oxford University Press, Oxford, 2013, vol. 6, pp. 421–425.
- 12 A. R. West, in *Solid State Chemistry and its Applications*, Wiley, 2nd edn, 2012, pp. 359–373.
- 13 G. Inzelt, in *Conducting Polymers: A New Era in Electrochemistry*, Springer, Berlin, 2nd edn, 2008, pp. 1–12.

- 14 H. Letheby, On the production of a blue substance by the electrolysis of sulphate of aniline, *J Chem Soc*, 1862, **15**, 161–163.
- 15 H. Shirakawa, E. J. Louis, A. G. MacDiarmid, C. K. Chiang and A. J. Heeger, Synthesis of electrically conducting organic polymers: halogen derivatives of polyacetylene, $(\text{CH})_x$, *J Chem Soc Chem Commun*, 1977, **16**, 578–580.
- 16 S. Etemad, A. J. Heeger and A. G. Macdiarmid, Polyacetylene, $(\text{CH})_x$: The Prototype Conducting Polymer, *Ann Rev Phys Chem*, 1982, **33**, 443–69.
- 17 A. J. Heeger, Polyaniline with surfactant counterions: Conducting polymer materials which are processible in the conducting form, *Synth Met*, 1993, **57**, 3471–3482.
- 18 C. K. Chiang, C. R. Fincher, Y. W. Park, A. J. Heeger, H. Shirakawa, E. J. Louis, S. C. Gau and A. G. MacDiarmid, Electrical conductivity in doped polyacetylene, *Phys Rev Lett*, 1977, **39**, 1098–1101.
- 19 A. J. Epstein, S. Etemad, A. F. Garito and A. J. Heeger, Metal-Insulator Transition and Antiferromagnetism in a One-Dimensional Organic Solid, *Phys Rev B*, 1972, **5**, 952.
- 20 O. H. Leblanc, On the Electrical Conductivities of Tetracyanoquinodimethan Anion-Radical Salts, *J Chem Phys*, 1965, **42**, 4307–4308.
- 21 M. M. Labes, R. Sehr and M. Bose, Organic Semiconductors. II. The Electrical Resistivity of Organic Molecular Complexes, *J Chem Phys*, 1960, **33**, 868–872.
- 22 L. R. Melby, R. J. Harder, W. R. Hertler, W. Mahler, R. E. Benson and W. E. Mochel, Substituted Quinodimethans. II. Anion-radical Derivatives and Complexes of 7,7,8,8-Tetracyanoquinodimethan, *J Am Chem Soc*, 1962, **84**, 3374–3387.
- 23 H. L. Van De Wouw, J. Chamorro, M. Quintero and R. S. Klausen, Opposites Attract: Organic Charge Transfer Salts, *J Chem Educ*, 2015, **92**, 2134–2139.
- 24 A. J. Berlinsky, Organic metals, *Contemp Phys*, 1976, **17**, 331–354.
- 25 T. Naito, Modern History of Organic Conductors: An Overview, *Crystals*, 2021, **11**, 1–53.
- 26 B. Masao Mizuno, A. F. Garito and M. P. Cava, ‘Organic Metals’: Alkylthio Substitution Effects in Tetrathiafulvalene-Tetracyanoquinodimethane Charge-transfer Complexes, *J Am Chem Soc, Chem Commun*, 1978, **1**, 18–19.
- 27 J. Ferraris, D. O. Cowan, V. Walatka and J. H. Perlstein, Electron Transfer in a New Highly Conducting Donor-Acceptor Complex, *J Am Chem Soc*, 1973, **95**, 948–949.
- 28 D. Jerome, A. Mazaud, M. Ribault and K. Bechgaard, Superconductivity in a synthetic organic conductor $(\text{TMTSF})_2\text{PF}_6$, *J Phys (Paris) Lett*, 1980, **41**, 95–98.

- 29 H. Kamerlingh-Onnes, The liquefaction of helium, *K Ned Akad Wet Proc*, 1908, **11**, 168–185.
- 30 H. Kamerlingh-Onnes, Disappearance of the Electrical Resistance of Mercury at Helium Temperatures, *K Ned Akad Wet Proc*, 1911, **14**, 113–115.
- 31 H. Kamerlingh-Onnes, Further experiments with Liquid Helium. G. On the electrical resistance of Pure Metals etc. VI. On the Sudden Change in the Rate at which the Resistance of Mercury Disappears, *K Ned Akad Wet Proc*, 1913, **15**, 1406–1430.
- 32 J. Bardeen, L. N. Cooper and J. R. Schrieffer, Microscopic Theory of Superconductivity, *Phys Rev*, 1957, **106**, 162–164.
- 33 W. Meissner and R. Ochsenfeld, Ein neuer effekt bei eintritt der supraleitfähigkeit, *Sci Nat*, 1933, **21**, 787–788.
- 34 J. C. Maxwell, VIII. A dynamical theory of the electromagnetic field, *Philos Trans R Soc Lond*, 1865, **155**, 459–512.
- 35 J. C. Maxwell, *A Treatise on Electricity and Magnetism*, Clarendon Press, 1873.
- 36 P. Mangin and R. Kahn, *Superconductivity: An introduction*, Springer, 2015.
- 37 F. London and H. London, The electromagnetic equations of the supraconductor, *Proc R Soc Lond Ser A Math Phys Sci*, 1935, **149**, 71–88.
- 38 C. J. Gorter and H. Casimir, Zur Thermodynamik des Supraleitenden Zustandes, *Arch Musée Teyler*, 1935, 55–60.
- 39 L. D. Landau and V. L. Ginzburg, On the theory of superconductivity, *Zh Eksp Teor Fiz*, 1950, **20**, 1064.
- 40 A. B. Pippard, The surface energies of superconductors, *Math Proc Camb*, 1950, **47**, 617–625.
- 41 E. Maxwell, Isotope Effect in the Superconductivity of Mercury, *Phys Rev*, 1950, **78**, 477.
- 42 C. A. Reynolds, B. Serin, W. H. Wright and L. B. Nesbitt, Superconductivity of Isotopes of Mercury, *Phys Rev*, 1950, **78**, 487.
- 43 J. W. Garland, Isotope Effect in Superconductivity, *Phys Rev Lett*, 1963, **11**, 114.
- 44 H. Fröhlich, Theory of the Superconducting State. I. The Ground State at the Absolute Zero of Temperature, *Phys Rev*, 1950, **79**, 845.
- 45 L. N. Cooper, Bound Electron Pairs in a Degenerate Fermi Gas, *Phys Rev*, 1956, **104**, 1189.
- 46 L. Shubnikov, Destruction of Supraconductivity by Electric Current and Magnetic Field, *Nature*, 1936, **138**, 545–546.

- 47 A. Pippard and W. L. Bragg, An experimental and theoretical study of the relation between magnetic field and current in a superconductor, *Proc R Soc Lond A Math Phys Sci*, 1953, **216**, 547–568.
- 48 A. A. Abrikosov, The magnetic properties of superconducting alloys, *J Phys Chem Solids*, 1957, **2**, 199–208.
- 49 M. Tinkham, in *Introduction to Superconductivity*, Courier Corporation, 2nd edn, 2004, pp. 1–16.
- 50 A. A. Abrikosov, in *Vortices in Unconventional Superconductors and Superfluids*, Springer, 2002, pp. 7–20.
- 51 U. Essmann and H. Träuble, The direct observation of individual flux lines in type II superconductors, *Phys Lett A*, 1964, **24**, 526–527.
- 52 W. J. De Haas and J. M. Casimir-Jonker, Penetration of a Magnetic Field into Supra-Conductive Alloys, *Nature*, 1935, **135**, 30–31.
- 53 G. N. Rjabinin and L. W. Shubnikow, Dependence of Magnetic Induction on the Magnetic Field in Supraconducting Lead, *Nature*, 1934, **134**, 286–287.
- 54 K. Mendelssohn and J. R. Moore, Supra-conducting Alloys, *Nature*, 1935, **135**, 826–827.
- 55 L. V. Shubnikov, V. I. Khotkevich, Yu. D. Shepelev and Yu. N. Ryabinin, Magnetic Properties of Superconducting Metals and Alloys, *Zh Eksper Teor Fiz*, 1937, **7**, 221–237.
- 56 L. Gor'kov, Microscopic derivation of the Ginzburg–Landau equation in the theory of superconductivity, *Zh Eksper Teoret Fiz*, 1959, **36**, 1918–1923.
- 57 L. P. Gor'kov, The Critical Supercooling Field in Superconductivity Theory, *J Exptl Theoret Phys. (U.S.S.R.)*, 1960, **37**, 833–842.
- 58 J. E. Kunzler, Superconductivity in High Magnetic Fields at High Current Densities, *Rev Mod Phys*, 1961, **33**, 501.
- 59 I. Giaever, Electron Tunnelling Between Two Superconductors, *Phys Rev Lett*, 1960, **5**, 464.
- 60 Charles. Kittel, in *Introduction to solid state physics*, John Wiley & Sons, Inc, 8th edn, 2005, pp. 257–296.
- 61 B. D. Josephson, The discovery of tunnelling supercurrents, *Rev Mod Phys*, 1974, **46**, 251.
- 62 B. D. Josephson, Possible new effects in superconductive tunnelling, *Phys Lett* 1962, **1**, 251–253.

- 63 B. D. Josephson, Supercurrents through barriers, *Adv Phys*, 1965, **14**, 419–451.
- 64 H. K. Onnes, Further Experiments with liquid helium. H. On the electrical resistance etc. (continued). VIII. The sudden disappearance of the ordinary resistance of tin, and the super-conductive state of lead, *K Ned Akad Wet Proc*, 1913, 51–67.
- 65 J. R. Gavaler, Superconductivity in Nb–Ge films above 22 K, *Appl Phys Lett*, 1973, **23**, 480–482.
- 66 K. H. Bennemann, in *Encyclopedia of Condensed Matter Physics*, Elsevier, 2005, pp. 72–81.
- 67 J. G. Bednorz and K. A. Müller, Possible high T_c superconductivity in the Ba-La-Cu-O system, *Ze Phys B: Condens Matter*, 1986, **64**, 189–193.
- 68 J. Georg Bednorz, K. Alex Müller and M. Takashige, Superconductivity in Alkaline Earth-Substituted $\text{La}_2\text{CuO}_{4-y}$, *Science*, 1987, **236**, 73–75.
- 69 M. K. Wu, J. R. Ashburn, C. J. Torng, P. H. Hor, R. L. Meng, L. Gao, Z. J. Huang, Y. Q. Wang and C. W. Chu, Superconductivity at 93 K in a new mixed-phase Y-Ba-Cu-O compound system at ambient pressure, *Phys Rev Lett*, 1987, **58**, 908.
- 70 A. Aliabadi, Y. Akhavan Farshchi and M. Akhavan, A new Y-based HTSC with T_c above 100 K, *Physica C: Supercond*, 2009, **469**, 2012–2014.
- 71 M. A. Subramanian, C. C. Torardi, J. C. Calabrese, J. Gopalakrishnan, K. J. Morrissey, T. R. Askew, R. B. Flippen, U. Chowdhry and A. W. Sleight, A New High-Temperature Superconductor: $\text{Bi}_2\text{Sr}_{3-x}\text{Ca}_x\text{Cu}_2\text{O}_{8+y}$, *Science (1979)*, 1988, **239**, 1015–1017.
- 72 Z. Z. Sheng and A. M. Hermann, Bulk superconductivity at 120 K in the Tl–Ca/Ba–Cu–O system, *Nature*, 1988, **332**, 138–139.
- 73 M. Cyrot and D. Pavuna, in *Introduction to Superconductivity and High-Tc Materials*, World Scientific, 1992, pp. 1–19.
- 74 E. V. Antipov, S. M. Loureiro, C. Chailout, J. J. Capponi, P. Bordet, J. L. Tholence, S. N. Putilin and M. Marezio, The synthesis and characterization of the $\text{HgBa}_2\text{Ca}_2\text{Cu}_3\text{O}_{8+\delta}$ and $\text{HgBa}_2\text{Ca}_3\text{Cu}_4\text{O}_{10+\delta}$ phases, *Physica C: Supercond*, 1993, **215**, 1–10.
- 75 A. P. Drozdov, M. I. Eremets, I. A. Troyan, V. Ksenofontov and S. I. Shylin, Conventional superconductivity at 203 kelvin at high pressures in the sulfur hydride system, *Nature*, 2015, **525**, 73–76.
- 76 A. P. Drozdov, V. S. Minkov, S. P. Besedin, P. P. Kong, M. A. Kuzovnikov, D. A. Knyazev and M. I. Eremets, Superconductivity at 215 K in lanthanum hydride at high pressures, *arXiv preprint arXiv: 1808.07039*, 2018, 1–7.

- 77 A. F. Hebard, M. J. Rosseinsky, R. C. Haddon, D. W. Murphy, S. H. Glarum, T. T. M. Palstra, A. P. Ramirez and A. R. Kortan, Superconductivity at 18 K in potassium-doped C₆₀, *Nature*, 1991, **350**, 600–601.
- 78 J. Nagamatsu, N. Nakagawa, T. Muranaka, Y. Zenitani and J. Akimitsu, Superconductivity at 39 K in magnesium diboride, *Nature*, 2001, **410**, 63–64.
- 79 K. Bechgaard and D. Jérôme, Organic Superconductors, *Sci Am*, 1982, **247**, 52–61.
- 80 S. S. P. Parkin, M. Ribaultz, D. Jérôme and K. Bechgaard, Superconductivity in the family of organic salts based on the tetramethyltetraselenafulvalene (TMTSF) molecule: (TMTSF)_x (X = ClO₄, PF₆, AsF₆, SbF₆, TaF₆), *J Phys C: Solid State Phys*, 1981, **14**, 5305–5326.
- 81 G. Saito, T. Enoki, K. Toriumi and H. Inokuchi, Two-dimensionality and suppression of metal-semiconductor transition in a new organic metal with alkylthio substituted TTF and perchlorate, *Solid State Commun*, 1982, **42**, 557–560.
- 82 S. S. P. Parkin, E. M. Engler, R. R. Schumaker, R. Lagier, V. Y. Lee, J. C. Scott and R. L. Greene, Superconductivity in a New Family of Organic Conductors, *Phys Rev Lett*, 1983, **50**, 270.
- 83 E. B. Yagubskii, in *Organic Conductors, Superconductors and Magnets: From Synthesis to Molecular Electronics*, Kluwer Academic Publishers, 2003, pp. 45–64.
- 84 É. B. Yagubskii, I. F. Shchegolev, V. N. Laukhin, P. A. Kononovich, M. V. Karatsovnik, A. V. Zvarykina and L. I. Buravov, Normal-pressure superconductivity in an organic metal (BEDT-TTF)₂I₃ [bis (ethylene dithiolo) tetrathiofulvalene triiodide], 1984, 213–217.
- 85 V. N. Laukhin, E. E. Kostiuchenko, Iu. V. Sushko, I. F. Shchegolev and E. B. Yagubskii, Effect of pressure on the superconductivity of β-(BEDT-TTF)₂I₃, *Sov Phys JETP Lett*, 1985, **41**, 81–84.
- 86 K. Murata, M. Tokumoto, H. Anzai, H. Bando, G. Saito, K. Kajimura and T. Ishiguro, Superconductivity with the Onset at 8 K in the Organic Conductor β-(BEDT-TTF)₂I₃ under Pressure, *J Phys Soc Jpn*, 1985, **54**, 1236–1239.
- 87 K. Bender, I. Hennig, D. Schweitzer, K. Dietz, H. Endres and H. J. Keller, Synthesis, Structure and Physical Properties of a Two-Dimensional Organic Metal, Di [bis(ethylene-dithiolo)tetrathiofulvalene]triiodide, (BEDT-TTF)₂I₃, *Mol Cryst Liq Cryst*, 1984, **108**, 359–371.
- 88 R. Kato, H. Kobayashi, A. Kobayashi, S. Moriyama, Y. Nishio, K. Kajita and W. Sasaki, A New Ambient-pressure Superconductor, κ-(BEDT-TTF)₂I₃, *J Chem Soc Jpn, Chem Lett*, 1987, **16**, 507–510.

- 89 K. Kajita, Y. Nishio, S. Moriyama, W. Sasaki, R. Kato, H. Kobayashi and A. Kobayashi, New organic superconductors K- and θ -(BEDT-TTF)₂I₃: Transport property, *Solid State Commun*, 1987, **64**, 1279–1284.
- 90 J. M. Williams, H. H. Wang, M. A. Beno, T. J. Emge, L. M. Sowa, P. T. Copps, F. Behroozi, L. N. Hall, K. Douglas Carlson and G. W. Crabtree, Ambient-pressure superconductivity at 2.7 K and higher temperatures in derivatives of (BEDT-TTF)₂IBr₂: Synthesis, structure, and detection of superconductivity, *Inorg Chem*, 1984, **23**, 3839–3841.
- 91 K. D. Carlson, G. W. Crabtree, L. Nuñez, H. H. Wang, M. A. Beno, U. Geiser, M. A. Firestone, K. S. Webb and J. M. Williams, Ambient pressure superconductivity at 4–5 K in β -(BEDT-TTF)₂AuI₂, *Solid State Commun*, 1986, **57**, 89–92.
- 92 H. Urayama, H. Yamochi, G. Saito, K. Nozawa, T. Sugano, M. Kinoshita, S. Sato, K. Oshima, A. Kawamoto and J. Tanaka, A New Ambient Pressure Organic Superconductor Based on BEDT-TTF with T_c Higher than 10 K (T_c=10.4 K), *Chem Lett*, 1988, **17**, 55–58.
- 93 A. M. Kini, U. Geiser, H. H. Wang, K. D. Carlson, J. M. Williams, W. K. Kwok, K. G. Vandervoort, J. E. Thompson, D. L. Stupka, D. Jung and M. H. Whangbo, A New Ambient-Pressure Organic Superconductor, κ -(ET)₂Cu[N(CN)₂]Br, with the Highest Transition Temperature Yet Observed (Inductive Onset T_c= 11.6 K, Resistive Onset = 12.5 K), *Inorg Chem*, 1990, **29**, 2555–2557.
- 94 T. Mori, Structural Genealogy of BEDT-TTF-Based Organic Conductors I. Parallel Molecules: β and β' Phases, *Bull Chem Soc Jpn*, 1998, **71**, 2509–2526.
- 95 T. Mori, H. Mori and S. Tanaka, Structural Genealogy of BEDT-TTF-Based Organic Conductors II. Inclined Molecules: θ , α , and κ Phases, *Bull Chem Soc Jpn*, 1999, **72**, 179–197.
- 96 T. Mori, Structural Genealogy of BEDT-TTF-Based Organic Conductors III. Twisted Molecules: δ and α' Phases, *Bull Chem Soc Jpn*, 1999, **72**, 2011–2027.
- 97 L. Martin, S. S. Turner, P. Day, P. Guionneau, J. A. K. Howard, D. E. Hibbs, M. E. Light, M. B. Hursthouse, M. Uruichi and K. Yakushi, Crystal chemistry and physical properties of superconducting and semiconducting charge transfer salts of the type (BEDT-TTF)₄[A^IM^{III} (C₂O₄)₃]·PhCN (A^I = H₃O, NH₄, K; M^{III} = Cr, Fe, Co, Al; BEDT-TTF = bis(ethylenedithio)tetrathiafulvalene), *Inorg Chem*, 2001, **40**, 1363–1371.
- 98 T. Mallah, C. Hollis, S. Bott, M. Kurmoo, P. Day, M. Allan and R. H. Friend, Crystal structures and physical properties of bis(ethylenedithio)-tetrathiafulvalene charge-

- transfer salts with FeX_4^- ($\text{X} = \text{Cl}$ or Br) anions, *J Chem Soc, Dalton Trans*, 1990, 859–865.
- 99 L. Martin, S. S. Turner, P. Day, K. M. A. Malik, S. J. Coles and M. B. Hursthouse, Polymorphism based on molecular stereoisomerism in tris(oxalato) Cr(III) salts of bedt-ttf [bis(ethylenedithio)tetrathiafulvalene], *Chem. Commun*, 1999, **0**, 513–514.
- 100 V. Krstić, S. Roth, M. Burghard, K. Kern and G. L. J. A. Rikken, Magneto-chiral anisotropy in charge transport through single-walled carbon nanotubes, *J Chem Phys*, 2002, **117**, 11315–11319.
- 101 G. L. J. A. Rikken and E. Raupach, Observation of magneto-chiral dichroism, *Nature*, 1997, **390**, 493–494.
- 102 G. L. J. A. Rikken, J. Fölling and P. Wyder, Electrical Magneto-chiral Anisotropy, *Phys Rev Lett*, 2001, **87**, 236602.
- 103 F. Pop, P. Auban-Senzier, E. Canadell, G. L. J. A. Rikken and N. Avarvari, Electrical magnetochiral anisotropy in a bulk chiral molecular conductor, *Nat Commun*, 2014, **5**, 1–6.
- 104 T. Yokouchi, N. Kanazawa, A. Kikkawa, D. Morikawa, K. Shibata, T. Arima, Y. Taguchi, F. Kagawa and Y. Tokura, Electrical magnetochiral effect induced by chiral spin fluctuations, *Nat Commun*, 2017, **8**, 1–6.
- 105 F. Qin, W. Shi, T. Ideue, M. Yoshida, A. Zak, R. Tenne, T. Kikitsu, D. Inoue, D. Hashizume and Y. Iwasa, Superconductivity in a chiral nanotube, *Nat Commun*, 2017, **8**, 1–6.
- 106 N. Mroweh, C. Mézière, F. Pop, P. Auban-Senzier, P. Alemany, E. Canadell and N. Avarvari, In Search of Chiral Molecular Superconductors: κ -[(S,S)-DM-BEDT-TTF]₂ClO₄ Revisited, *Adv Mater*, 2020, **32**, 2002811.
- 107 E. Coronado, J. R. Galán-Mascarós, C. J. Gómez-García and V. Laukhin, Coexistence of ferromagnetism and metallic conductivity in a molecule-based layered compound, *Nature*, 2000, **408**, 447–449.
- 108 A. W. Graham, M. Kurmoo and P. Day, β'' -BEDT-TTF₄[(H₂O)Fe(C₂O₄)₃]·PhCN: the first molecular superconductor containing paramagnetic metal ions, *J Chem Soc Chem Commun*, 1995, 2061–2062.
- 109 B. Zhang, Y. Zhang and D. Zhu, (BEDT-TTF)₃Cu₂(C₂O₄)₃(CH₃OH)₂: an organic–inorganic hybrid antiferromagnetic semiconductor, *Chem Commun*, 2011, **48**, 197–199.
- 110 A. Akutsu-Sato, H. Akutsu, S. S. Turner, P. Day, M. R. Probert, J. A. K. Howard, T. Akutagawa, S. Takeda, T. Nakamura and T. Mori, The first proton-conducting metallic ion-radical salts, *Angew Chem - Int Ed*, 2005, **44**, 292–295.

- 111 J. D. Wallis, A. Karrer and J. D. Dunitz, Chiral metals? A chiral substrate for organic conductors and superconductors, *Helv Chim Acta*, 1986, **69**, 69–70.
- 112 S. J. Krivickas, C. Hashimoto, J. Yoshida, A. Ueda, K. Takahashi, J. D. Wallis and H. Mori, Synthesis of racemic and chiral BEDT-TTF derivatives possessing hydroxy groups and their achiral and chiral charge transfer complexes, *Beilstein J Org Chem* **11**:172, 2015, **11**, 1561–1569.
- 113 C. Réthoré, N. Avarvari, E. Canadell, P. Auban-Senzier and M. Fourmigué, Chiral molecular metals: Syntheses, structures, and properties of the AsF_6^- salts of racemic (\pm)-, (R)-, and (S)-tetrathiafulvalene-oxazoline derivatives, *J Am Chem Soc*, 2005, **127**, 5748–5749.
- 114 S. Yang, A. C. Brooks, L. Martin, P. Day, H. Li, P. Horton, L. Male and J. D. Wallis, Novel enantiopure bis(pyrrolo)tetrathiafulvalene donors exhibiting chiral crystal packing arrangements, *CrystEngComm*, 2009, **11**, 993–996.
- 115 M. Chas, M. Lemarié, M. Gulea and N. Avarvari, Chemo- and enantioselective sulfoxidation of bis(ethylenedithio)-tetrathiafulvalene (BEDT-TTF) into chiral BEDT-TTF-sulfoxide, *Chem Commun*, 2007, 220–222.
- 116 E. Gomar-Nadal, C. Rovira and D. B. Amabilino, Synthesis of optically active amphiphilic tetrathiafulvalene derivatives, *Tetrahedron*, 2006, **62**, 3370–3379.
- 117 M. Atzori, F. Pop, P. Auban-Senzier, C. J. Gómez-García, E. Canadell, F. Artizzu, A. Serpe, P. Deplano, N. Avarvari and M. L. Mercuri, Structural diversity and physical properties of paramagnetic molecular conductors based on bis(ethylenedithio)tetrathiafulvalene (BEDT-TTF) and the tris(chloranilato)ferrate(III) complex, *Inorg Chem*, 2014, **53**, 7028–7039.
- 118 C. J. Gómez-García, E. Coronado, S. Curreli, C. Giménez-Saiz, P. Deplano, M. L. Mercuri, L. Pilia, A. Serpe, C. Faulmann and E. Canadell, A chirality-induced alpha phase and a novel molecular magnetic metal in the BEDT-TTF/tris(croconate)ferrate(III) hybrid molecular system, *Chem Commun*, 2006, 4931–4933.
- 119 A. M. Madalan, E. Canadell, P. Auban-Senzier, D. Brânzea, N. Avarvari and M. Andruh, Conducting mixed-valence salt of bis(ethylenedithio)tetrathiafulvalene (BEDT-TTF) with the paramagnetic heteroleptic anion $[\text{Cr}^{\text{III}}(\text{oxalate})_2(2,2'\text{-bipyridine})]^-$, *New J Chem*, 2008, **32**, 333–339.
- 120 E. Coronado, J. R. Galán-Mascarós, C. J. Gómez-García, A. Murcia-Martínez and E. Canadell, A chiral molecular conductor: Synthesis, structure, and physical properties

- of [ET]₃[Sb₂(L-tart)₂]-CH₃CN (ET = bis(ethyldithio)tetrathiafulvalene; L-tart = (2R,3R)-(+)-tartrate), *Inorg Chem*, 2004, **43**, 8072–8077.
- 121 F. Riobé, F. Piron, C. Réthoré, A. M. Madalan, C. J. Gómez-García, J. Lacour, J. D. Wallis and N. Avarvari, Radical cation salts of BEDT-TTF, enantiopure tetramethyl-BEDT-TTF, and TTF-Oxazoline (TTF-Ox) donors with the homoleptic TRISPHAT anion, *New J Chem*, 2011, **35**, 2279–2286.
- 122 L. Martin, H. Engelkamp, H. Akutsu, S. Nakatsuji, J. Yamada, P. Horton and M. B. Hursthouse, Radical-cation salts of BEDT-TTF with lithium tris(oxalato)metallate(III), *Dalton Trans*, 2015, **44**, 6219–6223.
- 123 L. Martin, P. Day, S. Nakatsuji, J. Yamada, H. Akutsu and P. Horton, A molecular charge transfer salt of BEDT-TTF containing a single enantiomer of tris(oxalato)chromate(III) crystallised from a chiral solvent, *CrystEngComm*, 2010, **12**, 1369–1372.
- 124 L. Martin, H. Akutsu, P. N. Horton, M. B. Hursthouse, R. W. Harrington and W. Clegg, Chiral Radical-Cation Salts of BEDT-TTF Containing a Single Enantiomer of Tris(oxalato)aluminum(III) and -chromate(III), *Eur J Inorg Chem*, 2015, **2015**, 1865–1870.
- 125 L. Martin, H. Akutsu, P. N. Horton and M. B. Hursthouse, Chirality in charge-transfer salts of BEDT-TTF of tris(oxalato)chromate(III), *CrystEngComm*, 2015, **17**, 2783–2790.
- 126 L. Martin, P. Day, P. Horton, S. Nakatsuji, J. Yamada and H. Akutsu, Chiral conducting salts of BEDT-TTF containing a single enantiomer of tris(oxalato)chromate(III) crystallised from a chiral solvent, *J Mater Chem*, 2010, **20**, 2738–2742.
- 127 L. Martin, P. Day, H. Akutsu, J. I. Yamada, S. Nakatsuji, W. Clegg, R. W. Harrington, P. N. Horton, M. B. Hursthouse, P. McMillan and S. Firth, Metallic molecular crystals containing chiral or racemic guest molecules, *CrystEngComm*, 2007, **9**, 865–867.
- 128 M. Kurmoo, A. W. Graham, P. Day, S. J. Coles, M. B. Hursthouse, J. L. Caulfield, J. Singleton, F. L. Pratt, W. Hayes, L. Ducasse and P. Guionneau, in *Molecules into Materials: Case Studies in Materials Chemistry-Mixed Valency, Magnetism and Super Conductivity*, World Scientific Publishing Co, 2007, pp. 541–549.
- 129 L. Martin, Molecular conductors of BEDT-TTF with tris(oxalato)metallate anions, *Coord Chem Rev*, 2018, **376**, 277–291.
- 130 S. Imajo, H. Akutsu, A. Akutsu-Sato, A. L. Morritt, L. Martin and Y. Nakazawa, Effects of electron correlations and chemical pressures on superconductivity of β''-type organic compounds, *Phys Rev Res*, 2019, **1**, 033184.

- 131 H. Kobayashi, R. Kato, A. Kobayashi, Y. Nishio, K. Kajita and W. Sasaki, Crystals and Electronic Structures of Layered Molecular Superconductor, θ -(BEDT-TTF)₂(I₃)_{1-x}(AuI₂)_x, *Chem Lett*, 1986, **15**, 833–836.
- 132 S. Benmansour and C. J. Gómez-García, The Peter Day Series of Magnetic (Super)Conductors, *Magnetochemistry*, 2021, **7**, 93.
- 133 M. Kurmoo, A. W. Graham, P. Day, S. J. Coles, M. B. Hursthouse, J. L. Caulfield, J. Singleton, F. L. Pratt, W. Hayes, L. Ducasse and P. Guionneau, Superconducting and Semiconducting Magnetic Charge Transfer Salts: (BEDT-TTF)₄AFe(C₂O₄)₃·C₆H₅CN (A = H₂O, K, NH₄), *J Am Chem Soc*, 1995, **117**, 12209–12217.
- 134 R. J. Brown, A. C. Brooks, J. P. Griffiths, B. Vital, P. Day and J. D. Wallis, Synthesis of bis(ethylenedithio)tetrathiafulvalene (BEDT-TTF) derivatives functionalised with two, four or eight hydroxyl groups, *Org Biomol Chem*, 2007, **5**, 3172–3182.
- 135 T. Ozturk, N. Saygili, S. Ozkara, M. Pilkington, C. R. Rice, D. A. Tranter, F. Turksoy and J. D. Wallis, Novel organosulfur donors containing hydroxy functionalities: synthesis of bis[2,2-bis(hydroxymethyl)propane-1,3-diylidithio]tetrathiafulvalene and related materials, *J Chem Soc Perkin Trans 1*, 2001, 407–414.
- 136 Q. Wang, P. Day, J. P. Griffiths, H. Nie and J. D. Wallis, Synthetic strategies for preparing BEDT-TTF derivatives functionalised with metal ion binding groups, *New J Chem*, 2006, **30**, 1790–1800.
- 137 J. P. Griffiths, R. J. Brown, P. Day, C. J. Matthews, B. Vital and J. D. Wallis, Synthesis of bis(ethylenedithio)tetrathiafulvalene derivatives with metal ion ligating centres, *Tetrahedron Lett*, 2003, **44**, 3127–3131.
- 138 J. P. Griffiths, H. Nie, R. J. Brown, P. Day and J. D. Wallis, Synthetic strategies to chiral organosulfur donors related to bis(ethylenedithio)tetrathiafulvalene, *Org Biomol Chem*, 2005, **3**, 2155–2166.
- 139 A. Karrer, J. D. Wallis, J. D. Dunitz, B. Hilti, C. W. Mayer, M. Bürkle and J. Pfeiffer, Structures and Electrical Properties of Some New Organic Conductors Derived from the Donor Molecule TMET (S,S,S,S,-Bis(dimethylethylenedithio) tetrathiafulvalene), *Helv Chim Acta*, 1987, **70**, 942–953.
- 140 A. M. Kini, J. P. Parakka, U. Geiser, H. H. Wang, F. Rivas, E. DiNino, S. Thomas, J. D. Dudek and J. M. Williams, Tetraalkyl- and dialkyl-substituted BEDT-TTF derivatives and their cation-radical salts: synthesis, structure, and properties, *J Mater Chem*, 1999, **9**, 883–892.

- 141 R. J. Brown, G. Camarasa, J. P. Griffiths, P. Day and J. D. Wallis, Synthesis of BEDT-TTF derivatives with carboxylic ester and amide functionalities, *Tetrahedron Lett*, 2004, **45**, 5103–5107.
- 142 T. Komatsu, H. Sato, T. Nakamura, N. Matsukawa, H. Yamochi, G. Saito, M. Kusunoki, K. Sakaguchi and S. Kagoshima, The Electrical and Magnetic Properties of a Novel Two-Dimensional Antiferromagnet Based on BEDT-TTF: θ -(BEDT-TTF)₂Cu₂(CN)[N(CN)₂]₂, *Bull Chem Soc Jpn*, 1995, **68**, 2233–2244.
- 143 H. Mori, S. Tanaka and T. Mori, Systematic study of the electronic state in θ -type BEDT-TTF organic conductors by changing the electronic correlation, *Phys Rev B*, 1998, **57**, 12023.
- 144 J. R. Dunetz, J. Magano and G. A. Weisenburger, Large-Scale Applications of Amide Coupling Reagents for the Synthesis of Pharmaceuticals, *Org Process Res Dev*, 2016, **20**, 140–177.
- 145 G. Coulthard, W. P. Unsworth and R. J. K. Taylor, Propylphosphonic anhydride (T₃P) mediated synthesis of β -lactams from imines and aryl-substituted acetic acids, *Tetrahedron Lett*, 2015, **56**, 3113–3116.
- 146 C. F. Macrae, P. R. Edgington, P. McCabe, E. Pidcock, G. P. Shields, R. Taylor, M. Towler and J. Van De Streek, Mercury: visualization and analysis of crystal structures, *J Appl Crystallogr*, 2006, **39**, 453–457.
- 147 C. Wang, A. S. Batsanov, M. R. Bryce and J. A. K. Howard, An Improved Large-Scale (90 g) Synthesis of Bis(tetraethylammonium)bis(1,3-dithiole-2-thione-4,5-dithiol)zincate: Synthesis and X-ray Crystal Structures of Bicyclic and Tricyclic 1,4-Dithiocines Derived from 1,3-Dithiole-2-thione-4,5-dithiolate (DMIT), *Synth*, 1998, **1998**, 1615–1618.
- 148 N. Svenstrup and J. Becher, The Organic Chemistry of 1,3-Dithiole-2-thione-4,5-dithiolate (DMIT), *Synth*, 1995, **03**, 215–235.
- 149 K. S. Varma, A. Bury, N. J. Harris and A. E. Underhill, Improved Synthesis of Bis(ethylenedithio)tetrathiafulvalene (BEDT-TTF): π -Donor for Synthetic Metals, *Synth*, 1987, **1987**, 837–838.
- 150 H. H. Wang, P. E. Reed and J. M. Williams, Perdeuterio bis(ethylenedithio)tetrathiafulvalene, *Synth Met*, 1986, **14**, 165–172.
- 151 J. Larsen and C. Lenoir, 2,2'-Bi-5,6-Dihydro-1,3-Dithiolo[4,5-b][1,4]Dithiinylidene (BEDT-TTF), *Org Synth*, 2003, 265–265.
- 152 K. Hartke, T. Kissel, J. Quante and R. Matusch, Thion- und Dithioester, XXIV. Synthese von Tetrathiooxalestern, *Chem Ber*, 1980, **113**, 1898–1906.

- 153 G. G. Abashev and E. V. Shklyava, Synthesis of 1,3-dithiole-2-thiones and tetrathiafulvalenes using oligo-(1,3-dithiole-2,4,5-trithione)., *Chem Heterocycl Compd (N Y)*, 2006, **42**, 423–439.
- 154 O. Y. Neiland, Y. Y. Katsens and Y. N. Kreitsberga, Preparation of Substituted 4, 5-Ethylenedithio-1, 3-dithiol-2-thiones, *ChemInform*, 1989, **20** (27).
- 155 J. D. Wallis and J. P. Griffiths, Substituted BEDT-TTF derivatives: synthesis, chirality, properties and potential applications, *J Mater Chem*, 2005, **15**, 347–365.
- 156 M. Mizuno, A. F. Garito and M. P. Cava, 'Organic metals': alkylthio substitution effects in tetrathiafulvalene–tetracyanoquinodimethane charge-transfer complexes, *J Chem Soc Chem Commun*, 1978, 18–19.
- 157 L. Martin, J. R. Lopez, H. Akutsu, Y. Nakazawa and S. Imajo, Bulk Kosterlitz-Thouless Type Molecular Superconductor β'' -(BEDT-TTF)₂[(H₂O)(NH₄)₂Cr(C₂O₄)₃]-18-crown-6, *Inorg Chem*, 2017, **56**, 14045–14052.
- 158 L. Martin, A. L. Morritt, J. R. Lopez, H. Akutsu, Y. Nakazawa, S. Imajo and Y. Ihara, Ambient-pressure molecular superconductor with a superlattice containing layers of tris (oxalato) rhodate enantiomers and 18-crown-6, *Inorg Chem*, 2017, **56**, 717–720.
- 159 A. Akutsu-Sato, H. Akutsu, J. Yamada, S. Nakatsuji, S. S. Turner and P. Day, Suppression of superconductivity in a molecular charge transfer salt by changing guest molecule: β'' -(BEDT-TTF)₄[(H₃O)Fe(C₂O₄)₃](C₆H₅CN)_x(C₅H₅N)_{1-x}, *J Mater Chem*, 2007, **17**, 2497–2499.
- 160 T. G. Prokhorova, L. I. Buravov, E. B. Yagubskii, L. V. Zorina, S. S. Khasanov, S. V. Simonov, R. P. Shibaeva, A. V. Korobenko and V. N. Zverev, Effect of electrocrystallization medium on quality, structural features, and conducting properties of single crystals of the (BEDT-TTF)₄A^I[Fe^{III}(C₂O₄)₃]-G family, *CrystEngComm*, 2011, **13**, 537–545.
- 161 E. Coronado, S. Curreli, C. Giménez-Saiz and C. J. Gómez-García, The series of molecular conductors and superconductors ET₄[AFe(C₂O₄)₃]-PhX (ET = bis(ethylenedithio)tetrathiafulvalene; (C₂O₄)²⁻ = oxalate; A⁺ = H₃O⁺, K⁺; X = F, Cl, Br, and I): Influence of the halobenzene guest molecules on the crystal struct, *Inorg Chem*, 2012, **51**, 1111–1126.
- 162 S. Benmansour, Y. Sánchez-Máez and C. Gómez-García, Mn-Containing Paramagnetic Conductors with Bis(ethylenedithio)tetrathiafulvalene (BEDT-TTF), *Magnetochemistry*, 2017, **3**, 7.
- 163 T. G. Prokhorova, L. I. Buravov, E. B. Yagubskii, L. V. Zorina, S. V. Simonov, R. P. Shibaeva and V. N. Zverev, Metallic bi- and monolayered radical cation salts based on

- bis(ethylenedithio)tetrathiafulvalene (BEDT-TTF) with the tris(oxalato)gallate anion, *Eur J Inorg Chem*, 2014, **2014**, 3933–3940.
- 164 P. Guionneau, C. J. Kepert, G. Bravic, D. Chasseau, M. R. Truter, M. Kurmoo and P. Day, Determining the charge distribution in BEDT-TTF salts, *Synth Met*, 1997, **86**, 1973–1974.
- 165 T. G. Prokhorova, E. B. Yagubskii, L. V. Zorina, S. V. Simonov, V. N. Zverev, R. P. Shibaeva and L. I. Buravov, Specific Structural Disorder in an Anion Layer and Its Influence on Conducting Properties of New Crystals of the (BEDT-TTF)₄A⁺[M³⁺(ox)₃]G Family, Where G Is 2-Halopyridine; M Is Cr, Ga; A⁺ Is [K_{0.8}(H₃O)_{0.2}]⁺, *Crystals*, 2018, **8**, 92.
- 166 B. Zhang, Y. Zhang, F. Liu and Y. Guo, Synthesis, crystal structure, and characterization of charge-transfer salt: (BEDT-TTF)₅[Fe(C₂O₄)₃]·(H₂O)₂·CH₂Cl₂ (BEDT-TTF = bis(ethylenedithio)tetrathiafulvalene), *CrystEngComm*, 2009, **11**, 2523–2528.
- 167 N. Avarvari and J. D. Wallis, Strategies towards chiral molecular conductors, *J Mater Chem*, 2009, **19**, 4061–4076.
- 168 L. W. Y. Wong, J. W. H. Kan, T. H. Nguyen, H. H. Y. Sung, D. Li, A. S. F. Au-Yeung, R. Sharma, Z. Lin and I. D. Williams, Bis(mandelato)borate: an effective, inexpensive spiroborate anion for chiral resolution, *Chem. Commun*, 2015, **51**, 15760–15763.
- 169 L. W. Y. Wong, G. S. S. Tam, X. Chen, F. T. K. So, A. Soeipto, F. K. Sheong, H. H. Y. Sung, Z. Lin and I. D. Williams, A chiral spiroborate anion from diphenyl-L-tartramide [B{L-Tar(NHPh)₂}₂]⁻ applied to some challenging resolutions, *CrystEngComm*, 2018, **20**, 4831–4848.